Accelerated Life Testing of Solar Energy Materials

Case Study of Some Selective Solar Absorber Coating Materials for DHW Systems

A Report of Task X
Solar Materials Research
and Development
February 1994

INTERNATIONAL ENERGY AGENCY
Solar Heating & Cooling Programme

INTERNATIONAL ENERGY AGENCY

International Energy Agency, headquartered in Paris, was founded in November 1974 as an autonomous body within the framework of the Organization for Economic Cooperation and Development (OECD) to coordinate the energy policies of its members. The twenty-three member countries seek to create the conditions in which the energy sectors of their economies can make the fullest possible contribution to sustainable economic development and the well-being of their people and the environment.

The policy goals of the IEA include diversity, efficiency and flexibility within the energy sector, the ability to respond promptly and flexibly to energy emergencies, the environmentally sustainable provision and use of energy, more environmentally-acceptable energy sources improved energy efficiency, research, development and market deployment of new and improved energy technologies, and cooperation among all energy market participants.

These goals are addressed in part through a program of collaboration in the research, development and demonstration of new energy technologies consisting of about 40 Implementing Agreements. The IEA's R&D activities are headed by the Committee on Energy Research and Technology (CERT) which is supported by a small Secretariat staff in Paris. In addition, four Working Parties (in Conservation, Fossil Fuels, Renewable Energy and Fusion) are charged with monitoring the various collaborative agreements, identifying new areas for cooperation and advising the CERT on policy matters.

IEA SOLAR HEATING AND COOLING PROGRAM

The Solar Heating and Cooling Program was one of the first collaborative R&D agreements to be established within the IEA, and, since 1977, its Participants have been conducting a variety of joint projects in active solar, passive solar and photovoltaic technologies, primarily for building applications. The twenty members are:

Australia	France	Spain
Austria	Germany	Sweden
Belgium	Italy	Switzerland
Canada	Japan	Turkey
Denmark	The Netherlands	United Kingdom
European Commission	New Zealand	United States
Finland	Norway	

A total of nineteen projects or "Tasks" have been undertaken since the beginning of the Solar Heating and Cooling Program. The overall program is monitored by an Executive Committee consisting of one representative from each of the member countries. The leadership and management of the individual Tasks are the responsibility of Operating Agents. These Tasks and their respective Operating Agents are:

*Task 1:	Investigation of the Performance of Solar Heating and Cooling Systems - Denmark
*Task 2:	Coordination of Research and Development on Solar Heating and Cooling - Japan
*Task 3:	Performance Testing of Solar Collectors - Germany/United Kingdom
*Task 4:	Development of an Insulation Handbook and Instrument Package - United States
*Task 5:	Use of Existing Meteorological Information for Solar Energy Application - Sweden
*Task 6:	Solar Systems Using Evacuated Collectors - United States
*Task 7:	Central Solar Heating Plants with Seasonal Storage - Sweden
*Task 8:	Passive and Hybrid Solar Low Energy Buildings - United States
*Task 9:	Solar Radiation and Pyranometry Studies - Canada/Germany
*Task 10:	Material Research and Development - Japan
*Task 11:	Passive and Hybrid Solar Commercial Buildings - Switzerland
Task 12:	Building Energy Analysis and Design Tools for Solar Applications - United States
Task 13:	Advanced Solar Low Energy Buildings - Norway
Task 14:	Advanced Active Solar Systems - Canada
Task 15:	Not initiated
Task 16:	Photovoltaics in Buildings - Germany
Task 17:	Measuring and Modelling Spectral Radiation - Germany
Task 18:	Advanced Glazing Materials - United Kingdom
Task 19:	Solar Air Systems - Switzerland
Task 20:	Solar Energy in Building Renovation - Sweden
*Completed	

Task X - Solar Materials R&D

Task X was initiated to address the materials problems associated with improvements in cost, performance and reliability of solar heated domestic hot water, and space heating and cooling systems. Task X activities began in 1985 and were completed in 1991.

Task activities were organized in the following four subtasks:

Subtask A	Performance Criteria for New Solar Materials
Subtask B	Selective Absorber Materials
Subtask C	Collector and Window Glazings

- Subtask A, involved modelling and (sub)system performance studies of new or proposed solar materials with respect for energy benefits. Failure conditions were studied.
- Subtask B, addressed issues of optical measurements, characterization of microclimate, failure, degradation and accelerated life testing of absorbers.
- Subtask C, involved the study of electochromic optical switching devices, and testing and analysis of low emittance coatings and transparent insulation.

The following countries participated in this task:

Austria	Germany	The Netherlands	United Kingdom
Canada	Italy	Spain	United States
Denmark	Japan (Operating Agent)	Sweden	

Accelerated Life Testing of Solar Energy Materials

Case study of some selective solar absorber coating materials for DHW-systems

Bo Carlsson
Swedish National Testing and
Research Institute
P.O. Box 857, S-501 15 Borås
Sweden

Ulrich Frei
Solar Energy Laboratory School of
Engineering, ITR
CH - 8640 Rapperswil
Switzerland

Michael Köhl
Fraunhofer Institute for Solar Energy
Systems
D - 7800 Freiburg
Germany

Kenneth Möller
Swedish National Testing and
Research Institute
P.O. Box 857, S - 501 15 Borås
Sweden

February. 1994

This report is part of the work within the IEA Solar Heating and Cooling Programme Task X Solar Materials Research and Development

---

Distribution: unrestricted
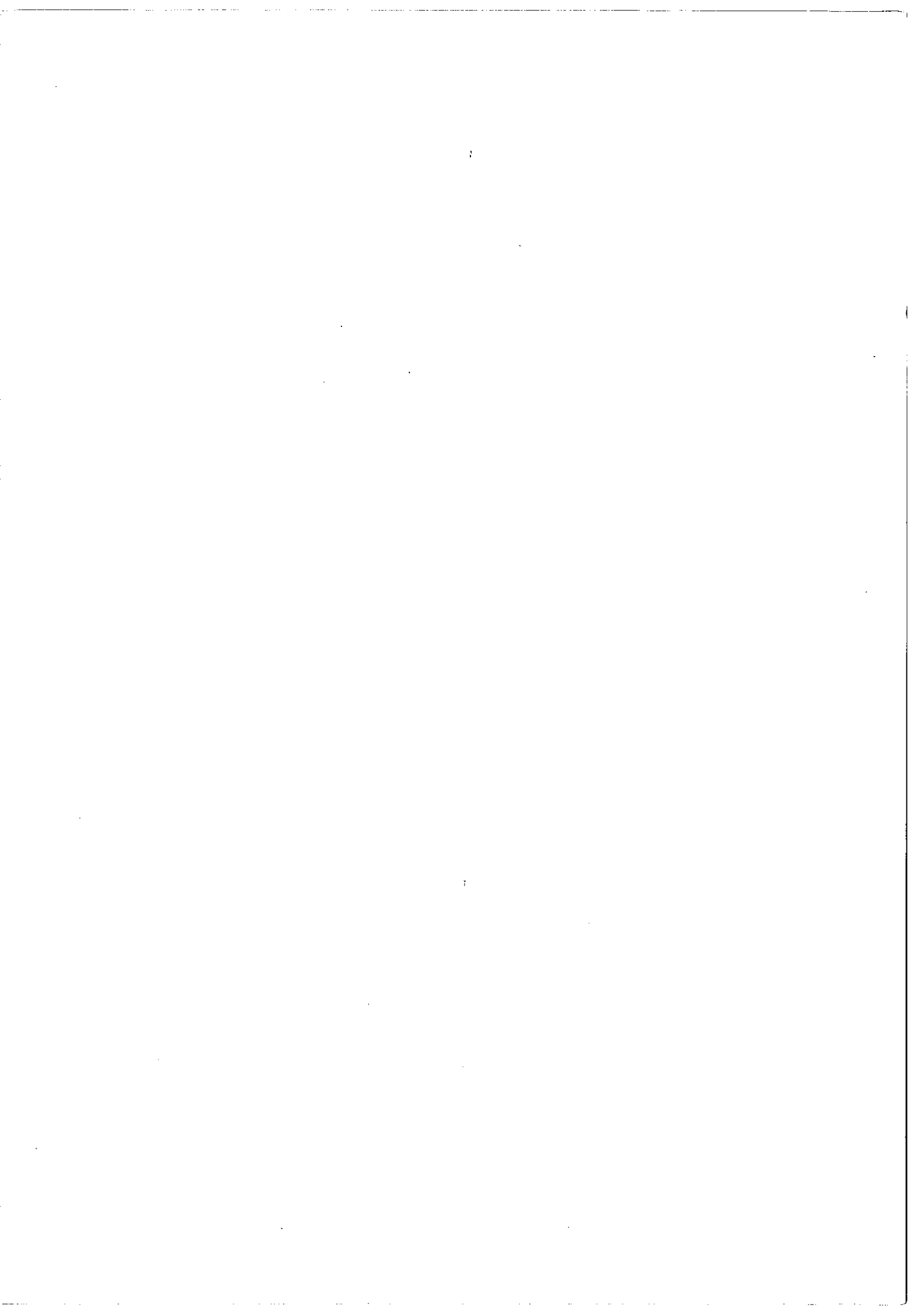
ABSTRACT

Accelerated life testing offers the possibility to forecast material service life prior to installation. For the development of new components and systems it, thus, opens a possibility for systematic life cost analysis and material selection.

The present report documents the results of a joint study aimed at establishing the use and limitations of methods for accelerated life testing applicable to materials used in solar heating and cooling applications. The study was conducted as part of the work in Task X "Solar Materials Research and Development" of the International Energy Agency Solar Heating and Cooling Programme.

The work was organized as a case study in which four commercially-available selective absorber materials were selected for study. These materials are used in single-glazed flat plate solar collectors for domestic hot water production.

The systematic approach to accelerated life testing employed in the case study involved a large number of activities. Analysis was made to find a relationship between the optical properties of an absorber and the thermal performance of a solar system. Recommended procedures for measurements of optical properties of absorber coatings were developed. Three different ageing test programmes were conducted simulating the effect of high temperature, high humidity and condensation, and sulphur dioxide at high humidity. To identify dominant mechanisms of degradation, techniques such as UV-VIS-NIR and IR spectroscopy, SEM, EDX, AES (depth profiling) and XRD were used.

To characterize quantitatively the effective levels of the different environmental factors which might contribute to material degradation under in-service conditions, theoretical models were developed for calculation of microclimatic data (temperature, and humidity). Measurement of microclimatic data (temperature, humidity, and corrosivity) was also carried out on collectors tested under operating and stagnation conditions.

To predict or estimate the service life of the coatings studied, time-transformation functions elaborated from the results of the accelerated tests were used. Failure criteria for absorbers in accelerated tests were also worked out. To validate derived models for service life estimation, absorber samples were taken from the collectors tested for three years.

Key words: Selective absorber coatings, black chrome coating, nickel-pigmented anodized aluminium coating, optical performance and measurement, accelerated aging, degradation, durability assessment, microclimatic conditions in solar collectors, service life prediction.
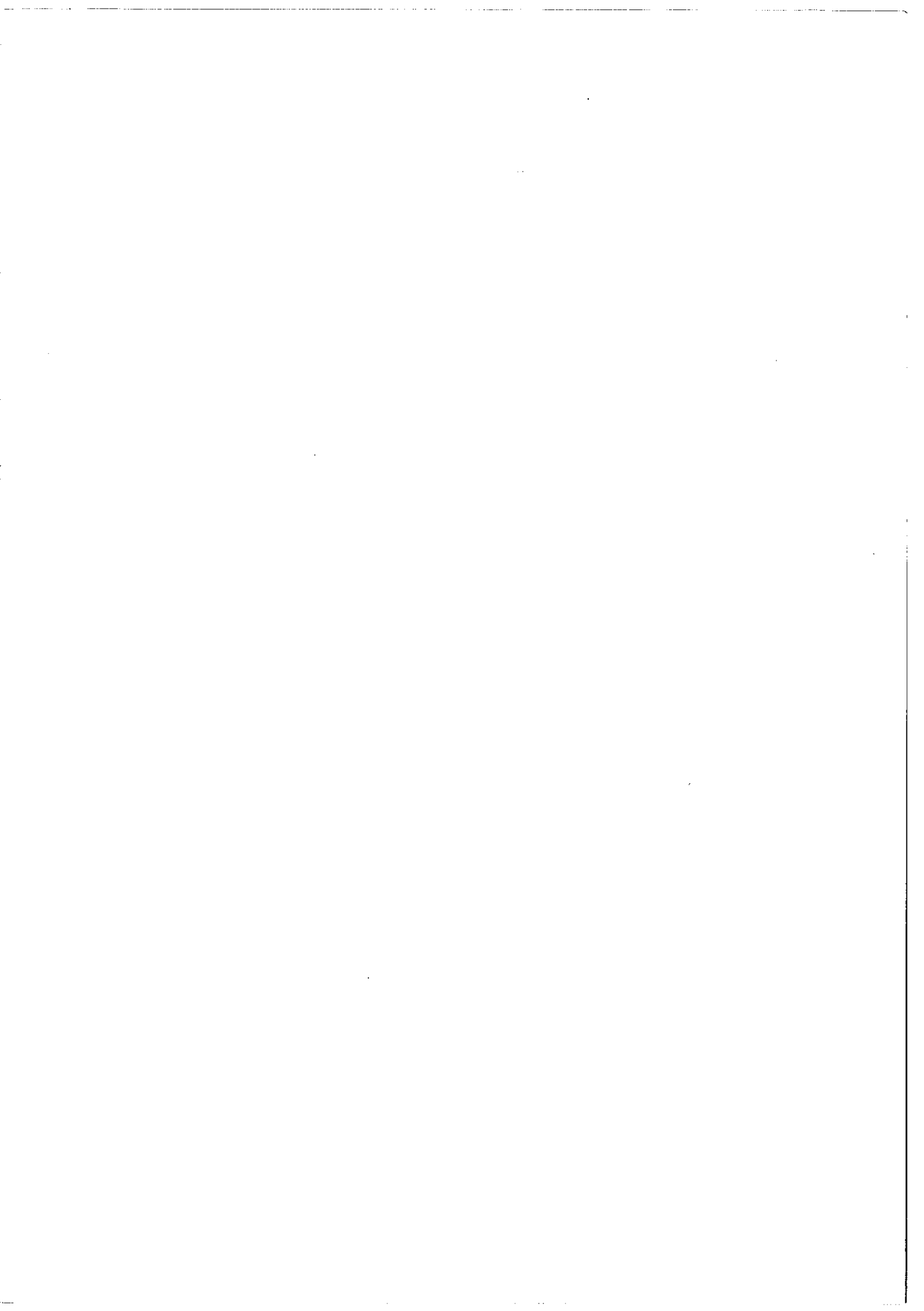
TABLE OF CONTENTS

CHAPTER 1

INTRODUCTION AND EXECUTIVE SUMMARY

1.1 Objectives of Case Study

In the design of solar heating and cooling systems, material questions associated with performance, cost and durability are closely related to each other. To select the most cost-effective material therefore requires durability to be expressed in quantitative terms in the form of an expected service life for the material in the application considered.

As solar heating and cooling is a new technology, service life data on materials from actual experience is limited. Consequently it is necessary to use service life prediction methods based on accelerated life testing to forecast materials service life prior to installation and to aid the development of new components and systems .

In Task X, "Solar Materials R & D" of the International Energy Agency Solar Heating and Cooling Programme, a survey was carried out to identify currently available methods for accelerated life testing that might be applicable to materials used in solar heating and cooling applications [1,1]. The present Task X study was intended to establish the use and limitations of the methods identified in the survey, and also to validate them experimentally .

The work was organized as a case study in which four commercially-available solar collector selective absorber materials were chosen for study, see **Table 1;1**. The application was use in single-glazed flat plate solar collectors for domestic hot water production.

Absorber coating material	Manufacturer
- black chrome on nickel on copper	MTI INC, USA
- black chrome on stainless steel	Energie Solaire, Switzerland
- nickel-pigmented anodized aluminium	Sunstrip, Sweden
- nickel-pigmented anodized aluminium	Showa, Japan

Table 1;1: *Absorber materials for study of accelerated life testing.*

From the survey research it was apparent that considerable efforts have been made to investigate the durability properties of most kinds of materials used in solar heating and cooling applications. A large number of accelerated ageing test methods have been used. But only a few have proven adequate for reliably predicting service life. In the survey, no systematic approach covering all aspects of service life prediction was identified.

It was concluded that many measures were needed to establish accelerated life testing in the application area of solar heating and cooling:

- Service life requirements should be formulated in terms of performance levels of materials.

- Methods should be developed to characterize quantitatively the in-use environmental conditions of materials.

- Relationships between the degradation mechanisms of materials and environmental influences should be evaluated and formulated mathematically.

- Experimental procedures for accelerated life testing should be developed and adopted to permit mathematical treatment of test results for life data analysis.

The objectives of the case study work were to develop both experimental and theoretical tools to meet those needs. This entailed the development of recommended procedures for measurement and testing, and of theoretical models to be used in life testing and life data analysis.

1.2 Scope and Accomplishments of the Case Study

In the systematic approach to accelerated life testing employed in the case study, a step was taken from a qualitative approach towards a quantitative approach for durability assessment. The methodology comprised a large number of activities encompassing a broad range of technical expertise in solar energy engineering, environmental testing, and material science, both at an applied and at a more basic level.

Performance analysis was needed for material failure to be defined. It was necessary first to establish a relationship between the optical properties of an absorber and the thermal performance of a solar system, and then to define a performance criterion for the absorbers in the application considered.

Failure was defined in terms of changes in the absorptance and emittance of absorber coating corresponding to a 5 % loss in solar system performance. This required the development of a theoretical model for use in computer simulation. This work was organized as a joint activity of the absorber and performance groups of Task X.

Failure analysis was needed to identify degradation mechanisms in optical performance of absorber coatings, and to establish relationships between deterioration in performance and changes in the chemical and physical properties of studied materials. This required the development of recommended procedures for measurements of optical performance of coatings. It further required the use of techniques for surface analysis such as UV-VIS-NIR and IR spectrophotometry, SEM, EDX and Auger Electron Spectroscopy, and X-ray diffraction. The benefit of also using theoretical tools, such as an effective medium theory model for optical characterization of absorber coatings, was demonstrated in the interpretation of ageing data .

Stress analysis, i.e. characterizing quantitatively the effective levels of different environmental factors that might contribute to material degradation under in-use conditions, was another important part of the case study work. In another joint effort with the performance group of Task X, a theoretical model was developed for calculation of microclimatic data (temperature, humidity) for absorbers in collectors. Measurement of microclimatic data (temperature, humidity, corrosivity) was also carried out for validation purposes on eight collectors tested by the Task X group at Rapperswil, Switzerland. In this activity, two collectors of each absorber coating material selected for case study work were used.

Accelerated ageing testing was the central activity of the case study work, and entailed simulating identified processes of degradation in laboratory tests at enhanced levels of stress to establish relationships between failure times and environmental influence. Three different ageing test programmes were conducted simulating the effect of (a) high temperature, (b) high humidity and condensation and (c) sulphur dioxide at high humidity. Considerable efforts were made to improve the test techniques so that ageing tests performed fulfilled the requirement of being quantitative. As a result, recommended procedures for ageing testing were worked out.

Life data analysis, which constituted the final step in the systematic approach for accelerated life testing chosen, comprised mathematical modelling of ageing test results to predict or estimate the service lives of the coatings studied. In the case study work, efforts were directed, not only at estimating the service lives of the coatings selected for case study, but also at establishing failure criteria for accelerated ageing tests to be used in the testing of new materials.

Finally, absorber samples taken from the collectors tested at Rapperswil by the Task X group were used to validate derived models for service life estimation. From the comparison between predicted and measured in-service degradation of the absorber coatings it could be concluded that the agreement was fairly good in most cases both from a qualitative and a quantitative point of view. However, the time available for the collector tests was short, making it difficult to judge how accurate the predicted service lives are.

The specific results for the selected coatings of the case study can be summarized as follows:

- Detailed knowledge of the degradation behaviour of the coatings has been gained.

- The relative importance of the different degradation mechanisms and how they influence the service life of the coatings have been clarified.

- Potential measures and tools for the improvement of solar collector design as regards ventilation have been identified. For the anodized aluminium coatings of the case study, the design of the solar collector with respect to ventilation was found to be the most critical factor for the service life.

The work of the case study has proved that the most important step in accelerated life testing is the identification and understanding of the mechanisms of material changes leading to degradation. It has further proved the importance of measurements and analysis of microclimatic data in terms relevant for the degradation processes observed in laboratory tests. However, it should be pointed out that an estimated service life should not be interpreted as an actual life. It should rather be seen as a quantitative measure of durability for processes observed at accelerated ageing.

This Task X report summarizes the results of the activities performed in the absorber group case study between 1987 and 1993. Some of the work conducted in the case study is presented in more detail in other publications such as conference proceeding papers and interim reports of Task X.

1.3 Recommendations for Future Research

The work conducted on accelerated life testing in the case study is unique due to its systematic and quantitative approach towards durability assessment. It treats the problem of service life prediction on both a system and material level and compiles contributions gained from a broad field of technical expertise. Its results therefore, are not only of value to solar energy engineers but also to material scientists and test engineers working with service life assessment and design of materials in other areas of application.

As the research work of the case study has the potential of generating many additional contributions, especially to solar collector and absorber development, it is recommended to continue and extend the scope of work in order to:

- better validate and refine the durability test procedures developed for solar absorbers,

- develop guidelines for solar collector design to accomplish the most favourable microclimatic conditions in collectors, and

- generalize recommended test procedures for standardization purposes.

Such work should include refinement of methods used for microclimate characterization, such as:

- analysis of condensation conditions and condensation frequencies in solar collectors of different designs for improvement of existing model for computer simulation,

- elaboration of relationships between microclimate and corrosivity of air in solar collectors using results from metal coupon exposures,

- definition of standardized microclimatic data to be used in service life prediction models.

In order to develop guidelines for design of solar collectors, work should be undertaken to:

- measure and evaluate the importance of air ventilation on microclimate in solar collectors of various designs,

- develop test methods for measurements of ventilation rates of air in solar collectors.

In order better to validate existing models for service life assessment of absorber coatings based on the accelerated indoor tests, absorber samples taken from collectors used in existing solar heating systems should be analyzed with respect to loss of optical performance over time, material changes and environmental influences. Based on the accelerated indoor tests used for simulating the influence of high temperature, condensed water and a highly corrosive atmosphere with sulphur dioxide, standardized durability test procedures for solar absorbers should be developed. These methods should be applied for testing of new emerging types of solar absorber coatings, such as selective paints, vacuum-deposited coatings and new kinds of electroplated coatings.

1.4 Participants in the Case Study

The Task X, Subtask B group on selective absorber materials, which conducted this study, included representatives from seven countries. The principal participants in the case study work were:

Germany	M. Köhl	Fraunhofer Institute for Solar Energy Systems in Freiburg
	K. Gindele	University of Stuttgart
Japan	S. Tanemura	National Industrial Research Institute in Nagoya
The Netherlands	J. van der Linden	Institute of Applied Physics TNO-TH in Delft
Spain	A. Gonzales	National Institute for Aerospacial Technology in Madrid
Sweden	B. Carlsson (Subtask Leader)	Swedish National Testing and Research Institute in Borås
	K. Möller	Swedish National Testing and Research Institute in Borås
Switzerland	U. Frei	Solar Energy Laboratory School of Engineering in Rapperswil
United Kingdom	M. Hutchins	Oxford Polytechnic School of Engineering

The following participating experts and contributors from Subtask A (Performance) of Task X, were involved in the joint activities with Subtask B:

Canada	T. Hollands	University of Waterloo
Denmark	S.A. Svendsen	Technical University of Denmark
The Netherlands	J. Havinga and A.C. de Gues	Institute of Applied Physics TNO-TH in Delft
	G. Brouwer (Subtask A Leader)	Van Heugten Consulting Engineers in Nijnegen

CHAPTER 2

GENERAL METHODOLOGY EMPLOYED FOR ACCELERATED LIFE TESTING

2.1 Principles of Accelerated Life Testing and Service Life Prediction

2.1.1 Durability tests for service life prediction

In service life prediction based on accelerated life testing, life data are calculated by extrapolating test results. Accordingly, in ageing procedures used the stress levels of one or more degradation factors are kept higher relative to the real use conditions. The advantage is of course that considerable time is saved with such a procedure. Moreover, for the development of new materials, accelerated life testing is, as a rule, the only realistic way to get information on the durability properties of materials prior to their market introduction.

However, despite the fact that a great number of laboratory test methods are available for determining the durability properties of materials, only a few are adequate for reliably predicting service life. Among the problems faced, the following can be mentioned [2,1]:

- Most existing short-term durability tests are intended only for comparative testing, i.e. only qualitatively compare the results of a test material with the results of a similar control material when exposed to identical conditions. Moreover, recommendations are seldom given as how to relate the results of these short-term tests to in-service performance.

- In the laboratory, materials and components are frequently tested in configurations far different from in-service configurations, making the results of laboratory tests difficult to relate to in-service performance.

- The degradation mechanisms of materials are complex and not well understood, so that it is difficult to design meaningful short-term tests.

- The degradation factors affecting service life, especially those involving natural weathering, are difficult to quantify. Many current tests therefore do not take into account all of the important factors, and the factors that are taken into account are seldom quantitatively related to actual exposure conditions.

- Methodologies, e.g. mathematical models, for relating results of laboratory tests to actual performance, are hard to develop because of the complexity of the mechanisms leading to material degradation.

Many efforts have been made to develop systematic approaches to service life prediction so that all essential aspects of the problem will be taken into consideration. The requirements for such a methodology can be summarized as [2,1]:

1   It must be generic.

2   It must lead to identification of all data needed for service life prediction, e.g. environmental degradation factors in service, possible degradation mechanisms of the material or component, quantitative performance requirements, internal maintenance methods, design features, etc.

3   It must be based upon the use of reliable test methods or feedback data. All tests must be designed for, and be of relevance to, requirements dictated by item 2 above.

4   It must provide guidance for data interpretation. Suitable methods and tools for this purpose, e.g. mathematical models, must be specified.

2.1.2   Systematic methodologies for service life prediction

In almost all existing systematic methodologies for service life prediction based on accelerated life testing, four basic themes appear [1, 1].

-   Performance analysis
-   Failure analysis
-   Laboratory ageing testing
-   Mathematical modelling for service life prediction

Performance analysis includes such elements as defining in-use performance requirements, formulating the service life requirement in terms of some functional property of the material and characterization of environmental influence on the material under service conditions which might contribute to degradation in material performance.

Failure analysis means finding interrelationships between deterioration in functional and physical/chemical properties of materials caused by environmental degradation factors. It may preferably comprise studies of morphological and compositional changes induced by artificial ageing and theoretical interpretations in terms of dominant mechanisms of degradation of materials.

Laboratory ageing testing includes evaluation of influence from different degradation factors on material durability. Tests used may simulate the effect of a single degradation factor or the simultaneous action of many degradation factors. Tests can be conducted under a constant environmental stress load or under a cyclic stress load. To ensure that the accelerated test methods will be of relevance for the prevailing in-use requirements, it is sometimes recommended to carry out long-term tests under in-service conditions in parallel with the accelerated tests. If the results from the two types of tests are not in qualitative agreement with respect to observed changes, the accelerated test is considered irrelevant.

Mathematical modelling for service life prediction means firstly to define the performance requirement for the accelerated test in terms of a performance level for at least one measureable physical or chemical property of the material. Secondly, to find a numerical expression which relates the change in the material property selected to the environmental stress factors contributing to the degradation of the material, and, lastly, to characterize the environmental stress factors under service conditions in order to be able to extrapolate the results of the accelerated tests to service life.

Two different kinds of approach to mathematical modelling exist - the deterministic and the probabilistic or statistical approach. The most pronounced problem of both is to find numerical expressions to describe accelerated life data in terms of environmental stress factors so that all factors in the environment contributing to degradation are taken into account. Another problem may be that the mechanism of degradation or the rate of degradation may be different at the elevated stress levels of accelerated testing compared to the situation under service conditions. In such cases, the numerical expressions set up to model accelerated life data may lead to erroneous results when used for extrapolation to in-use conditions. In the probabilistic approach, both variations in material properties and environmental influence are taken into consideration. This implies that a probabilistic approach to accelerated life testing may be preferable.

2.2 Failure Analysis Scheme for Planning of Accelerated Life Tests and Interpretation of Results

The methodology adopted for accelerated life testing in the present case study can be illustrated by a failure analysis scheme as is shown in *Figure* 2;1.

The failure analysis scheme in *Figure* 2;1 describes the degradation process in terms of six key words: PENALTY, FAILURE, DAMAGE, CHANGE, EFFECTIVE STRESS and LOADS. The key words and basic idea behind the scheme illustrated originate from a failure-analysis matrix formulated by the Jet Propulsion Laboratory. They developed it as an aid for unifying and integrating all data and relationships useful in assessing the service life of photovoltaic modulus [2,2]. Each step in the scheme on the left hand side of *Figure* 2;1 may be related to the subsequent step by an appropriate deterministic or statistical relationship. The relation should define the expected results of all the various activities involved in life testing and life data analysis, as indicated on the right hand side of *Figure* 2;1.

In the present case study only, one kind of failure was taken account of; namely, the loss in solar system performance caused by a deterioration of the optical properties of the absorber. This of course limited the scope of study but, on the other hand, made it possible to go into the details of how different environmental factors can generate material changes and cause a deterioration of the optical properties of coatings studied.

Penalty

A 5 % reduction in solar system performance

Failure

Corresponding deterioration of the solar absorptance α and/or thermal emittance ε of the absorber coating

Damage

Spectral changes in VIS-, NIR- and IR-reflectance of absorber coating

Change

Compositional, structural and morphological changes in coating properties

Effective stress

Environmental influence on the material or the micro-level related to temperature, humidity, moisture and pollutants (microclimate)

Loads

Environmental influence on the macro-level related to solar radiation, ambient temperature, wind, humidity and pollutants (macroclimate)

Formulation of performance criterion in terms of $\Delta\alpha$ and $\Delta\varepsilon$

Constant load accelerated ageing meaning determination of failure times for constant load accelerated ageing tests at different elevated levels of stress

Analysis of spectral changes during ageing to identify the mechanisms of degradation

Analysis of aged coatings by AES (depth profiling), XRD, Diffuse reflectance FTIR and SEM for identification of mechanisms

Characterization of microclimate

Mathematical modelling of results

Prediction of service life
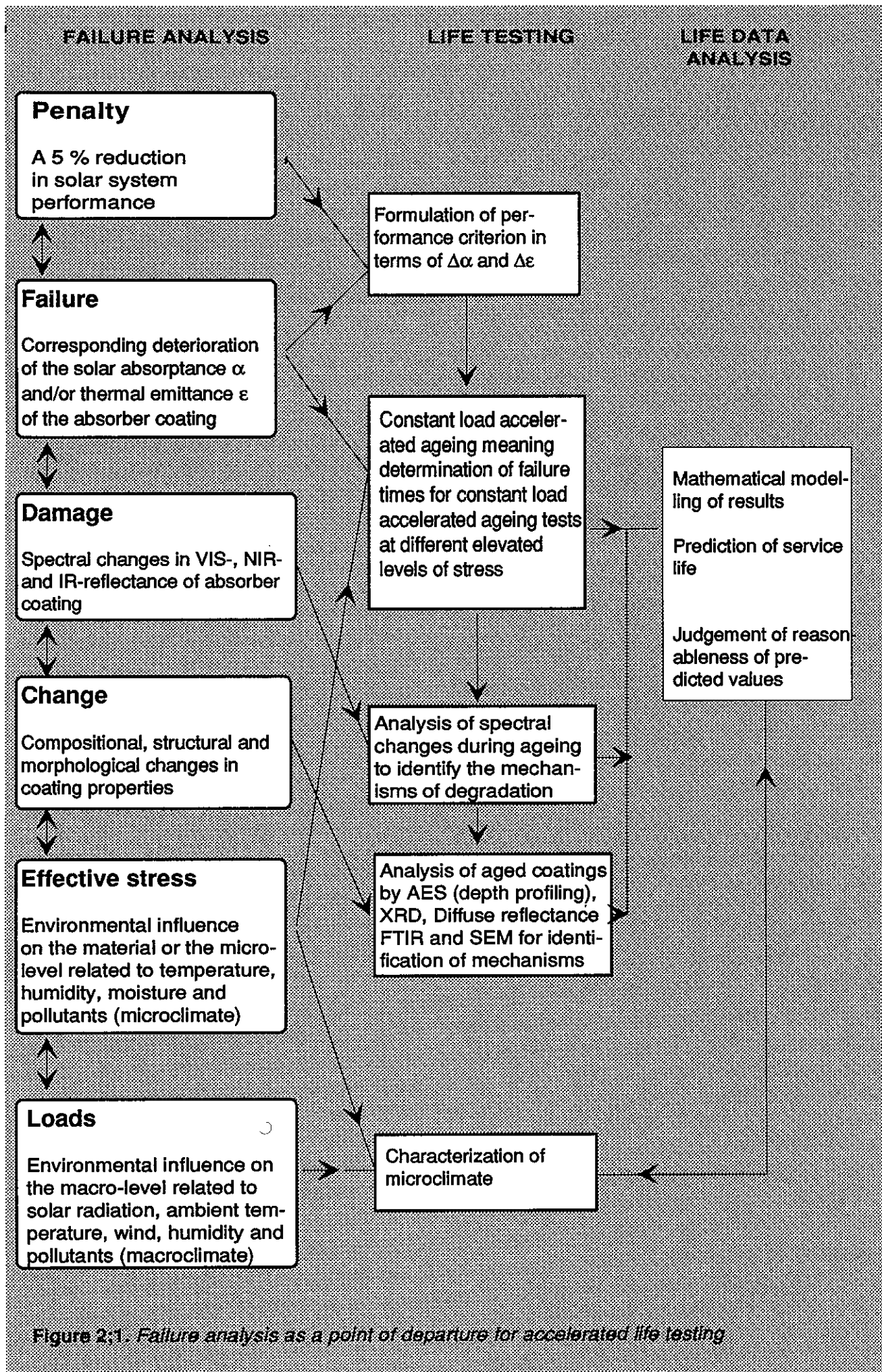
Judgement of reasonableness of predicted values

Figure 2:1. Failure analysis as a point of departure for accelerated life testing

2.2.1   Performance criterion for coatings studied

In order to formulate the criterion for the failure of an absorber coating, the relationship between the deterioration of the optical properties of coating and loss in solar fraction of DHW system had to be determined.

The optical performance of an absorber coating can be characterized in terms of its solar absorptance α_s and its thermal emittance ε. As the solar radiation absorbed by a solar collector is directly proportional to the solar absorptance, and the radiative heat losses from the collector depend on the thermal emittance, no simple relation exists between the thermal performance of the system and the optical performance of the absorber coating. However, as failure was defined as the deterioration of the optical performance corresponding to a 5 % loss in solar fraction, a performance criterion function PC of the following linear form was set up, ie:

$$PC = -\Delta\alpha_s + k_1 \Delta\varepsilon \leq k_2 \tag{2,1}$$

When PC has reached the value of k_2, the solar fraction has been reduced by 5 % in a relative sense and the absorber coating is considered to have failed.

The values of the two constants k_1 and k_2 are unique for every solar system/site/time period combination and depend on climate, system design, collector design and area, hot water demand, set point temperature of tap water and operation strategy of the system. Accordingly, it may be necessary to use different performance criteria for different solar systems in different types of climate.

In **Section 3.1** of the present report, results of computer simulation calculations performed in the case study are presented, aimed at analyzing this problem in more detail. Despite the complexity involved, the variations are not that high and for the case study the following values may be fairly representative for low-fraction solar systems, namely.

$k_1 = 0,25$

$k_2 = 0,05$ (2,2)

It should be pointed out, however, that this definition of failure should not be considered as a general recommendation, as will be discussed further in **section 3.1**. It should rather be seen as an example of how loss in system performance can be related to the deterioration of material performance upon which failure can be defined.

2.2.2 Constant load accelerated ageing testing

To find relationships between failure times of studied coatings and environmental influence at the micro or the material level, a constant-load accelerated ageing test programme was set up taking into account different environmental stress factors that might generate loss in the optical performance of selected coatings. Included in the programme were three different kinds of ageing tests related to (a) high-temperature degradation, (b) degradation by the action of moisture and high-humidity air, and (c) degradation caused by sulphur dioxide at high humidity, see **Table 2;1**.

A. Exposures at high temperatures (200-500 °C) and low humidities	- accelerated tests enhancing the environmental influence on the absorber under operating and stagnant conditions of solar collector at high levels of solar insolation
B. Exposures at service temperatures (10-90°C) but at high air humiditities(95-99 % RH). Tests are carried out both in the absence and presence of high con centrations of sulphur dioxide (ca 1 ppm)	- accelerated tests enhancing environmental influence on the absorber under starting-up and under non-operating conditions of the solar collector
C. Exposures at service temperatures (10-90°C) under condensation conditions	- accelerated tests under more extreme humidity conditions than B

Table 2;1: The joint test programme of constant load accelerated ageing, comprising three different kinds of environmental tests.

Besides these kinds of tests, some UV-irridiation tests were also performed. **Chapter 5** of this report gives a detailed presentation of the test programme, test and measurement procedures employed, reproducaibility of test results and critical factors of testing, together with ageing test results.

The choice of specific tests in the programme was partly based on previous knowledge of the durability properties of selected coatings.

2.2.3 Analysis of changes in optical properties and changes in chemical composition resulting from ageing

In the case study, considerable efforts was directed to the analysis of spectral, morphological and compositional changes induced by artificial and natural ageing, in order to be able to identify mechanisms of degradation. Based on this knowledge, reasonable mechanistic models could be formulated.

By use of both theoretical tools and advanced techniques for surface analysis, dominent mechanisms of degradation of absorber coatings studied could be identified, see *Figure* 2;2.

Black chrome coatings	High temperature degradation in α_S	Oxidation of metallic chromium to chromium oxide
Nickel-pigmented anodized aluminium coatings	High-temperature degradation in α_S	Oxidation of metallic nickel to nickel oxide
	Degradation in ε during condensation and at high humidities	Hydratization of Al_2O_3 to Pseudoboehmite and to Boehmite
	Degradation in α_S at SO_2-exposures and at high humidities	Electrochemical oxidation of metallic nickel to nickel sulphate

Figure 2;2: *Identified dominent mechanisms of degradation of absorber coatings in the case study.*

Chapter 6 of this report gives a detailed presentation of the results and theoretical analysis to identify dominent mechanisms of degradation. This chapter also reports the development of kinetic models for describing degradation data in terms of environmental factors.

2.2.4 Mathematical modelling for life data analysis

For mathematical modelling of life data obtained from the test programme of accelerated ageing, deterministic models based on the acceleration factor or a time transformation function approach were used.

The general principles for the mathematical approach chosen can be expressed as follows.

Consider an absorber coating with a solar absorptance α_S which is changed during ageing. Assume that the change in α_S can be expressed by the following kind of relation

$$\frac{\partial \alpha_S}{\partial t} = f(\alpha_S) \cdot g(\overline{S}) \tag{2,3}$$

where $f(\alpha_S)$ is a function which depends only on α_S and which remains the same independently of applied stress as long as degradation follows the same path, or mechanism. The function $g(\overline{S})$, the stress function, is dependent on the vector $\overline{S}$ which describes the influence of all the environmental factors acting on the coating.

Eq. (2,3) can be solved according to

$$\int_0^y g(\overline{S}) \, dt = \int_{\alpha_{S,0}}^{\alpha_{S,y}} \frac{d\alpha_S}{f(\alpha_S)} = B(\alpha_{S,0}, \alpha_{S,y}) \tag{2,4}$$

where $\alpha_{S,y}$, is the absorptance value at a certain ageing time y.

If $\overline{S}$ is constant in time during an ageing test, then:

$$B(\alpha_{S,0}, \alpha_{S,y}) = g(\overline{S}) \cdot y \tag{2,5}$$

meaning that, if R denotes the reference ageing test, for which $B(\alpha_{S,0}; \alpha_{S,y_R}) = B(\alpha_{S,0}; \alpha_{S,y})$ or $\alpha_{S,y} = \alpha_{S,y_R}$ then:

$$A = \frac{y_R}{y} = \frac{g(\overline{S})}{g(\overline{S}_R)} \tag{2,6}$$

where A is called the acceleration factor. The ratio $g(\overline{S})/g(\overline{S}_R)$ is called the time-transformation function.

If $\overline{S}$ varies periodically with time during an ageing process, the following equation may be derived

$$n \cdot \int_0^{y_p} g(\overline{S}) \, dt = g(\overline{S}_R) \cdot y_R \tag{2,7}$$

where y_p is the length of the period and n is the number of periods untill $\alpha_{S,y}$ is reached.

Analogous relations can be derived for the change in the emittance of the coating during ageing .

To be able to apply equation (2,7), use must be made of the time transformation functions derived from the results of constant-load accelerated ageing tests. The following simplifications therefore need to be introduced:

- When calculating the extent of degradation, only the time period at a certain state of environmental influence is of importance, not the history of changes in the environmental stress factors with time.

- Degradation processes taking place under service conditions proceed by the same mechanism as those conducted at elevated levels of stress during laboratory tests.

- Different processes of degradation proceed in parallel and independently of each other. The   contributions of the different processes to the changes in solar absorptance and thermal emittance are additive.

To distinguish between processes induced by test conditions A and B, see **Table 2;1**, it can be assumed that there exists a certain threshold value for the relative humidity, RH_C, such that for humidity levels below this value the effect of water vapour on the rate of degradation is negligible.

Accordingly, equation (2,7) can be rewritten as follows:

$$\frac{1}{n} = \sum_{i=A,B,C} \int_0^{y_i} (g_i\,(\bar{S})\,/g_i\,(\bar{S}_R)\,) \cdot \frac{1}{y_{R,\,i}}\,dt \tag{2.8}$$

or

$$\frac{1}{n} = \frac{1}{n_A} + \frac{1}{n_B} + \frac{1}{n_C} \tag{2,9}$$

where

y_i = time period of a year when service conditions according to test category i (A, B or C) prevail

$y_{R,\,i}$ = reaction time to predetermined value of $\Delta\alpha_s$ or $\Delta\varepsilon$ for a reference ageing test of category i (A, B or C)

$g_i\,(\bar{S})\,/\,g_i\,(\bar{S}_R)$ = time-transformation function for tests according to category i (A, B or C).

The quantity $1/n_A$ represents testing according to category A and service conditions when the relative humidity is less than RH_C; the quantity $1/n_B$, represents testing according to category B and service conditions when the relative humidity is between RH_C and 100 %, and the quantity $1/n_C$, represents testing according to category C and service conditions during condensation.

From the above, it can be concluded that the parameter n_A is the expected reaction time for predetermined values of $\Delta\alpha_S$ or $\Delta\varepsilon$ when only processes of category A contribute to the overall degradation. The parameters n_B and n_C are the corresponding reaction times when processes of categories B and C respectively act alone. The tentative model described enables processes of each category A, B or C to be evaluated separately. Reference constant-load tests can also be selected for each humidity interval, so that the acceleration factor or time-transformation functions will be as simple as possible.

In case of high-temperature degradation, the time-transformation function can be expressed, for example, in terms of a simple Arrhenius relation, see **Section 6.2**, and equation (2,8) be rewritten as

$$\frac{1}{n_A} = \int\limits_{}^{1\ year} exp\ (\frac{-E_A}{R}\ (\frac{1}{T} - \frac{1}{T_R}))\ \cdot \frac{1}{y_{R,A}} \cdot f\ (T) \cdot dT \qquad (2,10)$$

where E_A = activation energy and f (T) is the temperature distribution function for one year, when air humidity is less than RH_C.

Based on the model as expressed by equation (2,8), $\Delta\alpha_S$ and $\Delta\varepsilon$ relations for service conditions can be estimated for the overall process and the expected service life thereafter can be calculated using equation (2,1).

The tentative model used is relatively simple but of course very approximative. However, it can be a useful tool for making rough estimates of service lives from constant-load accelerated ageing data. Alternatively, the model can be useful when formulating failure time requirements for constant-load accelerated ageing tests.

In **Chapter 7** of the present report, both the formulation of performance requirements for accelerated ageing tests and estimation of service life of studied coatings are treated in detail.

2.2.5 Characterization of microclimate to quantify effective stress on absorber coatings under in-service conditions

The development of suitable time-transformation functions requires not only knowledge of the variations in the rate of degradation with parameters of constant-load accelerated testing, but also detailed insight into the environmental influence or effective stress on material level under service conditions.

In the case study, two different methods of generating microclimatic data for the absorber coatings in the application considered were employed:

- Computer simulation calculations using theoretical models to describe climatic conditions in collectors.

- In-situ measurements on long-term test collectors under operating and stagnant conditions.

It should be pointed out that the measurements performed on the long-term test collectors were mainly intended to serve as a basis for the development and validation of the theoretical models used to generate microclimatic data.

Chapter 4 of the present report describes the different methods employed and results obtained in the form of temperature and humidity frequency diagrams and effective levels of corrosivity in the collectors tested.

From a methodology point of view, it should be mentioned that, to a large extent, the methods available for characterization of microclimate determined the precision of estimated service lives.

CHAPTER 3:

PREREQUISITES FOR ACCELERATED LIFE TESTING IN THE CASE STUDY

3.1 Performance of Solar Domestic Hot Water Systems and Its Dependence on Degradation in Optical Performance of Solar Collector Absorbers

3.1.1 Computer simulations of solar domestic hot water systems

To quantify the effect of degradation in the optical performance of absorber coatings on solar system efficiency, computer simulations were carried out by the performance group of Task X, see also [3,1].

As this study is reported in detail by Hollands et al in ref [3,2], only a summary of their results and conclusions will be given in the present report.

The objective of the study was to use computer simulation of solar domestic hot water systems to calculate relationships between change in solar absorbtance $(-\Delta\alpha_s)$ and change in thermal emittance $(\Delta\varepsilon)$ at the relative decreases of the annual solar fraction F_s of 5 % and 10 %, see equation (2,1). A further objective was to study and interpret the nature of these relationships on a range of solar system parameters, such as geographical location, collector area and setpoint temperature of hot water.
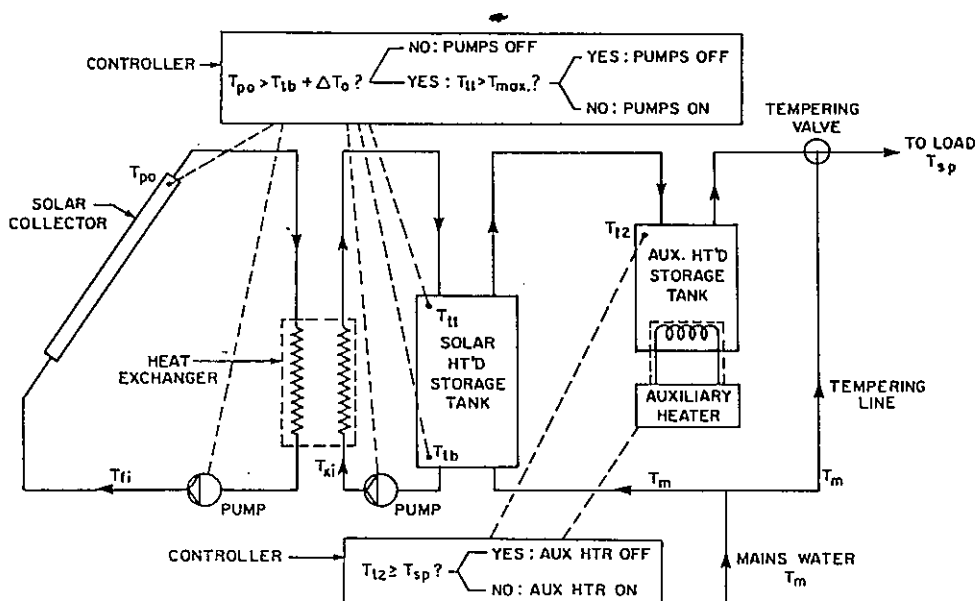
Figure3;1 *Schematic diagram of solar domestic hot water system in simulation studies.*

Simulations were performed using the "WATSUN" computer program to simulate the solar heating system sketched in *Figure 3;1*. Like other similar programs, WATSUN works through the simulated year in hourly time steps of simulated time. At each step, it reads from storage the mean weather data (solar irradiance on a horisontal surface and ambient temperature) and, using modelling algorithms, calculates the mean solar irradiance on the collector for the hour, calculates the collector output for the hour, reverses the status of the storage tank, and finally calculates the solar energy supplied to the load. Summed over the year, the latter quantity represents the annual solar energy delivered to the load. Dividing this value by the yearly energy demand gives the solar fraction F_s. The program used is fully documented in its instruction manual [3,3] .

The input weather data used by Hollands et. al. in the simulations were typical meteorological year (TMY) data for North American cities. The data for the European cities were synthetic data created from knowledge of certain monthly means for the locations. In the case of Rapperswil, Switzerland, real data for one particular year was used.

Quantity	Assumed value
Ambient temperature T_a	283 K
Mean absorber plate temperature T_n	308 K
Back and edge heat loss coeff., $U_b + U_e$	1 W/m^2 K
Convective heat transfer coefficient from cover to ambient air, h_w	15 W/m^2 K
Glass cover solar transmittance t_s	0.91
Glass cover solar absorptance $\alpha_{s, c}$	0.01
Spacing from absorber plate to glass cover	0.02 m
Bond conductance, C_b*	∞
Fin efficiency parameter $k\delta/W^{2*}$	27.7 W/m^2
Group $[h_{fi}(\pi D_i/W)]$*	36 W/m^{2}K
Collector tilt angle	45 deg

Table 3.1: Assumed values of input parameters to collector simulation program
    *(*These values make the fin efficiency F'= 0.95 and F = 0.86 when ε = 0.1)*

For information on the modelling algorithms used in WATSUN for the simulations, the reader is referred to reference [3,2]. *Tables 3;1 and 3;2* present assumed values of input parameters to the collector simulation program and system simulation program, respectively, as used by Hollands et al. The remaining parameters were variations on the "Base case 1 setting" given in *Table 3;3*.

Quantity	Assumed value
Collector tilt	45 deg.
Collector orientation	South-facing
Maximum allowable preheat tank temperature, T_{max}	90 °C
Controller differential, ΔT_o	1 K
Collector fluid specific heat	4200 J/kg K
Preheat tank heat loss coefficient	2 W/K
Tank room temperature	20 °C
Heat exchanger efficiency, ε_x	0.85
Heat exchanger heat capacity ratio	1

Table 3,2: Assumed values of input parameters to system simulation program

	Base Case 1	Base Case 2
Collector area, A_c	4.8 m^2	3.0 m^2
Preheat tank vol.	180 l	100 l
Daily total load draw-off	350 l	100 l
Setpoint temperature, T_{sp}	50 °C	55 °C
Heat exchanger effeciency, ε_x	0.85	0.85
Collector flow rate to collector area ratio: High flow Low flow	0.025 kg/s, m^2 0.0022 kg/s, m^2	0.025 kg/s, m^2
$\alpha_{s0}/\varepsilon_0$	0.95/0.1	0.95/0.1
F_s/F_{s0}	0.9	0.9

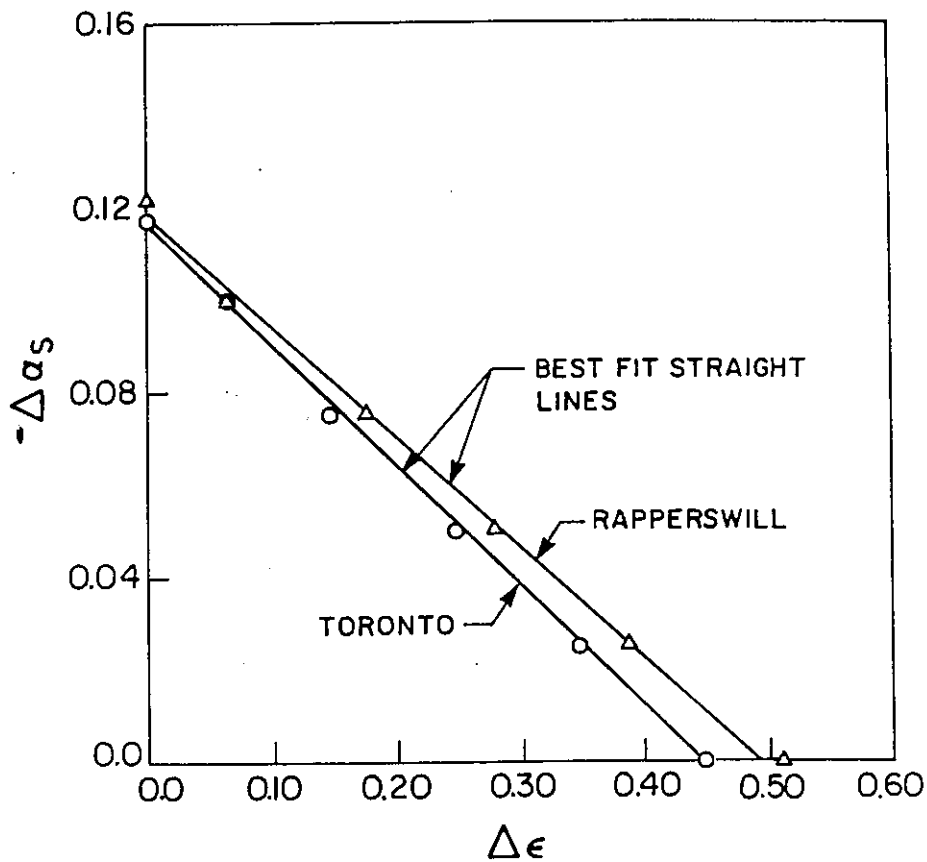*Table 3,3:* Base case input data to computer simulations

Figure 3;2: Plots of - $\Delta\alpha_S$ vs $\Delta\varepsilon$ for Base case 1, see Table 3;3.

Figure 3;2 shows plots of - $\Delta\alpha_S$ versus $\Delta\varepsilon$ using initial values $\alpha_{S,0} = 0,95$ and $\varepsilon_0 = 0,1$ and based on $F_S/F_{S,0} = 0,9$. Any point on a curve represents a combination of -$\Delta\alpha_S$ and $\Delta\varepsilon$ that will give a 10 % loss in system performance. Both curves are seen to be very close to linear and can, cf eq (2,1), be closely matched by

$$- \Delta\alpha_S = a - \frac{a}{b} \cdot \Delta\varepsilon \qquad\qquad (3,1)$$

where a and b are parameters that will depend on the geographical location and other input parameters.

3.1.2 Dependences of geographical location, solar collector area and other solar system variables

Plots such as that in *Figure 3;2* were accordingly prepared to show the effect of various circumstances on how the plot depends on geographical location, on collector

area, on thermostat setpoint temperature, on the (arbitrarily-chosen) ratio $\Delta F_s/F_{s,0}$ and on the collector flow rate.

The resulting plots all showed a nearly constant value for the slope $k_1 = a/b$ of about 0.27, but the intercept varied from about 0.10 to about 0.35 at $F_s/F_{s,0} = 0.9$. That the parameter $k_1 = a/b$ is relatively insensitive to a wide range of system variables can also be explained in theoretical terms as presented in detail by Hollands et al in reference [3,2].

To explain the variation in the parameter $a = k_2$, the ratio $(a/\alpha_{s,0}) / (\Delta F_s/F_{s,0})$ was plotted against the initial annual solar fraction $F_{s,0}$, see **Figure 3;3**.
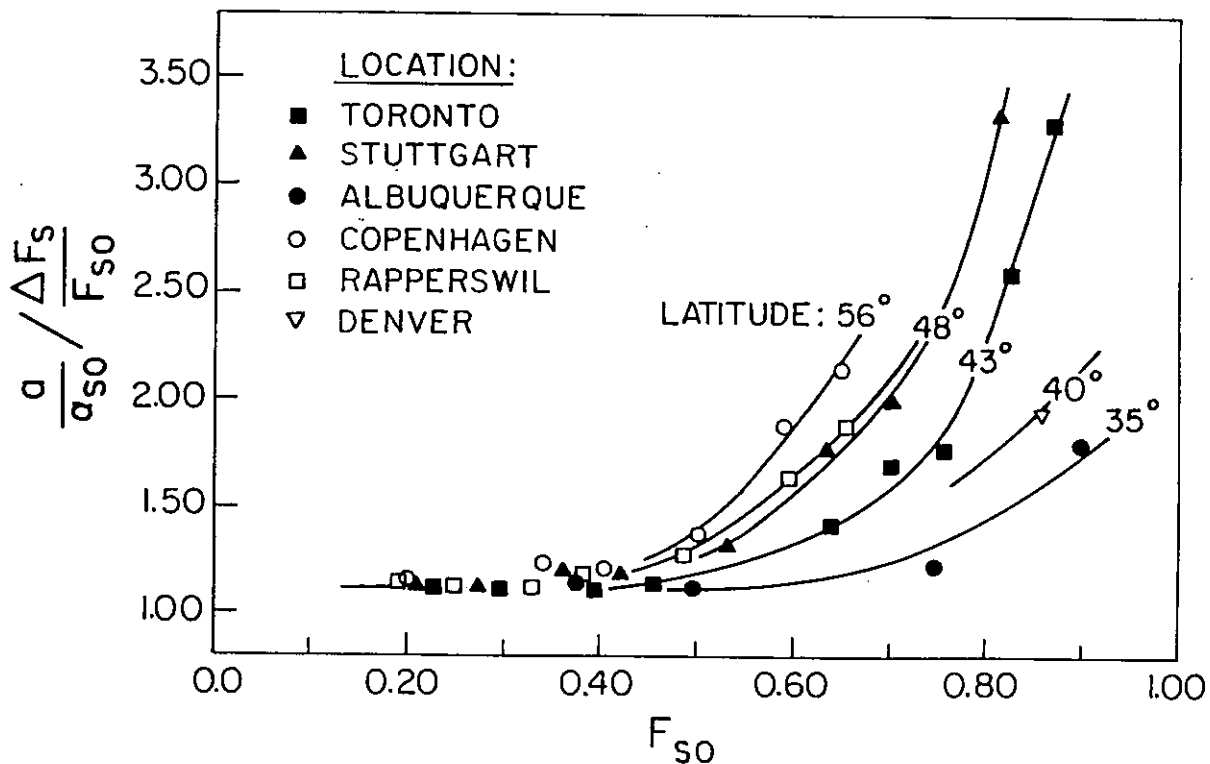
Figure 3,3: Plots of $(a/\alpha_{s,0}) / (\Delta F_s/F_{s,0})$ vs $F_{s,0}$ for all simulations performed in [3,2]

As expected, at low solar fraction, the ratio approaches unity (or a value just above unity 1,1) and it asymptotically approaches infinity as $F_{s,0}$ increases to high values.

The unexpected dependence on location for high values of $F_{s,0}$ as illustrated in **Figure 3;3** is explained by Hollands et al as follows. For extreme nothern locations, the available solar radiation in the month near the winter solstice is very small, and so these locations have an effective upper limit for F_s which is less than unity. Thus, for a given value of $F_{s,0}$, nothern locations would have higher values for the ratio $(a/\alpha_{s,0})$ /($\Delta F_s / F_{s,0}$). This is indeed what is observed in **Figure 3;3**, in which the lattitude of the individual cities has been indicated by a different symbol.

The conclusion is that for large values of the solar fraction, it should be possible to estimate the value of parameter a from the plots shown in **Figure 3;3**, using the latitude of the location in question.

3.1.3 Formulation of performance criterion for absorbers in the case study

In order to formulate the criterion for failure of an absorber coating in the present case study, the relationships between deterioration of the optical properties of coating and loss in solar system performance as described by Hollands et.al. in [3,2] were taken as a point of departure.

As discussed already in **Section 2.2.1**, a performance criterion function PC of the following linear form may seem the most preferable, as justified by the calculations made by Hollands et. al. in [3,2], i.e.

$$PC = -\Delta\alpha_s + k_1 \Delta\varepsilon \leq k_2 \qquad (2,1)$$

Following the recommendations by Hollands et. al in [3,2], the value of k_1 = a/b may be set equal to about 0.27 (or 0.25 in equation (2,1), which value is based on some more preliminary results by Hollands et. al.).

Failure in the case study was arbitrarily chosen as the deterioration of the optical performance of the absorber which corresponded to a 5 % loss in system performance. This means that $\Delta F_s/F_{s,0}$ = 0.05 in terms of loss of the annual solar fraction.

From **Figure 3;3** it can be seen that at a low solar fraction, ≤ 0.5, the ratio $(a/\alpha_{s,0})/(\Delta F_s/F_{s,0})$ is fairly constant (about 1.1) and, consequently:

$$k_2 = a = \alpha_{s,0} \cdot 0,05 \cdot 1,1 \approx 0,05 \qquad (3,2)$$

as $\alpha_{s,0}$ varies between 0.90 - 0.95 for the studied coatings in the case study, see **Section 3.3**.

Accordingly, the definition of failure used in the case study as expressed by eq (2.1) with values of k_1 and k_2 inserted will be

$$PC = -\Delta\alpha_s + 0.25 \cdot \Delta\varepsilon \leq 0.05 \qquad (3,3)$$

This definition of absorber failure seems quite well to correspond to a 5% loss in performance of solar systems having an initial annual solar fraction of 0.5 or less. For higher values of the initial annual solar fraction, the plots in **Figure 3;3** may be used to interpret absorber failure or estimated service lives of coatings in terms of loss in solar system performance.

3.2 Procedure Worked Out in the Case Study for Measurement and Determination of Optical Performance of Absorber Coatings

3.2.1 Round-robin programmes on optical property measurements in the case study

The definition of failure adapted in the case study required first of all, development of an accurate measurement procedure for determination of the solar absorptance and thermal emittance of the absorber coatings. It was therefore imperative for interlaboratory comparisons to be made to determine the relative accuracy of the measurement techniques used by the participating laboratories.

Three round-robin programmes were executed during this study. In the first action undertaken by six laboratories, each participant received four samples of a chemically oxidized blue stainless steel selective absorber coating provided by the Yazaki Corporation, Japan. In the second action, in which eight laboratories took part, a single sample from the Yazaki Corporation was circulated in turn to each participant and optical properties were measured and reported. In the third programme, of eight participating laboratories, a white ceramic tile (Zeiss 21819) sample and a Labsphere Infragold diffusely reflecting gold sample were circulated to each participant for measurements.

For determination of the optical properties, measurements were carried out using the procedures established and agreed by the participants and as summarized in **Section 3.2.2** of the present report.

As the round robin optical properties measurements in the case study have been reported in a separate publication [3,4], only some of the main conclusions and recommendations from this study will be reviewed here. A more detailed presentation of the study and results are given in [3,5].

Determination of solar absorptance from reflectance measurements in the solar range showed variations caused by inhomogenities of samples and in between samples from the same batch, by different measuring facilities and/or calibration techniques. The mean of the integrated solar reflectance obtained for the 24 measured samples in the first round-robin action was 0.129 ± 0.019. In the second round-robin activity, where all participants performed measurements on one and the same sample, the result was 0.122 ± 0.009.

In the visible wavelength region, the agreement between different laboratories was relatively good, but in the near-infrared wavelength region reflectance data differed markedly. An important cause of error here is the reflectance properties of the integrating sphere wall. It was recommended, therefore, that each participant should have a properly coated integrating sphere wall and that recoating should be performed at the outset of the measurements to be executed in connection with ageing testing in the case study.

In the third round-robin activity, measurements were performed on standards com-
monly employed for reference in the UV-VIS-NIR wavelength range. The ceramic
white tile sample was chosen in order to get a measure of the accuracy for the upper
end of the reflectance scale in the UV-VIS wavelength region. The diffusely reflecting
gold sample was selected for the same purpose in the NIR spectral range. The results
are given i **Table 3;4.**

Labora-tory	ρ_SWhite Tile	ρ_SInfra-gold	Calibration reference	Instrumentation
1	0.802	0.857	MgO	Beckman DK-2A
2	0.747	0.805	$BaSO_4$	Zeiss PMQ
3	0.768	0.836	$BaSO_4$	Zeiss PMQ
3	0.751	0.803	Spectralon	- " -
4	0.773	0.846	$BaSO_4$	Beckman 5240
5	0.698	0.806	Ceramic white tile (SRM2020)	Perkin Elmer Lambda 9
6	0.760	0.816	Spectralon	Zeiss PMQ
7	0.740	0.824	$BaSO_4$	Hitachi U 3400
8	0.654	0.848		Gier-Dunkle MS 251
	0.744±0.044	0.827±0.021		

*Table 3;4: Solar reflectance values (ρ_S) for the Zeiss 21819 ceramic white tile
and the diffusely reflecting Labsphere Infragold sample*

For the white tile the results agree only to within about 5 %. For the Labsphere Infra-
gold sample a wide scatter in data was observed in the near infrared region where
reflectance values of the sample are high. As some values were above unity, this
clearly demonstrated the inadequacy of reporting uncorrected $BaSO_4$ referenced data
for high reflectance materials. It was also concluded that all participants should use
the same reflectance standard and a suitable choice would be either Labsphere
Spectralon or NBS SRM 2020.

Determination of thermal emittance showed encouraging agreement, particularly when
taking into account the special difficulties associated with infrared measurements and
the different techniques empolyed by the participants, see *Table 3;5.*

Laboratory	ε_n	ε_h	Measurement technique
1	0.104	-	Gier-Dunkle DB-100
2	0.136	-	In-house radiometric (373K)
3	0.121	0.146	In-house radiometric (373K) for ε_n McDonald emissiometer (373K) for ε_h
3	0.123	0.149	Integrated spectral values (373K) for ε_n Integrated angular values (373K) for ε_h
5		0.13	Devices & Services AE (355K)
6	0.126	0.131	Integrated spectral values (373K) for ε_n Devices &Services AE (355K) for ε_h
7	0.129	0.127	Integrated spectral values (373K) for ε_n Modified Devices and Services AE (373K) for ε_h
8	0.09	-	Gier-Dunkle DB 100

Table 3;5:Total near-normal (ε_n) and total hemispherical (ε_h) thermal emittance values determined for the Yasaki blue stainless steel sample circulated in the second round-robin activity.

The average of the total near-normal thermal emittance measurements was 0.122 ±0,010 and the average of the total hemispherical thermal emittance values was 0.137 ±0.04. The results obtained from spectral reflectance techniques using diffuse gold integrating spheres agree well with the spectral radiometric results. Only at the low wavelength limits of the radiometric measurements were there any higher deviations.

3.2.2 Summary of recommended procedures for the measurement and evaluation of solar absorptance α_S and thermal emittance ε

Recommended procedure adopted by the IEA Task X participants for measurement and evaluation of solar absorptance and thermal emittance can be summarized as below.

A. Solar Range

Required properties: spectral directional absorptance $\alpha(\lambda)$ and directional solar absorptance α_S, for near-normal incidence.

Measured property: spectral (near-normal) directional/hemispherical reflectance $\rho(\lambda)$ of opaque samples within solar spectral range.

Spectral range: 0.32 µm - 2.5 µm

Angle of incidence: near-normal, i.e. 8° ... 10° to the surface normal.

Sample temperature: room temperature

Photometric integration: integrating sphere with $BaSO_4$-based sphere wall coating; specular component of reflected radiation has to be included.

Sphere design:

Sample position:	sample is part of sphere wall;
Detector position:	detector has to be shielded against radiation received directly from the sample;
Geometry:	if possible, use the comparison method (i.e. sample and reference are simultaneously part of the sphere wall); when using the substitution method (i.e. sample and reference are alternately covering the measuring port) the sphere error must be corrected by measuring the respectively corresponding brightnesses of the sphere wall.
Calibration:	use as a reference freshly pressed $BaSO_4$ - powder or a diffusely reflecting white title (e.g. "Spectralon", sold incl. calibration certificate by Labsphere Inc., North Sutton, NH 03260, USA).
Measured wavelengths:	depending on convolution method for calculation of solar absorptance, either about 40 wavelengths in the range 0.32 µm - 2.50 µm for weighted ordinates or the 20 selected ordinates for AM1.5 given below:

Selected ordinates (nm)			
389.8	592.6	795.4	1144.4
446.0	629.5	844.8	1253.5
483.3	666.7	896.7	1524.3
519.1	707.0	979.0	1700.1
555.4	750.5	1041.4	2322.0

Table 3;6: 20 selected ordinates for air mass 1.5 (Source ASTM E891).

Evaluation of spectral data:

$$\rho(\lambda) = (R_s(\lambda) / R_r(\lambda)) \cdot \rho_r(\lambda) \tag{3,4}$$

where R_s is the sample reading; R_r is the reference reading and ρ_r is the near-normal/hemispherical reflectance of the reference.

No correction of possible distortion of the measured result when a specular component of the reflected radiation exists.

$$\alpha(\lambda) = 1 - \rho(\lambda) \tag{3,5}$$

Evaluation of solar absorptance:

Convolution with solar spectrum AM1.5 for direct normal irradiance according to ASTM E891.

a) selected ordinates method:

$$\alpha_s = \frac{1}{20} \sum_{i=1}^{20} \alpha(\lambda_i) \tag{3,6}$$

the set of λ_i are the selected ordinate wavelengths of *Table 3;6*.

b) weighted ordinates method:

$$\alpha_s = \left(\sum_{i=1}^{n} \alpha(\lambda_i) S_{\lambda i} \Delta\lambda_i \right) / \left(\sum_{i=1}^{n} S_{\lambda i} \Delta\lambda_i \right) \tag{3,7}$$

the set of λ_i are the chosen measuring wavelengths; $\Delta\lambda_i$ the respective wavelength interval; $S_{\lambda i}$ the spectral solar irradiance according to ASTM E891 Table1, correctly summed over the respective wavelength interval.

Attention should be paid to:

- Possible anisotropies of the samples, i.e. the samples should be marked to allow mounting of the samples at the measuring port using the same orientation and ensuring that the same areas of samples are measured.

- The different weighting of different directions of polarisation by the monochromator may distort the measurement (but this is not a great effect for near-normal inciddence).

B.   Thermal range

Required properties: total directional emittance ε_n (373 K) for near-normal incidence and spectral near-normal directional emittance ε (λ) and total hemispherical emittance ε_h (373 K).

Measured properties: total hemispherical/directional reflectance ρ (373 K) for thermal radiation incident from a black-body radiator of 373 K or total directional emittance ε(373 K) of heated samples (both yielding ε_n(373 K)), and spectral directional/hemispherical reflectance $\rho(\lambda)$ of total hemispherical emittance ε_h (373 K) of heated samples (whenever the reflection method is used, transmittance has to be zero within spectral range measured).

Spectral range: 2.0 μm - 50.0 μm

Angle of incidence or emission: near-normal, i.e. 8° / 10 ° to the surface normal.

Sample temperature: 373 K in radiometric measurements on heated samples; room temperature when using spectrophotometric reflectance method.

Photometric integration: (for spectral measurements) integrating sphere with diffusely reflecting gold coating as sphere wall; specular component has to be included; (for "sphere design" see **A. Solar Range**).

Calibration: use as reference:

a) when using Devices and Services Emissiometer Model AE: references supplied by the manufacturer with the instrument.

b) for broad-band instruments, high emittance: Nextel Velvet Coating 2010 black
    ε_n (373 K) = 0.95; ε_h = 0.90
    (Source: J. Lohrengel, PTB Braunschweig, F.R.G.)

c) for spectral measurements, high reflectance: Labsphere diffusely reflecting gold coating "Infragold".

Evaluation:

a) broad-band measurements: use procedure given by manufacturer of measuring instrument.

b) spectral measurements:

$$\rho \, (\lambda) \quad = (R_s \, (\lambda) \, / \, R_r \, (\lambda) \,) \cdot \rho_r \, (\lambda) \tag{3,8}$$

where R_s is the sample reading; R_r is the reference reading and ρ_r is the near-normal/hemispherical reflectance of the reference.

No correction of possible distortion of the measured result in the case of specular component of the reflected radiation exists.

$$\epsilon \, (\lambda) \; = \; 1 \; - \; \rho \, (\lambda) \tag{3,9}$$

Total emittance from spectral measurements is convoluted with the aid of the Planck function P_λ for a black-body radiator temperature of 373 K.

$$\epsilon \, (373 \text{ K}) \; = (\int_0^\infty \epsilon(\lambda) \, P_\lambda \, d \, \lambda) \, / \, (\int_0^\infty P_\lambda \, d\lambda) \tag{3,10}$$

Attention: as in the solar range.

3.2.3 Optical property measurements in ageing testing of case study

Commercially available selective absorber coatings usually exhibit variations in optical properties which may typically be of the order of 2 % in solar absorptance. Sometimes, even higher deviations in absorptance of different samples taken from the same batch can be obtained. Some coatings also have a surface structure such that anisotropic effects may influence the measurements. If, for example, the reflectance is measured with one such sample mounted in two orientations perpendicular to each other, the reflectance values obtained may in some cases differ by as much as 0.3%.

When studying degradation in optical properties of absorber coatings in the case study, it should be possible accurately to measure changes in the absorptance and emittance of less than 0.1 %.

To ensure this, the following practice are recommended for measurements and evaluation of degradation data.

- When establishing degradation-over-time relationships in an ageing test, measurements of extent of degradation at different testing times should be performed on one and the same sample.

- The sample should be marked to allow mounting of the sample at the measuring port in exactly the same position as previously used, to ensure that the same area of sample is measured and that the orientation of the sample is also the same.

- When analysing degradation data, differences in solar absorptance or thermal emittance should be used as an indicator for degradation, i.e.

$$\Delta \alpha_S, (t) = \alpha_S (t) - (\alpha_S (0) \qquad (3,11)$$

where $\alpha_S(t)$ denotes absorptance measured at testing time t, and $\alpha_S(0)$ denotes initial value of absorptance

and

$$\Delta \varepsilon_n(t) = \varepsilon_n(t) - \varepsilon_n(0)$$

where $\varepsilon_n(t)$ denotes thermal emittance measured at testing time t, and $\varepsilon_n(0)$ denotes initial value of thermal emittance.

Alternatively, normalized values can be used, i.e

$$\alpha_{S,N} (t) = \alpha_S (t) \cdot / \alpha_S (0) \qquad (3,12)$$

where $\alpha_{S,N}(t)$ denotes normalized absorptance value at testing time t.

3.3 Absorber Coating Materials for the Case Study

3.3.1 Factors taken into account when selecting materials for the case study

In the choice of selective absorber materials for the case study, various factors were taken into consideration: technical and scientific requirements on materials, commercial interests in participating countries of IEA Task X, and requirements on materials dictated by practical considerations such as availability of materials and the need for feed-back data from practice.

- The results of the case study should be as generic as possible.

- Materials of good commercial interest should be used to generate data for solar collector manufactures.

- At least some qualitative information on durability properties of the selected materials should be available from previous research and testing.

- The materials selected should be well definied and exhibit small variations in quality.

- Samples of materials should be readily available for measurement and testings. For validation purposes, single-glazed collectors with the absorber materials selected should also be available for long-term durability tests under in-use conditions.

- For analysis of mechanisms of natural degradation under service conditions, absorber material samples from at least three years of in-service exposure should be available.

These requirements narrowed down the number of potential materials for study considerably. The final choice of materials was made as follows:

- black chrome on nickel on copper (MTI Solar Inc., USA)

- black chrome on stainless steel (Energie Solaire, Switzerland)

- nickel-pigmented anodized aluminium (Sunstrip, Sweden)

- nickel-pigmented anodized aluminium (Showa, Japan)

Coatings selected are of considerable commercial interest. Consequently, a good durability of a material selected should be expected, with the result that difficulties in the testing and analysis of its degradation over time can be expected.

3.3.2   General characteristics of the selected coatings for the case study

Black chrome coatings

Generally speaking, black chrome coatings consist of a mixture of small metallic chromium particles and chromium oxide. The metallic chromium particles are small, of the order of 10 nm in diameter, and are probably entirely embedded in the oxide phase, Lampert and Washburn [3, 6]. The solid oxide phase appears as distinguishable particles with sizes of about 100 nm in the black chrome coating, the latter having a high void fraction, Sweet et. al [3, 7].

Black chrome coatings can be electrodeposited on various substrates. For the Energie Solaire absorber material the substrate is a stainless steel, and for the MTI absorber material the substrate is electrodeposited nickel on copper, see *Figure 3;4 and 3;5, Table 3;7.*
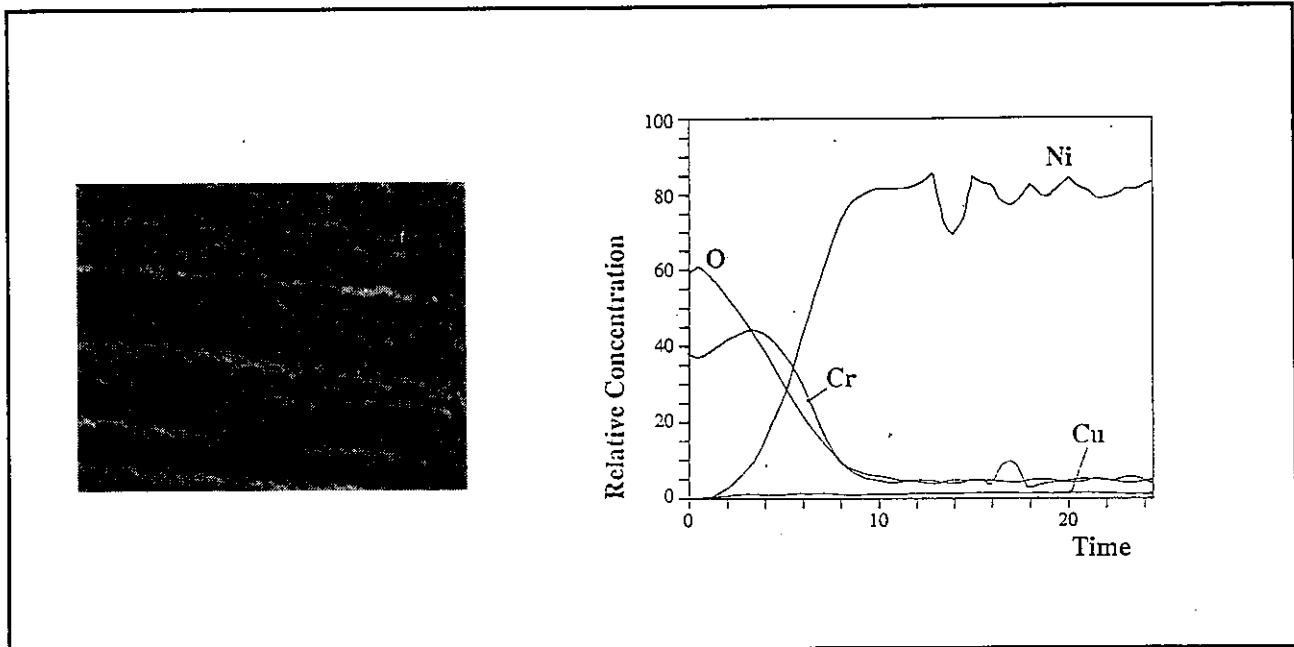
Figure 3;4 Scanning Electron Microscopy (SEM) micrograph (x 1500) and AES depth profiles of Cr, Cu, Ni and O for the MTI black chrome coating selected in the case study. For experimental details, see Tanemura [3,8].
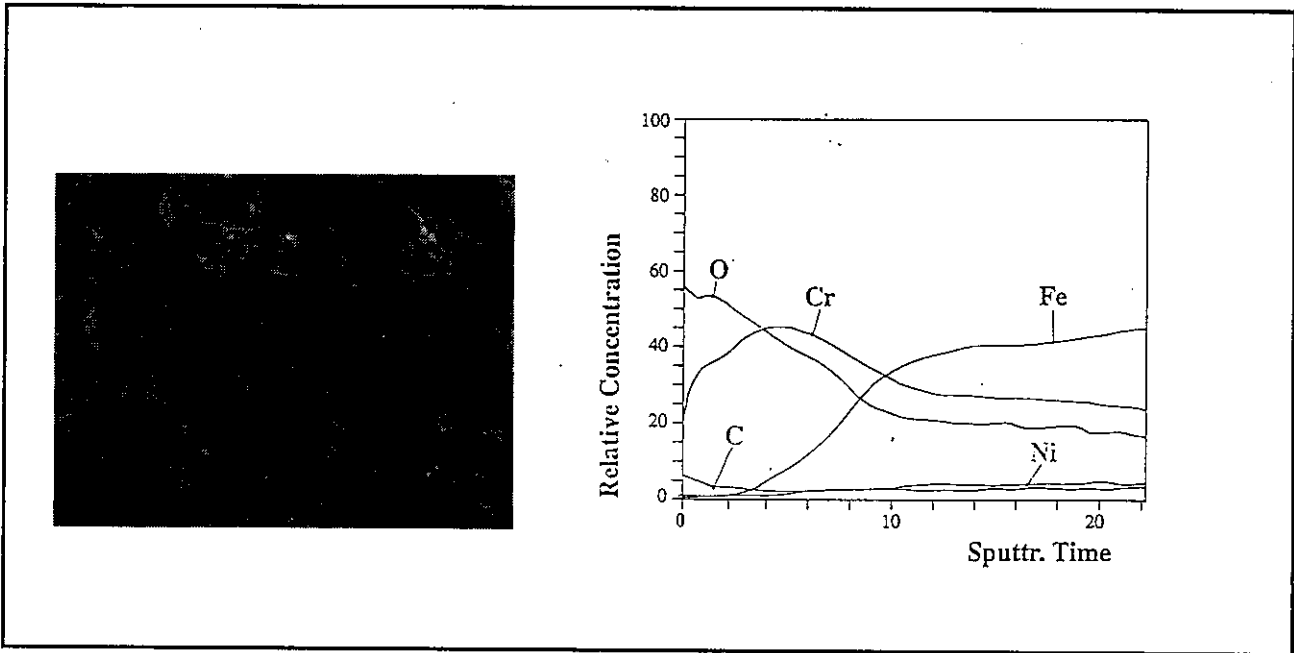
Figure3;5   *Scanning Electron Microscopy (SEM) micrograph (x 1500) and AES depth profilesof Cr, Fe, Ni and O for the Energie Solaire black chrome coating selected in the case study. Experimental details,are given in [3.8].*

Solar absorptance and thermal values for the two black chrome coating materials are given in **Figures 3;6 and 3;7**, together with reflectance spectra for the VIS-NIR and NIR-IR wavelength regions. The high solar absorptance of this kind of coating is due to the metallic chromium particles and a pronounced surface roughness effect is also important, according to Smith et al [3,9].

The optical properties of black chrome coatings are not so well understood but there are some theoretical models for calculation of optical properties, see eg. Niklasson [3.9] for av brief review.
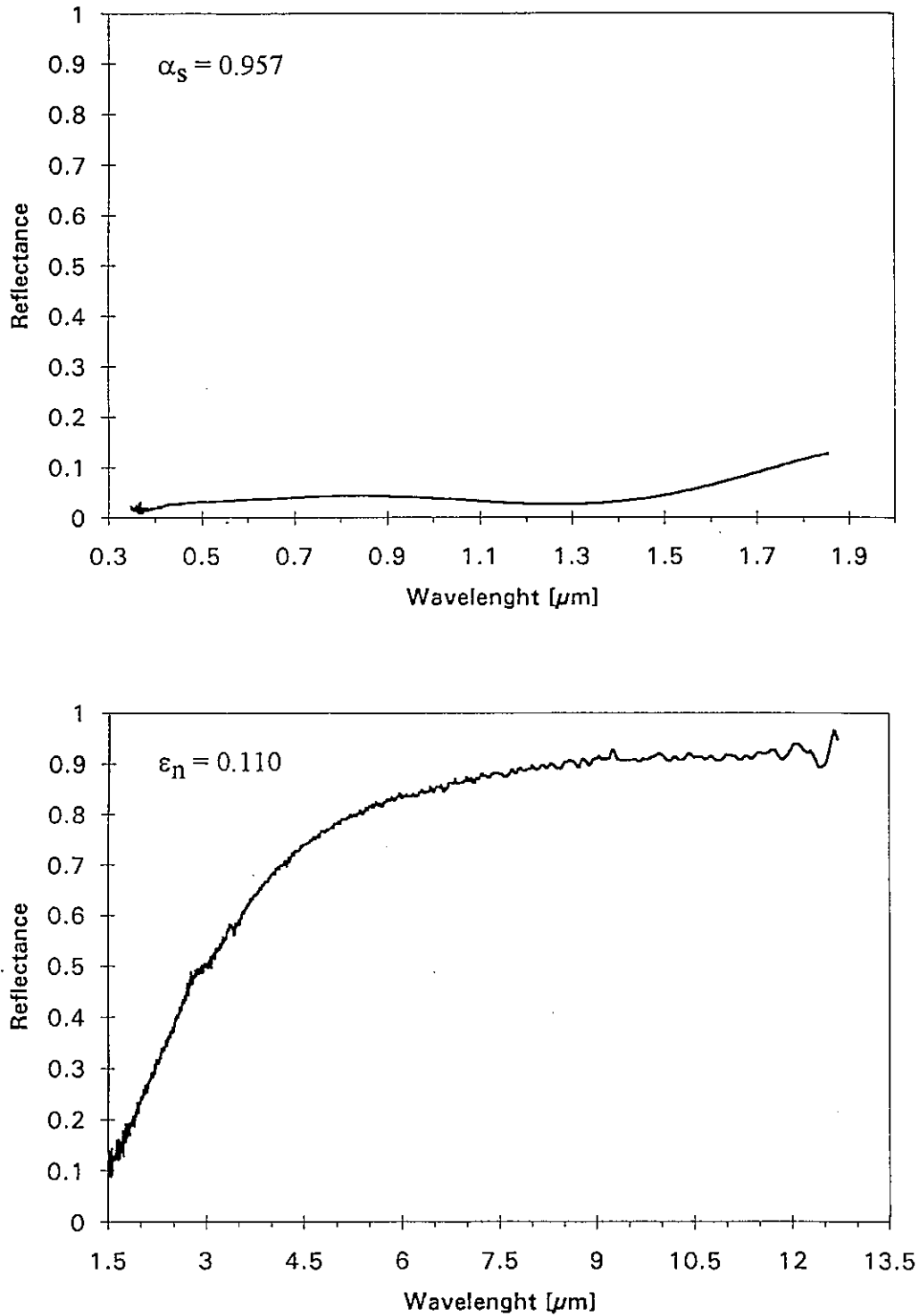
Figure 3;6: VIS-NIR near-normal reflectance spectrum and NIR-IR near-normal reflectance spectrum of the MTI black chrome coating selected for the case study.

The substrate material for a black chrome coating should be corrosion-resistant. An electrodeposited layer of metallic nickel is used for the MTI black chrome absorber material and a stainless steel for the Energie Solaire black chrome absorber. The stainless steel substrate of the Energie Solaire absorber is basically a chrome nickel steel of 18-20 % Cr, 8-10 % Ni, 0.08 % C, 0.1 % Si, 2.0 % Mn, 0.05 % P and 0.03 %.S.
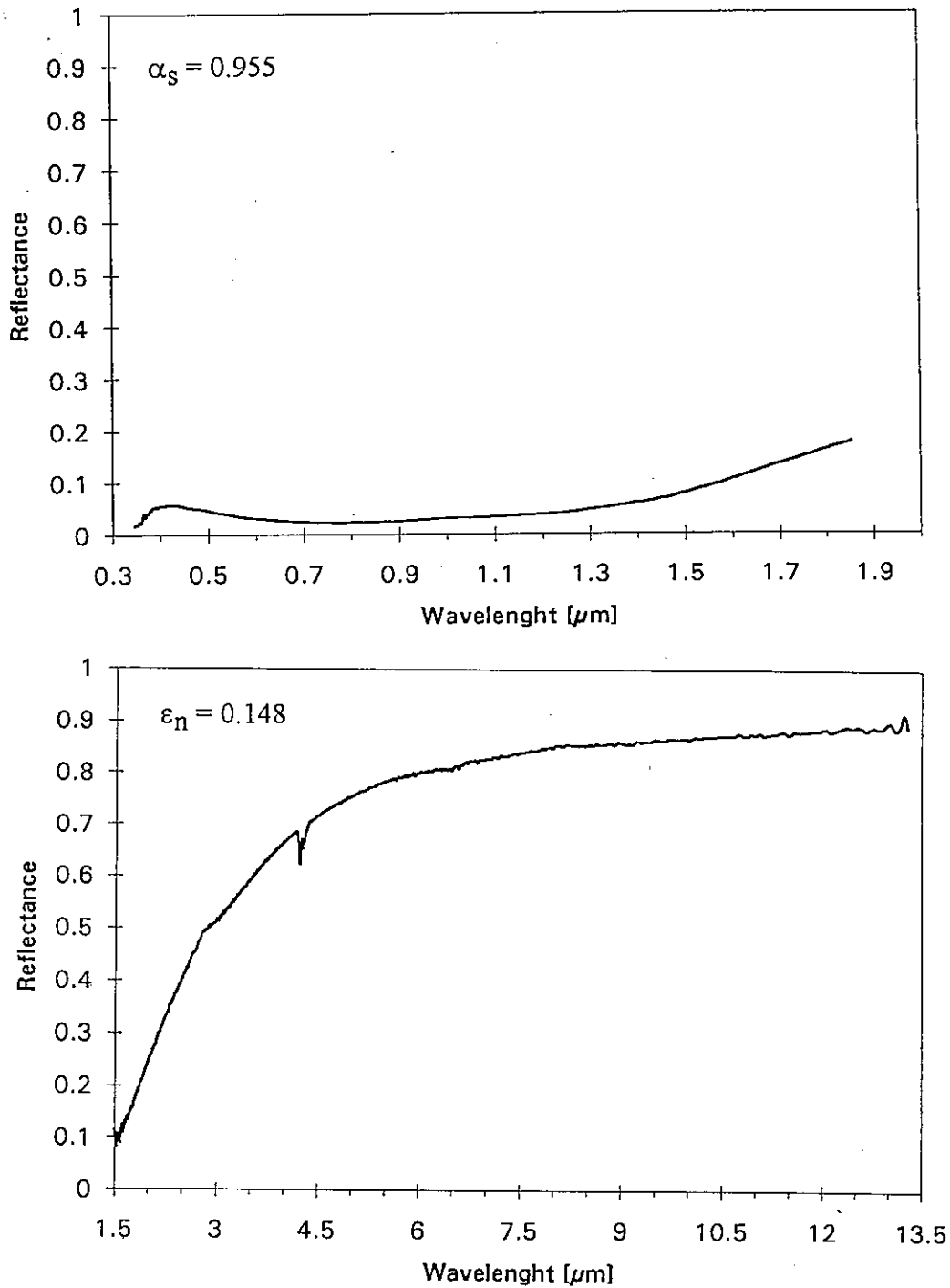
Figure 3;7: VIS-NIR near-normal reflectance spectrum and NIR-IR near-normal reflectance spectrum of the Energie Solaire black chrome coating selected for the case study.

Nickel-pigmented anodized aluminium

The two nickel-pigmented anodized aluminium coatings studied are very similar, see *Figures 3;8* and *3;9*. They are produced by first dc-anodizing aluminium sheets in a phosphoric acid solution to generate a porous layer of aluminium oxide on the substrate surface. This layer is then used as a matrix for small metallic nickel particles which are made to precipitate in the pores of the aluminium oxide layer in a subsequent process of electrochemical reduction of nickel from a solution containing $NiSO_4$, see eg [3,11] and [3,12].
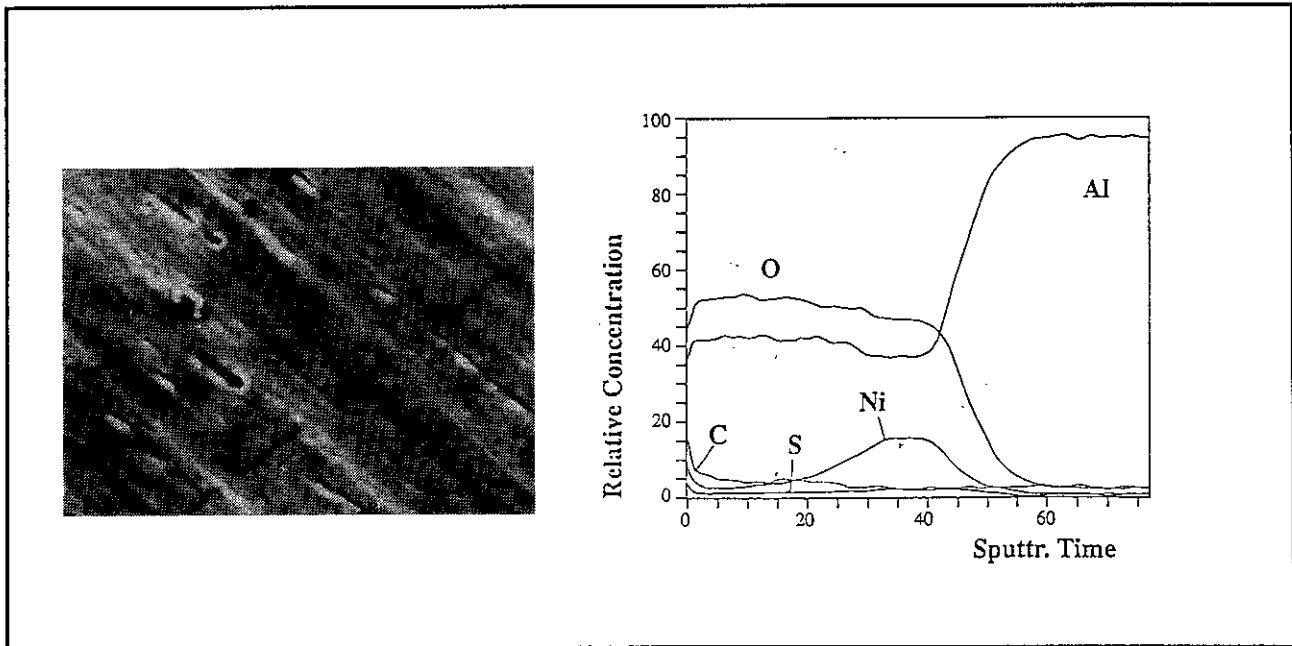
Figure 3;8: Scanning Electron Microscopy (SEM) micrograph (x 1500) and AES depth profiles of Al, Ni, O, P and S for the Sunstrip nickel-pigmented anodized aluminium coating selected for the case study. For experimental details, see [3,8].
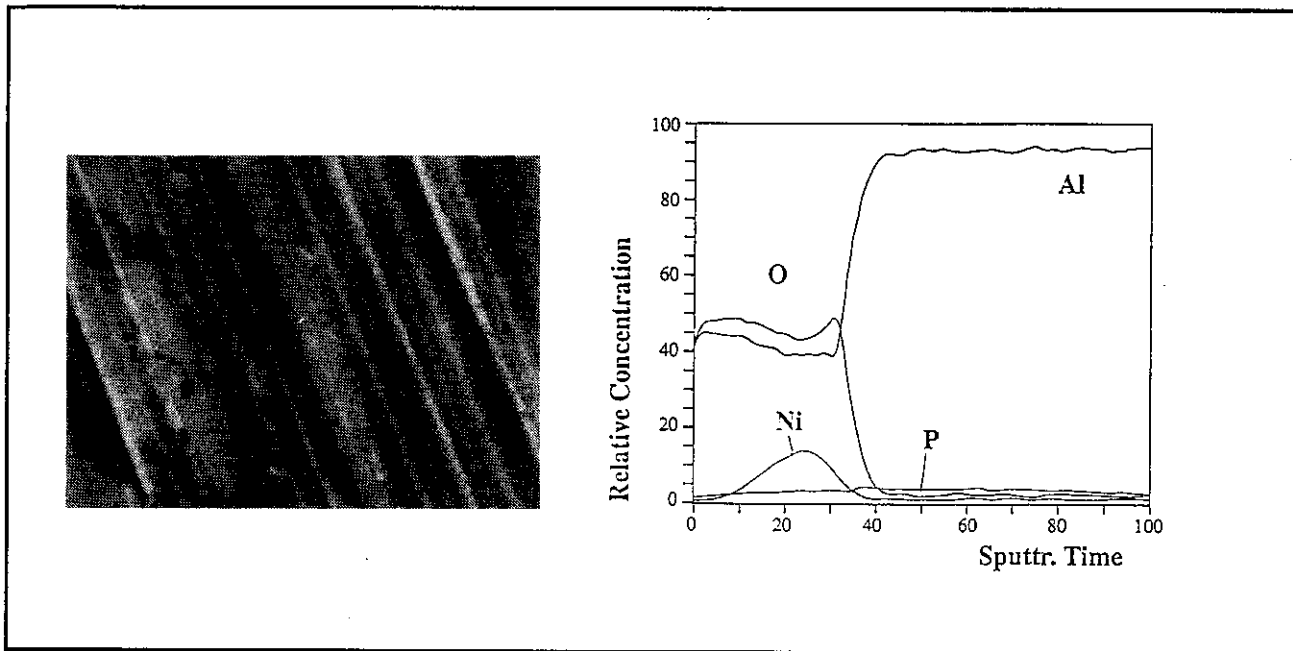
Figure 3;9: Scanning Electron Microscopy (SEM) micrograph (x 1500) and AES depth profile of Al, Ni, O, P, and S for the Showa nickel-pigmented anodized aluminium coating selected for the case study. For experimental details, see [3,8].

Solar absorptance, thermal emittance values and corresponding reflectance spectra for the two nickel-pigmented anodized aluminium materials are given in **Figures 3;10** and **3;11**.

Commercially produced nickel-pigmented anodized aluminium absorbers may exhibit large variations in optical properties. The value of solar absorptance may vary from 0.89-0.95 between different batches. The Sunstrip samples investigated in the case study represent accordingly a low-performance batch of coating. A special programme has recently been undertaken to improve optical performance of coating by optimization of preparation conditions. In the laboratory, coatings have been prepared with α_s = 0.96 and ε_h = 0.15 [3, 13].

The high absorptance of these coatings is due to the metallic nickel particles which are located at the bottom of the pores of the aluminium oxide, see **Figures 3;8** and **3;9**. The particles are believed to be nearly spherical in shape and have sizes of the order of 10-30 nm [3,11].
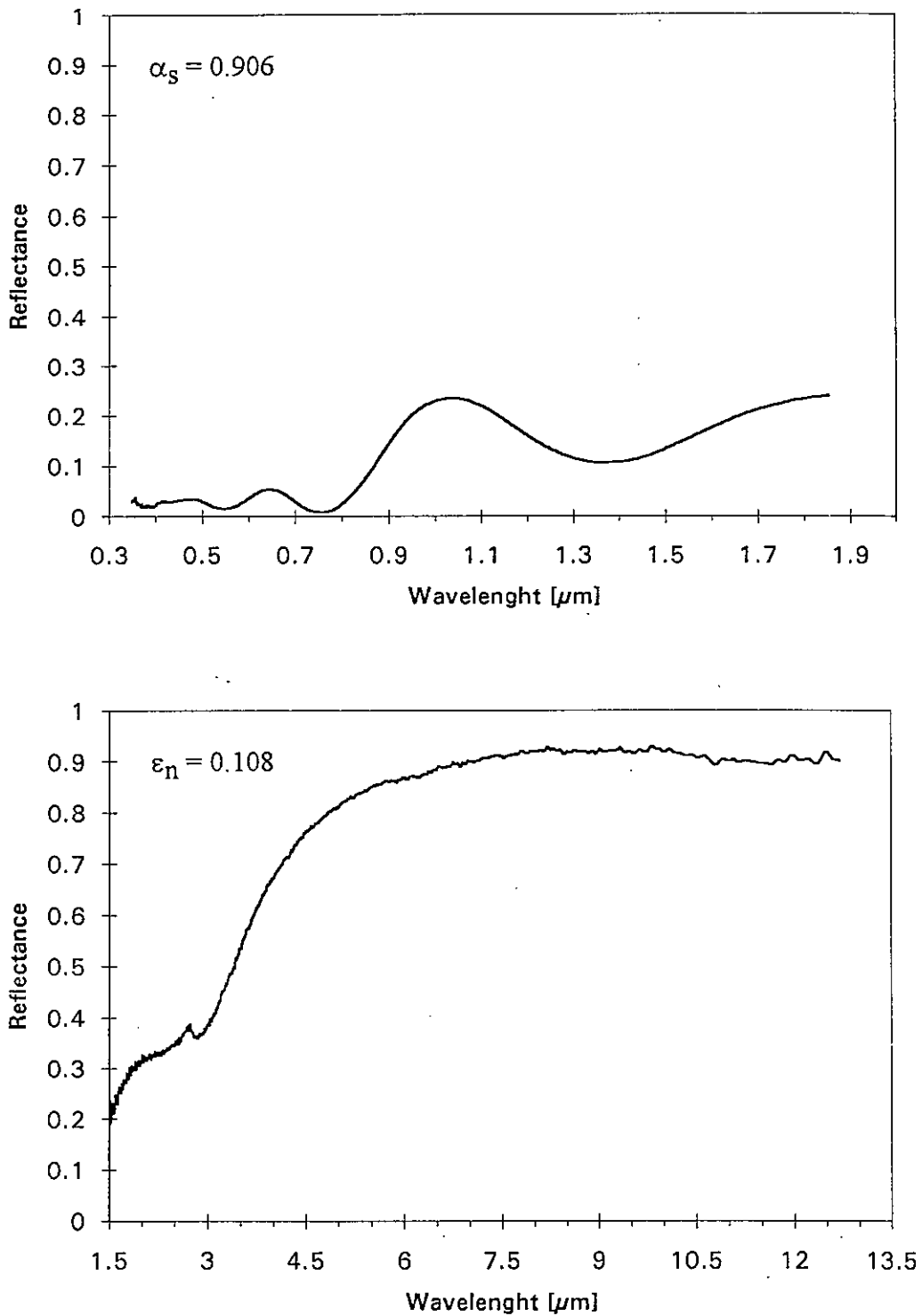
Figure 3;10: VIS-NIR near-normal reflectance spectrum and NIR-IR near-normal reflectance spectrum for the Sunstrip nickel-pigmented anodized aluminium coating selected for the case study.
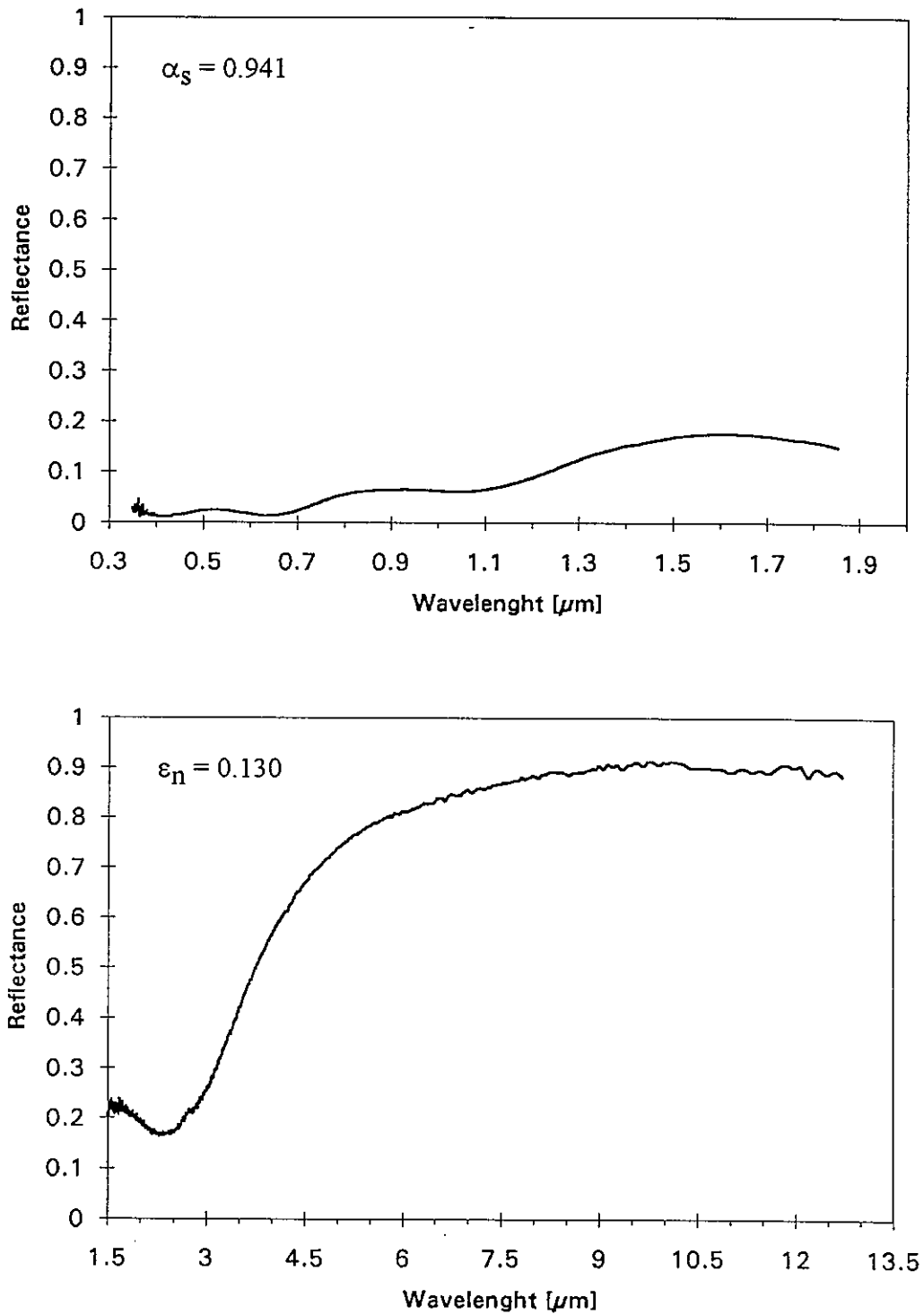
Figure 3;11: VIS-NIR near-normal reflectance spectrum and NIR-IR near-normal
reflectance spectrum for the Showa nickel-pigmented anodized
aluminium absorber coating selected for the case study

The nickel-pigmented anodized aluminium coatings can be described by a structural model as has been proposed by Andersson et, al, [3,11], see *Figure 3;12*.

Porous Al₂O₃

Ni particles

Homogeneous Al₂O₃

Metallic Al
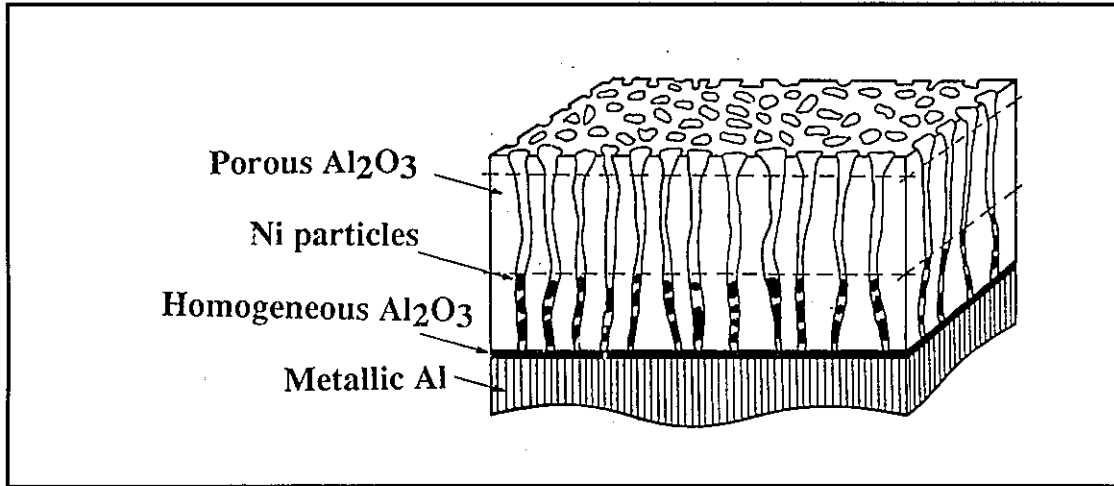
Figure 3;12: Structural model for a nickel-pigmented anodized aluminiuim absorber coating as proposed by Andersson et. al. [3,11].

Based on this structural model, the Bruggeman theory was used by Andersson et. al [3,11] to set up an effective medium theory model for calculation of the optical properties of coating. This theoretical model, somewhat refined, was used by Nicklasson in the present case study to calculate the optical properties of the two nickel-pigmented anodized aluminium coatings selected, [3,14].

As shown in *Figure 3;13*, the reflectance spectrum of the two coatings can be reproduced quite well by assuming the coating system to consist of three layers. Next to the aluminium substrate there is in the Showa coating; a layer of porous aluminium oxide of thickness 0.25 μm filled with metallic nickel particles to a volume fraction of 0.25. Above that there is a layer of unfilled porous aluminium oxide of thickness 0.22 μm, and then a layer of 0.15 μm for which is assumed a composition grading of aluminium oxide with air. Corresponding parameters for the Sunstrip coating are slightly different, c.f. also *Figures 3;8 and 3;9*.
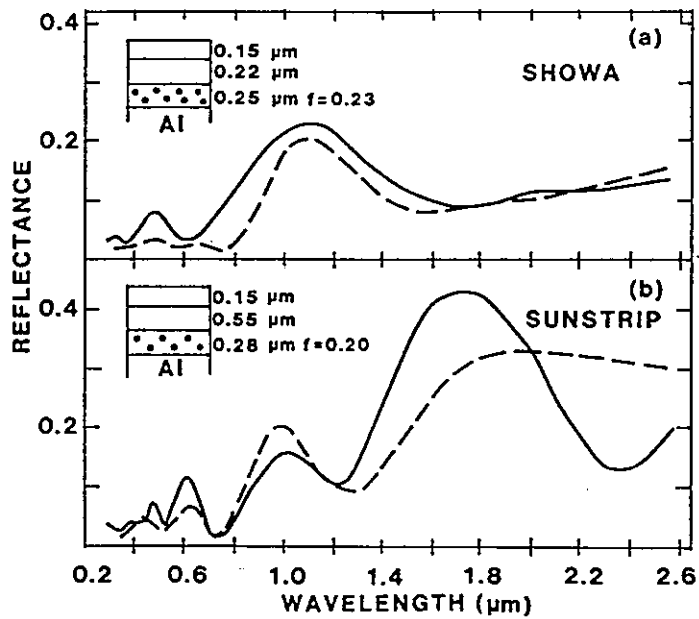
Figure 3;13 *Reflectance spectrum for the two nickel-pigmented anodized aluminium absorber coatings selected for the case study. Dashed curves show experimental data and continous curves show result of calculations using the structural models and parameter values shown in the figure.*

Niklasson also found that the normalized change in solar absorptance, i.e. 1- $(\alpha_s/\alpha_{s,0})$, can be related to the normalized change in metallic nickel content, 1-Q as expressed by equation (3,13)

$$1- (\alpha_s / \alpha_{s,0}) \approx (1 - Q)^\beta \qquad\qquad (3,13)$$

The value of parameter β was found to be equal to 2.5, see also *Figure 3;14*.
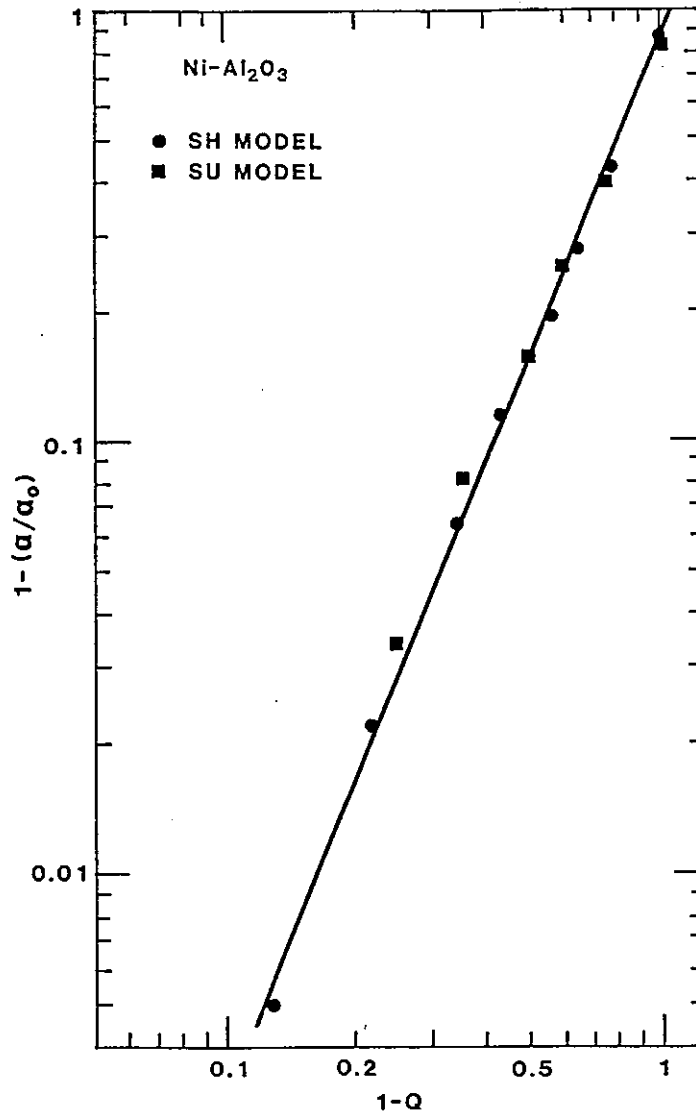
Figure 3;14 Normalized change in solar absorptance, 1- $(\alpha_S/\alpha_{S,0})$, as a function of normalized change in metal content, 1-Q, for nickel-pigmented aluminium oxide coatings. Points denote calculations with optical models pertinent to the Showa (SH) and Sunstrip (SU) coatings. The line was drawn as a guide for the eye [3,14].

CHAPTER 4

CHARACTERIZATION OF MICROCLIMATE FOR ABSORBERS IN SINGLE GLAZED SOLAR COLLECTORS FOR DHW-SYSTEMS

4.1 Important Environmental Factors of Absorber Coating Degradation

Environmental factors which may contribute to degradation of absorber coatings are numerous. To be able to identify the most important ones, it is essential to have some ideas and basic understanding of what the dominant mechanisms of degradation may be. This requires information on material compositions, material structures e.t.c., see Chapter 3.3.

For the absorber coating materials of case study of prime interest was environmental factors which may cause loss in optical performance. These were identified as high temperature, high humidity and moisture, airborne pollutants and solar radiation.

A high temperature accelerates all kinds of processes. For the selective absorber coatings of case study this means that a high temperature increases the oxidation rate of metal which may cause a decrease in the absorptance of coating.

High humidity may generate hydrolysis reactions. High humidity must prevail for electrochemical corrosion to take place causing oxidation of metal and decrease in absorptance of coating. Many airborne pollutants accelerates electrochemical corrosion also when present at very low concentrations. Solar radiation may initiate photochemical redox reactions leading to loss in optical performance.

When installed in a single flat plate collector for domestic hot water production an absorber coating is exposed to temperatures which may vary from minus 20 °C up to more than 200 °C. High temperature stability of the absorber coating is required.

As the casing of a flat plate collector is usually ventilated, this means that the absorber coating is in contact with the ambient air. Humid air from the ambient can flow in and out through the ventilation holes of the collector. Sometimes the temperature of the collector inside is so low related to the humidity level so that condensation of water may take place.

In the past some collector manufactures tried to develope air tight collectors equipped with desiccants and thus adopting the same technique as for the sealing of multiple glazings. After a short time period only, problems with the condensation of water appeared. New designs based on evacuating the collector casing look more promising. However, working pressures of less than 1 mbar are needed which means that an efficient vacuum pump and additional tubes have to be installed making the system much more expensive.

From field inspections of about 150 solar heating installations in Switzerland it could be concluded that the problem of water condensation on inside parts of collector has not yet been solved. In almost all of the systems inspected there were collectors which had condensed water on the inside surface of the collector cover plate. Rain penetration or improper design of collector as regards ventilation of air may be the causes to the condensed water observed. It can be concluded that an absorber coating for today's solar collectors has to resist exposure in a very humid atmosphere without loss in optical performance.

As a solar collector exchanges air with the ambient, this means also that airborne pollutants will be transported from the ambient into the collector and the absorber plate. As a consequence, air pollutants may be important degradation factors for absorber coatings and their influence on coating durability needs to be considered.

Sulphur dioxide present in air as a trace substance, accelerates greatly, as well known, electrochemical corrosion of most metallic materials at high humidities. It may, therefore influence the optical performance of an absorber by promoting corrosion attacks on the metallic substrate. It may also cause loss in the optical performance of selective absorber coatings pigmented with small metallic particles, due to oxidation/corrosion of the metal particles.

That the degradation factors chosen influence the durability of the absorber coating materials selected for case study have previously been demonstrated by many using accelerated laboratory testing, see eg. [4,1].

However, for the case study microclimatic data in the form of effective levels of the environmental factors chosen were needed. The generation of such data was accomplished by making use of

- computer simulation calculations based on theoretical models to describe climatic conditions in collectors,

- in-situ measurements on collectors at long-term testing under operating and stagnant conditions.

The measurements on the collectors were mainly intended to serve as a basis for the development and validation of the theoretical models used to calculate microclimatic data.

4.2 In-situ Measurements of Micro Climatic Data on Collectors Tested under Stagnation and Simulated Operation Conditions

To be able to measure microclimatic data in-situ two different collector test facilities were set up at the Solar Energy Laboratory ITR in Rapperswil Switzerland.

One set of collectors was operating under the same conditions as if the collectors had been installed in a real DHW systems. The other set of collectors was operating under stagnation conditions which meant that no thermal energy was extracted from the collector system during testing. Thus, the collectors were exposed to the maximum thermal load. Both set of collectors were installed on a test platform on the roof of a laboratory building. The collectors were facing south with a tilt angle of 30°. This geometrical arrangement results in an average yearly solar insolation of about 1200 kWh/m² of collector area.
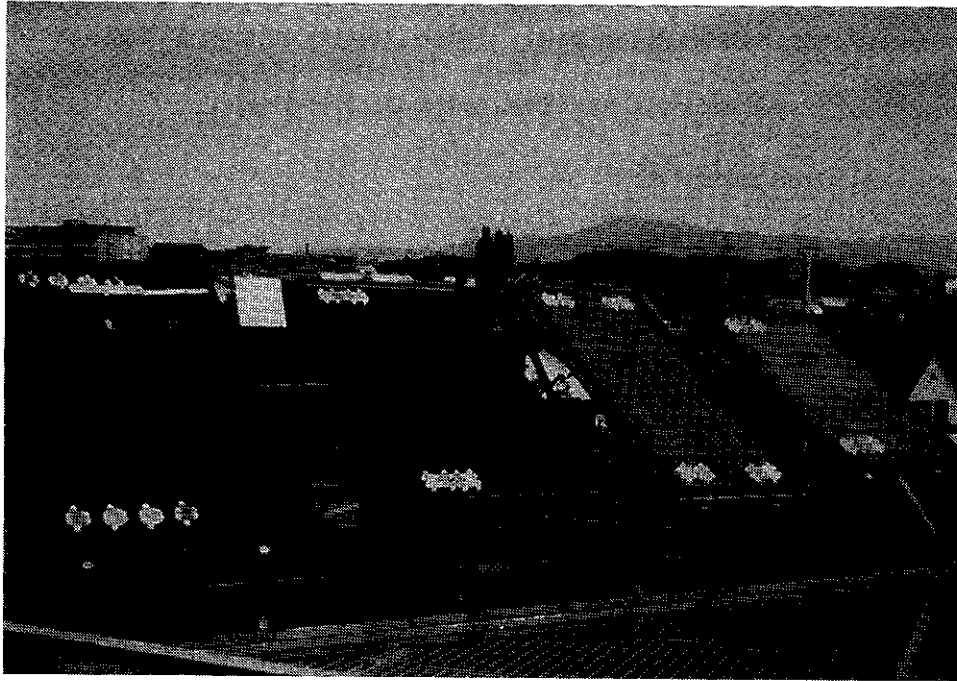
Figure 4;1: *The collector test facilities at the School of Engineering ITR, Switzerland*

Characteristic macro climatic data for the Rapperswil test site are given in *Table 4:1*.

M	1	2	3	4	5	6	7	8	9	10	11	12	Sum
G	33	55	93	130	151	160	173	146	116	74	36	25	1192
D	18	28	47	63	77	80	79	70	53	37	20	15	587
T	0.0	1.9	8.5	8.5	13.2	15.9	18.4	17.5	14.4	9.3	4.1	0.0	-

M:	: Number of the month (1 = January, 12 = December)
Sum	: Yearly sum of the global/diffuse radiation in the collectors plane [kWh/m^2]
G	: Monthly sum of the global radiation in the collectors plane [kWh/m^2]
D	: Monthly sum of the diffuse radiation in the collectors plane [kWh/m^2]
T	: Average ambient temperature [°C]
G, D, T	: Average values of 8 years measurement

Table 4:1   Monthly climatic data for Rapperswil.

The collectors were tested for a time period of three years. The first half year at the roof of the ITR-building. The second half of the first year and the second year, the test, however, was carried out at a field station located outside of Rapperswil because of rebuilding of the roof of the ITR-building. The third year of test was performed with the collectors once again placed on the roof of the ITR-building.

4.2.1   Test arrangements
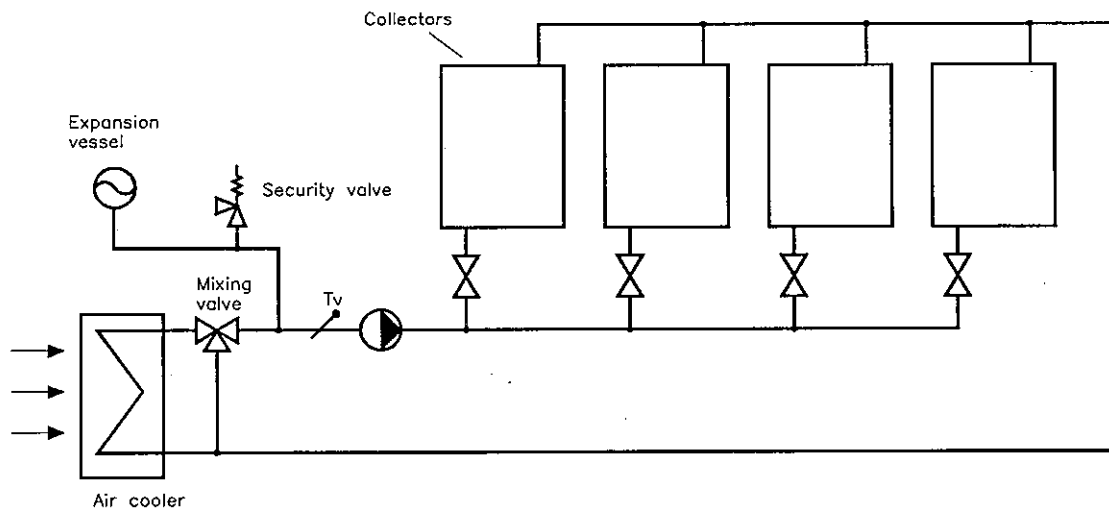
Figure 4;2:   Test loop to simulate the in-use conditions of a collector in a DHW system

The test loop shown in *Figure 4;2* was used to simulate the conditions prevailing in a DHW system during operation. It is a typical closed loop system as usually installed in Europe. The heat transfer fluid in the loop is an ethylenglycol/water mixture (33 Vol.-% ethylenglycol, 67 Vol.-% deionised water) with corrosion inhibitors added. Ethylenglycol is used to prevent freezing. Instead of a storage tank, an air heat exchanger with a fan is used in order to keep the service temperature of the loop at a maximum temperature of about 50 °C. The fan starts working if the global solar irradiation exceeds 200 W/m^2, measured in the collectors plane. Below that insolation level the fan is switched off. Similar to a real installation, a non return valve prevents the system to run in the reverse mode during night hours. The lowest temperature of the collector is reached during the night due to radiative cooling from the night sky. Without a non return valve a reverse flow would result and course warmer heat transfer fluid to enter the collector.

In *Figure 4;3* the installation scheme for stagnation testing is shown. As the maximum stagnation temperature in the collectors may exceed 200 °C, pure ethyleneglycol is used as heat transfer fluid to avoid boiling.

A : Test collector
B : Air ventilation valve
C : Expansion vessel
D : Pressure gauge
E : Pressure—release valve
F : Drain valve
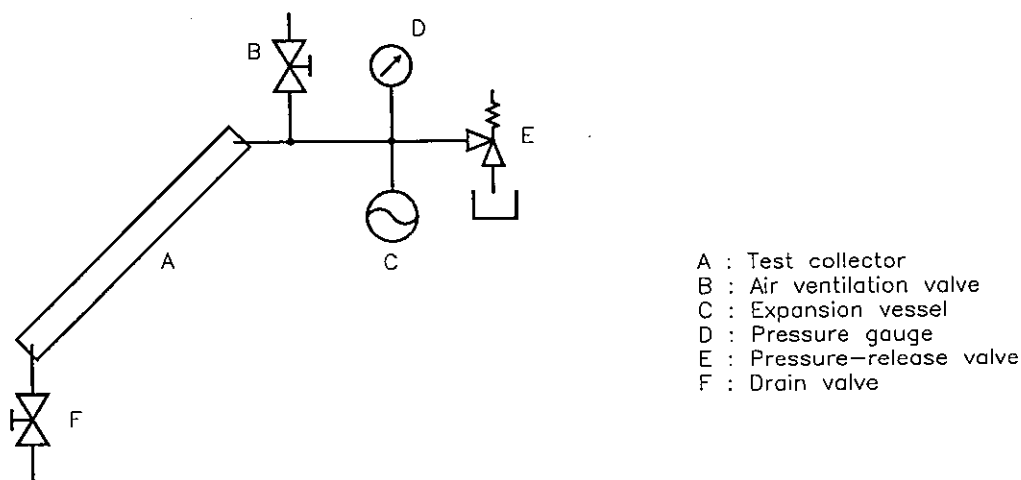
Figure 4;3   Test loop to operate the collectors under stagnation conditions

The four different single glazed flat plate collectors tested were all commercial products.

Test Collector 1:

Collector manufacturer	: Teknoterm, Sweden
Collector type	: Modified HT
Absorber coating	: Aluminium oxide pigmented with nickel
Absorber trade name	: Sunstrip
Absorber coating manufacturer	: Sunstrip Aluminium Finspång, Sweden
Ventilation[1]	: High because of untight backside (no ventilation holes)

Test Collector 2:

Collector manufacturer	: Showa Aluminium Corp., Japan
Collector type	: FAL-S2C
Absorber coating	: Aluminium oxide pigmented with nickel
Absorber trade name	: Showa
Absorber coating manufacturer	: Showa, Japan
Ventilation	: Low and controlled by special ventilation holes at the top and at the bottom of the collector

Test Collector 3:

Collector manufacturer	: Ernst Schweizer Metallbau, Switzerland
Collector type	: Sessatherm
Absorber coating	: Black chrome on nickel on copper
Absorber trade name	: North Star Fins
Absorber coating manufacturer	: MTI, USA
Ventilation	: Moderate because of slightly untight backside (no ventilation holes)

Test Collector 4:

Collector manufacturer	: Agena SA, Switzerland
Collector type	: Azur III
Absorber coating	: Black chrome on stainless steel
Absorber trade name	: Energie Solaire
Absorber coating manufacturer	: Energie Solaire SA, Switzerland
Ventilation	: Low and controlled by special ventilation holes at the top and at the bottom of the collector

---

[1] The Teknoterm collector used in the case study is intended to be installed as a roof integrated collector. Its backside is therefore not designed to be tight against wind and rain loads which may have a strong impact on the microclimate in the collector. Thus, the Teknoterm collector tested in the case study represents a highly ventilated kind of collector, which microclimate depends significantly on the outdoor climatic conditions.

Before testing, holes were drilled in the sides, bottom and top pieces of the collector frame to make measurements of the internal climate of collector possible, see *Figure 4;4.*
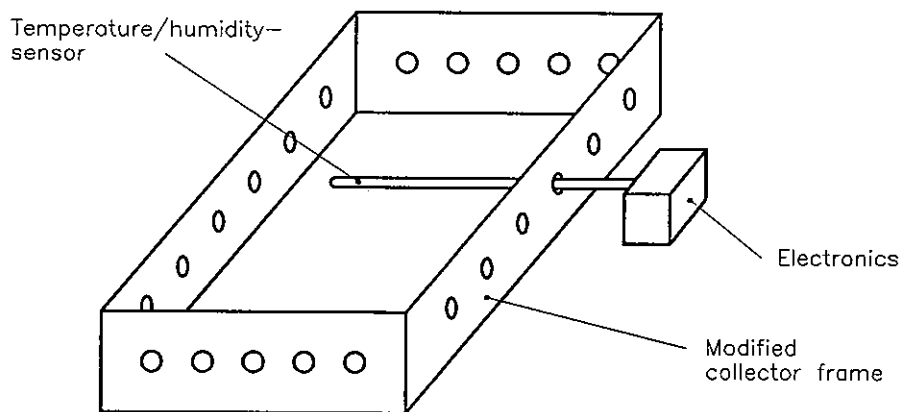
Figure 4;4: Collector with holes drilled for climatic measurements.

4.2.2 Measurements and monitoring of climatic data during testing

To characterize the environmental conditions for the absorber coatings during testing a variety of climatic variables were measured:

- ambient air temperature -
- ambient air humidity
- solar insolation
- absorber plate temperature
- humidity inside the collector
- time of wetness on the absorber surface and on the surface of cover plate
- corrosivity of the atmosphere outside and inside of the collector
- concentration of sulphur dioxide inside the collector

Macroclimate and absorber plate temperatures

Macroclimatic data or the climatic conditions outside of the collectors tested were measured with sensors placed within the test area. The ambient air temperature was measured with a Pt 100 sensor, the ambient air humidity with a capacitance humidity sensor (Rotronic) and the solar insolation with a Kipp and Zonen CM 11 pyranometer mounted coplanar to the plane of the aperture of collectors. On each of the collectors tested, the absorber plate temperature was measured as shown in *Figure 4;5.* The special sensor holder was screwed directly onto the absorber plate. To accomplish a good thermal contact a heat sink compound was used.
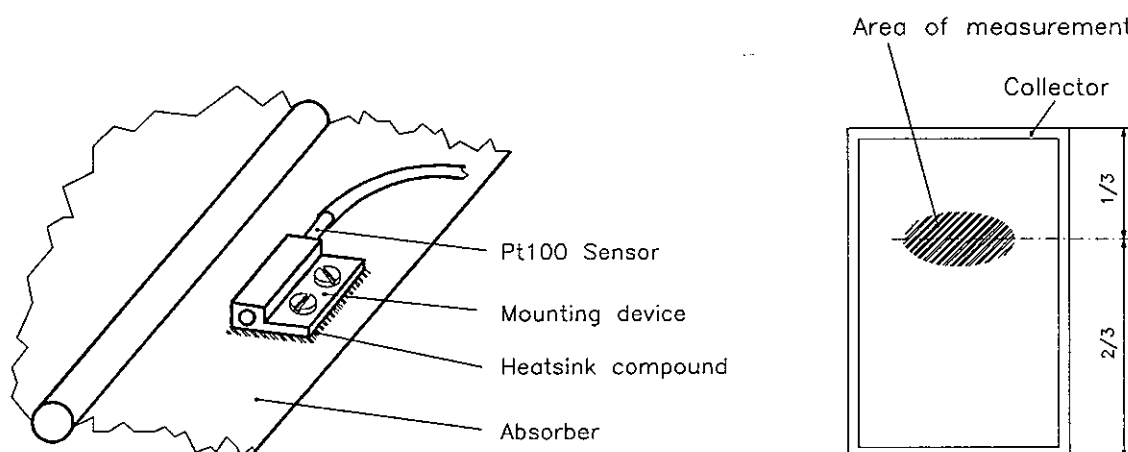
Figure 4;5: Measurement of absorber temperature.

For all the measurements performed, data were taken every 30 second. The data collected was used to calculate mean values for measurement intervals which varied from 2 minutes during day time up to 10 minutes during night time. The data logging system used (Acurex TEN/5) consists of a 16 bit A/D converter and different multiplex input cards for every type of sensor (Pt 100, Voltage, e.t.c.). The calculated mean values of climatic data were stored on a hard disc and back up's were generated on optical discs once a week.

Humidity inside the collector

The humidity of air inside the collector was measured between the absorber plate and the cover plate on two collectors - the Teknoterm collectors and the Agena collector both tested under simulated operation conditions.

A combined temperature and capacitance humidity sensor (Rotronic) was during measurement inserted in the collectors as shown in *Figure 4;6*. The sensor was equipped with a Teflon foam filter to avoid direct contact between the sensor and condensed water eventually formed. The sensor had an excellent stability over time as verified by calibration of the sensor before and after a measurement period.

An alternative measurement procedure would have been to use a dew point mirror instrument. However, in this case air from the collector must have been let out of the collector during measurement and then reinjected. This should have caused a change in the natural convection flow of air through the collector. As a result the humidity level measured should have been false.
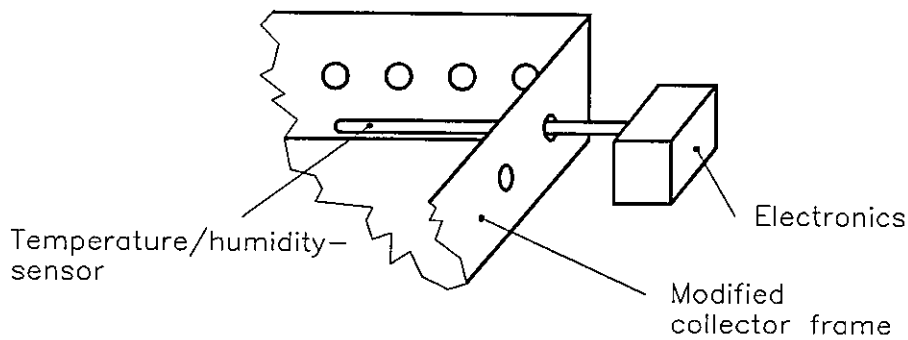
Figure 4;6: *Temperature/humidity sensor applied in a test collector.*

Time-of-wetness on the absorber surface and on the surface of cover plate

To be able to measure if and to what extent condensation of water occurs at the absorber surface a new instrument called "reflectance mode condensation sensor" (RMCS) developed by the Fraunhofer Institute for Solar Energy System in Freiburg was used.

The measurement principle is based on the fact that if condensation of water occurs on a surface its reflectance changes. The relative specular reflectance is measured by use of a very small monochromatic light source (laser) and a detector. The laser is pulsed to avoid measurement errors caused by straylight and the heating up of the measurement spot.

The advantages with this method compared to more conventional corrosion meters or time-of-wetness meters are that even very small quantities of condensed water can be detected, the measurement is performed directly on the surface, and radiation exchange between the absorber surface and the cover plate is not disturbed during measurement.

The RMCS sensor was used both for time-of-wetness measurements on the absorber surface and the inner surface of the cover plate.
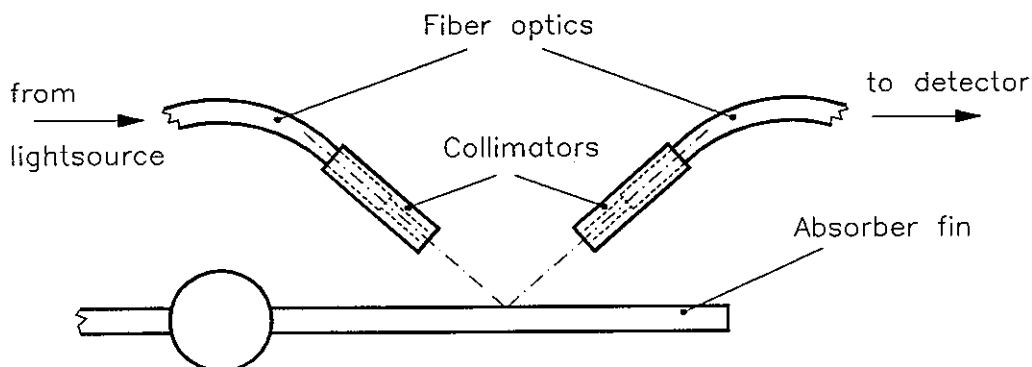
Figure 4;7: Reflectance mode condensation sensor (RMCS).

Corrosivity of the atmosphere outside and inside of the collector and the concentration of sulphur dioxide inside the collector

To measure the corrosivity of the atmosphere outside and inside of the collectors, standard metal coupons were used as proposed in ISO 9226. For each measurement,a set of four standard metal specimens was used:

- unalloyed carbon steel according to Swedish Standard SS 1147 (ISO 3574 CR4)
- zinc (impurity level 0.5 %)
- copper according to Swedish Standard SS 5013-02 (ISO R1336 Cu FRTP)
- aluminium according to Swedish Standard SS 4007-14 (ISO 6361 Al 99.5)

The dimensions of the specimens were 50x100x1 mm.

The corrosivity of the atmosphere outside of the collectors was determined by open air exposure of three sets of standard metal specimens mounted on the back side of a solar collector tested. The specimens were accordingly directed towards north and at an angle of 150° from the horizontal plane. The specimens were mounted on the solar collector with the aid of Teflon holders.

Standard metal specimens were used to determine also the corrosivity in the air space between absorber and cover plate of the collectors. One set of the four different specimens was attached to the absorber both at the upper and lower ends of it. The metal coupons were fixed to the absorber as described in *Figure 4;8*. Also in this case the specimens were attached by Teflon holders in order to electrically insulate them.
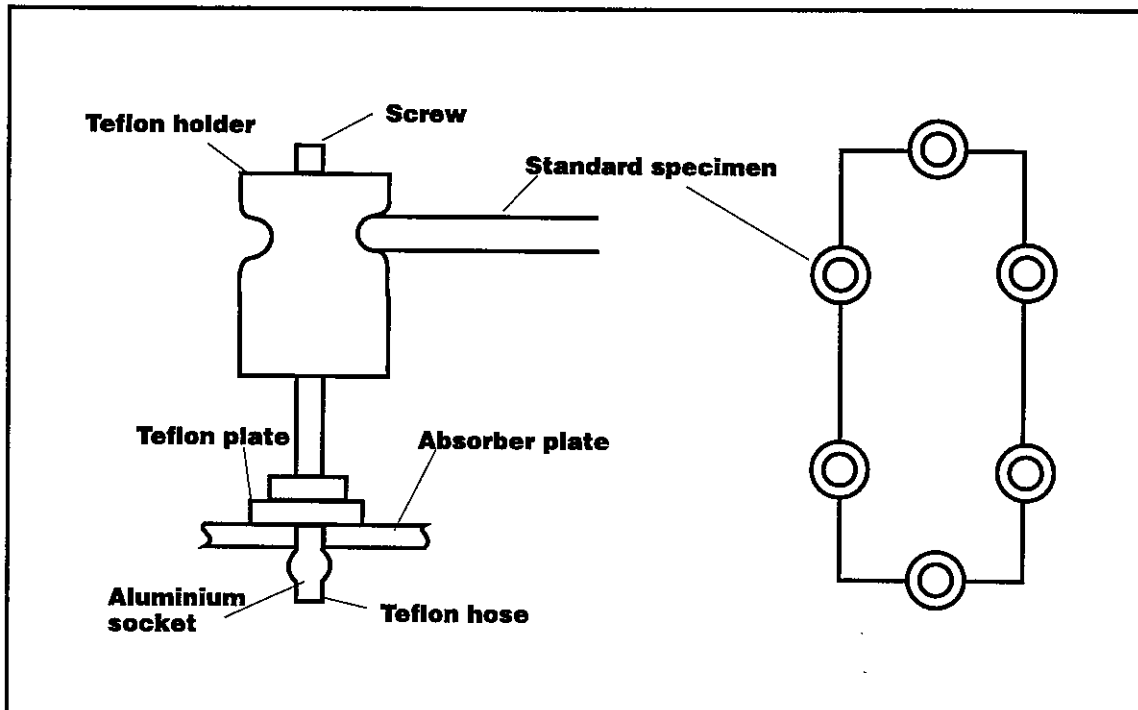
Figure 4;8: Mounting of the standard metal specimens used to determine the corrosivity inside the solar collector.

Before exposure the specimens were carefully cleaned with a hydrocarbon solvent in order to remove all marks of dirt, oil or other foreign matter capable of influencing the result from the corrosion rate determination. After drying the coupons were weighed to the nearest 0.1 mg.

After exposure the corrosion products were removed from the exposed coupons by chemical cleaning as described in ISO DIS 8407.

To determine the concentration of sulphur dioxide inside the solar collectors, some measurements with an UV-fluorescence instrument were performed. The measurements were intended mainly to gain a better knowledge of how fast a solar collector exchanges air with the ambient during different modes of operation.

4.2.3 Results from measurements of microclimatic data on the collectors tested

During the three years of test a huge amount of climatic data was collected and stored on data files. To make some of the data more accessible for future research, a special data file was made based on one year of measurements on the Teknoterm collector tested under simulated operation conditions [4,2].

Absorber temperatures during testing

Absorber plate temperatures measured on the eight collectors tested are illustrated as temperature histograms in *Figure 4;9.*

Temperature histogram
Stagnation

Temperature histogram
Operation
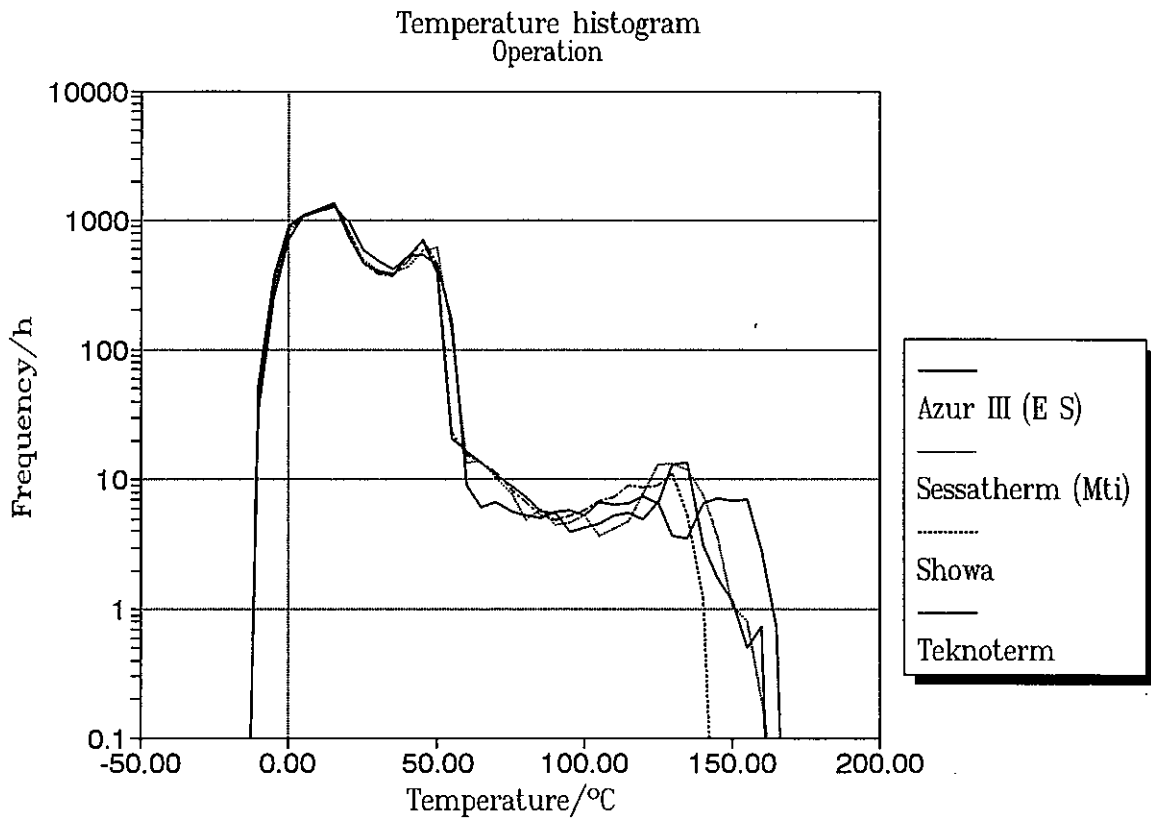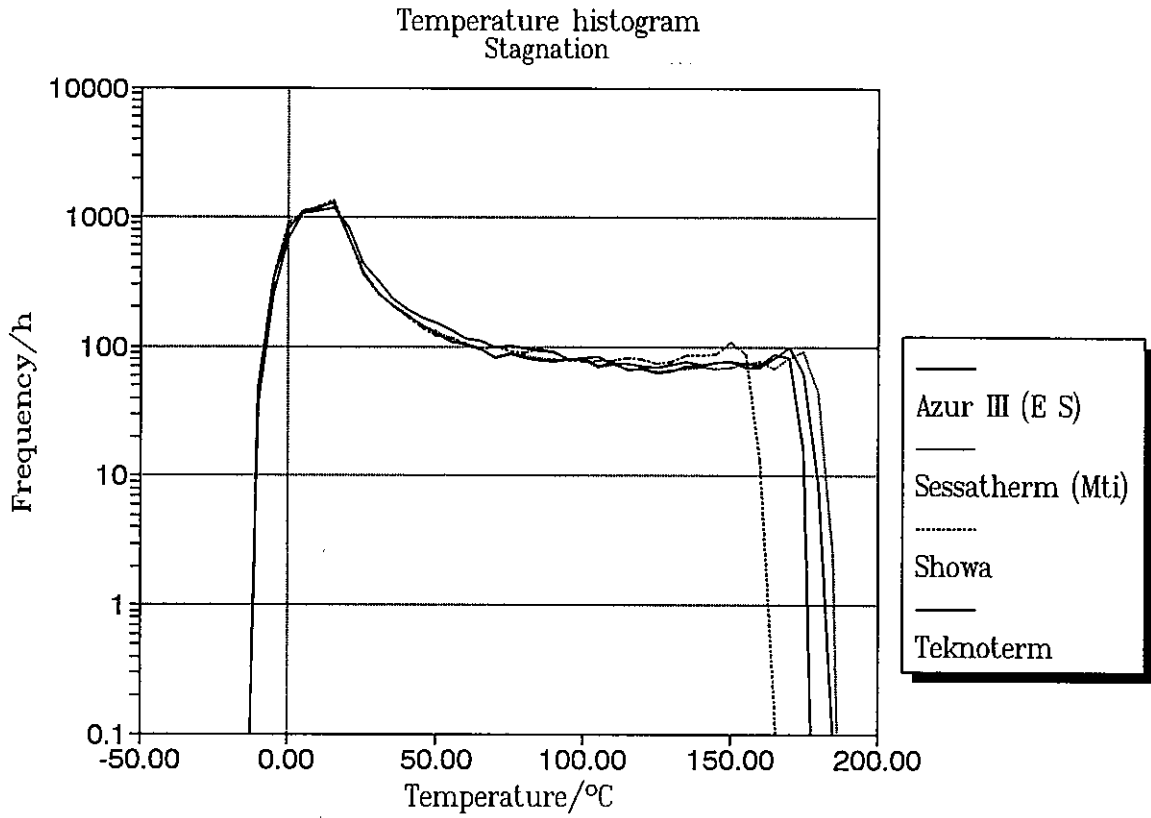
Figure 4;9 *Characteristic temperature data for the eight solar collectors tested.*

As can be seen the variation in temperatures of the different collectors tested is small when the collectors are working under the same mode or operation. It shold be pointed out, however, that the data for the collectors tested under operation conditions contains a period of fourteen days when the collectors were under stagnation conditions because of a pump failure.

Humidity condition inside the collectors

Measurements of the humidity conditions in the air gap between absorber plate and cover plate were made on two collectors; the Agena and the Teknoterm collectors tested under operation conditions. However, as the Agena collector had a collector frame of wood being hygroscopic the humidity data measured was difficult to interpret, see eg. [4,3]. Therefore, main part of humidity measurements were made on the Teknoterm collector constructed of nearly non-hygroscopic materials,

In *Figure 4;10*: temperature frequency diagrams for different humidity intervals are shown for the Teknoterm collector tested under operation conditions.
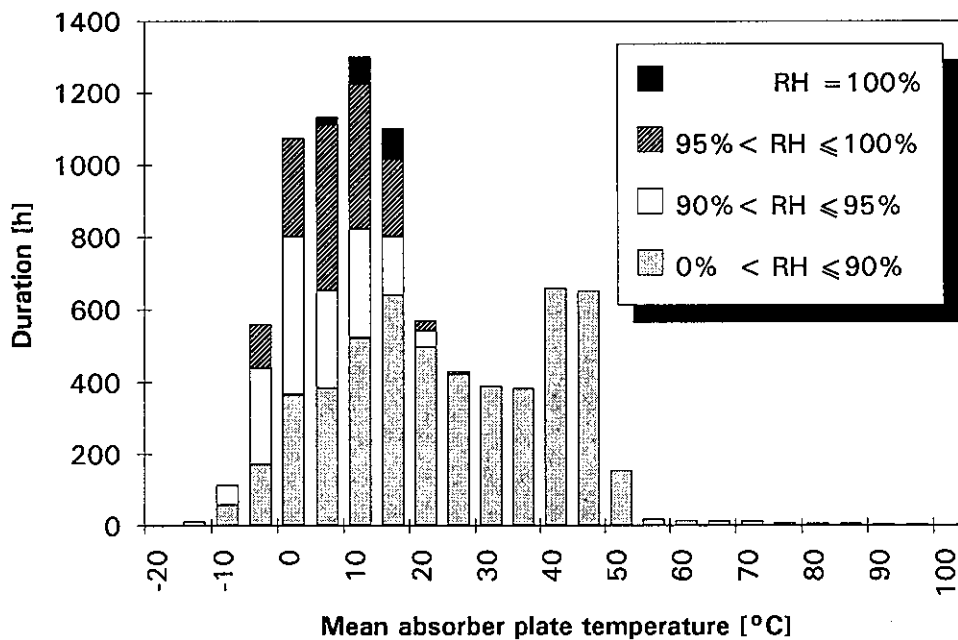
Figure 4;10 *Temperature frequency diagrams for different humidity intervals measured during long-term testing of the Teknoterm collector under operation conditions*

The relative humidity values given in the figure are measured in the air gap between absorber and cover plate.

It should be pointed out that the time-of-wetness measurements made with the RMCS sensor placed on the absorber plate in the middle part of the collector, gave no indication of the occurrence of condensed water on the absorber surface.

In *Figures 4;11*: measured data for two arbitrary chosen days are shown to illustrate the different kinds of humidity situations which may arise.

Time periods when the humidity level in the air gap may approach high values are during situations when the relative humidity of ambient air is close to 100 %. In particular during night hours and clear sky conditions the absorber temperature will be lower than the ambient temperature and as a result condensation may occur.
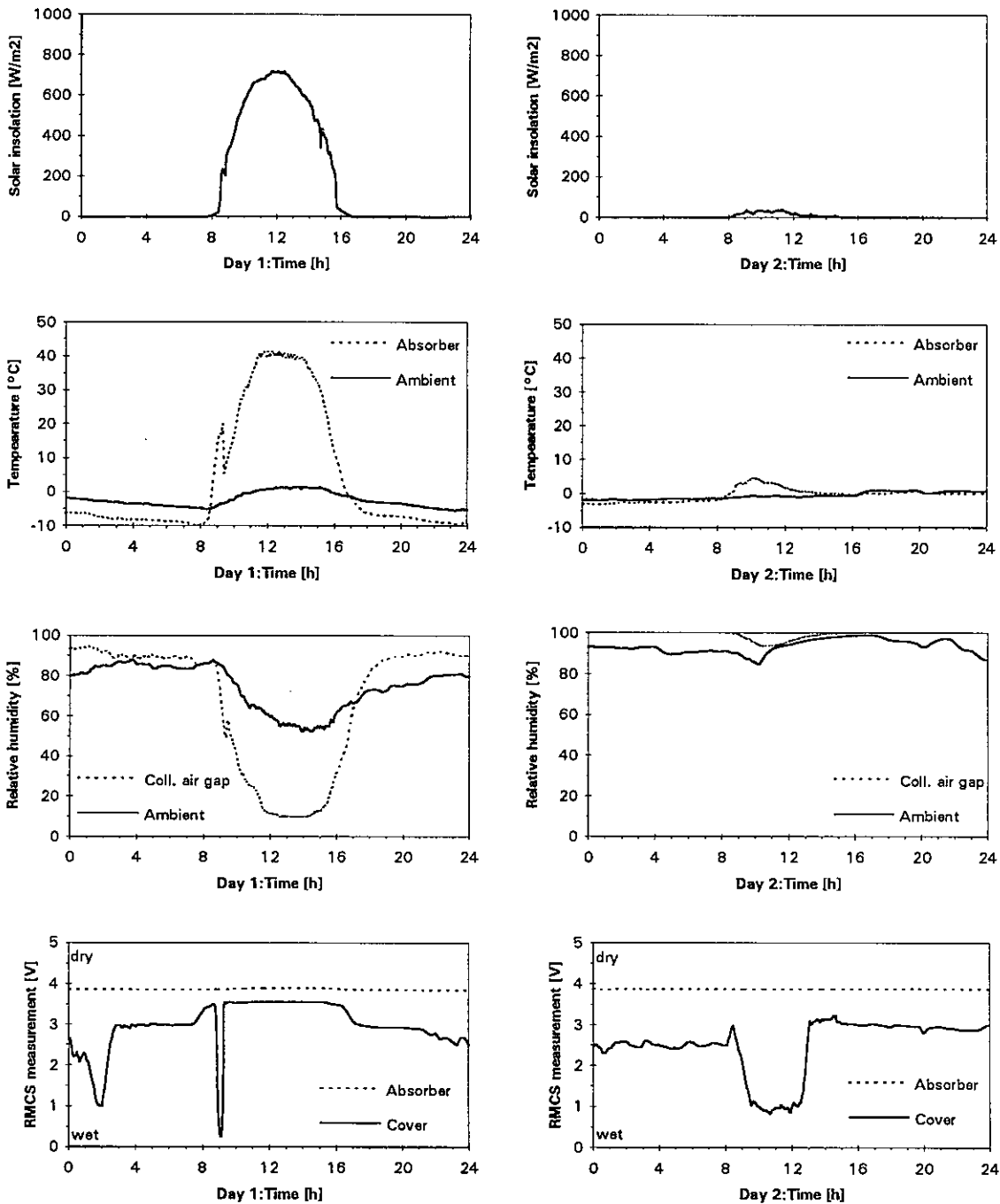
Figure 4;11:Measured climatic data on the Teknoterm collector tested under simulated operation conditions for two days

Corrosivity of the air outdoor and inside the collectors and the occurrence of sulphur dioxide

The results of the measurements of the corrosivity of air using standard metal coupons are given in *Table 4,2*. The exposure time for coupons placed outside and inside the collectors was two years in the first test and one year in the second test.

Location of Coupons	Metal weight loss of coupons								
	Steel (g/m²)			Zinc (g/m²)			Copper (g/m²)		
	1st and 2nd years	3rd year	Total	1st and 2nd years	3rd year	Total	1st and 2nd years	3rd year	Total
Collectors tested under simulated operation conditions									
Teknoterm									
top	1.0	8.8	9.8	0.4	0.5	0.9	2.2	0.9	3.1
bottom	0.5	0.1	0.6	0.4	0.5	0.9	0.6	0.3	0.9
Showa									
top	0.1	0	0.1	0.2	0	0.2	0.1	0.1	0.3
bottom	0.1	0.1	0.2	0.2	0.1	0.3	0.1	0.1	0.2
Sessatherm									
top	0.1	0.3	0.4	1.1	0.5	1.6	0.2	0.1	0.3
bottom	0.1	0.3	0.4	0.8	0.3	1.1	0.1	0.1	0.2
Azur III									
top	0.1	2.6	2.7	1.3	1.1	2.4	0.4	0.2	0.6
bottom	0.0	0.5	0.5	0.8	0.5	1.3	0.2	0.1	0.3
Collectors tested under stagnation conditions									
Teknoterm									
top	17.2	33.7	50.9	4.5	6.0	10.5	3.7	2.3	6.0
bottom	14.2	6.8	21.0	0.3	0.3	0.6	0.7	0.9	1.6
Showa									
top	0.1	0.1	0.2	0.2	0.1	0.3	0.4	0.3	0.7
bottom	0.1	0.1	0.2	0.2	0.2	0.4	0.2	0.2	0.4
Sessatherm									
top	1.1	0.1	1.2	1.2	0.2	1.4	0.5	1.0	1.5
bottom	0.1	0.2	0.3	0.5	0	0.5	0.2	0.5	0.7
Azur III									
top	0.1	51.4	51.5	0.6	2.5	3.1	2.2	1.7	3.9
bottom	0.1	2.3	2.4	0.6	0.5	1.1	0.4	0.9	1.3
Outdoor exposed coupons									
Mean value of two coupons exposed	73.2 ±0.2	65.2 ±0.2	138.4 ±0.2	2.3±0.1	1.9±0	4.2 ±0.1	4.8±0	6.4 ±0.2	11.2 ±0.2
Coupons exposed the first year of test		41.4			1.43			3.17	

Table 4;2   Metal weight losses of standard metal specimens exposed inside and outside of collectors tested.

Outdoor corrosivity at the test sites

The collectors were tested during a total period of three years. The collectors were first placed at the roof of an ITR-building. However, as previously mentioned due to rebuilding of the school the collectors were removed to a field station, located outside Rapperswil and also quite high above the town, after approximately half a year. The collectors were therefore exposed to two quite different environments. Rapperswil is situated very close to the Zürich Lake. The humidity can therefore be high. The climate at the field station is dryer. It is also very likely that the level of air-pollutants is lower compared to Rapperwil, especially during winter.

The difference in corrosivity between the two test sites is readily seen in the metal losses of the outdoor exposed coupons in *Table 4;2*.

In order to show the differences between the test sites, one year metal losses are calculated from the data given in *Table 4;2*. These data are given together with the location of the test sites in *Table 4;3*.

Time period (approxima- tely)	Test site	Metal weight loss of coupons		
		Steel (g/m^2)	Zink (g/m^2)	Copper (g/m^2)
1st year	Roof of ITR and field station	42	1.4	3.2
2nd year	Field station	32	0.8	1.6
3rd year	Roof of ITR	65	1.9	6.4

Table 4;3   Metal weight losses of standard metal specimens exposed outside of collectors tested at different test sites.

As is seen in *Table 4;3* there are large differences in weight losses for all metals between the second and third year, i. e. between the two different test sites.

Corrosivity inside the collectors

At first sight the results presented in *Table 4;2* seem to be hard to understand. One might suspect a very poor reproducibility in this type of tests. However, as pointed out above the outdoor environment has been changed during the test period. This fact, of course, complicates the interpretation of the results in *Table 4;2*.

Despite the change of test sites, the results contain a lot of information. Some conclusions can relatively easy be made.

A general observation is that the microclimate inside the collectors is milder than the macroclimate outdoors. This could at first sight seem to be self-evident, but one has to keep in mind that the temperature can reach much higher levels inside the collectors than outside. Nor are the outdoor coupons exposed to rain.

The corrosion of the steel coupons inside the collectors is, with few exceptions, very low compared to the outdoor corrosion. This indicates a very low humidity inside the collectors. The exceptions will be discussed below.

Another general observation is that in almost all collectors the corrosivity is higher at the top of the collectors. This is in contradiction to the observation that the most severe degradation of the aborber coatings usually takes place at the bottom.

Concerning the Showa and the Sessatherm collectors there are no major differences in corrosion rates of the metal coupons between the collectors working under simulated operation conditions and those working under stagnation conditions except for the copper coupons. For the copper coupons the corrosion rates are higher under stagnation.

During the third year of the collector test there was a small leak in a pipe for the cooling medium in the Azur III collector in stagnation. This leak resulted in a very drastic increase in the corrosion rate of the metal coupons as can clearly be seen in *Table 4;2*. The coupons, thus, responded strongly on the change in the environment.

The cover glass of the Teknoterm collector in stagnation was remounted since it came loose. The sealing seems to be very poor. This might explain the high corrosion rate of the metal coupons inside the collector, especially at the top of the collector. The corrosion rate also seems to increase as the time passes indicating a continuously deterioration of the sealing. A similar but less pronounced effect can also be seen at the top of the Teknoterm collector working under simulated operation conditions. No obvious leaks were, however, found.

It has to be pointed out that the rear sides of the Teknoterm collectors were made of corrugated aluminium plates, which, of course, makes the collectors very untight and the ventilation very uncontrolled.

The corrosion rates of the metal coupons inside the Showa collectors are very low. These collectors are also very tight. They are ventillated only through small holes at the top and bottom. By comparing the corrosion of the metall coupons inside the Teknoterm and the Showa collectors it seems to be quite clear that the design of the collectors is of great importance in the control of the microclimate inside the collectors and that metal coupons could be a very useful tool in the design of collectors.

The somewhat puzzling results of the corrosion of the coupons inside the collectors especially for zinc suggests that it is not only temperature and humidity that determine the corrosion rates, but also air pollutants such as SO_2 are of importance.

In *Table 4;4* some results from measurements of the sulphur dioxide concentration in the collector tested are presented. The measurements were performed at the field station during two consecutive days in November 1989. The weather the first day was cloudy and rainy, while the weather the second day was cloudless and sunny.

The outdoor concentration level of sulphur dioxide during the two days of measurements was 2-3 ppb, which is in the order of the stated accuracy of the instrument used. Nevertheless, due to the high reproducibility of the measured values, interesting results were obtained.

	Measured sulphur dioxide concentration (ppb)	
	Day 1 (cloudy)	Day 2 (cloudless)
Teknoterm Collector		
operation	0	2-3
stagnation	0	3-4
Showa Collector		
operation	0	2-3
stagnation	0	2-3
Sessatherm Collector		
operation	2	2
stagnation	1-2	4-6
Azur III Collector		
operation	10	38
stagnation	20	9
Out doors	2-3	2-3

Table 4;4 *The sulphur dioxide concentration levels measured in the collectors tested and out-doors during two consecutive days.*

* The Azur III collectors have a wooden frame, which may release other types of pollutants. This can explain the high values measured. It is known that the instrument used not always is capable of distinguish between SO_2 and other types of pollutants.

As is seen in **Table 4;4** the SO_2-level is zero in both of the nickel pigmented aluminium collectors (Teknoterm and Showa) when the weather is cloudy, i. e., when the absorbers are relatively cold and the humidity level is high. The SO_2-level in the black chrome collectors (Sessatherm and Azur III) is, however, the same as the outdoor level or higher (Azur III, see explanation above). When the weather is sunny on the other hand, i. e., when the absorbers are warm and the humidity low, the SO_2-levels are almost the same in all collectors (except in Azur III). The SO_2-levels inside the collectors are also the same as the outdoor level.

The observations above indicates that the nickel pigmented aluminium absorbers can absorb SO_2 when they are relatively cold and the humidity is high.

In order to get a better insight into the effects of sulphur dioxide air pollution on the corrosivity inside the collectors and out-doors, an EDX investigation was also performed on the steel coupons exposed two years before the descaling of corrosion products. The result of this investigation is given in **Table 4;5**.

| Location of coupons | Peak heights with EDX | | | Metal weight |
	O	S	Fe	loss (g/m^2)
Collectors tested under simulated operation conditions				
Teknoterm				
top	369	51	1890	0.97
bottom	228	55	1881	0.49
Showa				
top	69		1875	0.07
bottom	52		1979	0.08
Sessatherm				
top	245	56	1871	0.10
bottom	187	75	1874	0.08
Azur III				
top	57		1973	0.05
bottom	54		1884	0.03
Collectors tested under stagnation conditions				
Teknoterm				
top	989	91	1804	17.2
bottom	945	134	1892	14.2
Showa				
top	57		1986	0.08
bottom	54		1982	0.08
Sessatherm				
top	487	50	1872	1.12
bottom	88		1980	0.13
Azur III				
top	75		2042	0.06
bottom	55		1892	0.06
Outdoor exposed coupons				
Number 1*	1371	267	1869	41.5
Number 3**	1091	219	1852	73.6
Number 4**	1320	212	1839	72.8

Table 4;5 *EDX peak heights for oxygene (O), sulphur (S) and iron (Fe) of the steel coupons according to Table 4:2.*

Coupons exposed outdoor for one year.
** Coupons exposed outdoor for two years.*

As can be seen in *Table 4;5* sulphur containing corrosion products have been formed. It must, however, be pointed out that an EDX investigation of this kind is more qualitatively than quantitatively. The results can therefore not directly be used to calculate the amount of sulphate present in the corrosion products. For that reason

an ionchromotographic investigation (IPC) was performed on the corrosion products from the outdoor exposed coupons showing that 7 % of the corrosion products was iron-sulphate. The coupons from the Teknoterm collectors have a relatively high sulphur peak indicating the importance of SO_2 in the corrosion of these coupons.

4.3 Calculations of Micro Climatic Data by Use of Computer Simulation

The measurements of microclimatic data as described in **Section 4.2** were intended to serve mainly as a basis for validation of theoretically calculated data in the case study.

A joint effort with the performance group of Task X was made to develope suitable theoretical models to calculate by computer simulation microclimatic data of temperature and humidity for absorbers in collectors. The models developed should serve the purpose of being able to generate relevant microclimatic data for absorbers in DHW-systems of various designs and at different locations and climates.

A description of the models and the development work are also given in [4.2], [4.4] and [4.5]. In present report a summary of the work conducted will be given with main emphasis placed on its application for service life prediction.

4.3.1 Currently available computer models used for calculations of temperature and humidity data for absorbers in collectors

The problems involved in generating relevant microclimatic data by theoretical calculations varied considerably in complexity depending on which environmental factor that was taken into account.

To calculate mean solar absorber plate temperatures was rather straight forward. Data could be obtained on an hourly time basis using currently available computer simulation programs similar to what is described in **Section 3.1**. Input data needed for the calculations comprised solar system design parameters, operation parameters and macroclimatic data for reference years of climates of interest.

To generate data characterizing the humidity conditions on the absorber plate surface under in-use conditions was far more complicated.

The first approach here was to make the assumption that the absolute humidity inside and outside the collector is the same, which should hold true for a well-ventilated collector containing no accumulated liquid water.

Making this assumption Hollands et.al. [4.5]. made some calculations using the same computer simulation program as described in **Section 3.1** and with hourly values for ambient humidity as input data. Results are presented in *Figure 4;12.*
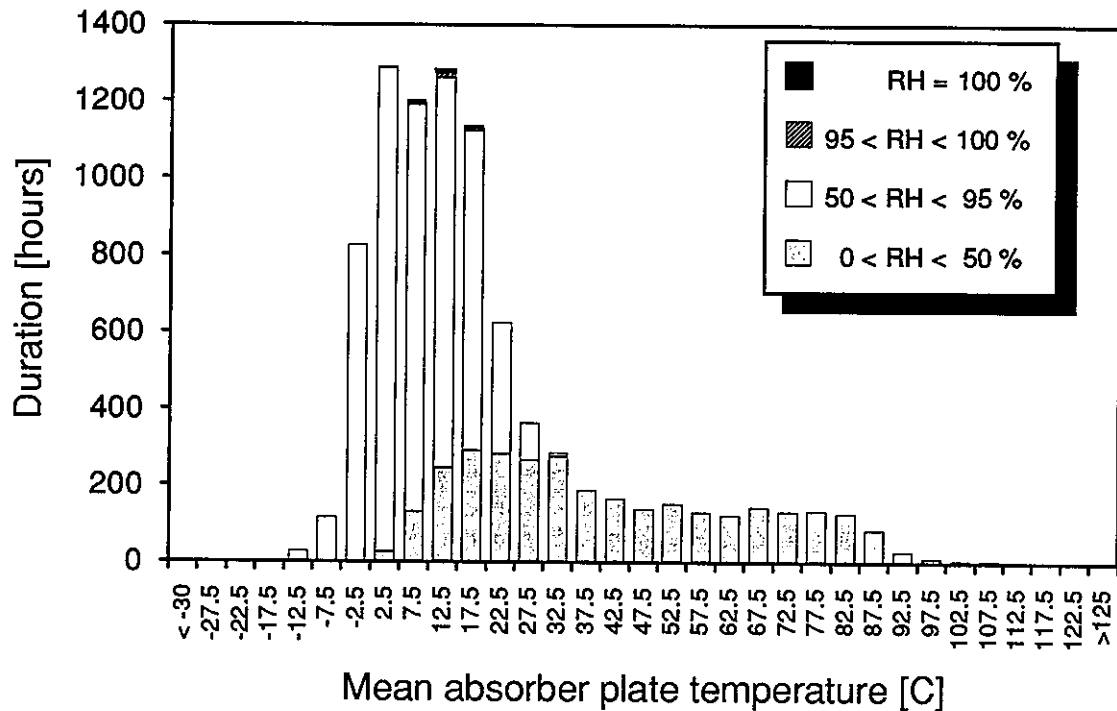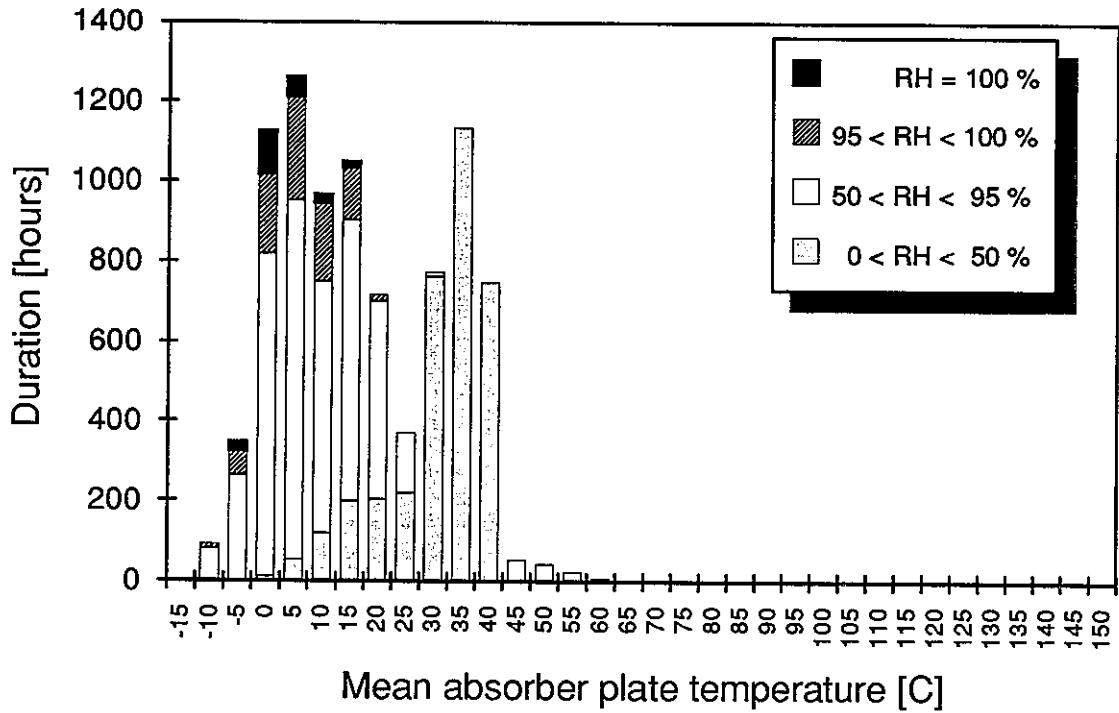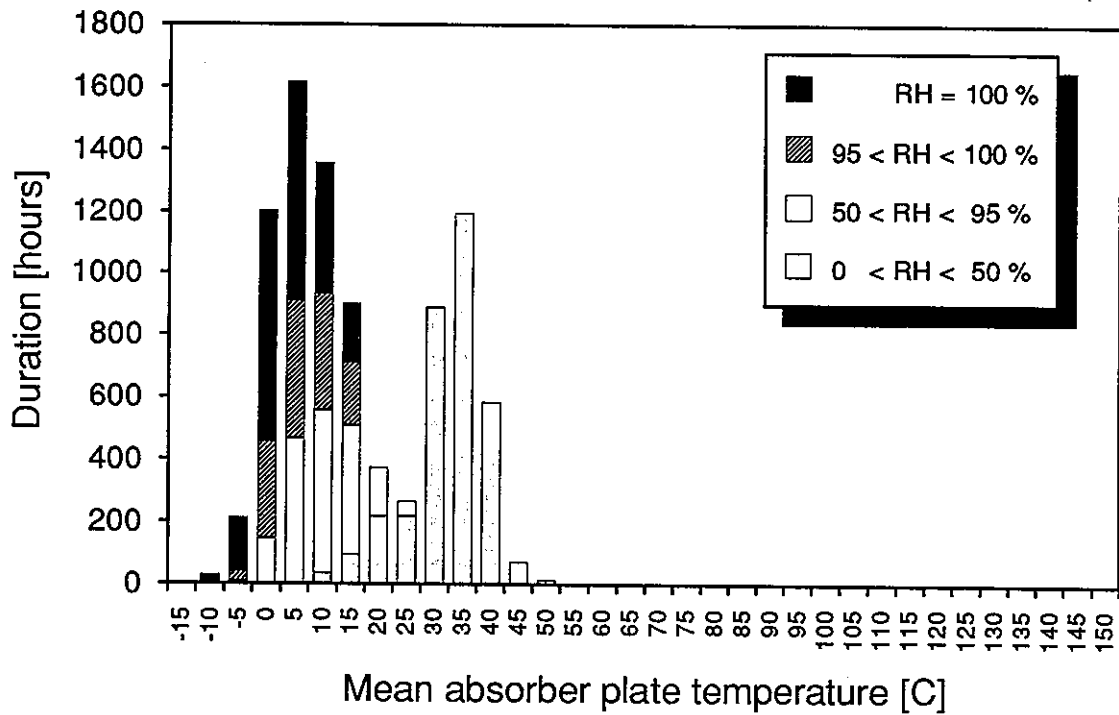
Figure 4;12 Yearly mean absorber plate temperature frequency diagrammes for different humidity intervals representative for a solar DHW-system located at Rapperswil (Hollands et.al.)

Of importance is to express humidity data related to the absorber temperature. Moreover a high accuracy in calculated data is needed in particular when the relative humidity approaches 100 %. The degradation rate for some coatings is several orders of magnitude higher when condensation takes place on the absorber surface compared to the situation when the relative humidity on the surface is around 95 %. The most important question, thus, was if or to what extent, condensation occurs on the absorber plate surface in a collector under in-use conditions.

As the mean absorber plate temperature does not represent the lowest absorber plate temperature and, consequently, not the worst case, Holland et.al. therefore extended their calculations to generate also relevant humidity data for the absorber plate near the collector inlet, see *Figure 4;13* . In *Figure 4;14* results are shown for a solar DHW - system located in a more humid climate, namely near Toronto.
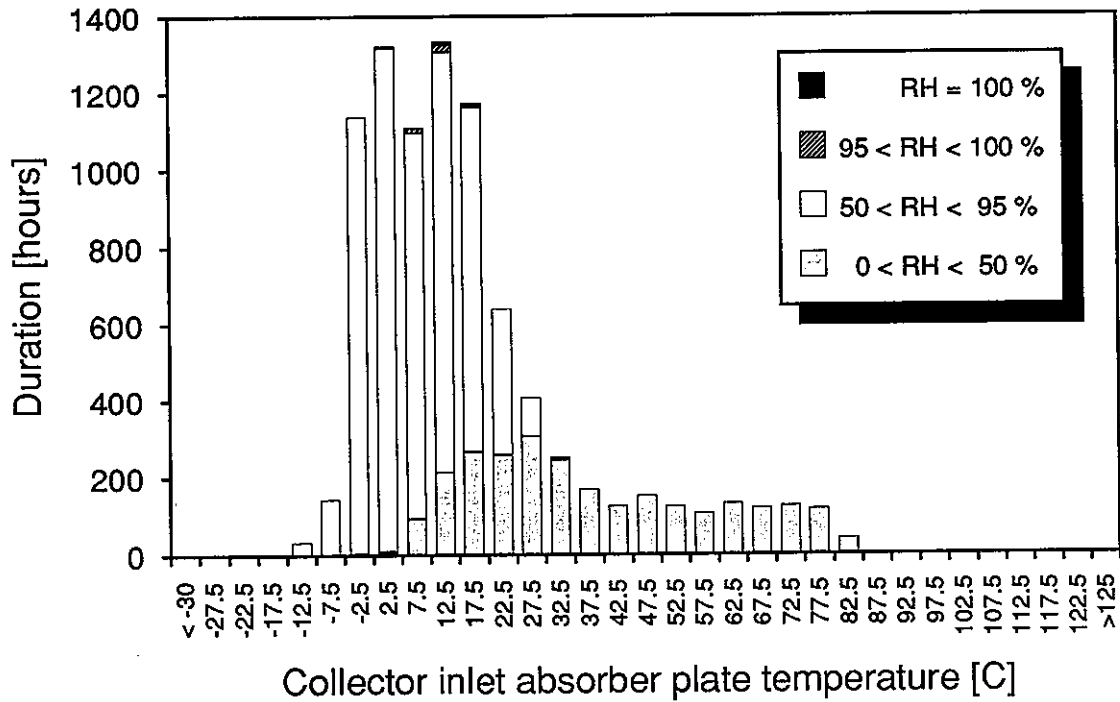
Figure 4;13 *Yearly frequency diagrams for absorber plate temperatures at collector inlet within different intervals representative for a solar DHW-system located at Rapperswil (Hollands et.al.).*
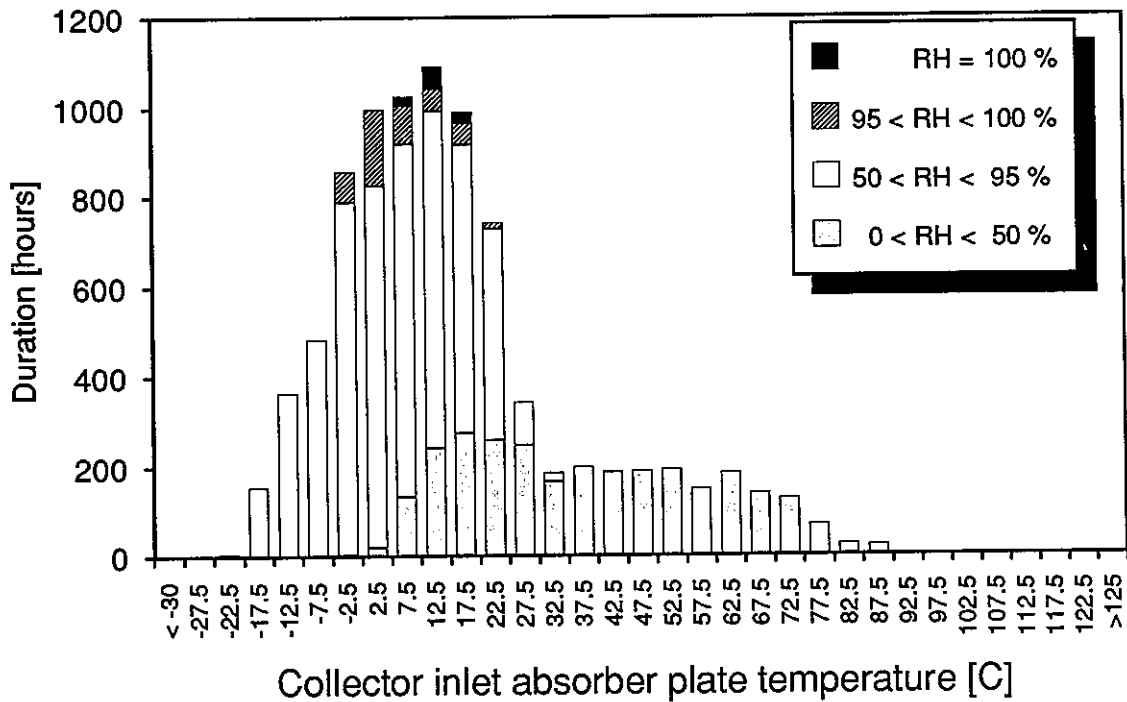
Figure 4;14 *Yearly frequency diagrams for absorber plate temperatures at collector inlet within different intervals representative for a solar DHW-system located at Toronto (Hollands et.al.).*

The calculations made by Hollands et.al. pointed to the fact that the relative humidity level is as expected low when the solar collector is under operation, the solar insolation is high enough. Periods when the relative humidity may approach 100 % can only occur when the collector is non-operating and, consequently, when the absorber plate temperature is low and close to the ambient temperature.

4.3.2 Development of a special computer model for calculations of humidity data for absorbers in a collector

As the time period of condensation occuring on the absorber plate surface under in-use conditions is a very important parameter for service life calculations, efforts were made to develope a more advanced heat and mass transfer model to describe the humidity conditions prevailing on the absorber surface in a collector. The model, which is described in detail by van der Linden et.al. in [4,2], requires the following input data for annual simulation of humidity conditions:

- ventilation rate coefficient
- collector dimensions
- temperature of the cover plate (hourly values)
- temperature of the absorber plate (hourly values)
- temperature of the ambient air (hourly values)
- water vapour pressure of the ambient (hourly values)

It is assumed that the temperatures of absorber, cover and air gap between the two are uniform. The air gap temperature is calculated as the mean temperature of the absorber and cover for each time step.

In the model the following processes are taken into account:

- ventilation caused by density differences between the air inside and outside of the collector, expansion/compression of the air in the collector due to heating up/cooling down of the air during the time step considered.

- condensation as a consequence of the fact that the dew point of air inside collector exceeds the temperature of the cover or absorber

- evaporation of condensed water on absorber (or cover plate) when the dew point of the air inside the collector is less than the temperature of absorber (or cover plate). Both the absorber plate and cover plate are assumed to be able to hold a maximal amount of water of 0.01 kg/m^2. If this amount is exceeded, excess water condensed is assumed to drip off and is transported out from the collector.

Within a time step - one hour - all processes are considered stationary.

The ventilation rate $\dot{V}$ of a collector is modelled by the following equation:

$$\dot{V} = C \ (\Delta P / \Delta P_R)^{1/2} + \frac{\Delta V}{\Delta t} \qquad\qquad (4,1)$$

where $\frac{\Delta V}{\Delta t}$ is the change in the volume of air in the collector caused by the thermal expansion/compression. This contribution to the ventilation rate is due to the fact that the temperature of air in the collector in the time step considered differs from that in the previous time step. The parameter ΔP, which should be expressed in Pa, is the difference in pressure due to density differences between ambient air and air inside the collector. The parameter ΔP_R is by definition equal to 1 Pa. The ventilation rate coefficient C depends on the collector design - tightness - and is a variable which needs to be determined as input parameter for an annual simulation.

The model requires normally the collector to be constructed of non-hygroscopic materials although it can be extended to take into account the effect of using hygroscopic construction elements as eg a wooden frame used in the Agena solar collector Azur III tested in the case study [4,2] .

In the calculations made by van der Linden et.al. the TPD solar energy system simulation package, see eg. [4,4] was used to generate input data, as absorber and cover plate temperatures, for each time step. These data were then fed into the humidity model described above. The results are shown
below.
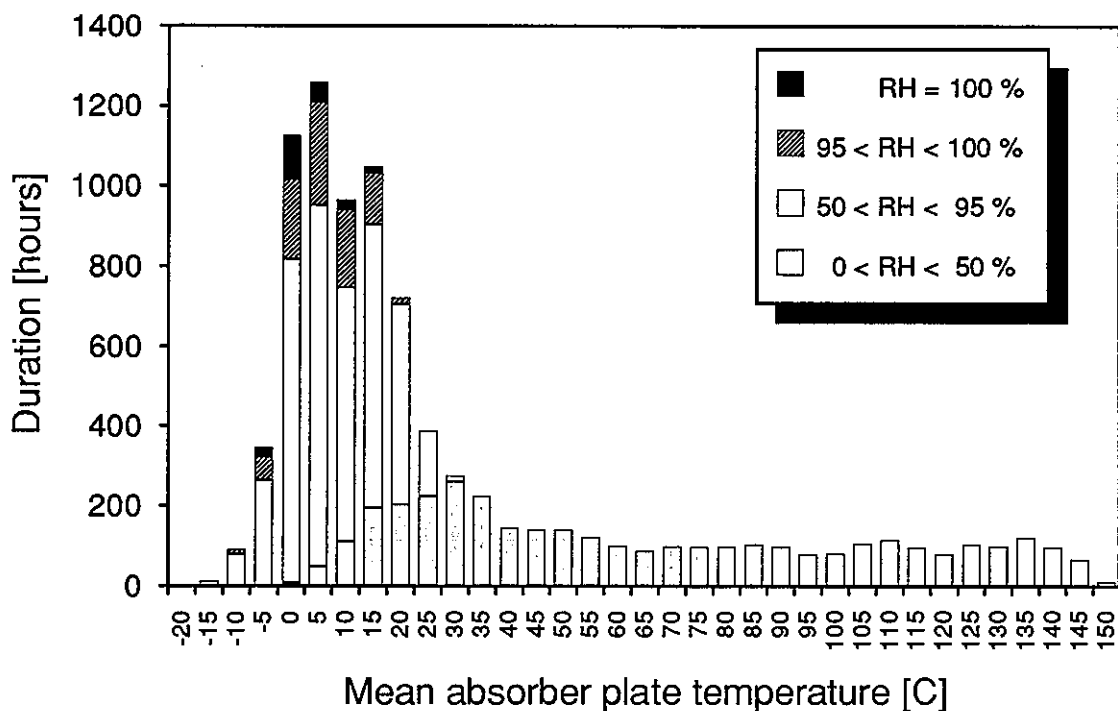
Figure 4;15 Yearly mean absorber plate temperature frequency diagrams for different humidity intervals representative for a collector tested under stagnation conditions at Rapperswil (Ventilation rate coefficient = 0.076 dm³ s⁻¹ (van der Linden et. al.)

Figure 4,16 *Yearly absorber plate temperature frequency diagrams for different humidity intervals representative for a collector tested under operation conditions at Rapperswil (Ventilation rate coefficient = 0.076 dm^3 s^{-1} (van der Linden et.al.)*

Figure 4;17: *Yearly mean absorber plate temperature frequency diagrams for different humidity intervals representative for a typical Dutch Solar DHW-system located at De Bilt, Netherland (van der Linden et.al.) (Ventilation rate coefficient = 0.076 dm^{3}s^{-1})*

4.3.3 Comparison between Calculated and Measured Microclimatic Data

To model the microclimate for an absorber in a solar collector is as has been shown quite a complex matter. The models developed to describe humidity accordingly are based on many approximations which correctnesses and limitations need to be fully validated. However, such work has not been possible to accomplish within the time frame of case study.

The correctness of the assumption that the absolute humidity inside and outside a solar collector could be set equal to each other may at a first sight look reasonable, see *Figure 4;18*. However, accumulation of water in the collector caused by condensation occurs which means that the absolute humidity inside the collector will sometimes be higher than outside of the collector. During such periods the relative humidity at the absorber surface may also approach 100 % giving rise to a high acceleration of degradation processes like hydrolysis reactions and electrochemical corrosion.
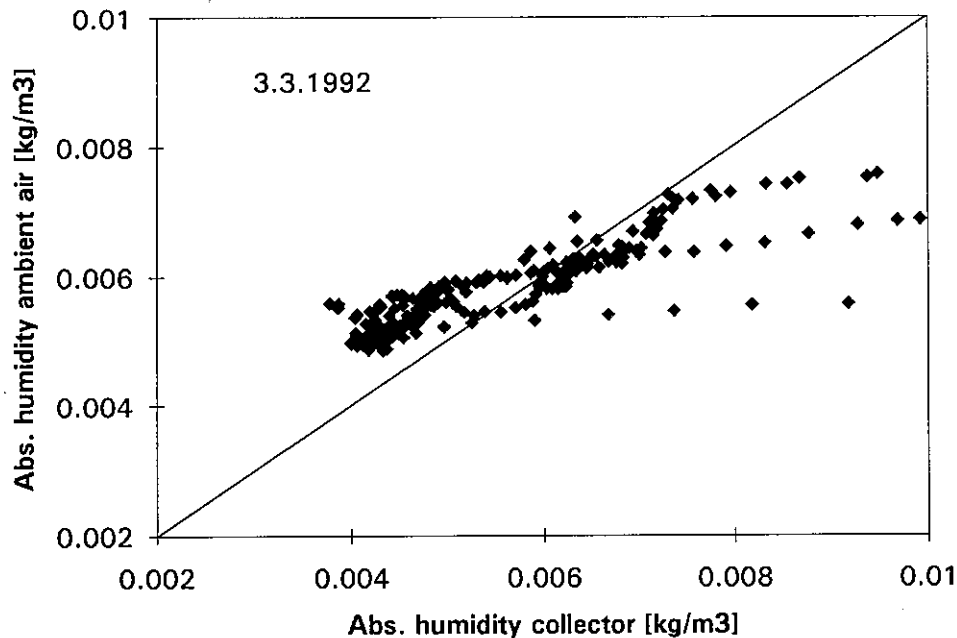
Figure 4;18 Comparison between absolute humidities measured outside of the collectors and in the air gap between the absorber and cover plate in the Teknoterm collector tested under simulated operation conditions.

A better agreement with measured data is obtained by making use of the more advanced heat and mass transfer model set up by van der Linden et.al. as shown in *Figure 4;19*. The results from calculations are in good qualitative agreement with the results from measurements. However, all parameters of the theoretical model used has not been fully optimized.

In the model set up by van der Linden et.al. ventilation through the collector has been considered independent on the wind conditions. According to Svendsen [4,6] wind have been found to greatly affect measurements on ventilation rates of air through collectors.
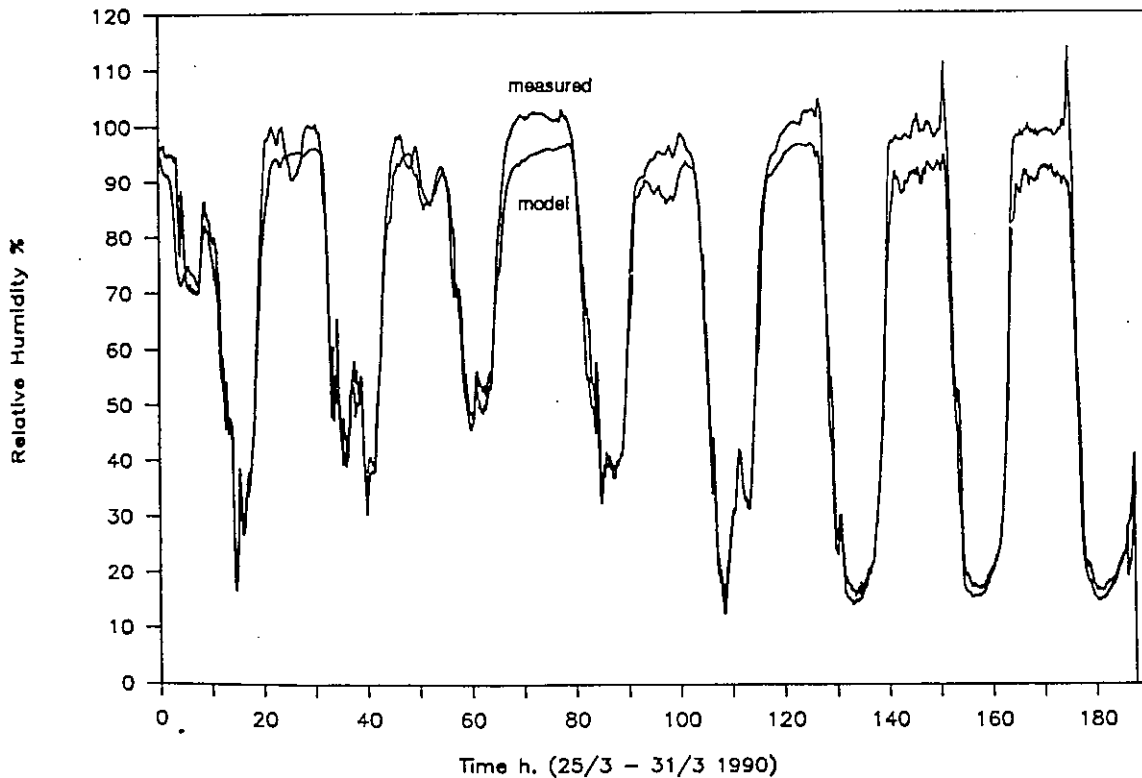
Figure 4;19 Comparison between measured and calculated air humidities in the Teknoterm collector tested under simulated operation conditions. For the calculation of data the model by van der Linden has been used.

To extend the microclimate model, in such a way that also effective levels of air borne pollutants inside the collectors may be calculated, is considered not possible due to too high complexity. Indirect methods of measurements as previously described in the report is here recommended.

The work on characterization of microclimate in solar collectors, constitutes one of the most important steps towards service life prediction. However, the results obtained so far have only partly been able to answer the very many questions that exist. More work is consequently needed to fully understand all results obtained and to refine the present model for calculations.
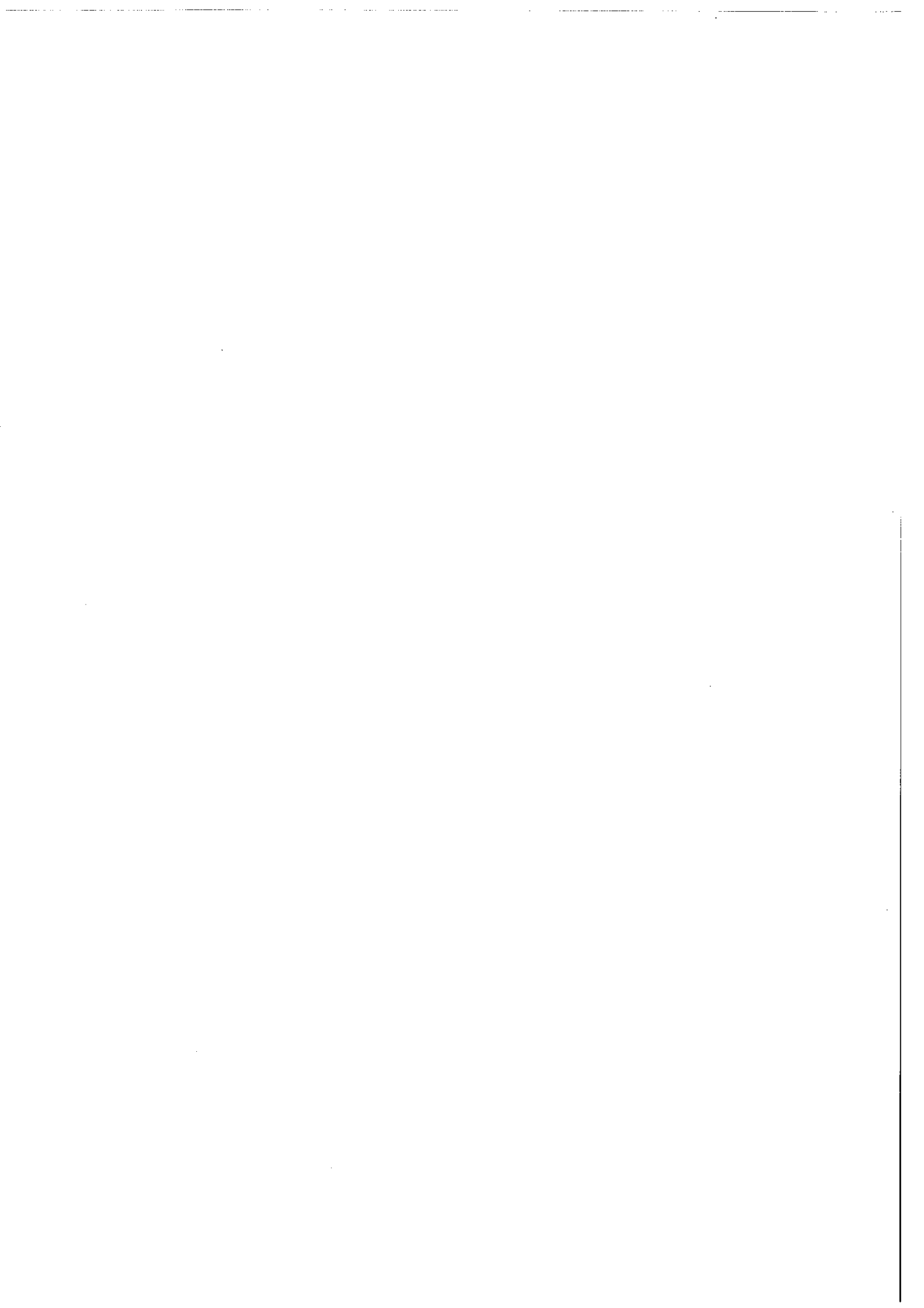
CHAPTER 5:

CONSTANT LOAD ACCELERATED AGEING TESTS

5.1 Purpose of Tests

To investigate the effects of the environmental parameters considered to be the dominating degradation factors for the selected coatings of case study, a constant load accelerated ageing test programme was set up by the Task X participants. The programme comprised four different kinds of ageing tests related to

- high-temperature degradation
- degradation by the action of condensation and high-humidity air
- degradation caused by sulphur dioxide as an air borne pollutant
- degradation caused by solar irradiation

The prime purpose for conducting the test programme was to generate data for service life prediction based on accelerated life testing as already outlined in **Chapter 2** of this report. A second purpose of conducting the tests was to improve existing test techniques so that quantitative interpretations of test results could be made possible.

High-temperature degradation

High-temperature ageing is frequently used in many technical application areas for the assessment of thermal stability of materials. In solar heating and cooling it has been used by many for determining the high-temperature resistance and expected service life times of absorber coatings [5,1; 5,2].

In this case study, the main efforts concerning high-temperature testing were directed towards refining the test technique in order to improve the accuracy in the determination of degradation rates. A round robin test was performed in order to identify possible systematic errors in the different test techniques used by the participating laboratories of the case study. A joint high-temperature test programme was also conducted in a work sharing manner. However, the systematic differences between the results of the different laboratories due to different equipment used made interpretation too difficult. Therefore only data from the Institute of Electrical Engineering, University of Stuttgart, Germany, are reported from this programme, since the largest number of tests was performed by them.

Degradation caused by the action of condensation and high-humidity air

Tests to simulate degradation caused by the action of condensation and high-humidity air can be performed in many different ways. However, most of such tests are used only for comparative testing. One problem is to control the test conditions at high humidities near the condensation limit. Cyclic tests comprising periods of condensation on the sample surface in between periods of sample exposure in a drying atmosphere are complex, and the results are difficult to interpret and make use of in connection with accelerated life testing.

The most frequently used high-humidity test for durability assessment of absorber coatings has been exposure of a sample at a constant temperature of 90 °C and at a constant humidity level of 95 % RH [5,1]. However, results obtained using this method have not been satisfactory for some coatings. Even after very long test periods no indication of lack of humidity resistance of these coatings has been found. Nevertheless, they have failed when placed under humid in-use conditions after too short a time period to be acceptable.

The work of the case study was therefore to conduct and evaluate more severe tests for use in connection with accelerated life testing. Tests were performed at humidities above 95 % RH. Tests were also conducted keeping the sample at a constant temperature below the dewpoint of surrounding air in order to maintain constant condensation of water on the sample surface during testing. As tests were also performed at different temperatures, the resulting programme of tests became quite comprehensive.

Due to the special technique needed for this, all tests were performed in only one laboratory - the Solar Energy Laboratory at ITR in Rapperswil, Switzerland.

Degradation caused by sulphur dioxide as an airborne pollutant

A special test technique has been developed during recent years for studying the influence of airborne pollutants on the corrosion resistance of materials. This new technique involves exposures of samples in a circulating air atmosphere with very low concentrations, less than 1 ppm, of pollutants added. It is presently used mainly for the testing of electronic components.

For the testing of absorber coatings, exposures of samples in high-humidity air containing small concentrations of sulphur dioxide has previously been used, adopting this new test technique [5,1]. Compared to other methods, this test technique has the potential for being more quantitative than other corrosion test techniques used today mainly for comparative testing.

The work of the case study was therefore directed towards evaluation of this new technique for accelerated life testing. Due to the special kind of test equipment needed, all tests were also in this case executed in only one laboratory - The Swedish National Test and Research Institute.

Degradation caused by solar irradiation

In order to investigate the influence of ultraviolet irradiation on the durability of selected coatings in the case study, some combined ultraviolet, condensation and humidity tests were performed by the Oxford Polytechnic, UK. The tests were carried out in a climatic cabinet equipped with a UV source which delivered an UV-irradiance of 50 ±5 mW/cm^2 to the surface of samples. The total UV dose to which the samples were exposed was calculated to be equivalent to more than 5 years, exposure to air mass 2 irradiation under a glass cover.

From the test result obtained it was concluded that UV irradiation is not a serious degradation factor for the materials investigated. Full results of the study are contained in [5,3].

5.2   High-temperature Testing

5.2.1   Round-robin programme on high-temperature ageing testing

In order to reduce potential sources of error in connection with high-temperature testing a round robin programme was undertaken with seven laboratories participating, see also [5,4].

Each laboratory was provided with samples of the Energie Solaire black chrome absorber coating material. All samples were cut from the same sheet in order to minimize deviations between samples distributed for testing. Each laboratory received three samples for constant-load high-temperature ageing at three temperatures: 450 °C, 480 °C and 500 °C.

It was agreed by the participants to carry out tests with the samples mounted on stainless steel sample holders (dimensions about 10 x 10 x 1 cm) to increase the thermal mass of system. This should prevent the samples from thermal shocks during heating-up and cooling-down periods in connection with optical measurements during testing. It should also smooth out temperature fluctuations. Temperature sensors should be mounted between the sample and holder.

The optical properties of the sample should be measured, according to the recommended procedure presented in **Section 3.2.2** of this report. Measurements should be performed at predetermined testing times for the three tests to be executed.

The results of the round robin test are presented in *Table 5;1* and *5;2*.

Lab	450 °C	3 h	10 h	50 h	480 °C	3 h	10 h	500 °C	3 h
1	0.946	0.902	0.889	0.842	0.949	0.896	0.863	0.945	0.868
2	0.939	0.903	0.884	0.839	0.938	0.873	0.837	0.938	0.840
3	0.936	0.904	0.882	0.822	0.940	0.874	0.823	0.935	0.851
4	0.952	0.910	0.891	0.837	0.952	0.874	0.830	0.951	0.842
5	0.937	0.907	0.882	0.815	0.943	0.872	0.830	0.943	0.845
6	0.934	0.899	0.890	0.843	0.940	0.883	0.845	0.936	0.864
7	0.934	0.883	0.872	0.825	0.937	0.878	0.841	0.943	0.876
α	0.9397	0.9012	0.8843	0.8319	0.9427	0.8786	0.8384	0.9416	0.8551
σ	0.068	0.088	0.066	0.111	0.057	0.086	0.131	0.057	0.141
σ/%	0.072	0.098	0.075	0.133	0.060	0.089	0.157	0.061	0.165

Table 5;1   *Solar absorptance of the Energie Solaire black chrome coating, measured at the different laboratories before, during and after the constant-temperature tests (α = average, σ = variance).*

Lab	450 °C	3 h	10 h	50 h	480 °C	3 h	10 h	500 °C	3 h
1	0.177	0.119	0.118	0.104	0.168	0.92	0.122	0.182	0.99
2	0.220		0.138	0.135	0.208		0.128	0.211	0.135
3	0.216	0.149	0.147	0.145	0.221	0.144	0.144	0.226	0.146
4	0.214	0.139	0.141	0.130	0.216	0.138	0.128	0.214	0.129
5	0.210	0.130	0.140	0.100	0.220	0.149	0.150	0.210	0.130
ε	0.215	0.139	0.142	0.128	0.216	0.141	0.138	0.215	0.135

Table 5;2 Thermal emittance of the Energie Solaire black chrome coating, measured at the different laboratories before, during and after constant-temperature tests (ε = average).

The agreement between the thermal emittance values evaluated from near-normal hemispherical reflectance measurements (laboratories 2 - 5) is surprisingly good. After an initial decay period the emissivity, however, stays constant.

The reported values for the solar absorptance of the unaged samples show clearly systematic difference between the laboratories. The differences among the three samples due to sample inhomogenities or statistical scattering in the measurements are much smaller. The systematic error (about 0.6) might be caused by the differences of the equipment used for optical measurement, eg. the integrating spheres, or be caused by use of different optical references, see **Chapter 3.2**. The error is increased to about 1.7 % after ageing, depending on the load.

A life data analysis was made to understand better the consequences of the systematic deviations in test results obtained by the different laboratories .

Using the solar absorptance values reported by the different laboratories, the following data were evaluated:

- the activation energy, E_A, according to the Arrhenius relation,
- the maximum working temperature, T_{MAX}, for an assumed time of 10 years,
- the life defined from a permitted decrease of α_s equal to 0.05,
- the life at a constant working temperature of 300 °C, y (300 °C).

A detailed description on how to evaluate those data is given in **Chapter 6** of present report. The results are shown in *Table 5;3*.

Lab.	E_A (kJ/mol)	T_{MAX} (°C)	y(300 °C) (years)
1	186	277	1.9
2	256	317	47.5
3	201	289	4.3
4	251	312	28.9
5	215	298	8.2
6	219	302	12.1
7	138	228	0.2
Arit. mean value	209.3	289	14.7
Standard deviation	40.2	30.1	17.4

Table 5;3 Activation energy (E_A), maximum temperature for a life of 10 years (T_{MAX}), and life at a constant working temperature of 300 °C, y(300 °C), evaluated from data obtained by each laboratory.

For a discussion on what kind of errors that may have caused the differences in the data of *Table 5.3*, the following relative normalized absorptance may be helpful, namely

$$R(t) = \alpha_N (t) / (\bar{\alpha} (t) / \bar{\alpha} (\theta)) \tag{5.1}$$

where $\alpha_N (t) = \alpha (t) / \alpha (0)$ or the normalized absorptance, $\bar{\alpha} (t)$ is the mean value of α at a certain testing time t for a particular high-temperature test calculated with data from all laboratories, and $\bar{\alpha} (0)$ is the corresponding mean value for the initial absorptance values. Values of this parameter are shown in *Figure 5;1*

As can be seen from the figure, the values from laboratory 7 (and also to a certain degree from laboratory 1) show a relatively stronger degradation at lower temperatures compared to the situation at higher temperatures. As a result, the activation energies calculated are the lowest, which leads to an under-estimated durability compared with the results from the other laboratories.

The values calculated from the data of laboratories 2 and 4 exhibit a temperature dependence which is the opposite. The activation energies calculated are the highest and the lives, y (300 °C), the longest.

The data in *Figure 5;1* from laboratory 3, 5 and 6 exhibit less variations with temperature. Accordingly, the lives, y (300 °C), calculated are closer to each other. Laboratory 5 reported higher degradation while laboratory 6 reported lower degradation than the average. This does not affect the calculated activation energies, however.
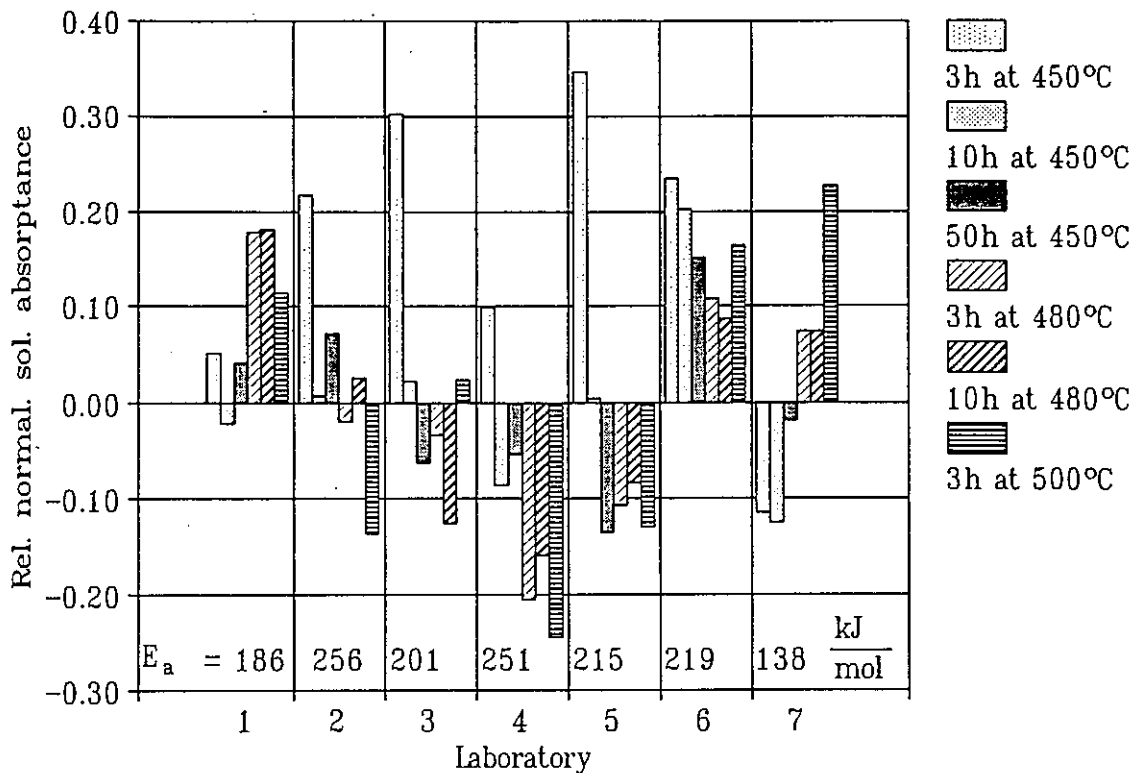
Figure 5;1 Relative normalized absorptance R (t) values for the different laboratories calculated for some selected testing time periods at the three test temperatures chosen.

It can be concluded that the systematic deviations observed between the results from the different laboratories can be due to a systematic temperature-independent or a temperature-dependent error. In the second case, the error introduces an increase or a decrease in the activation energy to be determined.

One reason for temperature-dependent errors in connection with the tests may be too high temperature fluctuations. Even a systematic variation around the set temperature results in a higher effective temperature according to the Arrhenius relation. The amplitude of the fluctuations varies with the set point and is proportional to the heating power. Ovens with a high maximum temperature and, therefore, a high heating power generate temperature fluctuations with a high amplitude.

Ovens with circulating air heating (used by laboratory 3 and 5) should be preferred because of the better temperature homogeneity in the ovens and especially between the temperature sensor and the sample. When radiation furnaces are used, the temperature of sample and "the temperature of the temperature sensor" strongly depend on the radiation exchange with the heater and therefore also on their optical properties. It is in this case preferable to measure the sample temperature for heating control (laboratory 6).

5.2.2 Crucial factors of testing and test procedure employed for accelerated life testing

The use of high-temperature ageing for accelerated life testing requires, as shown by the round robin test, a lot of measures to be taken.

These can be summarized and exemplified by the test procedure used by the University of Stuttgart laboratory as follows:

- The guidelines given in 3.2.2 and 3.2.3 should be followed for the optical measurements of samples. It is of great importance to measure the extent of degradation as a function of testing time on one and the same sample.

- The usage of circulating air ovens should be preferred, as discussed in 5.2.1 for the pertinent range of test temperatures, 250 °C - 600 °C. In *Table 5;4* the test equipment used by the University of Stuttgart laboratory is specified.

- Ideally, the test should be performed with the sample mounted on a holder with a high thermal mass or alternatively by heating up/cooling down the sample and oven simultaneously. With such a procedure, thermal shocks which might cause undesired degradation of the sample can be avoided. However, such a procedure requires that the temperature/time profiles during heating up/cooling down of the sample are measured so that corrections for this temperature effect can be taken into account when calculating the effective test time in connection with life data analysis of results. It should be pointed out, however, that the degradation of the sample during a heating up or cooling down period can often be neglected. The effective additional temperature load of a typical circulating air oven is about a quarter of an hour at a test temperature of 400 °C [5.5]. When conducting the tests, the results of which are presented in a later section of this report, the University of Stuttgart laboratory heated up and cooled down the oven with the sample placed in it during all the phases of high-temperature tests.

Table 5;4

Manufacturer:		Brabender Real test	Naber
Type		TSW 240/RV	N 30 A
Heat transfer		Circulating air	Circulating air
Temperature	range:	RT - 450 °C	RT - 750 °C
"	constance:	± 0.5 K	± 1 K
"	homogenity	± 2 K	± 1 K
Power:		3.4 kW	up to 5 kW
Inner Dimensions:		0.6 x 0.6 x 0.7 m³	0.3 x 0.35 x 0.45 m³
Volume		240 l	45 l
Materials		Stainless steel	Stainless steel ceramic

Table 5;4 Specification of high-temperature ovens used by the University of Stuttgart laboratory in the accelerated life tests of the case study.

5.2.3 Ageing test results

In the joint constant-load high-temperature test programme set up by the Task X group, test temperatures and testing times were chosen on the basis of previous durability studies performed on similar absorber coating materials by Köhl et.al. [5.5]. Test duration was not allowed to exceed one month, which determined the lowest test temperature of the programme.

Due to systematic deviations between test results from different laboratories, only the test results from the University of Stuttgart laboratory are presented in *Tables 5;5 - 5;8* of this report.

For additional information on the tests being performed in the case study, the reader is referred to [5.6].

Spectral reflectance data are presented only in the solar wavelength range because no complete set of data is available for the infrared region. The changes in the spectra resulting from high-temperature ageing in this wavelength region occur mainly at the beginning of the tests. It is caused by desorption of water and reduces the thermal emittance, as can be seen from the integral emittance values given.

Although not being included in the joint test programme, results from high-temperature ageing tests performed under vacuum conditions are also presented. Such data give valuable information when analyzing possible degradation mechanisms of the coatings studied.

Table 5;5 *Results from high-temperature ageing tests of the Energie Solaire black chrome absorber coating.*

300 °C

Time, h	α_s	ε_n (373 K)
0	0.942	0.20
3	0.939	
10	0.935	0.17
20	0.931	0.16
100	0.924	0.15
530	0.909	
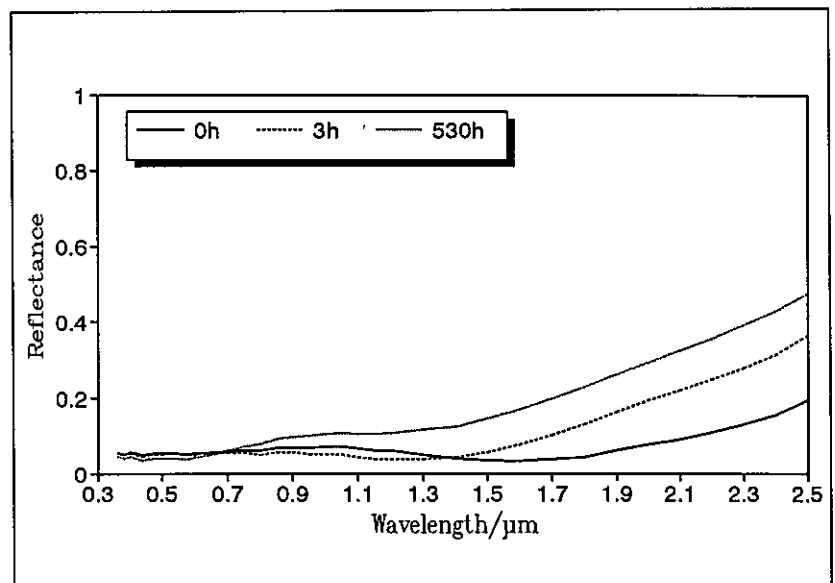
Table 5;5 cont.

330 °C

Time, h	α_s	ε_n (373 K)
0	0.943	0.20
3	0.935	0.15
6	0.931	0.14
10	0.925	0.14
20	0.918	0.13
100	0.909	
500	0.899	
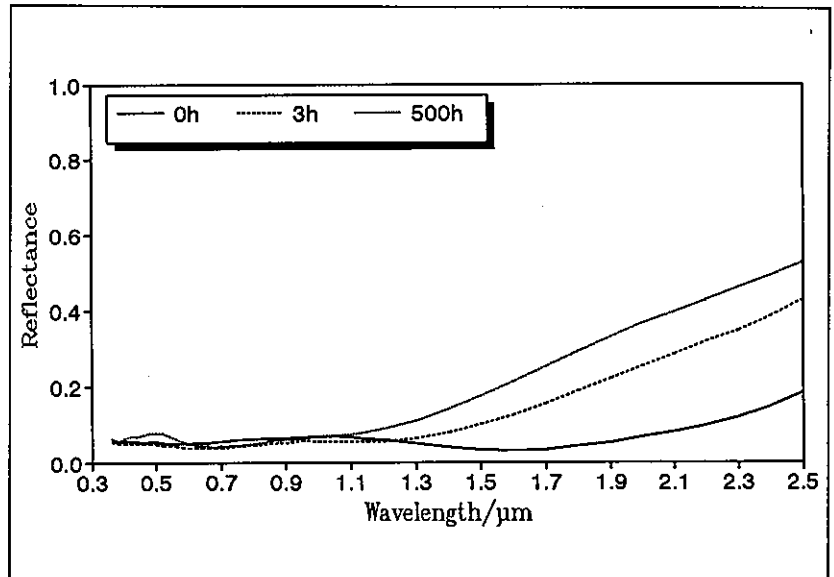
350 °C

| Time, h	α_s	ε_n (373 K)
0	0.938	0.20
3	0.923	0.15
6	0.914	
10	0.912	
20	0.903	
50	0.885	
100	0.874	0.14
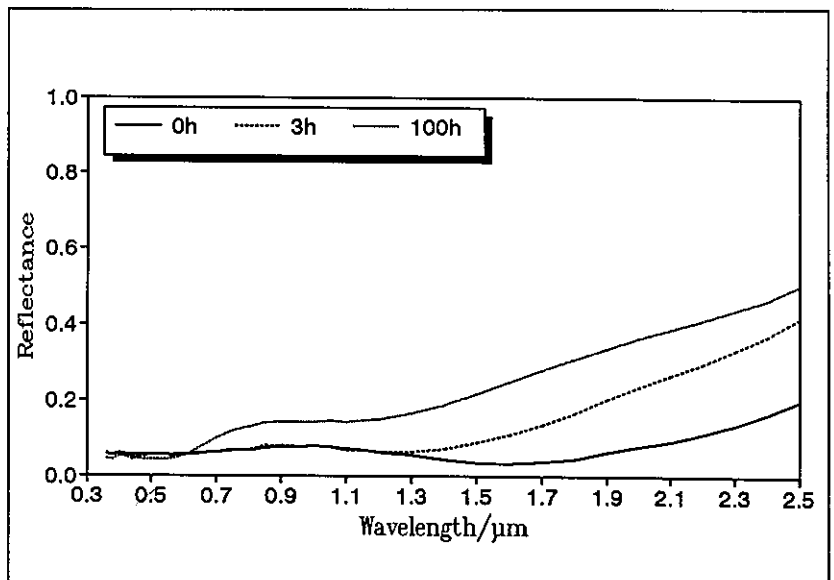
Table 5; cont

380 °C

Time, h	α_s	ε_n (373 K)
0	0.946	0.19
3	0.934	
10	0.931	
50	0.927	
100	0.921	
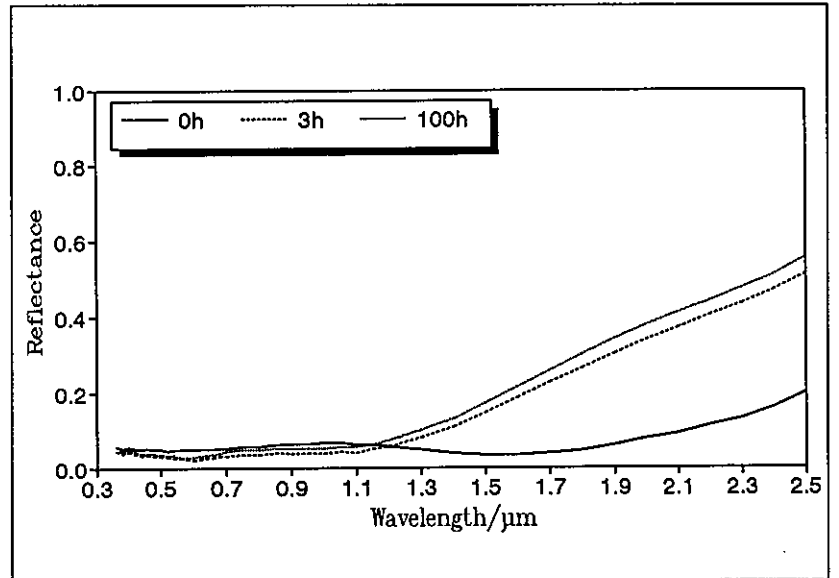
400 °C

Time, h	α_s	ε_n (373 K)
0	0.943	0.21
3	0.926	
6	0.928	
10	0.926	
20	0.920	
50	0.920	
100	0.911	0.13
500	0.849	0.14
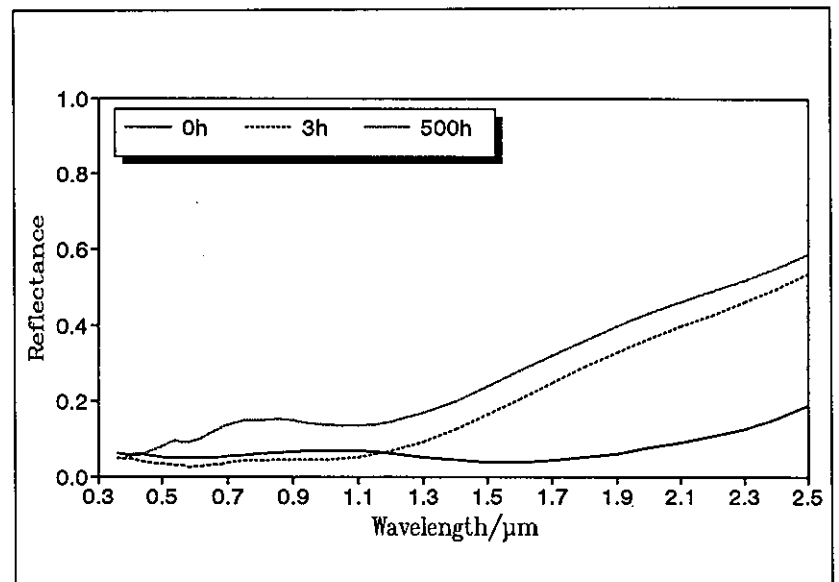
Table 5;5 cont

430 °C

Time, h	α_s	ε_n (373 K)
0	0.941	
3	0.873	
6	0.865	
20	0.848	
100		
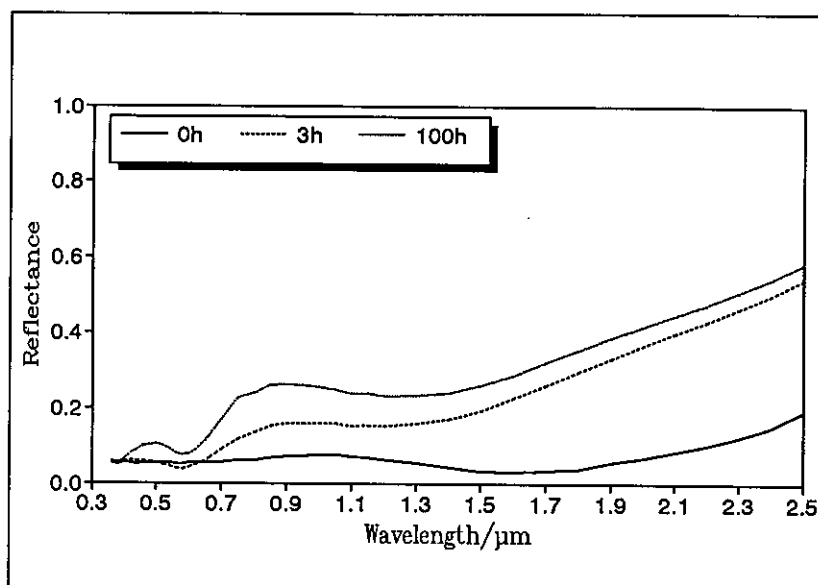
450 °C

Time, h	α_s	ε_n (373 K)
0	0.944	0.21
1	0.919	
3	0.910	
6	0.899	
10	0.885	
20	0.863	0.12
50	0.832	0.15
100	0.806	
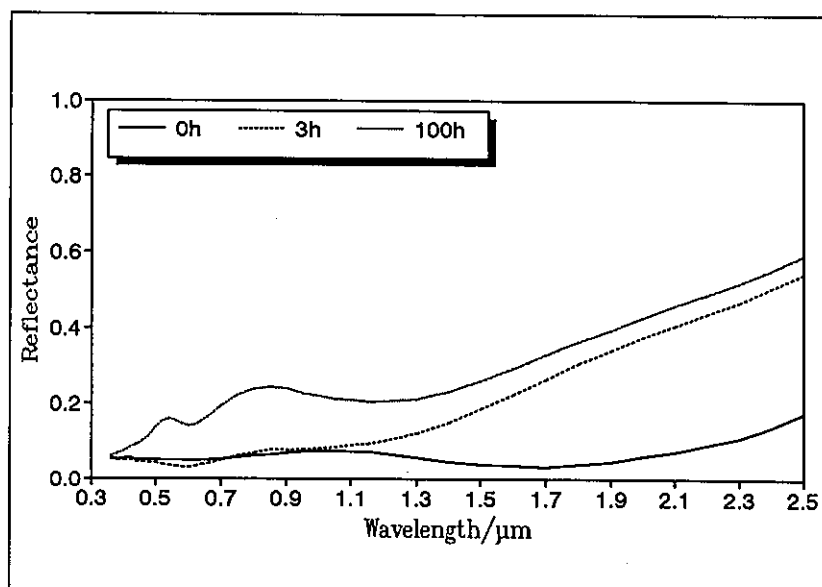
Table 5;5 cont.

500 °C

| Time, h	α_s	ε_n (373 K)
0	0.941	0.20
3	0.860	
6	0.835	
10	0.815	
20	0.794	0.13
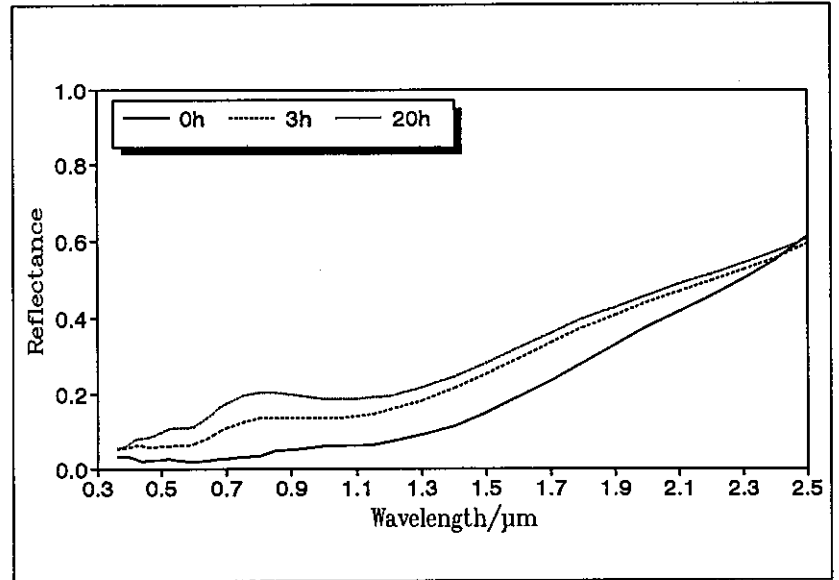
550 °C

Time, h	α_s	ε_n (373 K)
0	0.946	
1	0.831	0.20
3	0.794	
6	0.780	
10	0.770	0.14
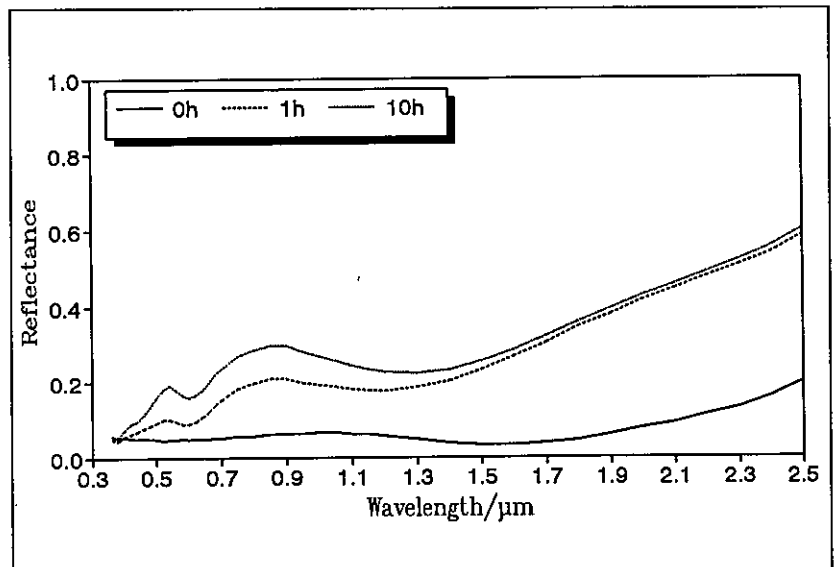
Table 5;5 cont.

600 °C

| Time, h	α_s	ε_n (373 K)
0	0.946	0.20
1	0.766	
3	0.754	
6	0.754	
10	0.741	0.12
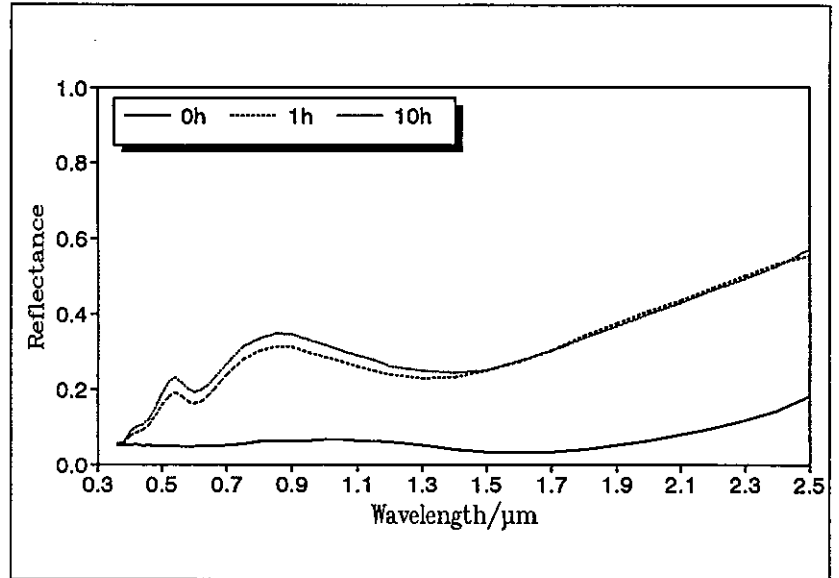
500 °C in vacuum
500 °C in air
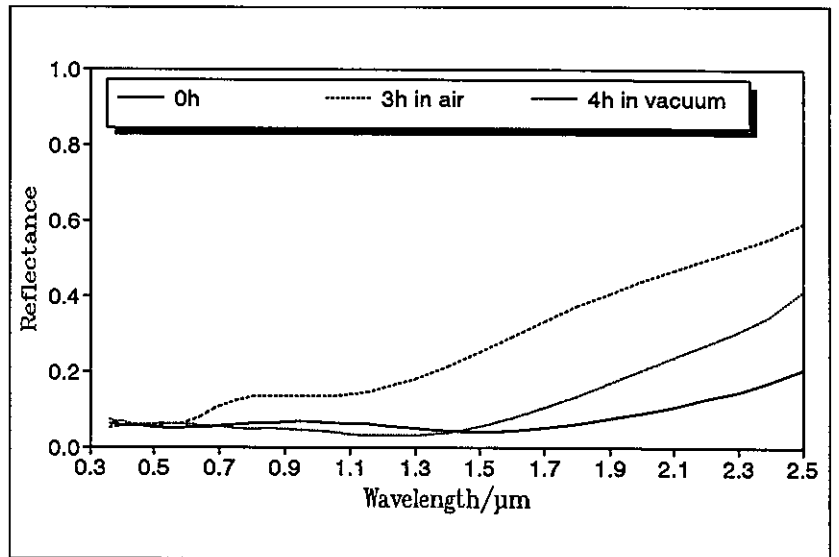
Table 5;6 *Results from high-temperature ageing tests of MTI black chrome absorber coating*

300 °C

Time, h	α_s	ε_n (373 K)
0	0.969	0.09
3	0.952	0.06
10	0.947	0.06
20	0.943	0.09
100	0.936	0.07
530	0.923	
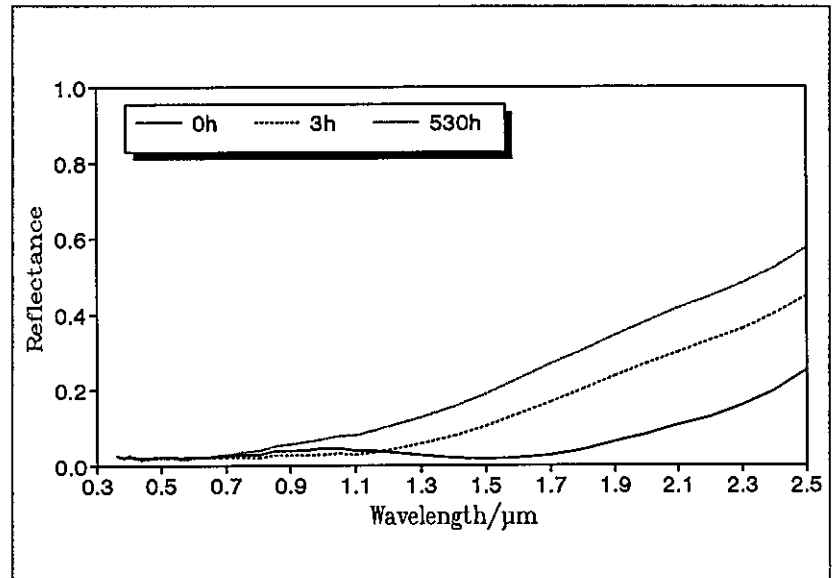
330 °C

Time, h	α_s	ε_n (373 K)
0	0.965	
20	0.927	
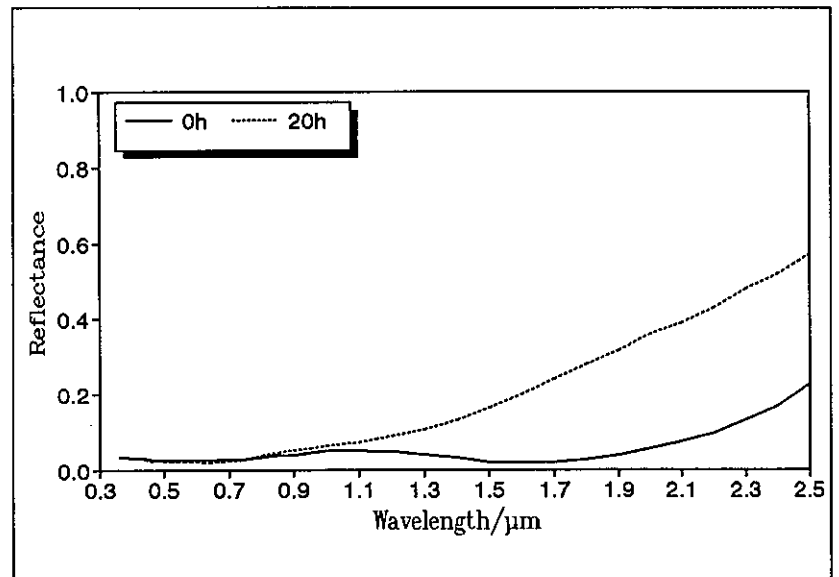
Table 5;6 cont.

350 °C

Time, h	α_s	ε_n (373 K)
0	0.970	0.08
3	0.938	0.06
6	0.930	
10	0.920	0.07
20	0.919	0.07
50	0.906	0.06
100	0.909	0.05
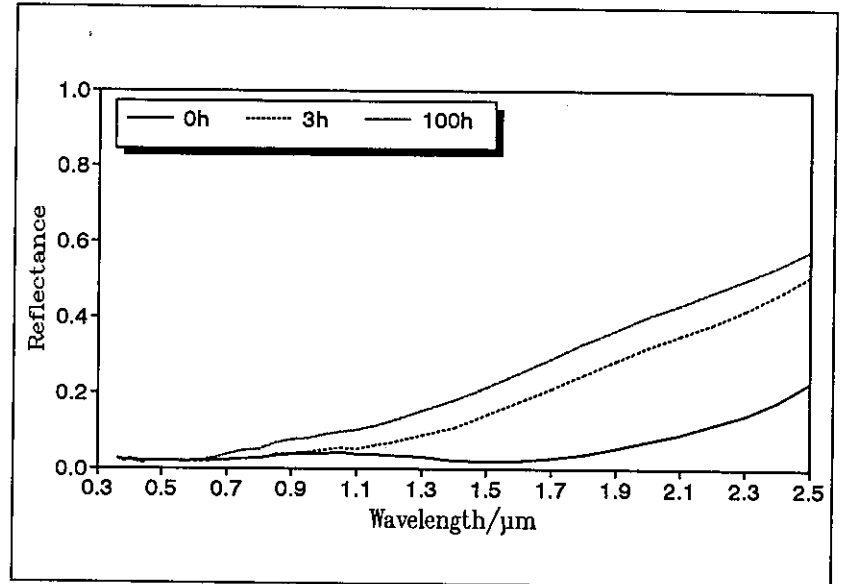
370 °C

| Time, h	α_s	ε_n (373 K)
0	0.972	
20	0.918	
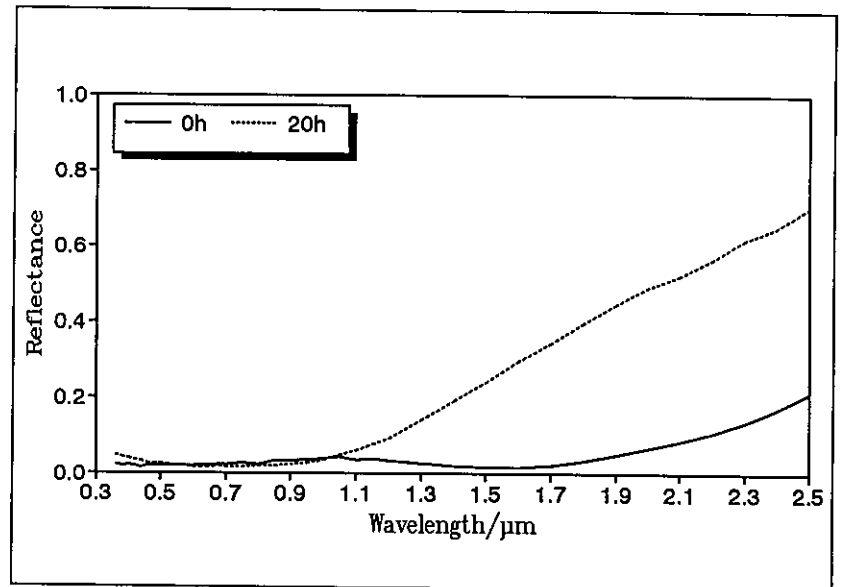
Table 5;6 cont.

400 °C

Time, h	α_s	ε_n (373 K)
0	0.971	
20	0.915	
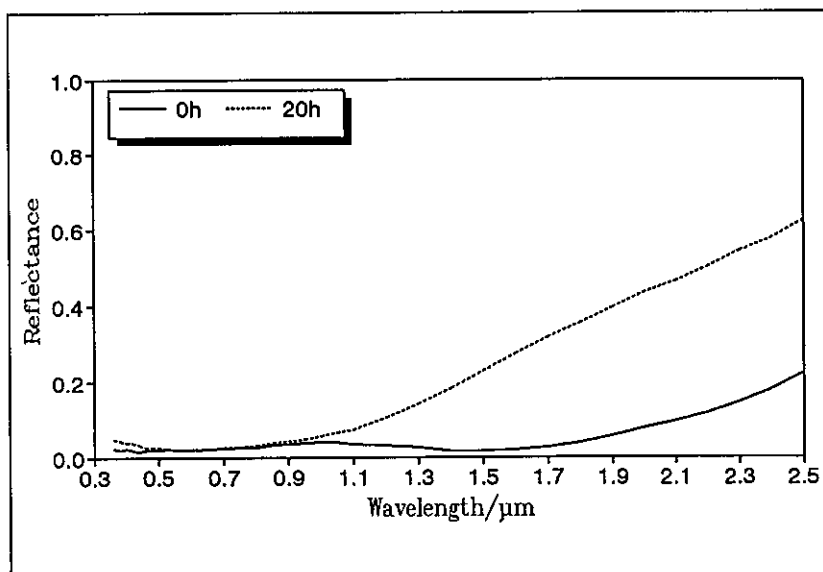
430 °C

| Time, h	α_s	ε_n (373 K)
0	0.971	0.08
3	0.894	0.05
6	0.884	0.06
20	0.866	0.07
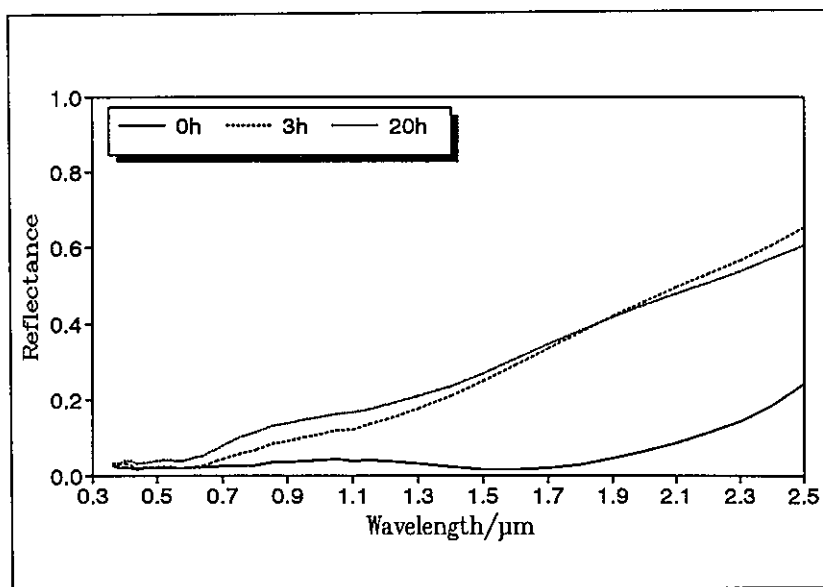
Table 5;6 cont.

450 °C

Time, h	α_s	ε_n (373 K)
0	0.969	
1	0.903	
3	0.880	
6	0.868	
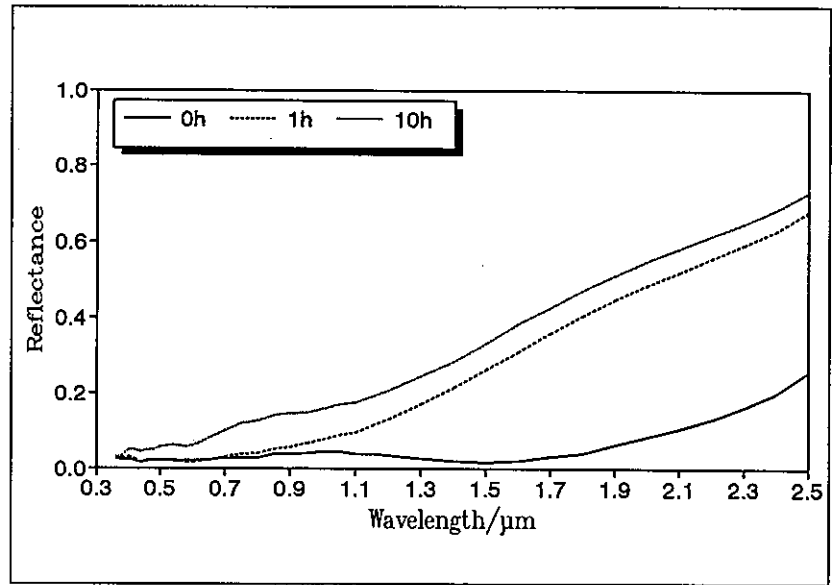
450 °C in vacuum
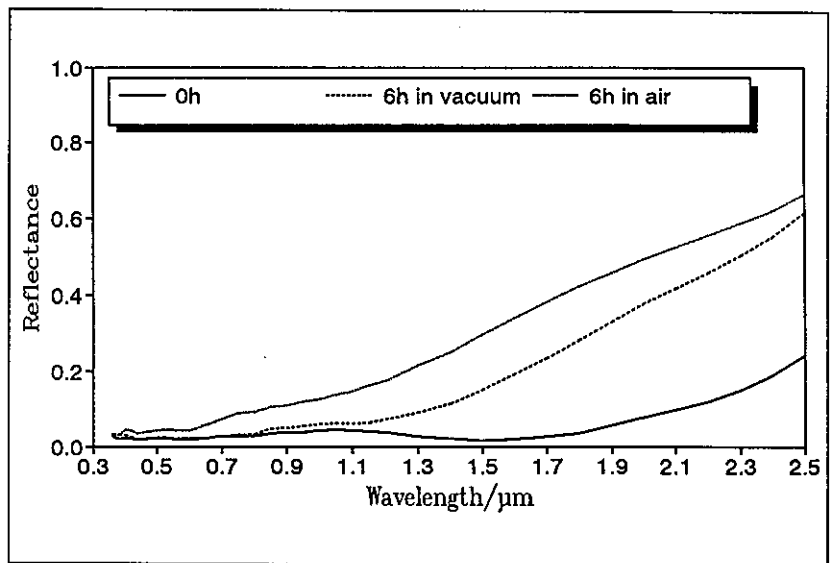
Table 5;7 *Results from high-temperature ageing tests of the Showa Nickel pigmented anodized aluminium absorber coating.*

300 °C

Time, h	α_s	ε_n (373 K)
0	0.928	0.12
3	0.907	
10	0.914	0.11
20	0.912	0.11
100	0.907	0.11
530	0.902	
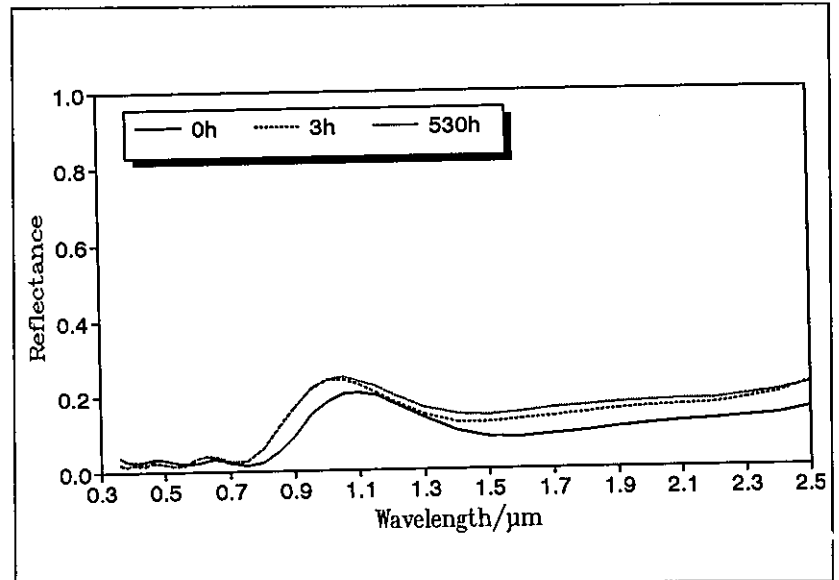
330 °C

Time, h	α_s	ε_n (373 K)
0	0.927	0.14
3	0.896	
20	0.896	0.10
100	0.892	0.10
500	0.892	0.11
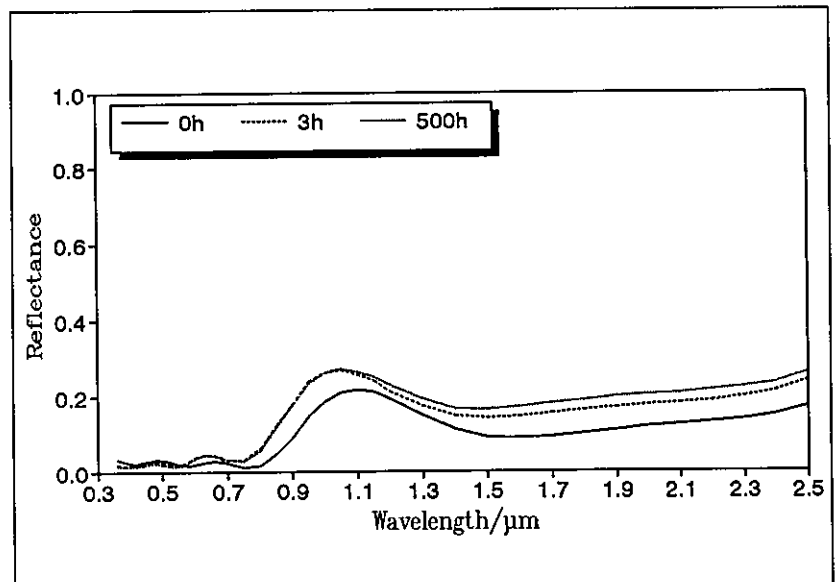
Table 5;7 cont.

350 °C

Time, h	α_S	ε_n (373 K)
0	0.924	0.12
3	0.884	0.12
6	0.891	
10	0.891	
20	0.889	
50	0.887	
100	0.874	
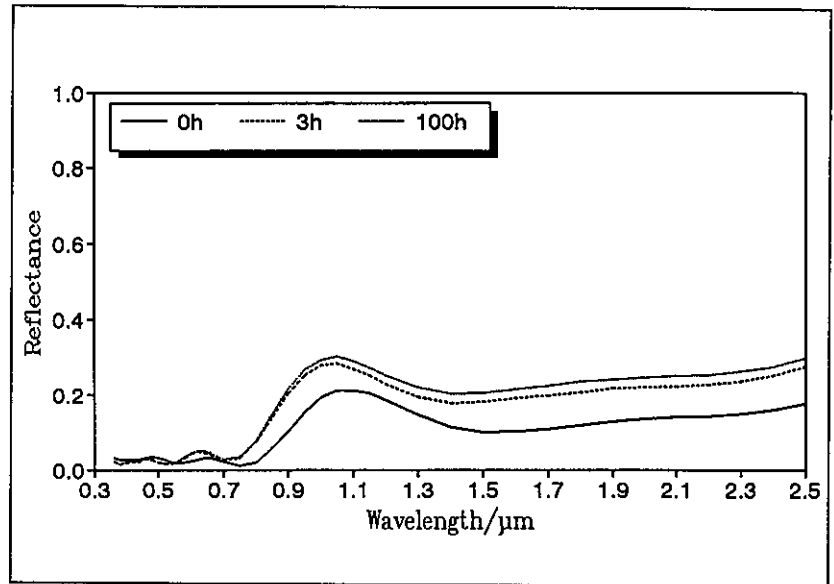
380 °C

Time, h	α_S	ε_n (373 K)
0	0.919	0.09
3	0.884	
10	0.881	
50	0.878	
100	0.875	0.08
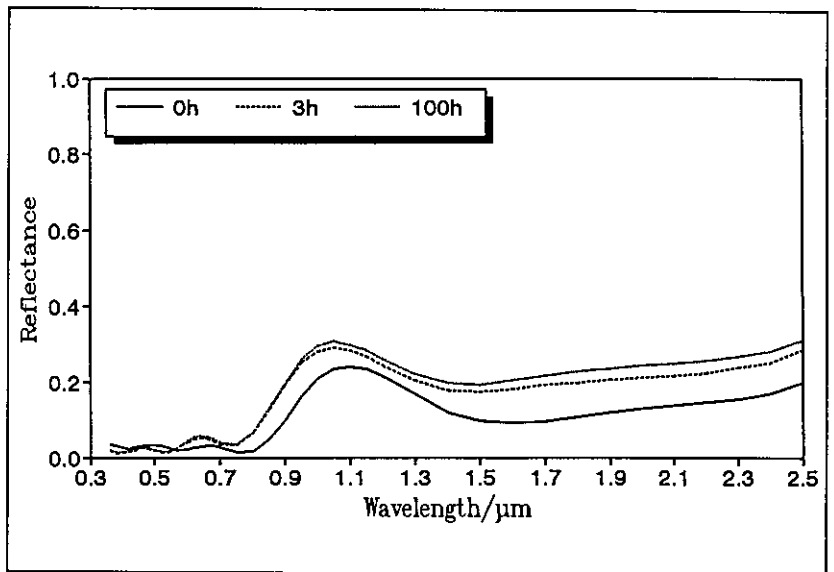
Table 5;7 cont.

400 °C

Time, h	α_s	ε_n (373 K)
0	0.938	0.14
3	0.906	
6	0.908	
10	0.907	
20	0.904	
50	0.905	
100	0.900	0.11
500	0.891	0.12
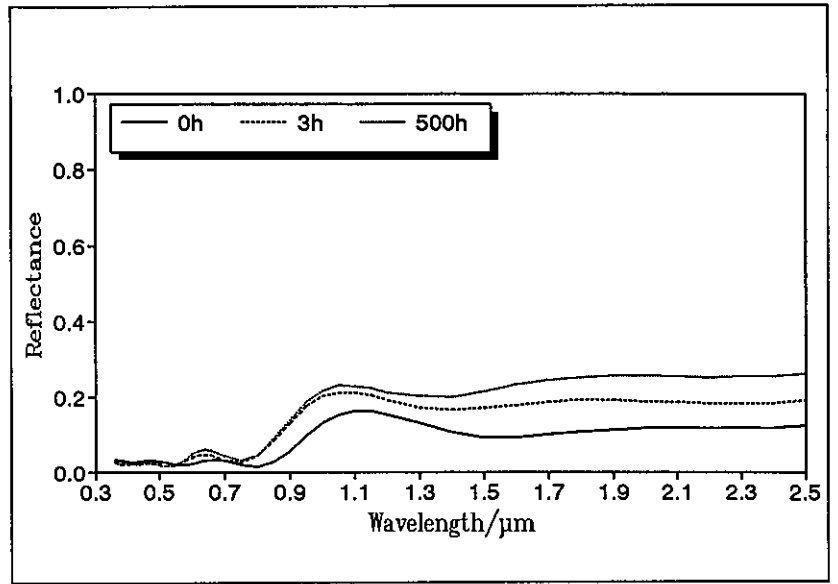
430 °C

| Time, h	α_s	ε_n (373 K)
0	0.939	0.12
3	0.905	
6	0.913	
20	0.899	0.10
100		
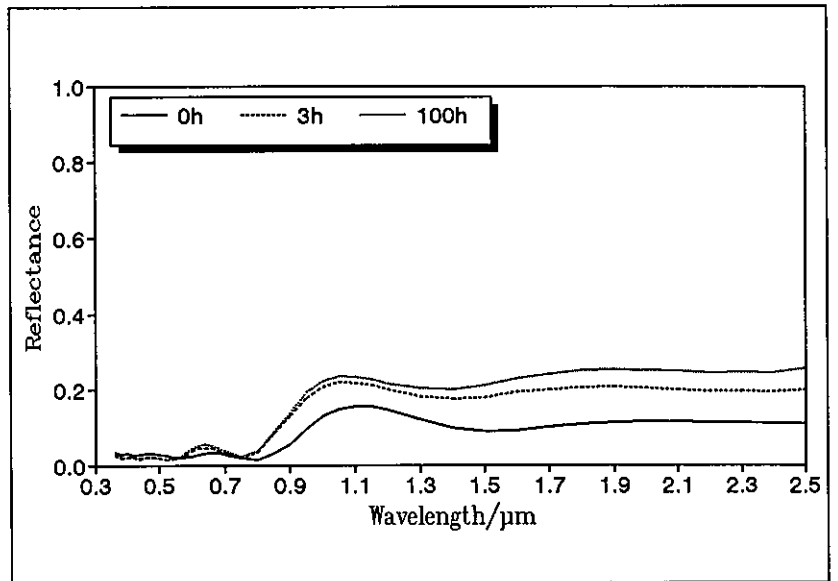
Table 5;7 cont.

450 °C

Time, h	α_s	ε_n (373 K)
0	0.935	0.14
3	0.900	
6	0.894	
10	0.895	
20	0.891	
50	0.887	
100	0.894	0.11
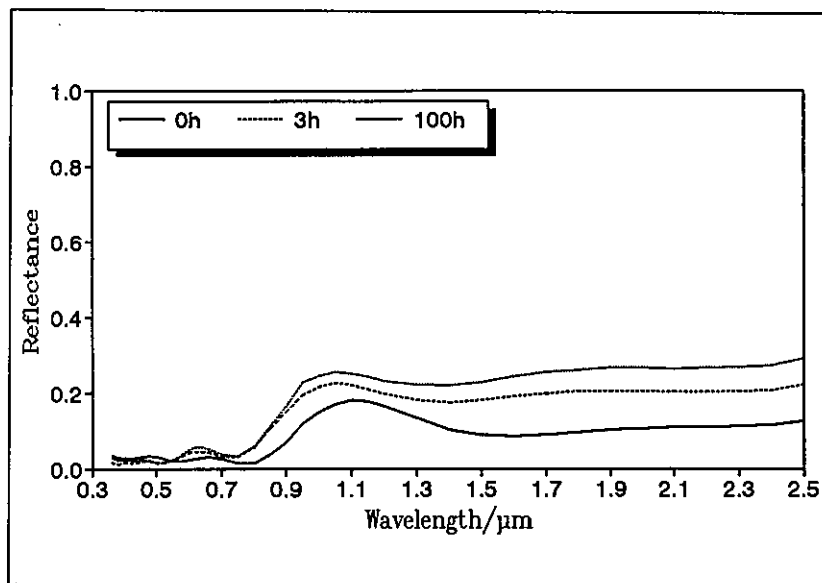
500 °C

Time, h	α_s	ε_n (373 K)
0	0.921	0.12
6	0.831	
10	0.823	
20	0.813	0.07
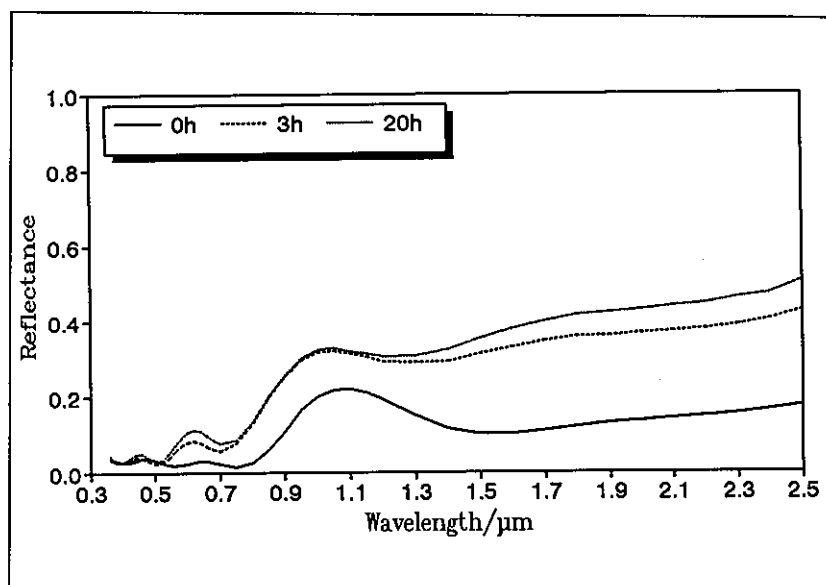
Table 5;7 cont.

550 °C

Time, h	α_s	ε_n (373 K)
0	0.919	
1	0.846	0.12
3	0.843	
6	0.82	
10	0.805	0.06
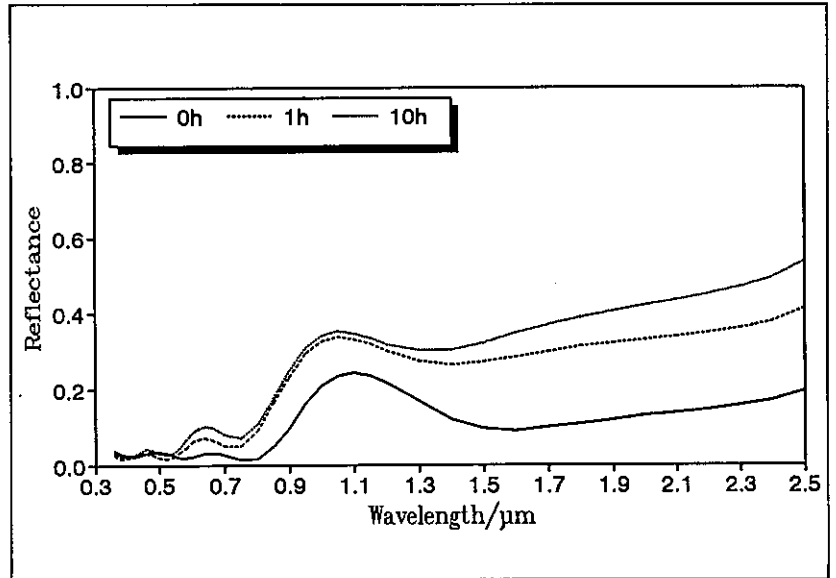
600 °C

Time, h	α_s	ε_n (373 K)
0	0.927	0.10
1	0.835	
3	0807	
6	0.764	
10	0.737	0.06
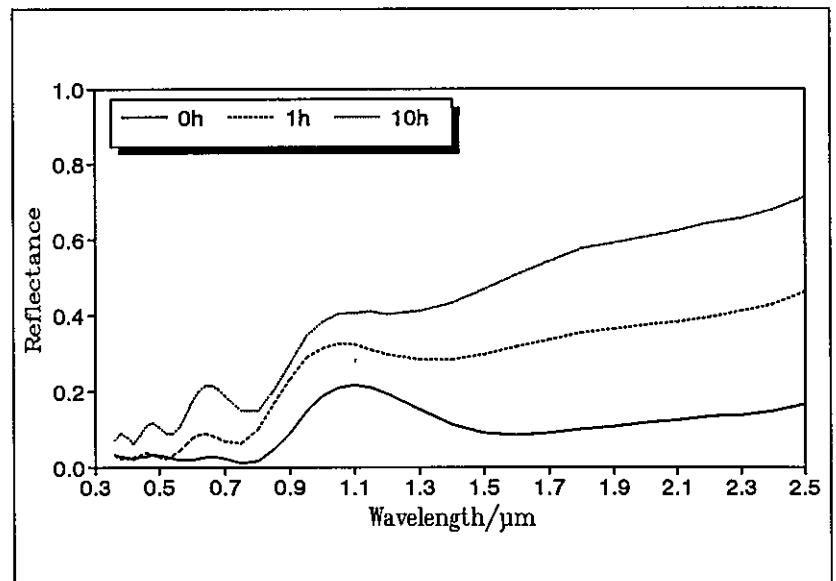
Table 5;7 cont.

500 °C in vacuum
500 ° in air

Legend: 0h — ; 6h in air ········ ; 6h in vacuum ———
Y-axis: Reflectance (0.0 to 1.0)
X-axis: Wavelength/µm (0.3 to 2.5)
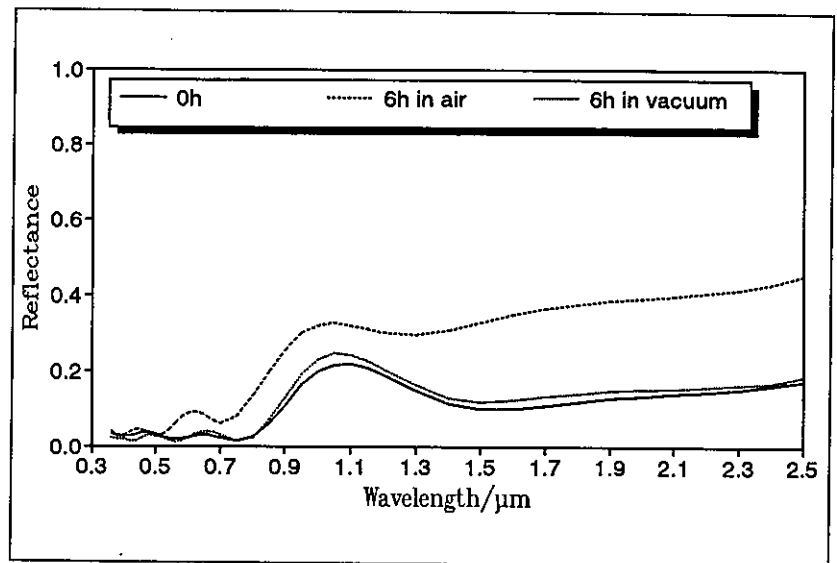
**Table 5;8** *Results from high-temperature ageing tests of the Sunstrip Nickel-pigmented anodized aluminium absorber coating.*

300 °C

Time, h	α_s	ε_n (373 K)
0	0.876	0.09
3	0.859	
10	0.851	
20	0.849	0.07
100	0.849	0.07
530	0.839	
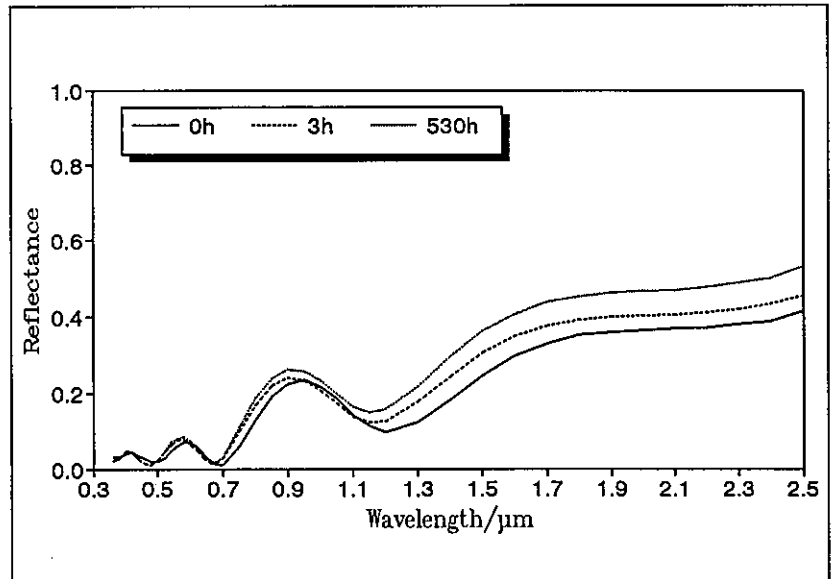
330 °C

| Time, h	α_s	ε_n (373 K)
0	0.893	0.12
3	0.876	
20	0.872	0.11
100	0.861	0.12
500	0.866	0.11
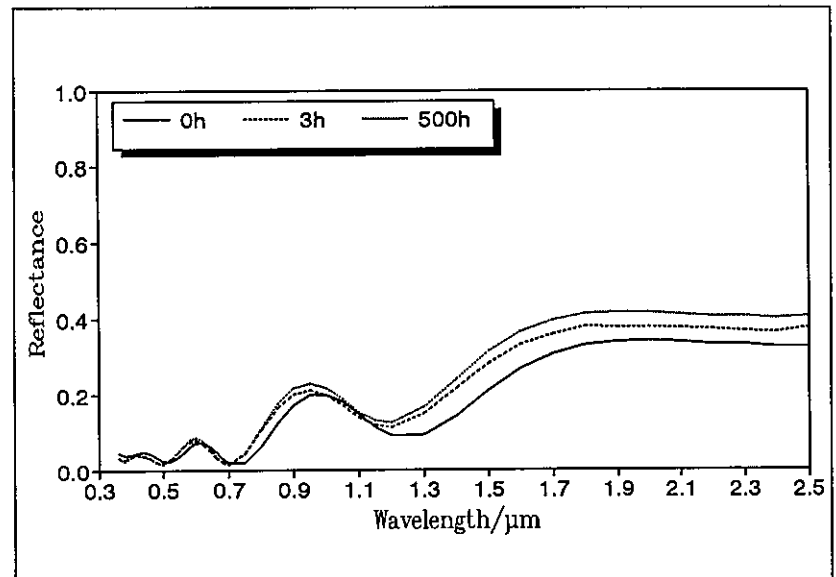
Table 5;8 cont.

350 °C

Time, h	α_s	ε_n (373 K)
0	0.887	0.09
3	0.863	0.09
6	0.869	
10	0.861	
20	0.867	
50	0.856	
100	0.852	
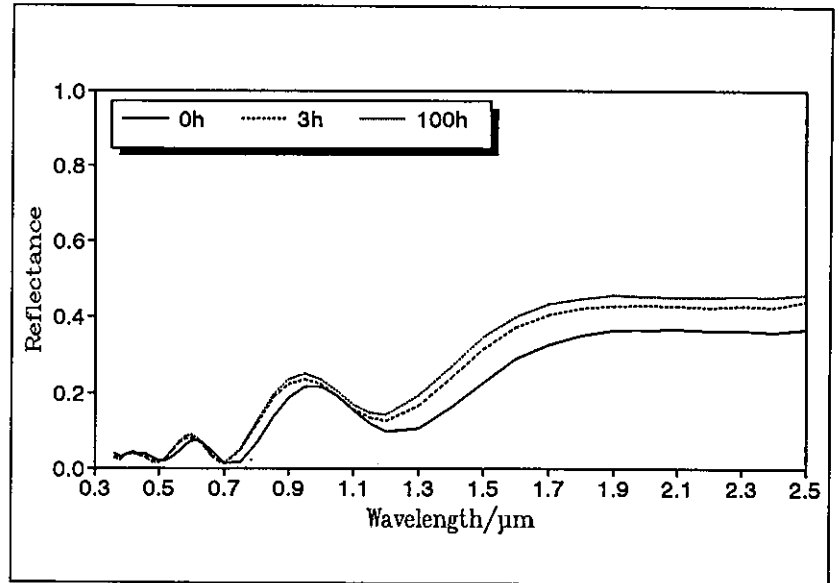
380 °C

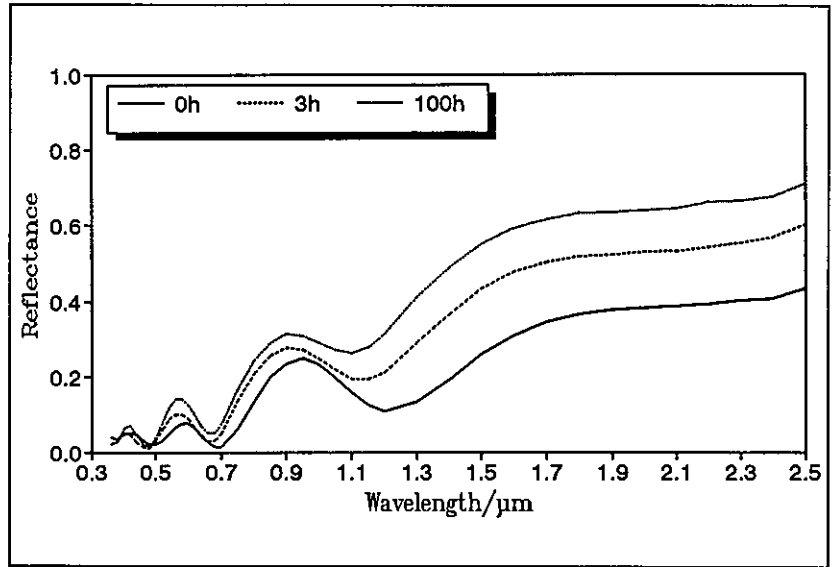| Time, h	α_s	ε_n (373 K)
0	0.888	0.11
3	0.864	
10	0.858	
50	0.855	
100	0.849	0.1
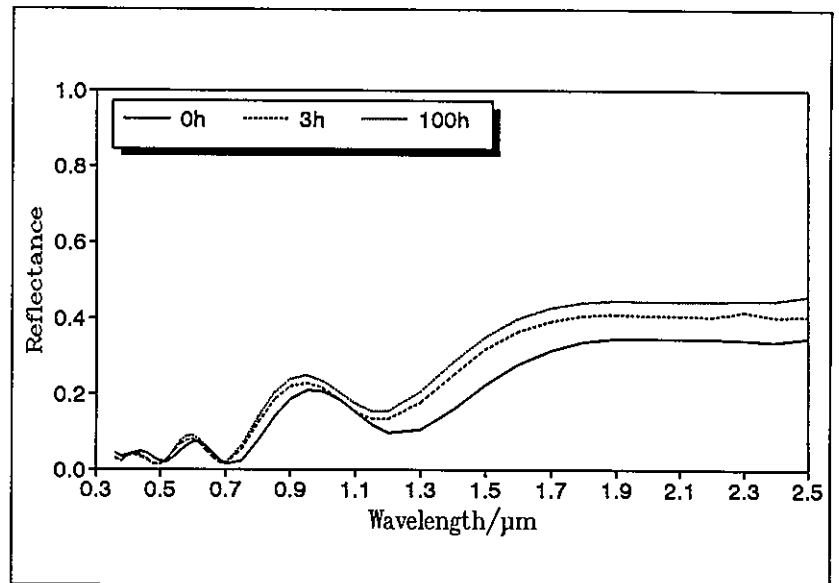
Table 5;8 cont.

400 °C

Time, h	α_s	ε_n (373 K)
0	0.871	0.07
3	0.831	
6	0.837	
10	0.834	
20	0.824	
50	0.82	
100	0.815	0.06
500	0.784	0.08
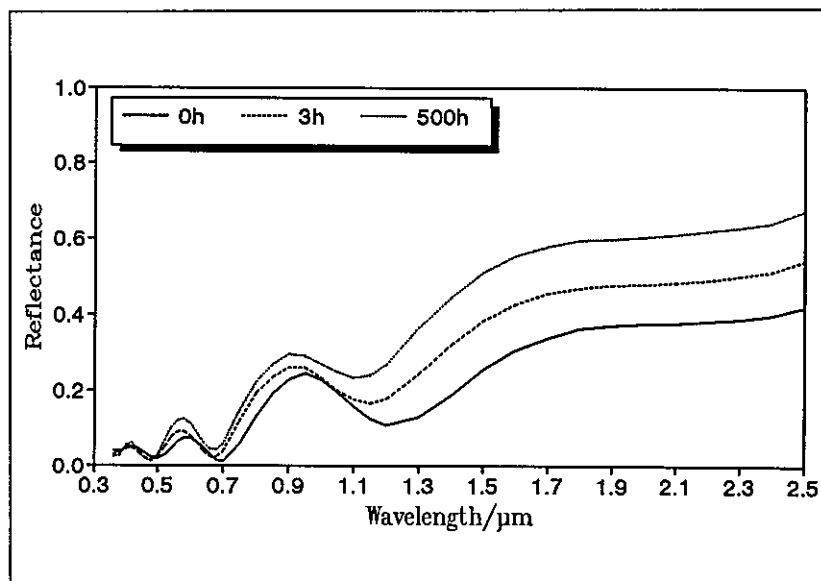
430 °C

Time, h	α_s	ε_n (373 K)
0	0.892	
3	0.857	
6	0.853	
20	0.844	
100		
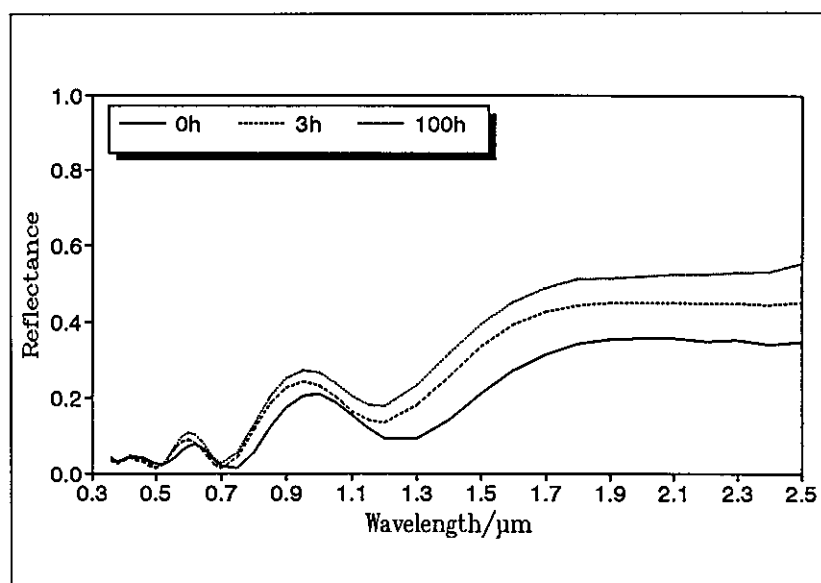
Table 5;8 cont.

450 °C

Time, h	α_s	ε_n (373 K)
0	0.868	0.14
3	0.812	
6	0.813	
10	0.801	
20	0.791	
50	0.772	
100	0.762	

500 °C

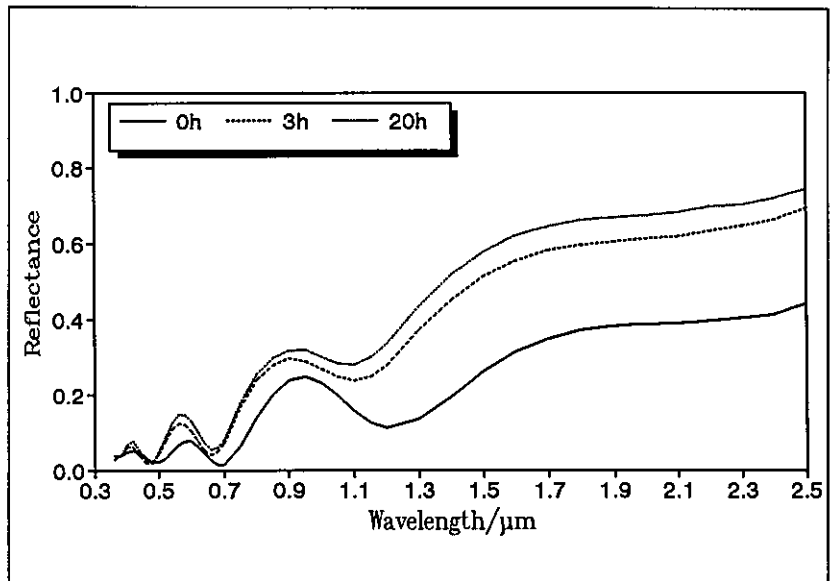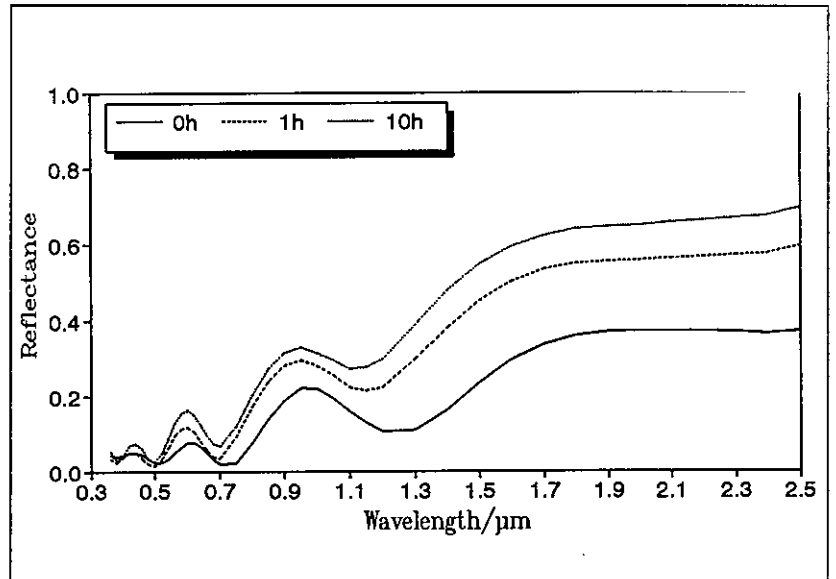| Time, h	α_s	ε_n (373 K)
0	0.867	0.07
3	0.779	
6	0.773	
10	0.751	
20	0.741	0.07

Table 5;8 cont.

550 °C

Time, h	α_s	ε_n (373 K)
0	0.883	
1	0.806	
3	0.790	
6	0.763	
10	0.762	

600 °C

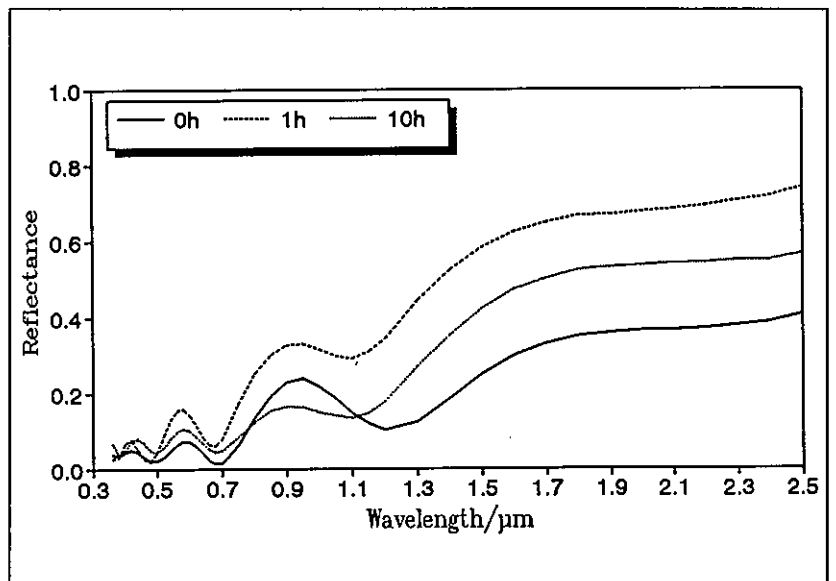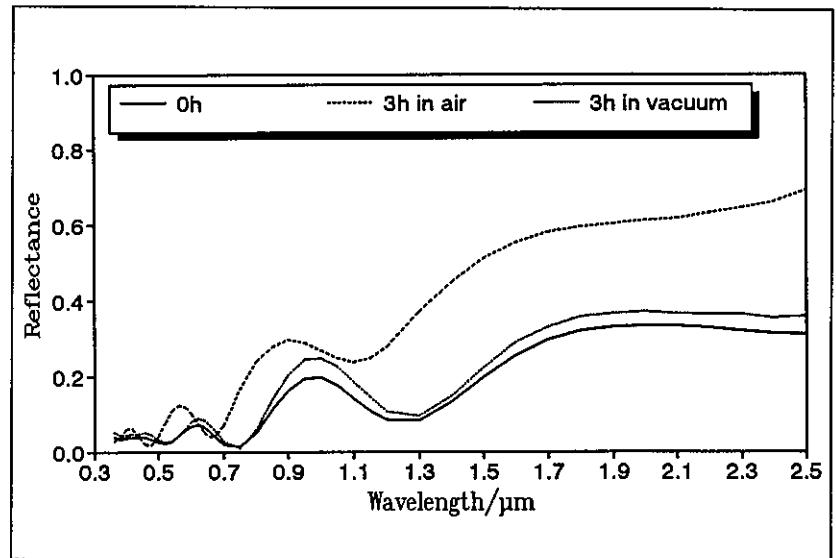| Time, h	α_s	ε_n (373 K)
0	0.874	
1	0.746	
6	0.842	
10	0.837	

Table 5;8 cont.

500 °C in vacuum
500 ° in air

5.3 High-humidity Exposure and Condensation Testings

The intent of conducting the humidity testing programme was above all to get a better insight into the durability properties of coatings when exposed to conditions close to condensation and at condensation conditions.

5.3.1 Equipment and ageing procedures for testing

High-humidity tests

A commercially available humidity cabinet was used for all tests. The only modification made was changing the temperature controller and the fan of the humidity bath. These changes were necessary in order to extend the humidity range at 90 °C from 95 % RH to 98 % RH. In addition, the temperature and humidity controls of the cabinet were carefully calibrated to improve the absolute accuracy of those parameters. Temperature and relative humidity were continuously measured near the samples by means of a combined temperature and capacitance humidity sensor (Rotronic) to check the functioning of the test cabinet during the whole test. This is of great importance as test periods up to more than 1000 hours were used. The specification of the cabinet used is given in *Table 5;9*.

Manufacturer	: Hubert Horstmann GmbH
Type	: HS 220 K30
Volume	: 0.22 m^3
Internal dimensions	: 0.61 x 0.61 x 0.61 m
Temperature range	: -20 - +180 °C
Humidity range (modified)	: 10 - 98 % RH (18 - 90 °C)
Materials	: Stainless steel, glass
Temperature measurement	: Pt 100 sensor
Humidity measurement	: Psychrometer with Pt 100 sensors

Table 5;9 Specification of climatic cabinet used for the humidity tests.

When performing a humidity test, the cabinet has to reach the specified levels of temperature and humidity before the samples are placed into the cabinet. They are mounted electrically isolated from each other. If samples have to be measured with respect to degradation after a certain time they are taken out of the cabinet in such a way that no condensation can occur on the surface of samples; this means that the temperature and humidity level is lowered to 25 °C and 50 % RH. This procedure, including the interruption after the specified testing time, is computer-controlled.

A comprehensive analysis of the reproducibility of the high-humidity test method used for the work of the case study requires detailed knowledge of coating properties and the variation in coating properties. It has therefore not been possible to carry out this work in a systematic way.

However, a critical point in performing high-humidity tests is the measurement and the control of the relative humidity and the temperature in the cabinet. *Table 5;10* lists requirements for temperature and humidity stability and accuracy which must be fulfilled.

|	
Temperature constancy over time	± 1 K
Relative humidity constancy over time	± 2 % RH
Absolute accuracy of temperature	± 0.3 K
Absolute accuracy of relative humidity	± 1 % RH

Table 5;10 *Requirements for the accuracy of temperature and relative humidity of a climatic cabinet to be used for high-humidity tests .*

Commercially available climatic cabinets to be used for high-humidity tests (98-99 % RH) must consequently be carefully checked to make sure that they fulfil these requirements.

Condensation tests

The same humidity cabinet, as described above, was also used for the condensation tests. The samples were fixed electrically isolated from each other and in very good thermal contact with a fluid-cooled sample holder (see *Figure 5;2*), specially developed for this purpose. During the test, the temperature of the holder was kept at about 5 K below the surrounding temperature, i.e. the temperature of cabinet. The cabinet was operating at a humidity level of about 95 % RH. These operating conditions led to constant condensation on the surface of samples during the test.

Apart from the different operating conditions for samples, the applied procedure for testing was the same as for the high-humidity tests described above.
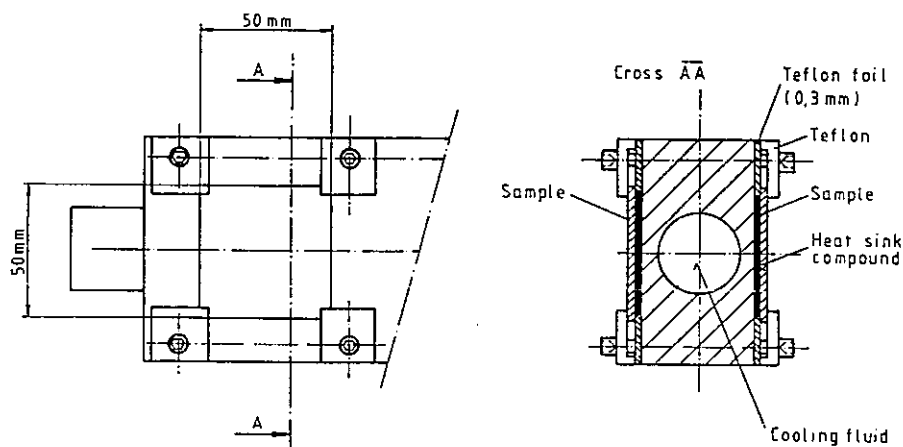
Figure 5;12   *Schematic drawing of the sample holder used for condensation testing*

The crucial point in ensuring a high reproducibility of the condensation tests is the careful mounting of the samples on the sample holder. A thin layer of an electrically isolating heat sink compound in combination with a teflon foil for distance control is needed to guarantee good thermal contact. The arrangement made also means that bimetallic corrosion will be prevented. In addition, the temperature of the fluid circulated through the sample holder has to be controlled by a thermostatic bath to within ± 0.5 K. The same requirements for the climatic chamber as listed in *Table 5;10* also apply for these tests.

To check the reproducibility of the condensation tests, a series of tests were performed under the same test conditions with different samples. The results are shown in *Figure 5;13*. Apart from · the fact that the initial condition of samples is different from one sample to another, due to inhomogenities, the results obtained are fairly good.
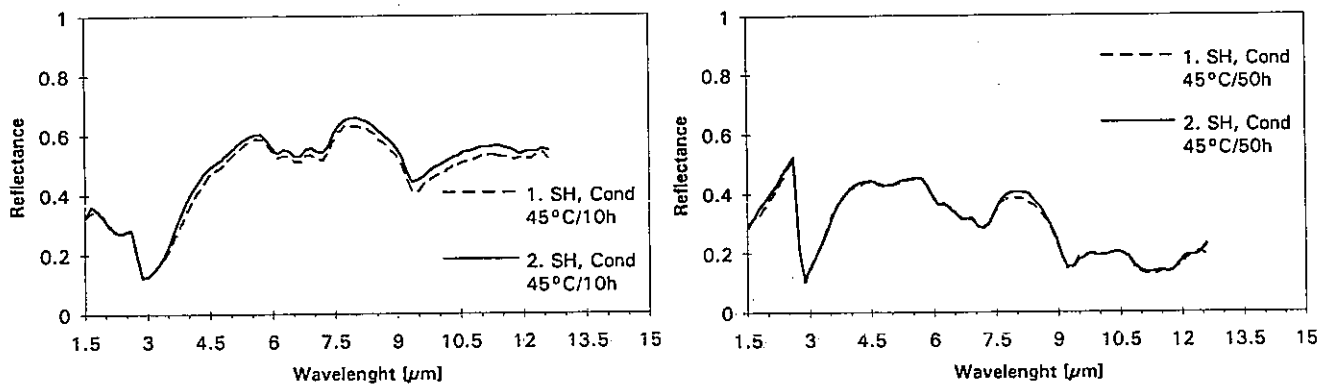
Figure 5;13 Check of reproducibility of condensation tests

5.3.2 Ageing test results

Table 5;11 presents an overview of all high-humidity tests and condensation tests performed in the case study. Results for the different absorber coating materials are presented in *Tables 5;12 - 5;15*.

Table 5;11 Overview of high-humidity and condensation tests performed

Test cond. A/B/C	Showa	Sunstrip	En.-Solaire	MTI	0	<3	<10	<50	<100	<200	<300	<700	<1000	<1300
50/95/50	×	×	×	×	×					×	×		×	
70/95/70	×	×	×	×	×					×	×		×	
90/95/90	×	×	×	×	×					×	×		×	
50/99/50	×	×	×	×	×					×	×		×	
90/99/90	×	×	×	×	×					×	×		×	
18/95/12	×	×	×	×	×	×				×	×			×
25/95/20	×	×			×			×		×	×			×
30/95/25	×	×			×					×		×		
35/95/30	×	×			×	×	×	×		×				
50/95/45	×	×	×	×	×	×	×	×		×	×	×		
50/95/40[1]	×	×	×	×	×	×	×	×			×			
50/95/45[2]	×	×			×	×	×	×						
50/95/45	×	×			×	×	×	×		×				
70/95/65	×	×	×	×	×	×	×	×		×	×	×		
90/95/85	×	×	×	×	×	×	×	×		×	×	×		

Column header: Tested absorber coatings (Showa, Sunstrip, En.-Solaire, MTI); Test duration, h (0, <3, <10, <50, <100, <200, <300, <700, <1000, <1300)

A: Temperature of the cabinet [°C]
B: Relative humidity of the cabinet [% RH]
C: Temperature of the sample [°C]

1):Serial test: high-temperature test (400 °C) followed by a condensation test
2):Serial test: condensation test followed by a high temperature test (400 °C)

Table 5;12   Results from high-humidity tests and condensation-tests for the Showa nickel-pigmented anodized aluminium absorber coating

High humidity Tests

Cabinet: 50 °C, 95 % RH
Sample: 50 °C

Time, h	α_s	ε_n(373 K)
0	0.916	0.131
150	0.916	0.134
300	0.917	0.129
800	0.916	0.133

Cabinet: 70 °C, 95 % RH
Sample: 70 °C

Time, h	α_s	ε_n(373 K)
0	0.932	0.150
150	0.928	0.151
300	0.929	0.154
800	0.930	0.151
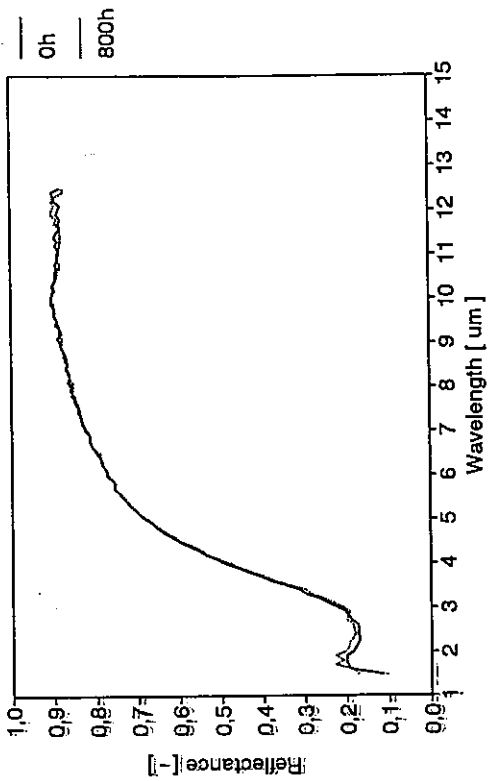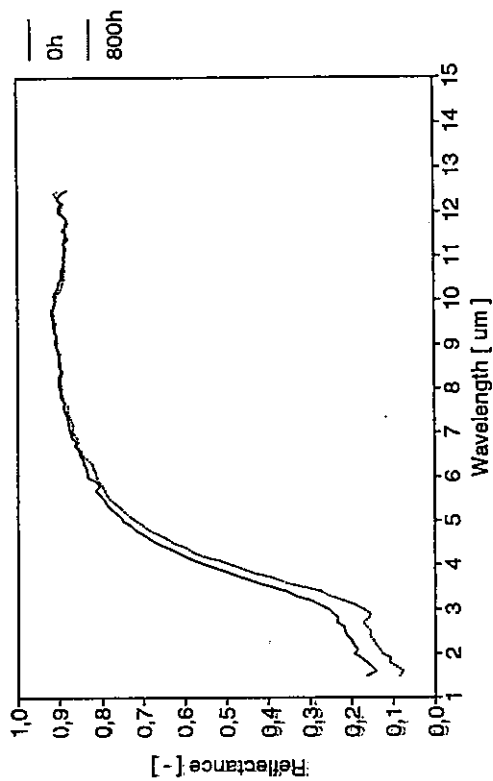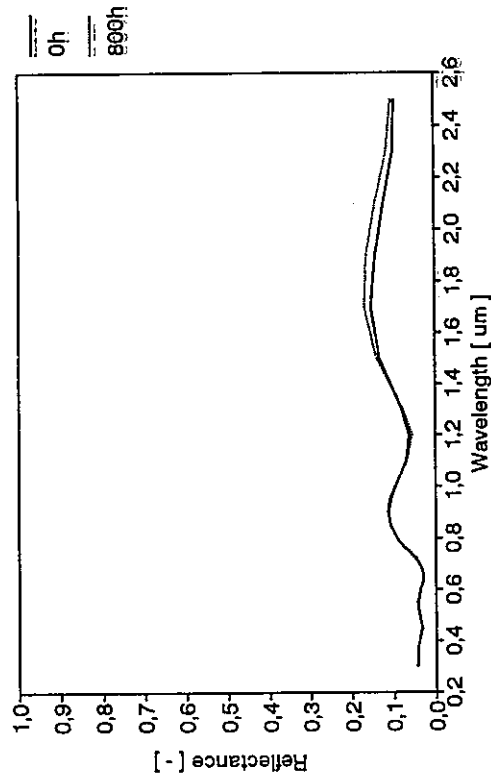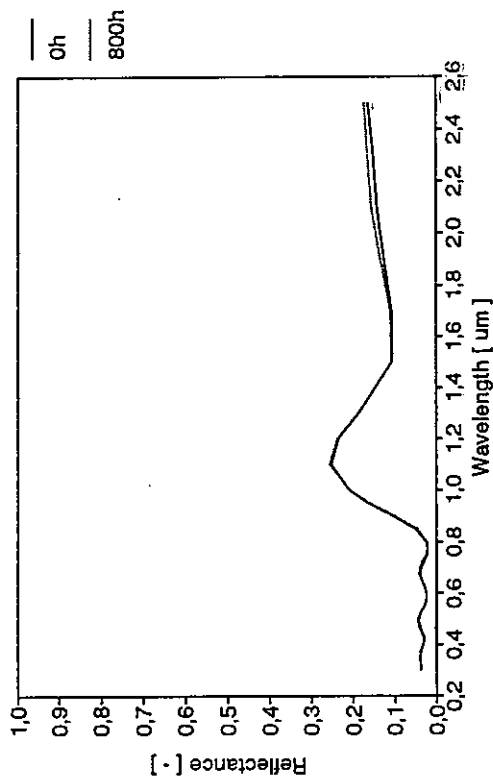
Table 5:12 cont.

Cabinet: 90 °C, 95 % RH
Sample: 90 °C

Time, h	α_s	$\varepsilon_n(373\ K)$
0	0.931	0.150
150	0.932	0.150
800	0.929	0.151

Cabinet: 50 °C, 99 % RH
Sample: 50 °C

Time, h	α_s	$\varepsilon_n(373\ K)$
0	0.879	-
150	0.921	0.120
300	0.920	0.120
900	0.919	0.122

Table 5;12 cont.

Cabinet: 90 °C, 99 % RH
Sample: 90 °C

Legend: 0h — 150h — 300h — 1000h
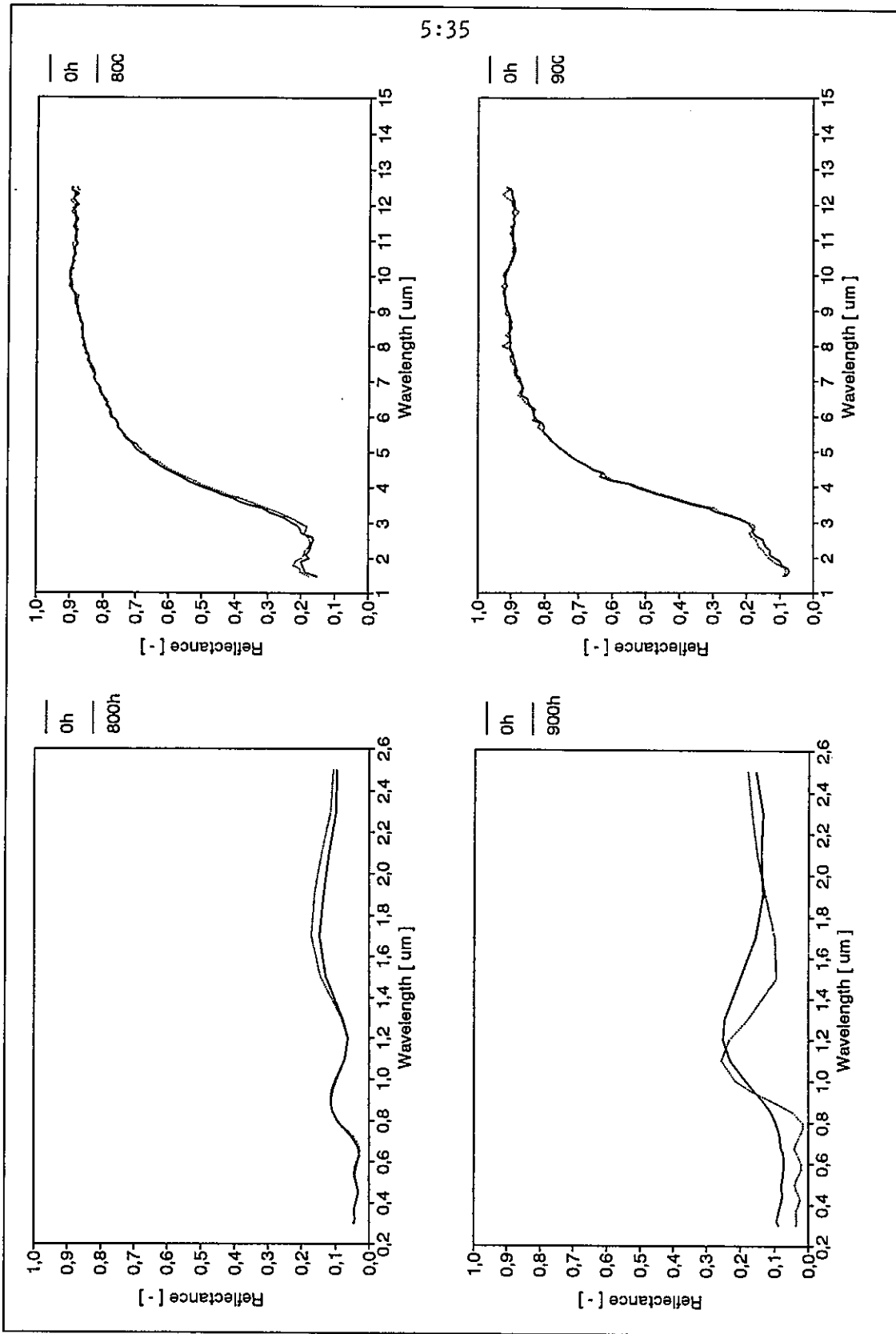
Time, h	α_s	ε_n(373 K)
0	0.880	0.126
150	0.912	0.127
300	0.897	0.148
1000	0.884	0.163

Reflectance [-] vs Wavelength [um]

Condensation Tests
Cabinet: 18 °C, 95 % RH
Sample: 12 °C

Legend: 0h — 1150h
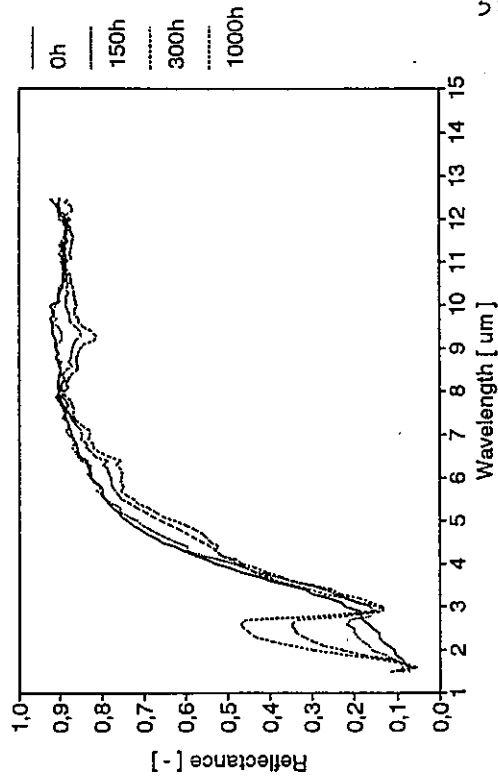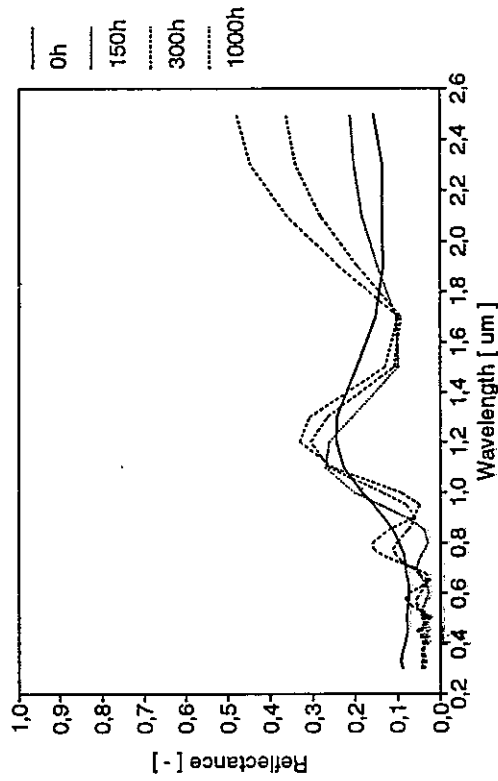
Time, h	α_s	ε_n(373 K)
0	0.878	0.125
3	0.920	0.121
10	0.922	0.127
110	0.923	0.122
300	0.924	0.129
650	0.925	-
1150	0.921	0.135

Reflectance [-] vs Wavelength [um]
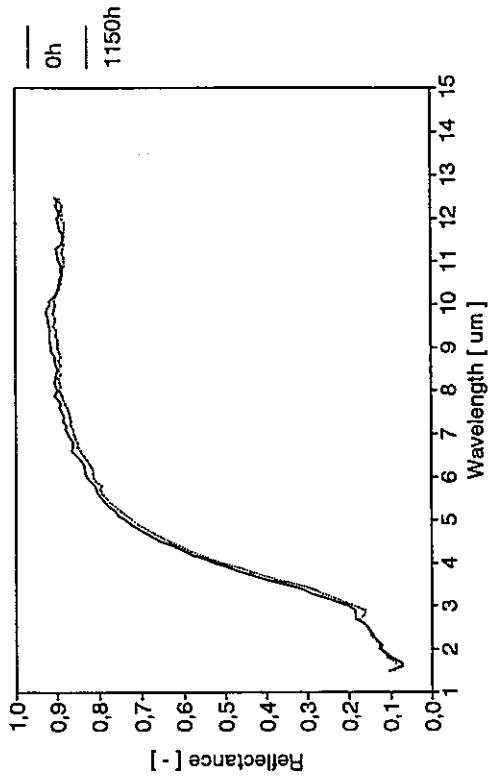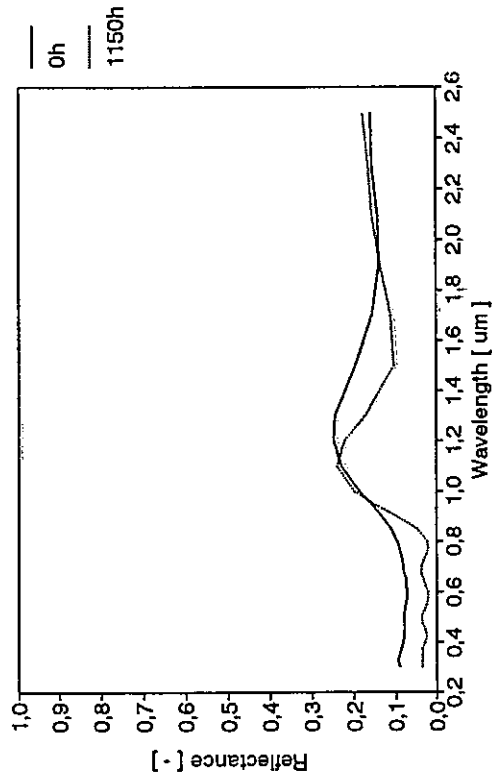
Table 5;12 cont.

Cabinet: 25 °C, 95 % RH
Sample: 20 °C

| Time, h	α_s	ε_n(373 K)
0h	0.934	0.136
50	0.935	0.133
150	0.935	0.135
300	0.938	0.142
650	0.941	0.228
1250	0.900	0.804

Cabinet: 30 °C, 95 % RH
Sample: 25 °C

Time, h	α_s	ε_n(373 K)
0	0.933	0.135
170	0.943	0.360
370	0.918	0.716
600	0.893	0.870
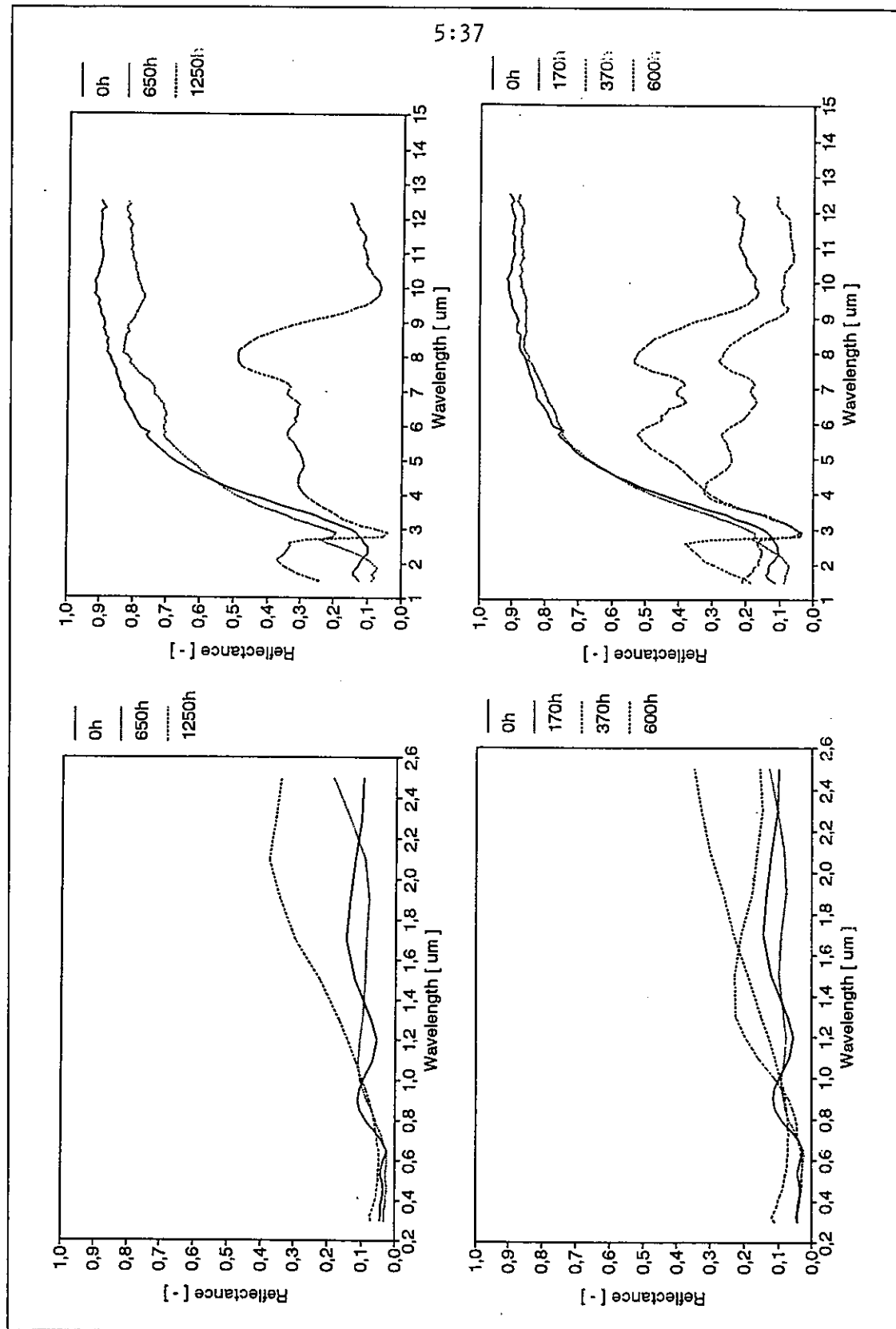
Table 5;12 cont.

Cabinet: 35 °C, 95 % RH
Sample: 30 °C

Time, h	α_S	ε_n(373 K)
0	0.933	0.138
3	0.933	0.139
10	0.937	0.138
50	0.941	0.204
200	0.912	0.869
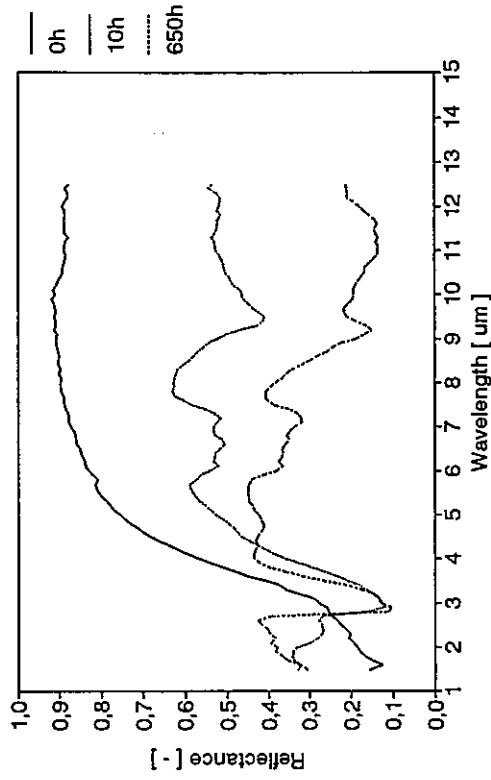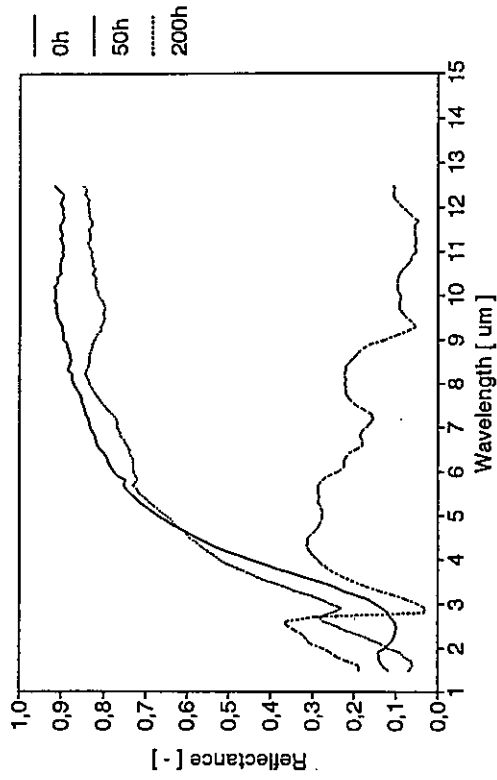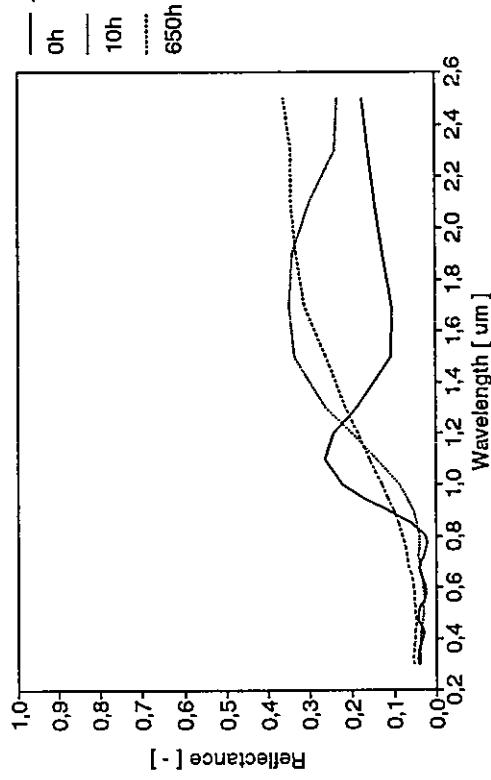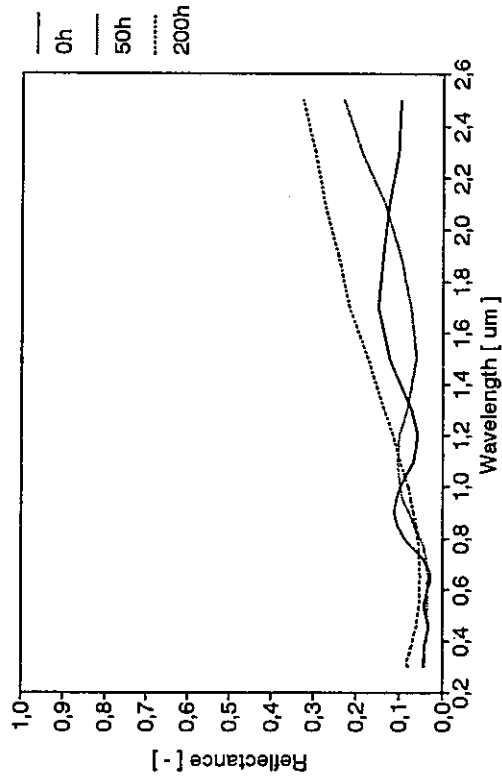
Cabinet: 50 °C, 95 % RH
Sample: 45 °C

Time, h	α_S	ε_n(373 K)
0	0.914	0.130
3	0.917	0.130
10	0.904	0.476
50	0.890	0.775
150	0.893	0.771
300	0.890	0.758
650	0.886	0.761

Table 12;5 cont.

Cabinet: 50 °C, 95 % RH
Sample: 45 °C

Time, h	α_s	ε_n(373 K)
0	0.910	0.134
20	0.880	0.710
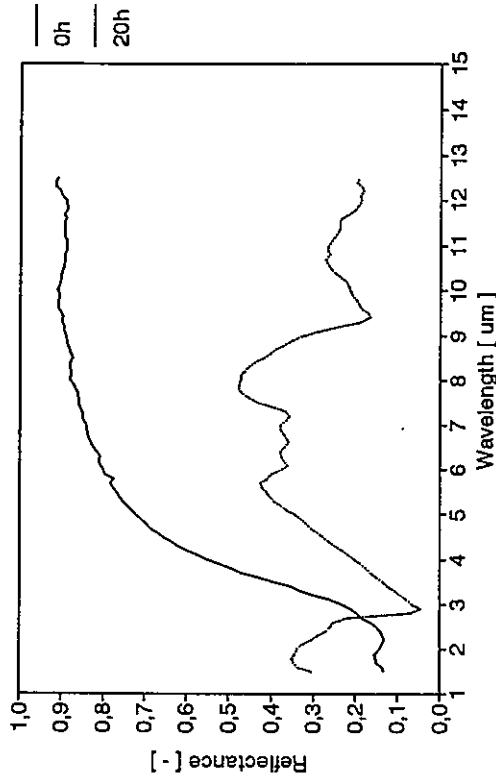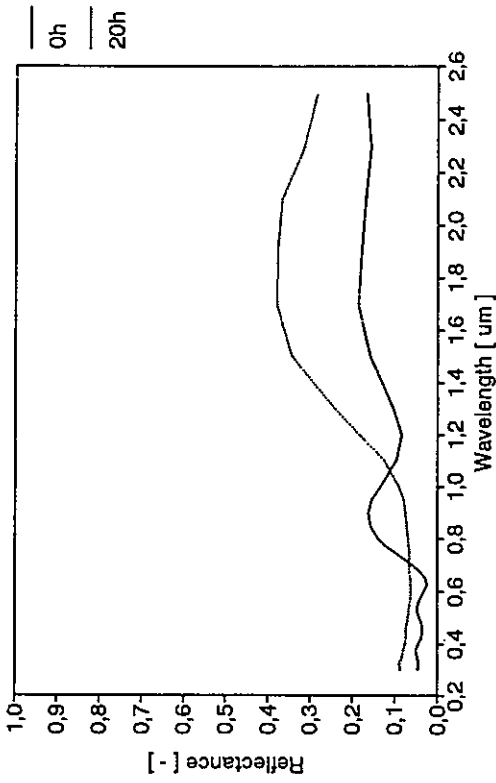
Cabinet: 70 °C, 95 % RH
Sample: 65 °C

| Time, h	α_s	ε_n(373 K)
0	0.916	0.132
3	0.910	0.249
10	0.898	0.272
50	0.888	0.321
150	0.880	0.317
300	0.865	0.336
650	0.845	0.332
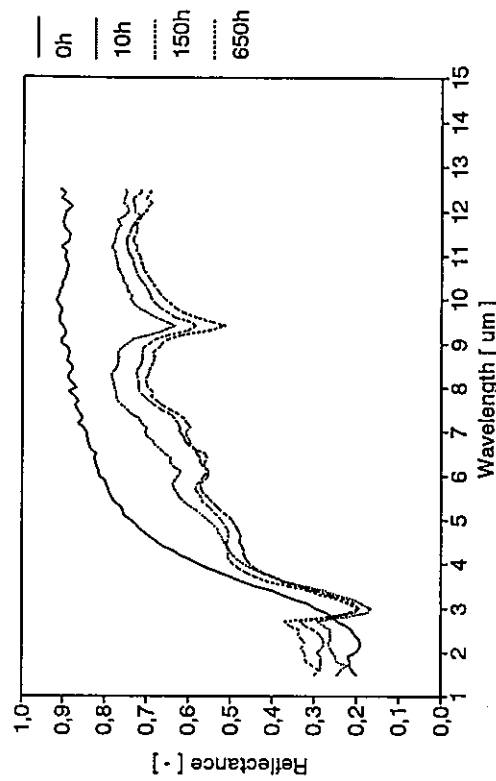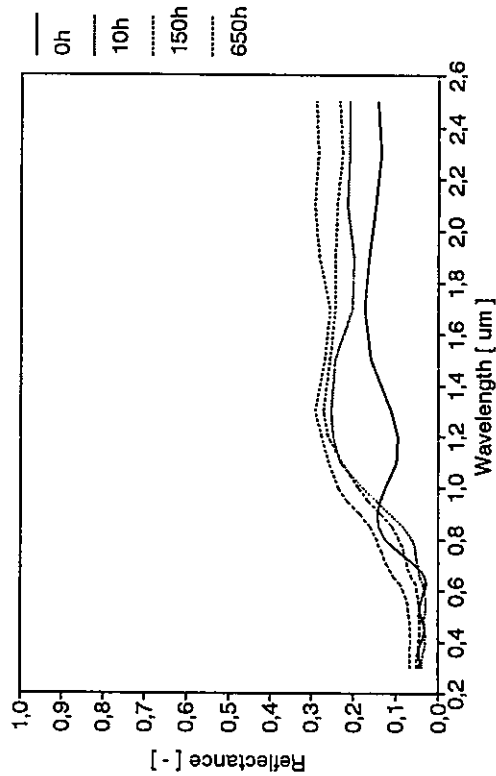
Table 5;12 cont.

Cabinet: 90 °C, 95 % RH
Sample: 85 °C

Time, h	α_S	ε_n(373 K)
0	0.916	0.134
3	0.908	0.235
10	0.900	0.240
50	0.889	0.296
150	0.879	0.358
300	0.856	0.403
650	0.838	0.419
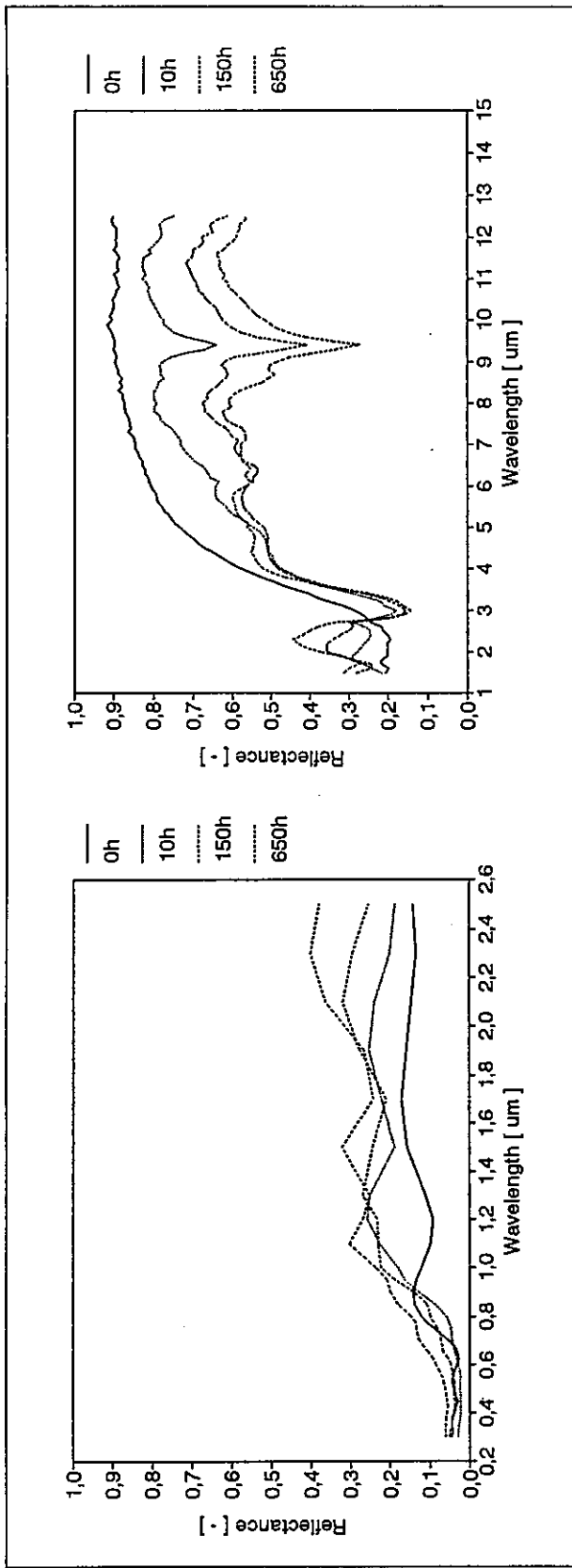
Table 5;12 cont.

Seriel Tests

1) High temperature test followed by a condensation test

5:41

Cabinet:	400 °C
Sample:	400 °C

Time, h	α_s	ε_n(373 K)
0		
100		

Cabinet: 50 °C, 95 % RH		
Sample:	45 °C	

Time, h	α_s	ε_n(373 K)
0	0.879	0.145
3	0.790	0.128
10	0.792	0.126
50	0.790	0.836
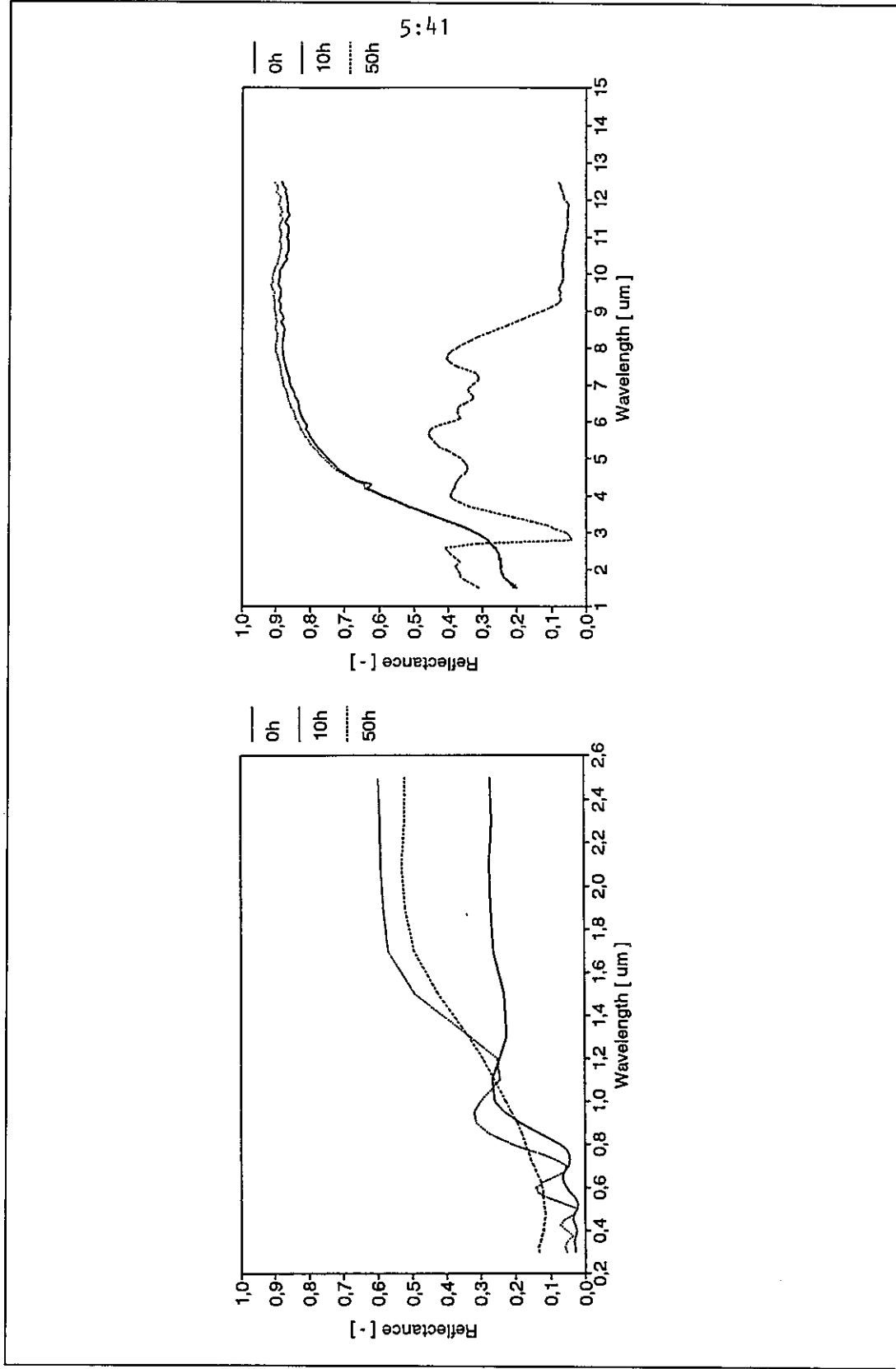
Table 5;12 cont.

2) Condensation test followed by a high temperature test

Cabinet: 50 °C, 95 % RH
Sample: 45 °C

Time, h	α_s	ε_n(373 K)
0	0.909	0.134
3	0.912	0.134
10	0.922	0.170
50	0.870	0.860
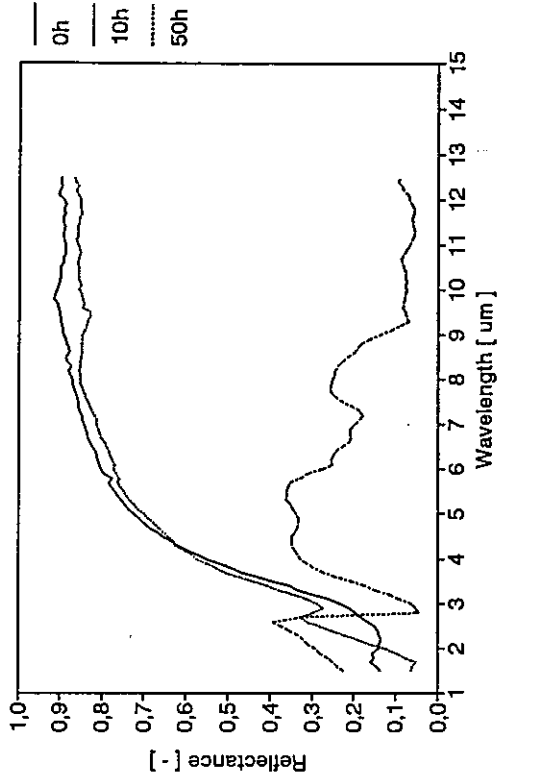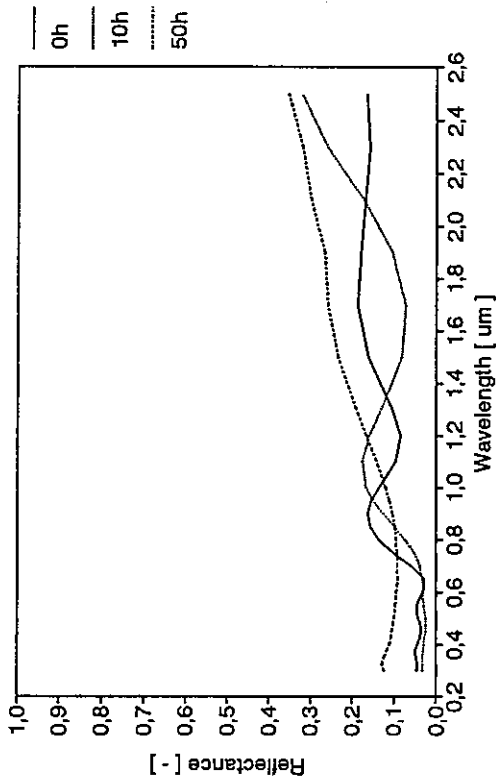
Cabinet: 400 °C
Sample: 400 °C

Time, h	α_s	ε_n(373 K)
0	0.870	0.860
3	0.642	0.659
10	0.589	0.678
50	0.507	0.644
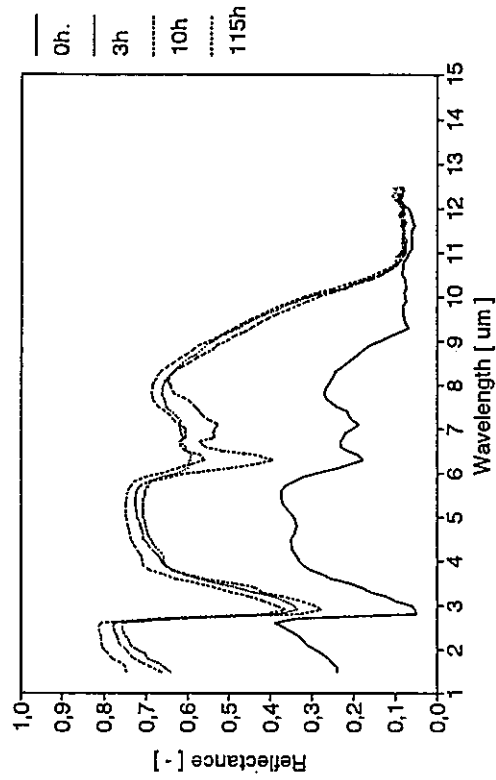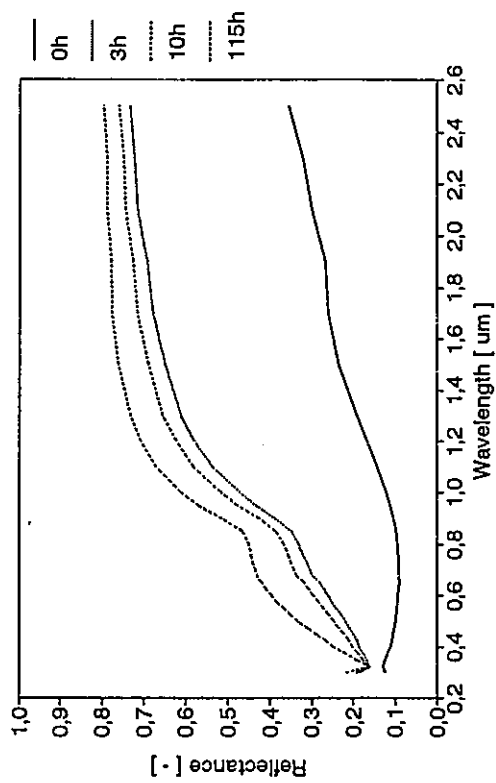
Table 5;13   Results fron high-humidity and condensation tests for the Sunstrip nickel-pigmented anodized aluminium absorber coating
High Humidity Tests

Cabinet: 50 °C, 95 % RH
Sample: 50 °C

Time, h	α_s	$\varepsilon_n(373\ K)$
0	0.884	0.105
15	0.878	0.109
300	0.877	0.109
800	0.876	0.123

Cabinet: 70 °C, 95 % RH
Sample: 70 °C

Time, h	α_s	$\varepsilon_n(373\ K)$
0	0.868	0.091
15	0.862	0.091
300	0.862	0.092
800	0.861	0.093

Table 5;13 cont.

5:44
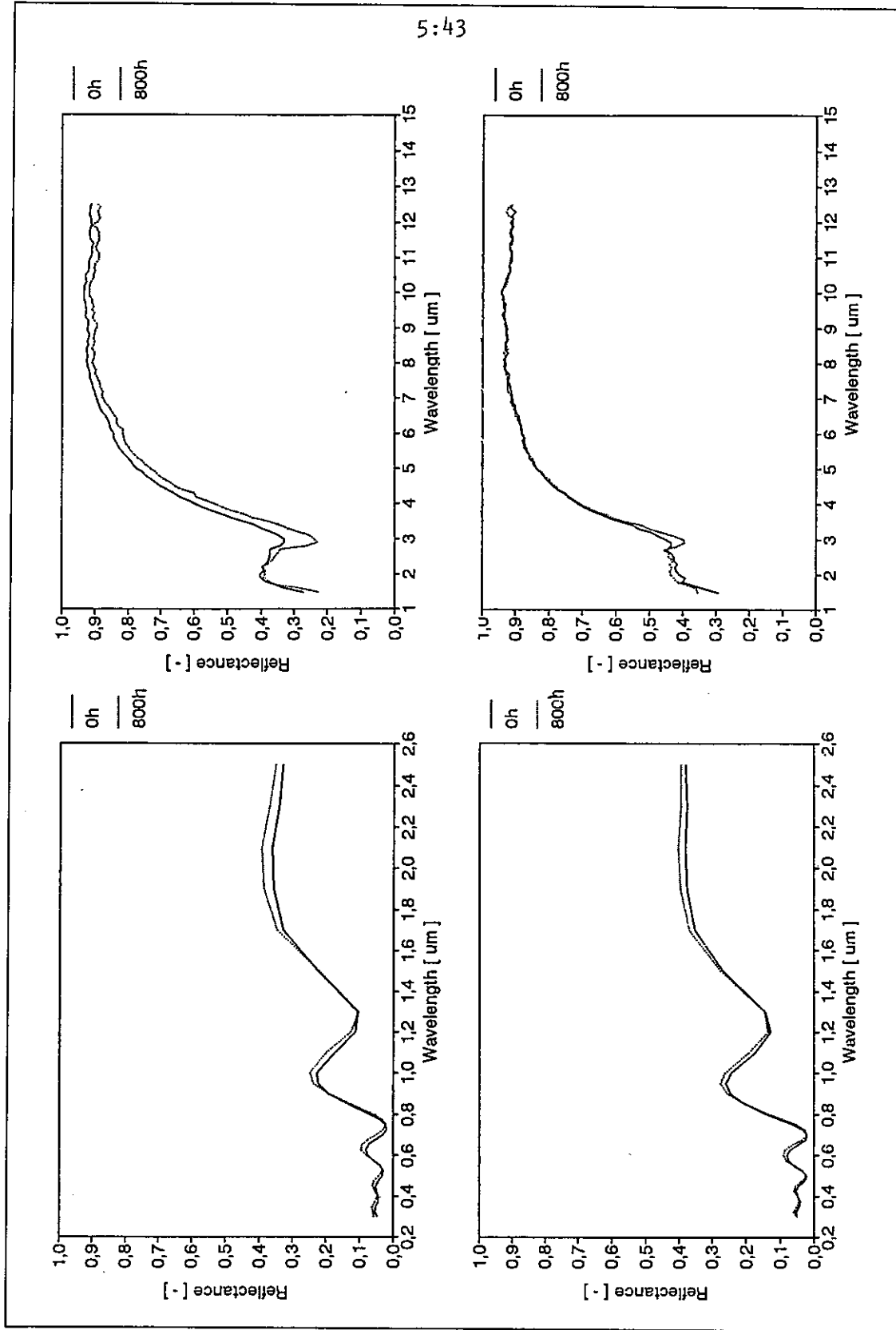
Cabinet: 90 °C, 95 % RH
Sample: 90 °C

Time, h	α_s	ε_n(373 K)
0	0.881	0.107
15	0.877	0.108
300	-	-
800	0.874	0.110

Cabinet: 50 °C, 99 % RH
Sample: 50 °C

Time, h	α_s	ε_n(373 K)
0	0.885	0.111
15	0.885	0.112
300	0.885	0.117
800	0.883	0.119
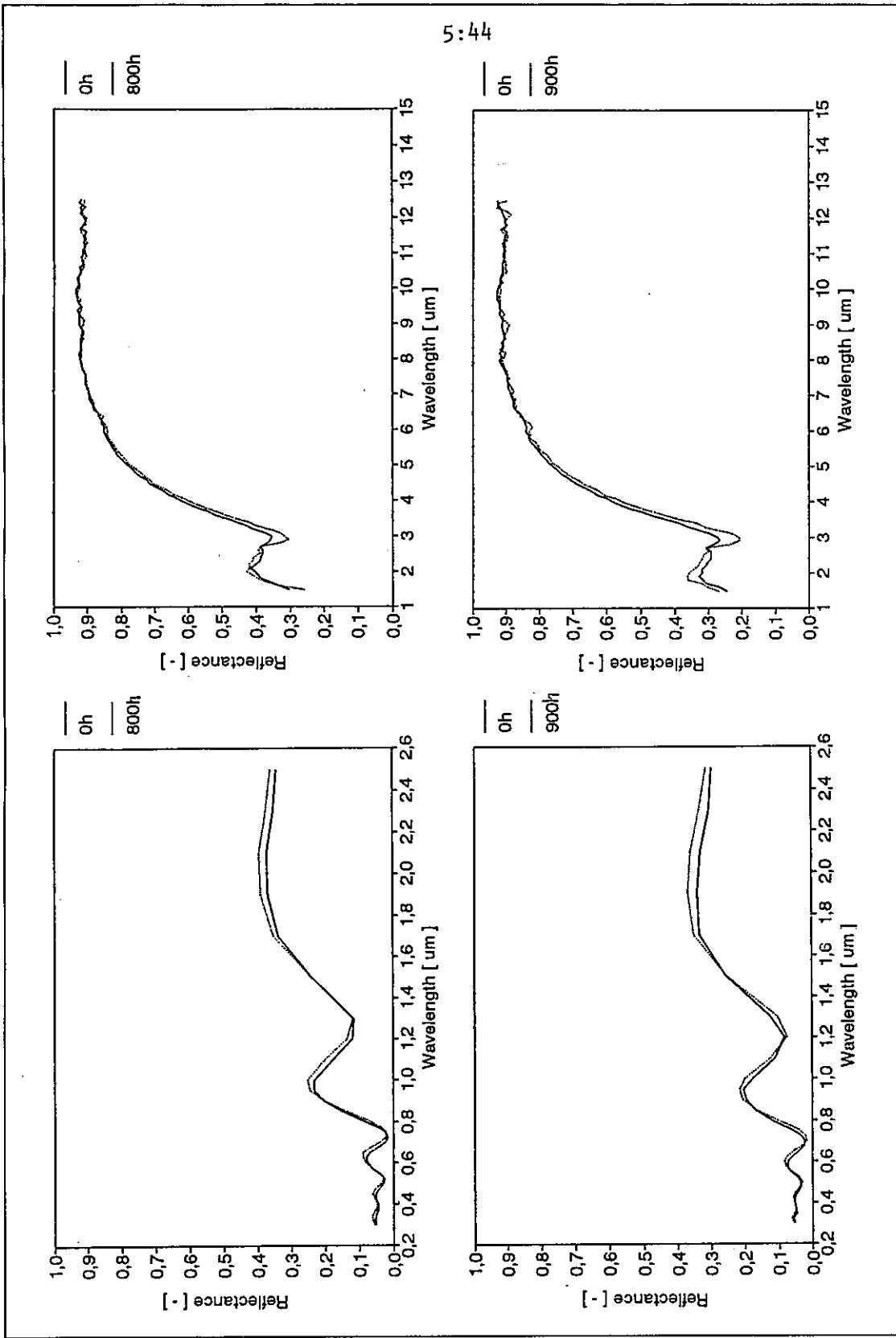
Table 5;13 cont.

Cabinet: 90 °C, 99 % RH
Sample: 90 °C

Time, h	α_s	ε_n(373 K)
0	0.884	0.109
15	0.869	0.129
300	0.870	0.129
1000	0.877	0.135
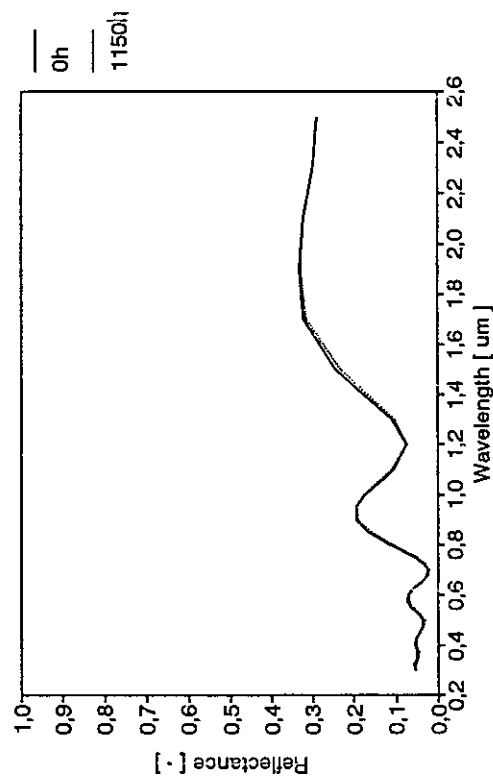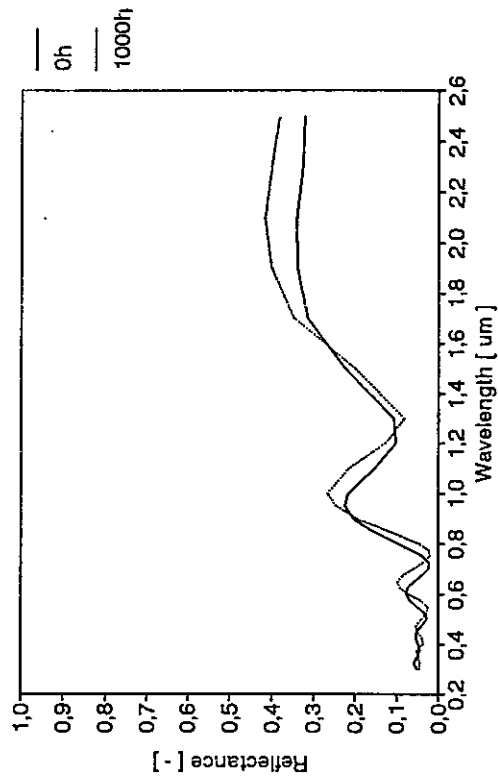
Condensation tests

Cabinet: 18 °C, 95 % RH
Sample: 12 °C

Time, h	α_s	ε_n(373 K)
0	0.889	0.118
3	0.888	0.116
10	0.894	0.123
110	0.888	0.127
300	0.897	0.120
650	0.898	0.123
1150	0.892	0.128
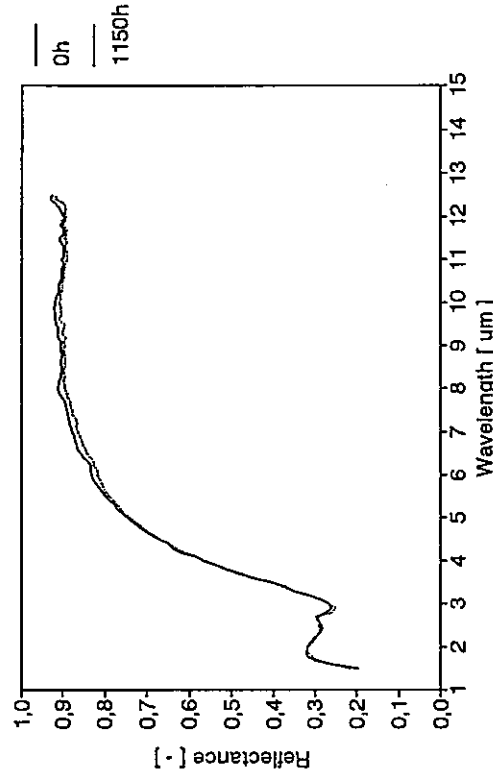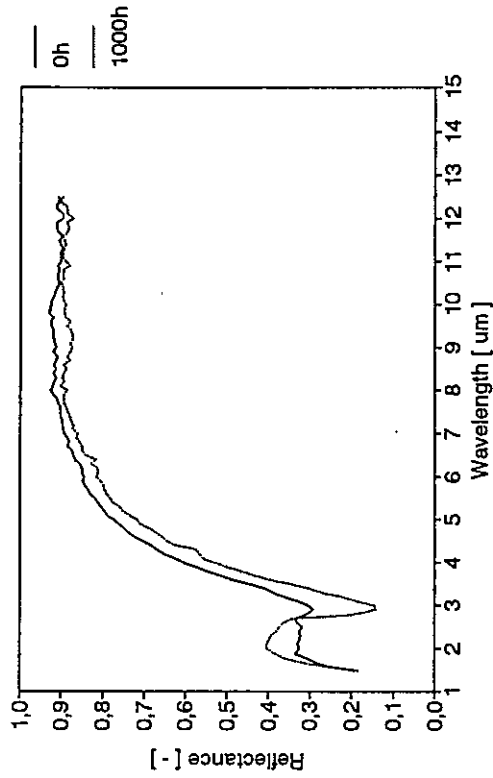
Table 5;13 cont.

Cabinet: 25 °C, 95 % RH
Sample: 20 °C

Time, h	α_s	ε_n(373 K)
0	0.883	0.141
50	0.888	0.139
150	0.888	0.144
300	0.897	0.150
650	0.903	0.168
1250	0.904	0.600

Cabinet: 30 °C, 95 % RH
Sample: 25 °C

Time, h	α_s	ε_n(373 K)
0	0.884	0.148
170	0.911	0.190
370	0.906	0.576
600	0.886	0.858

5:47
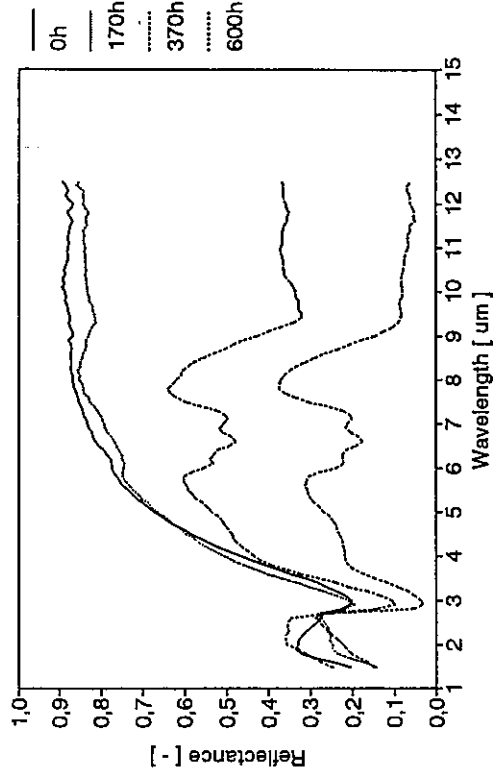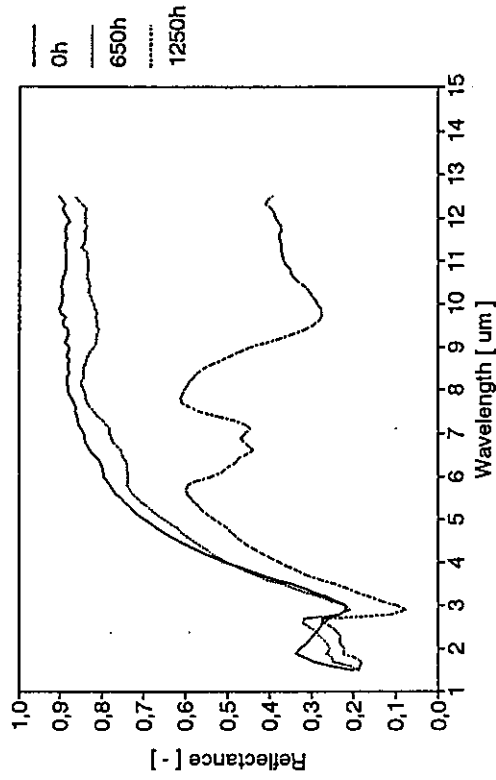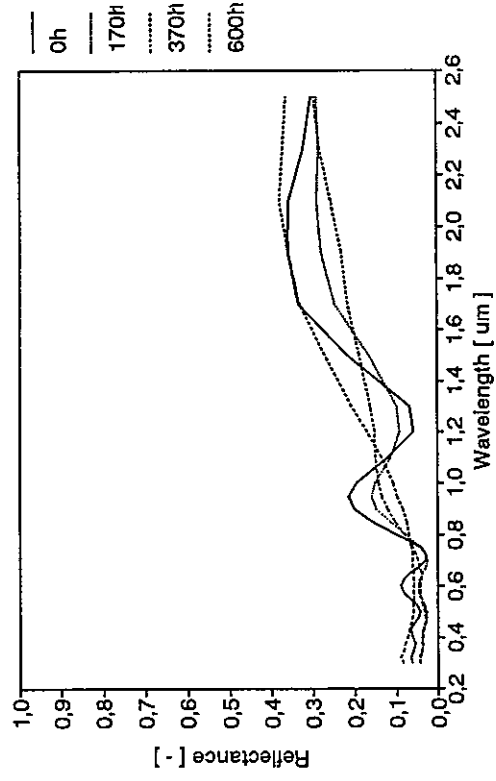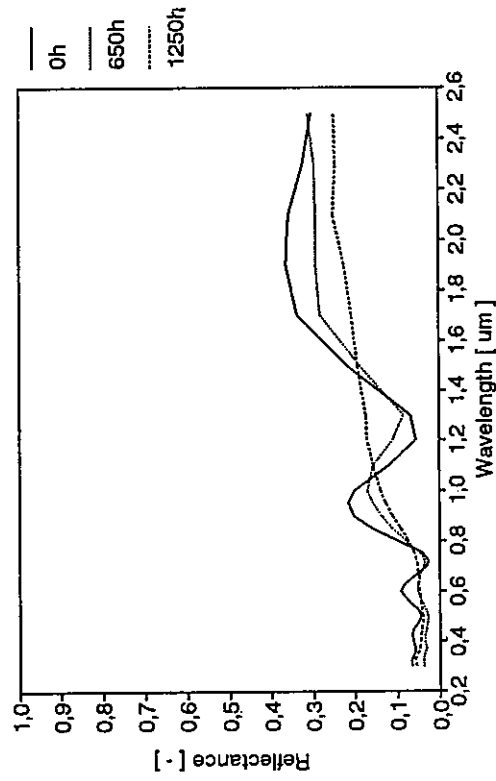
Table 5;13 cont.

Cabinet: 35 °C, 95 % RH
Sample: 30 °C

Time, h	α_s	$\varepsilon_n(373\ K)$
0	0.885	0.120
3	0.885	0.122
10	0.882	0.124
50	0.905	0.203
200	0.867	0.865

Cabinet: 50 °C, 95 % RH
Sample: 45 °C

Time, h	α_s	$\varepsilon_n(373\ K)$
0	0.882	0.111
3	0.883	0.110
10	0.916	0.170
50	0.883	0.585
150	0.886	0.763
300	0.881	0.752
650	0.877	0.756

Table 5;13 cont.

5:48
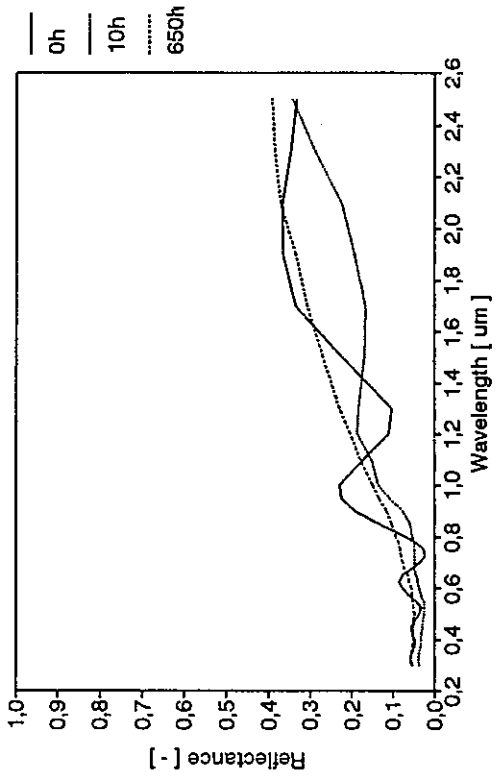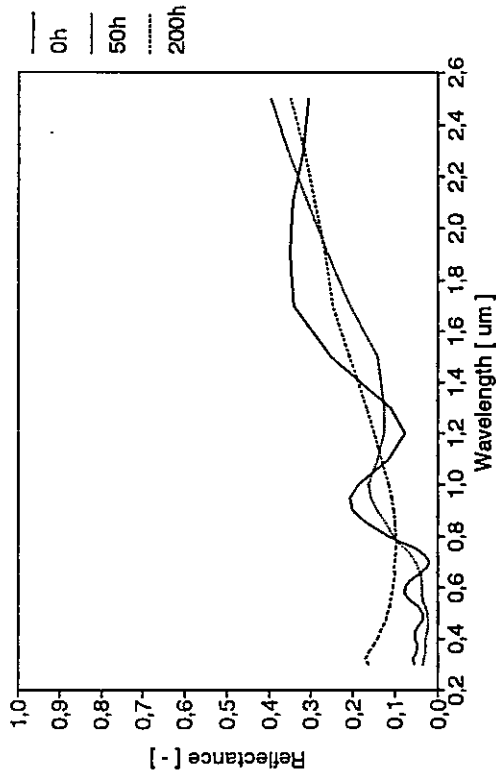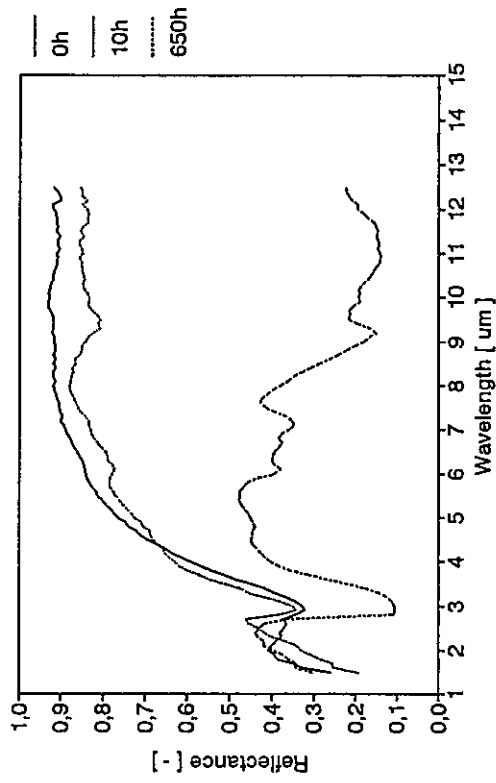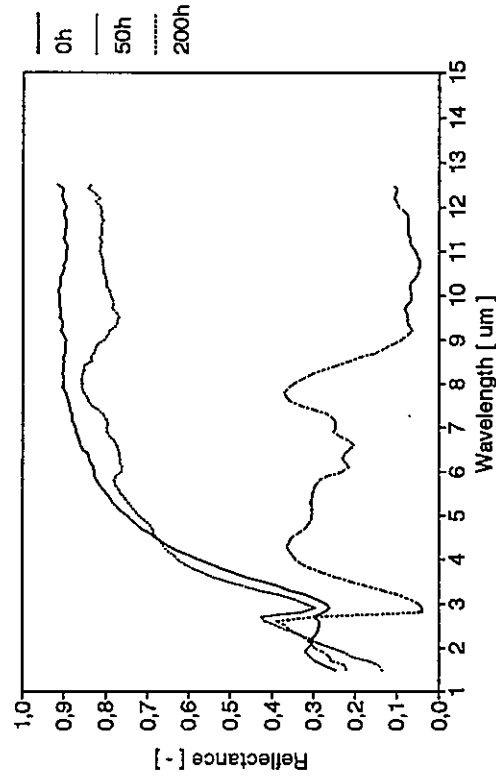
Cabinet: 50 °C, 95 % RH
Sample: 45 °C

Time, h	α_S	$\varepsilon_n(373\ K)$
0	0.889	0.118
20	0.873	0.680
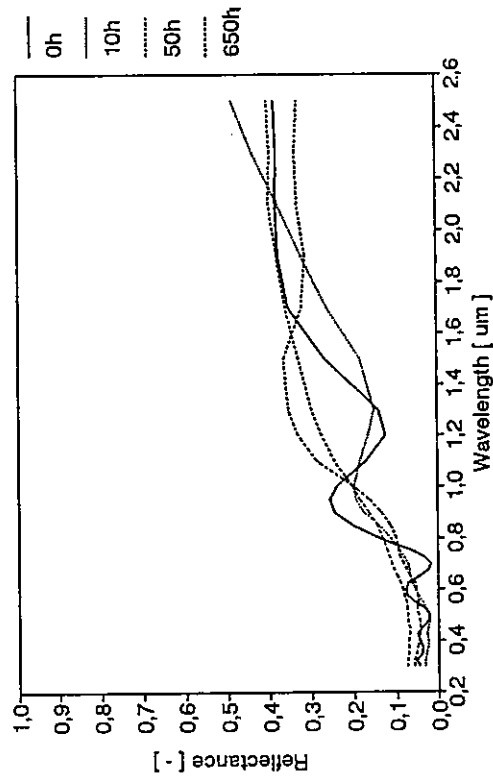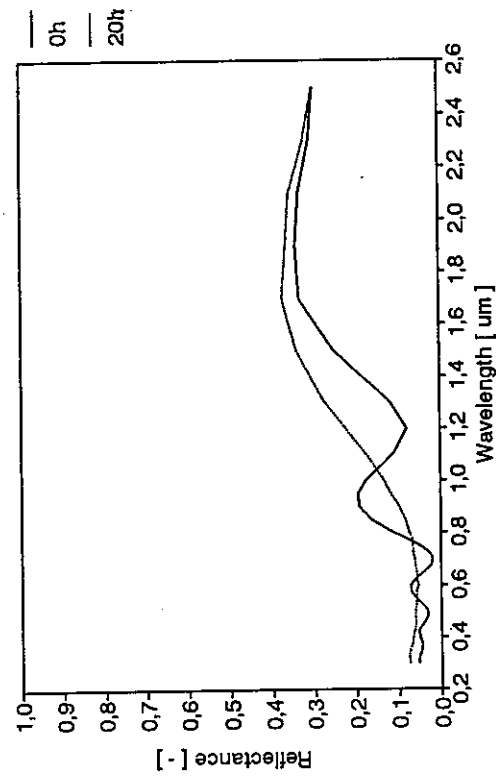
Cabinet: 70 °C, 95 % RH
Sample: 65 °C

Time, h	α_S	$\varepsilon_n(373\ K)$
0	0.869	0.090
3	0.865	0.088
10	0.882	0.122
50	0.856	0.341
150	0.833	0.710
300	0.840	0.752
650	0.839	0.751
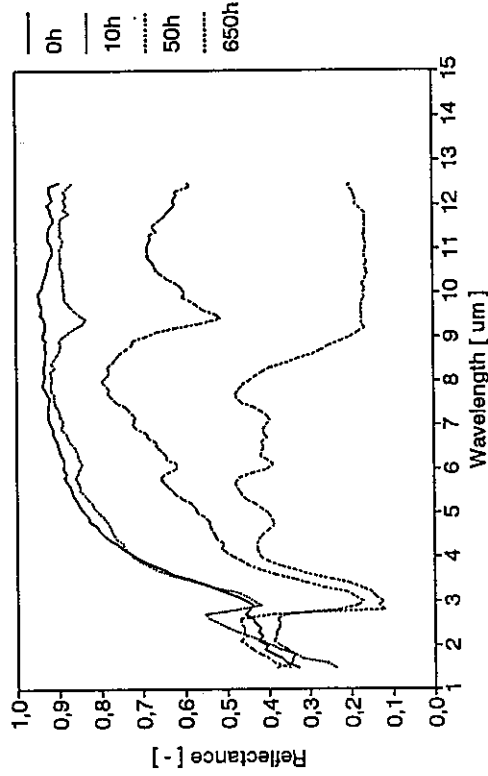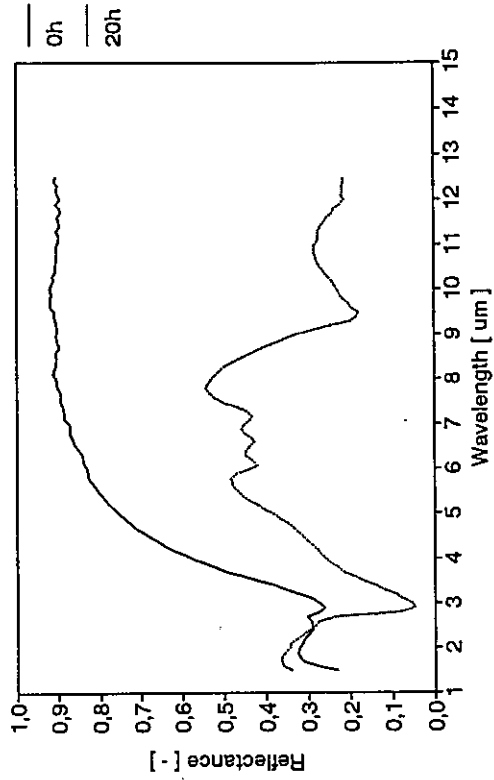
Table 5;13 cont.

Cabinet: 90 °C, 95 % RH
Sample: 85 °C

| Time, h	α_S	$\varepsilon_n(373\ K)$
0	0.867	0.092
3	0.866	0.172
10	0.843	0.261
50	0.822	0.498
150	0.831	0.657
300	0.820	0.677
650	0.788	0.678
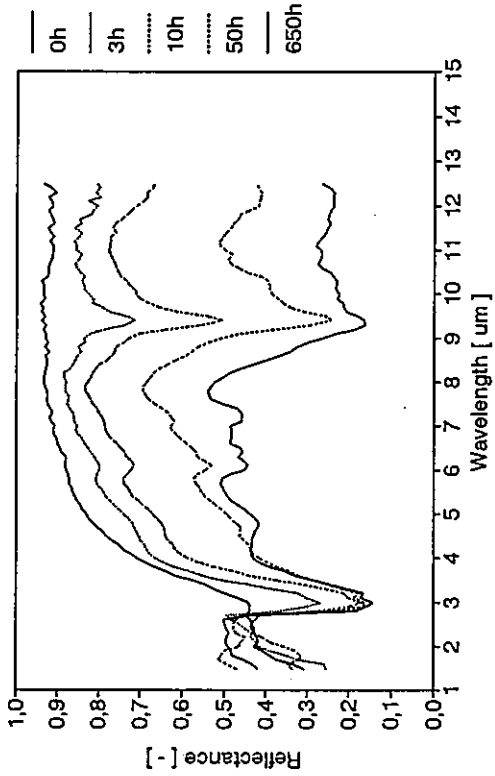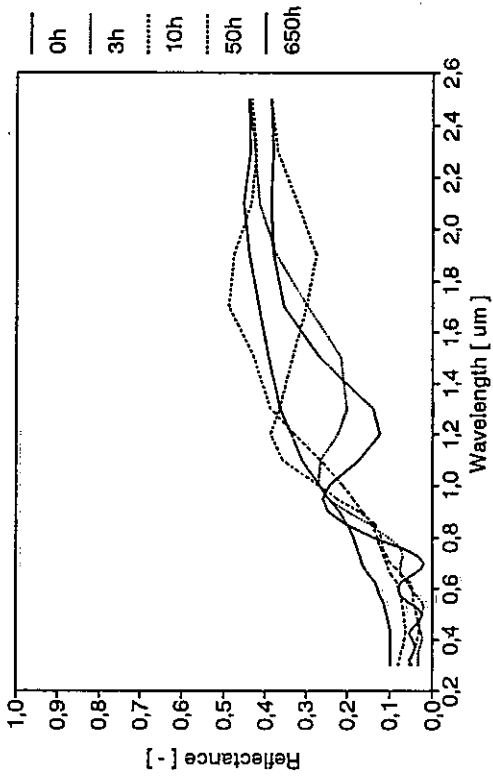
Table 5;13 cont.

Serial Tests

1) High-temperature test followed by a condensation test

Cabinet: 400 °C
Sample: 400 °C

Time, h	α_S	$\varepsilon_n(373\ K)$
0		
100		
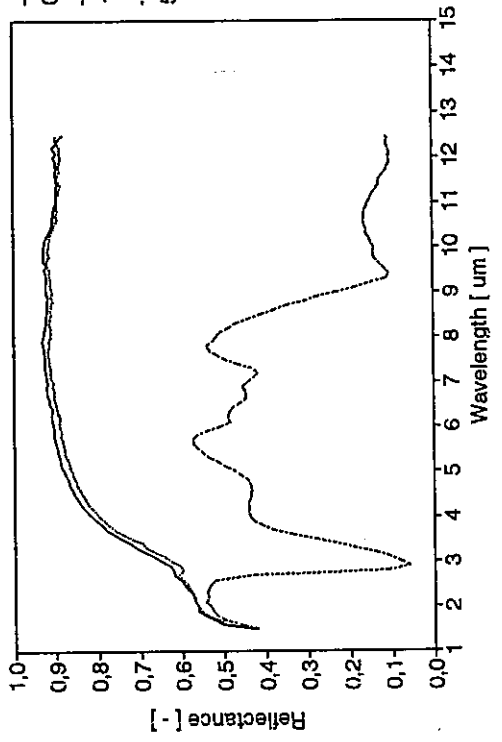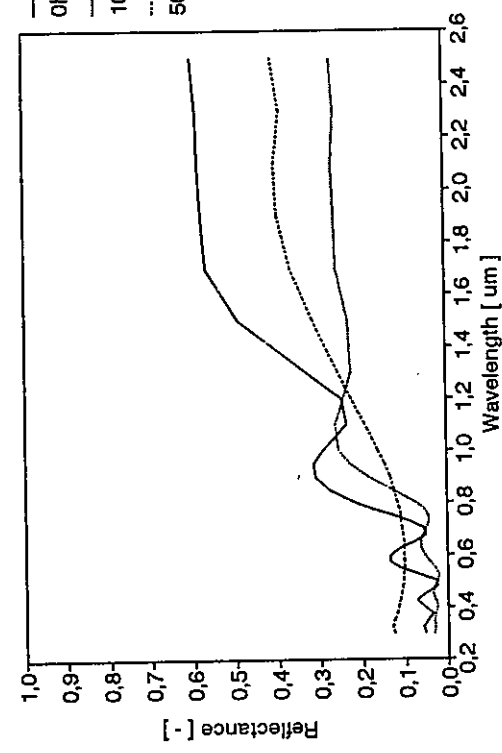
Cabinet: 50 °C, 95 % RH
Sample: 45 °C

| Time, h	α_S	$\varepsilon_n(373\ K)$
0	0.794	0.093
3	0.876	0.101
10	0.879	0.103
50	0.840	0.741

Table 5;13 cont.

## 2) Condensation test followed by high-temperature test

Cabinet: 50 °C, 95 % RH
Sample: 45 °C

Time, h	α_S	ε_n(373 K)
0	0.891	0.124
3	0.889	0.118
10	0.901	0.125
50	0.886	0.781
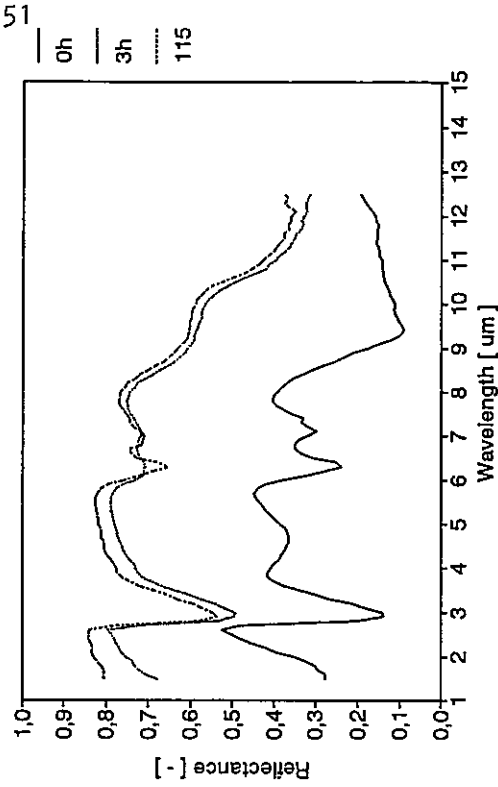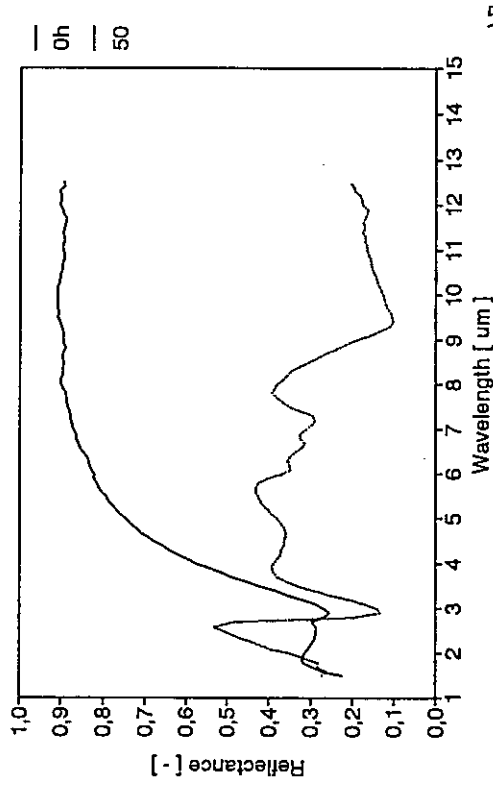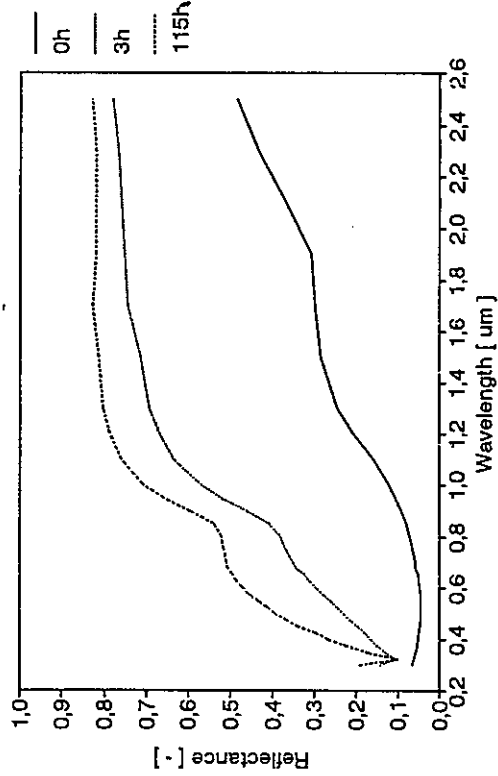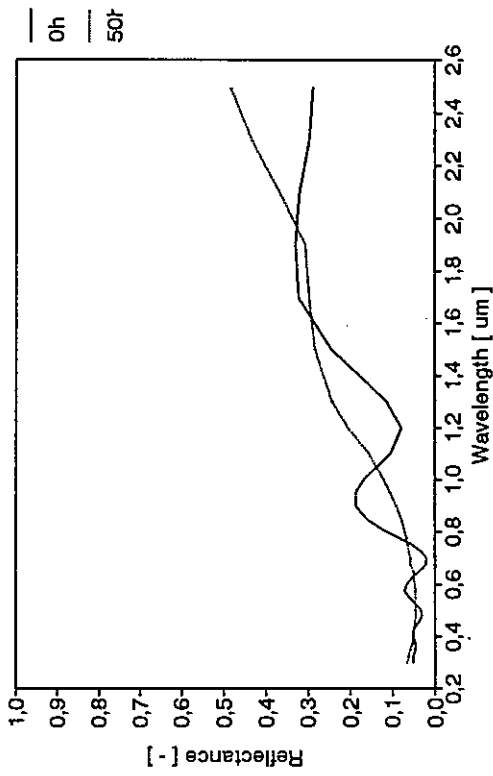
Cabinet: 400 °C
Sample: 400 °C

Time, h	α_S	ε_n(373 K)
0	0.886	0.781
3	0.577	0.437
10	0.504	-
115	0.442	0.542

Table 5:14   Results from high-humidity tests and condensation tests for the Energie Solaire black chrome absorber coating

High Humidity Tests

Cabinet: 50 °C, 95 % RH
Sample: 50 °C

Time, h	α_S	ε_n(373 K)
0	0.938	0.209
150	0.937	0.210
300	0.937	0.213
800	0.937	0.233

Cabinet: 70 °C, 95 % RH
Sample: 70 °C

Time/h	α_S	ε_n(373 K)
0	0.940	0.225
150	0.938	0.212
300	0.940	0.214
800	0.938	0.214
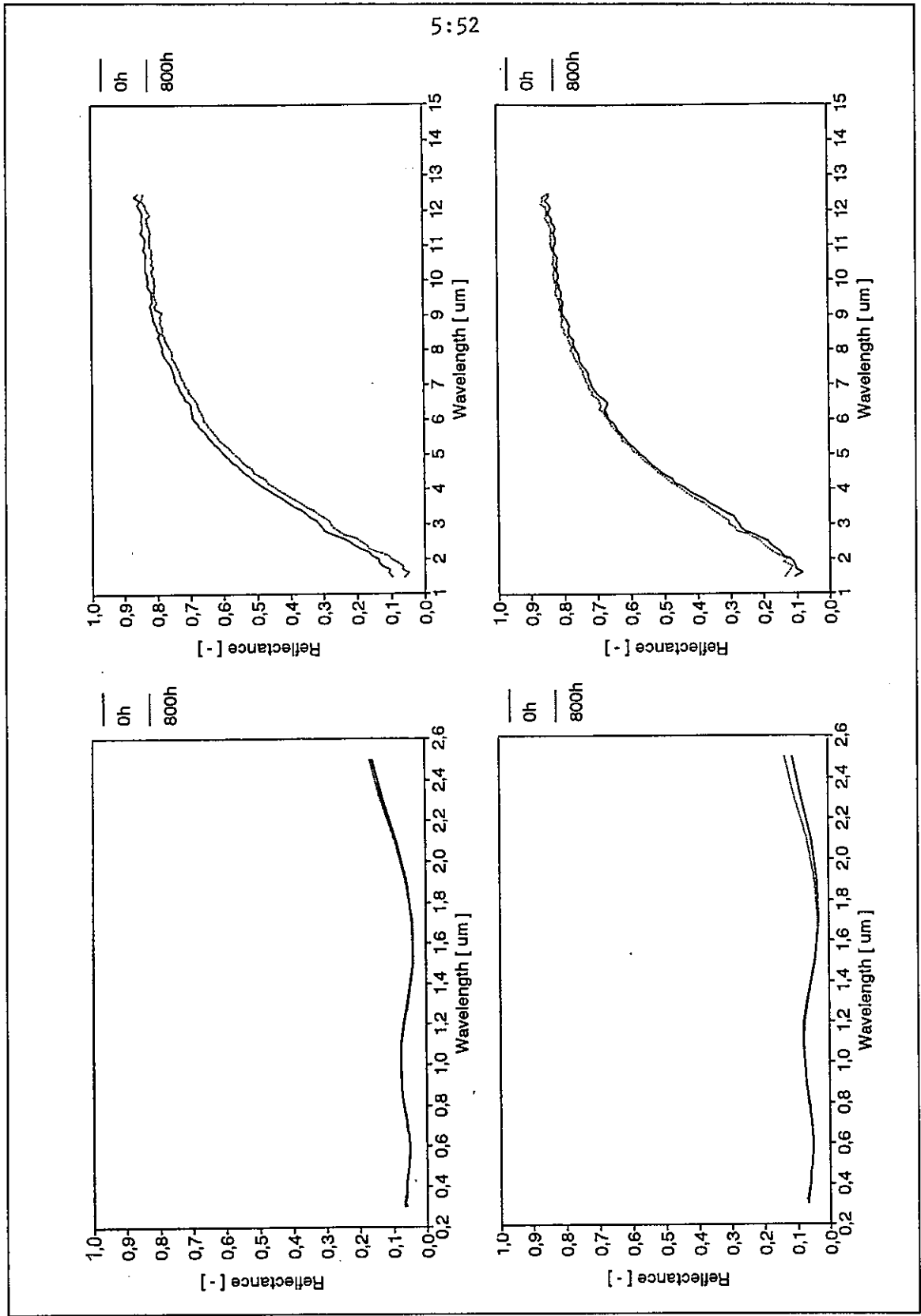
Table 5;14 cont.

Cabinet: 90 °C, 95 % RH
Sample: 90 °C

Time, h	α_s	ε_n(373 K)
0	0.938	0.210
150	0.938	0.207
300	-	-
800	0.938	0.206

Cabinet: 50 °C, 99 % RH
Sample: 50 °C

Time, h	α_s	ε_n(373 K)
0	0.936	0.222
150	0.943	0.224
300	0.942	0.221
900	0.943	0.222
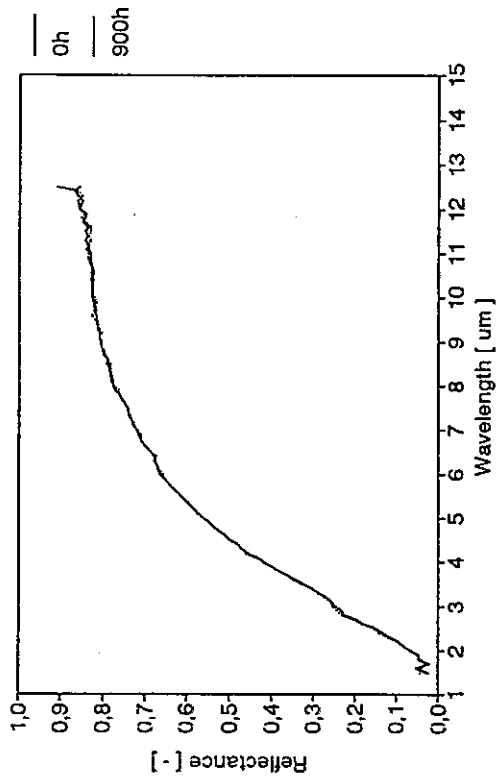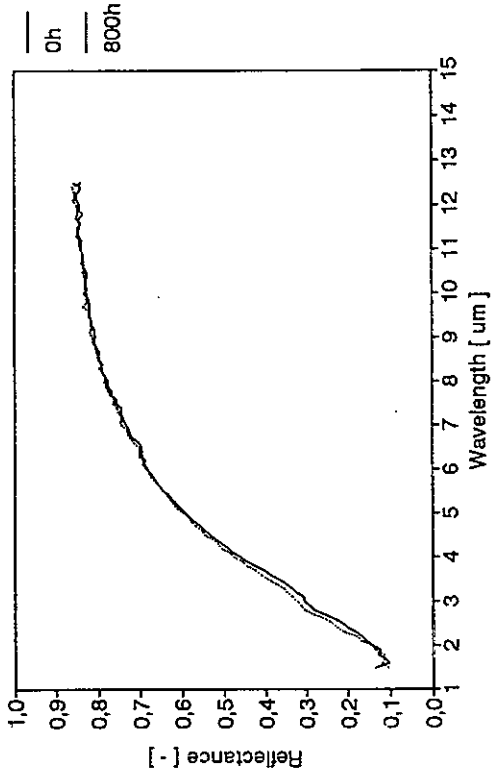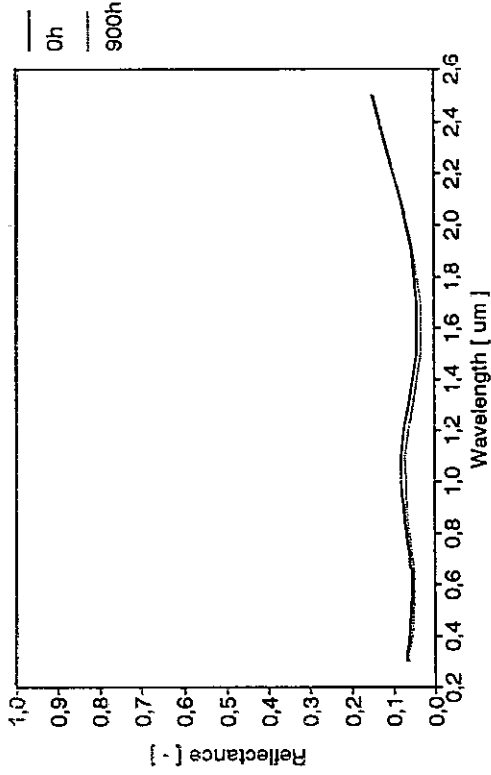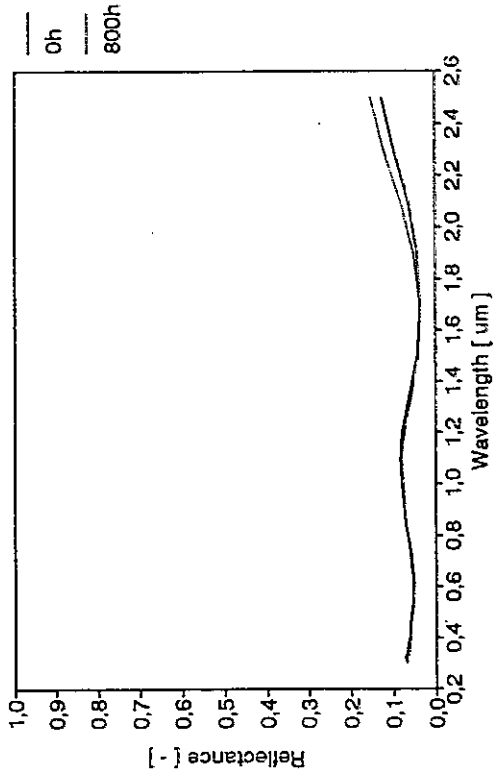
Table 5;14 cont.

Cabinet: 90 °C, 99 % RH
Sample: 90 °C

Time, h	α_s	ε_n(373 K)
0	0.937	0.220
150	0.937	0.218
300	0.938	0.218
1000	0.944	0.219
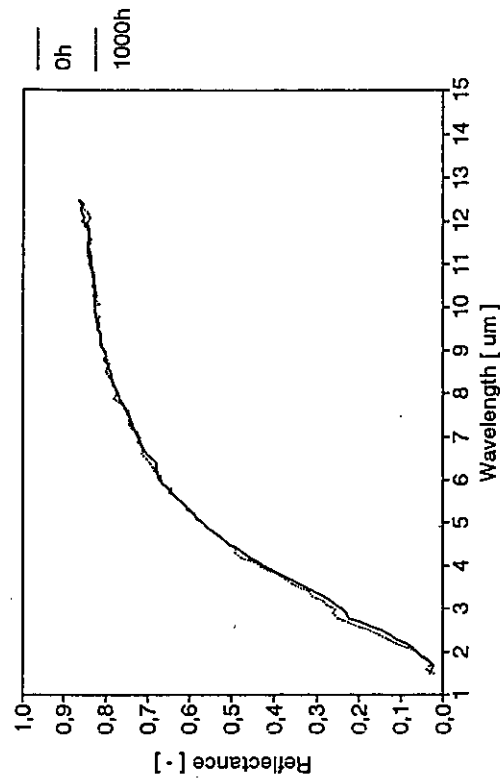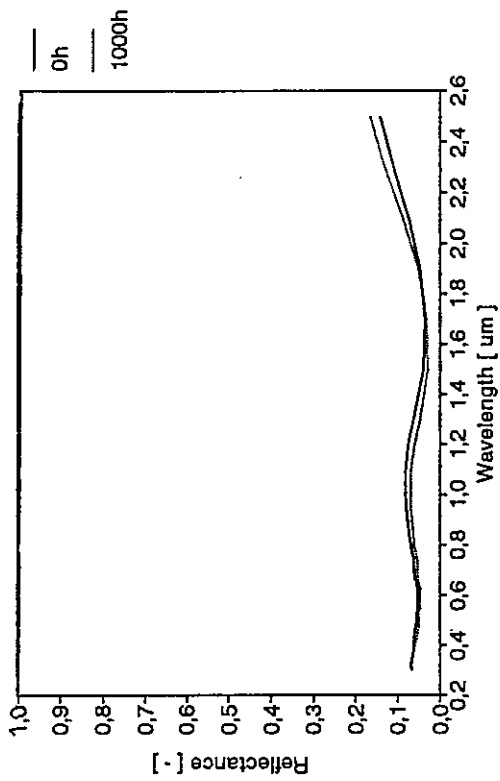
Condensation tests

Cabinet: 18 °C, 95 % RH
Sample: 12 °C

| Time, h	α_s	ε_n(373 K)
0	0.939	0.221
3	0.943	0.222
10	0.943	0.226
110	0.942	0.223
300	0.945	0.227
650	0.945	–
1150	0.940	0.229

5:54

Table 5;14 cont.

5:55
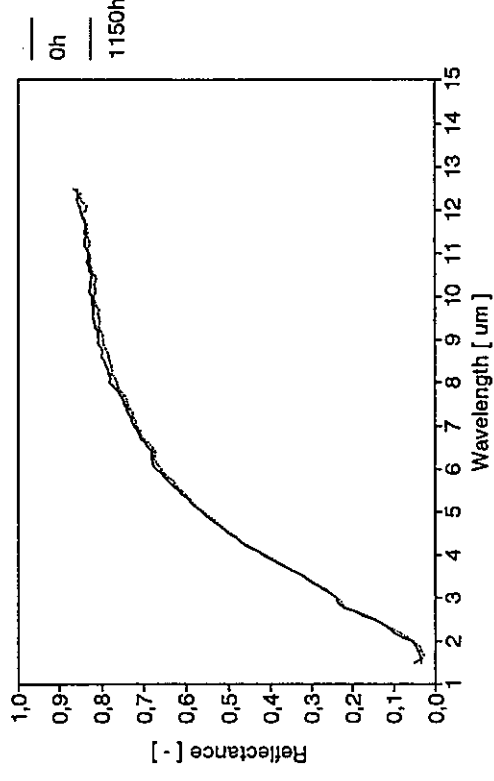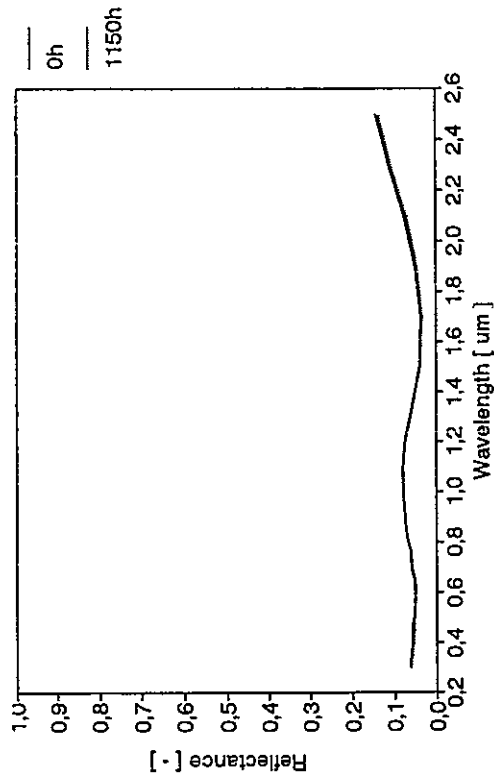
Cabinet: 50 °C, 95 % RH
Sample: 45 °C

Time, h	α_s	$\varepsilon_n(373\ K)$
0	0.936	0.217
3	0.937	0.218
10	0.938	0.216
50	0.940	0.217
150	0.940	0.219
300	0.941	0.220
650	0.940	0.220
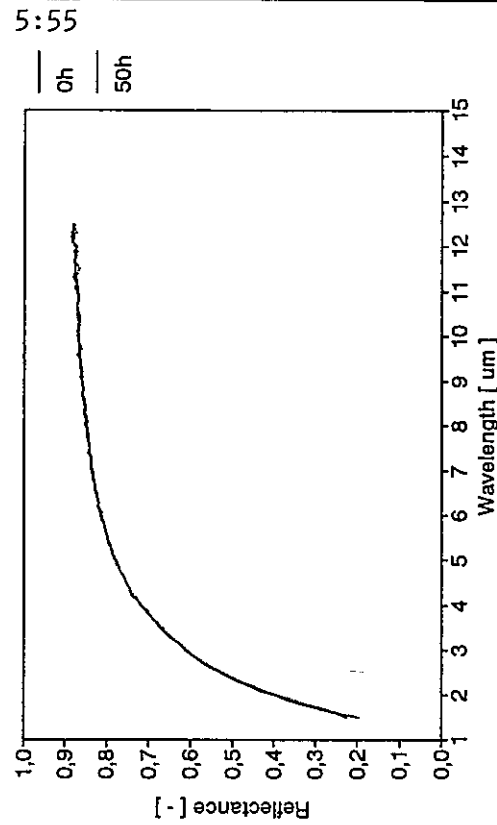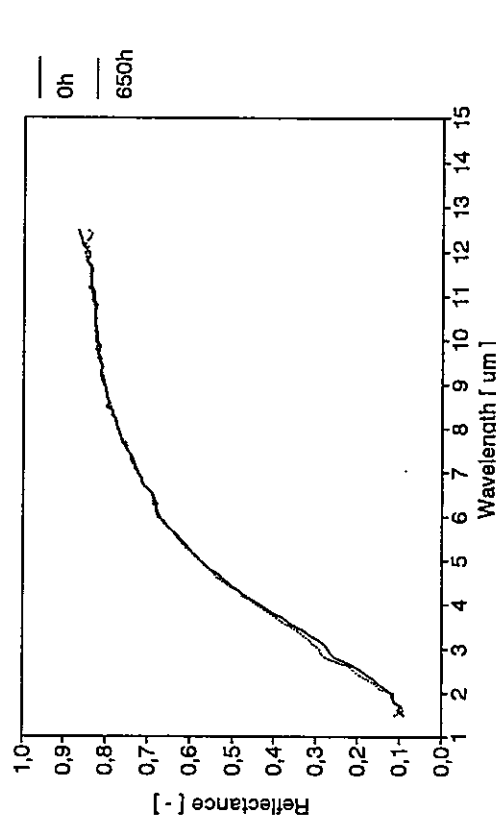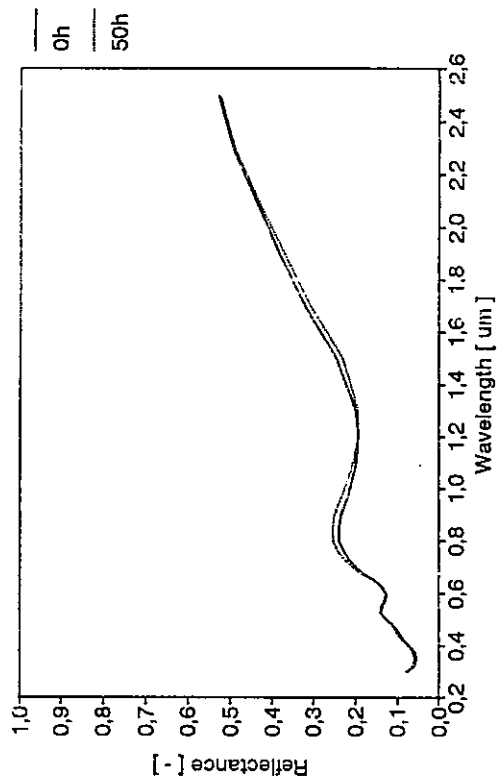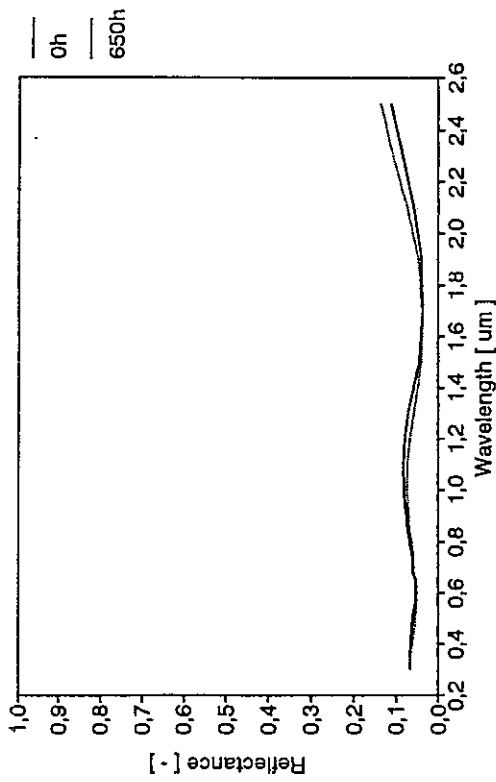
Cabinet: 50 °C, 95 % RH
Sample: 45 °C[1]

Time, h	α_s	$\varepsilon_n(373\ K)$
0	0.805	0.148
3	0.803	-
10	0.802	0.148
50	0.802	0.147

1) Condensation test followed after a high temperature test at 400 °C.

Table 5;15 cont.

Cabinet: 70 °C, 95 % RH
Sample: 65 °C

Time, h	α_s	ε_n(373 K)
0	0.939	0.212
3	0.939	0.208
10	0.939	0.207
50	0.940	0.207
150	0.940	0.208
300	0.939	0.207
650	0.936	0.208

Cabinet: 90 °C, 95 % RH
Sample: 85 °C

Time, h	α_s	ε_n(373 K)
0	0.943	0.216
3	0.940	0.210
10	0.942	0.210
50	0.942	0.210
150	0.943	0.209
300	0.941	0.209
650	0.943	0.209
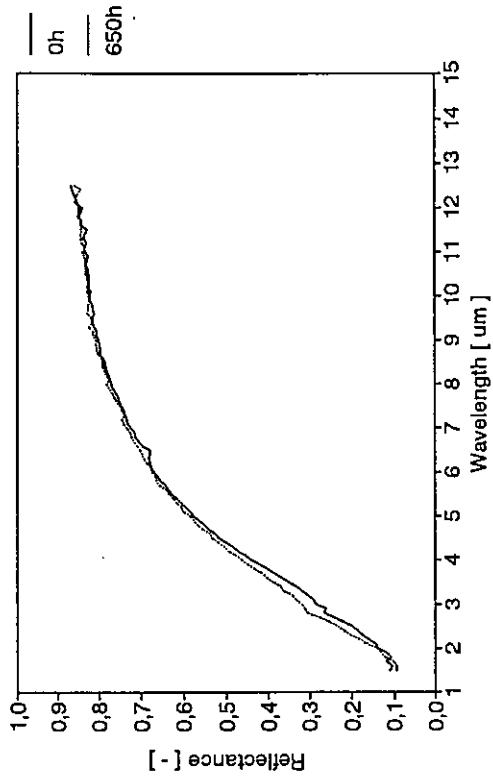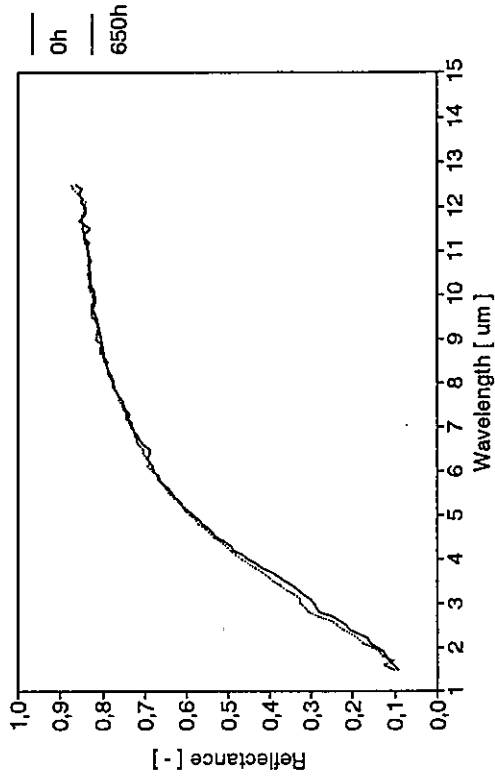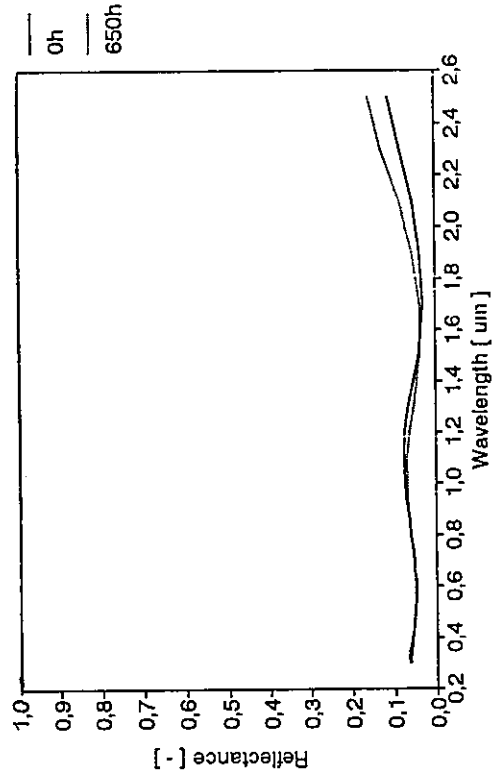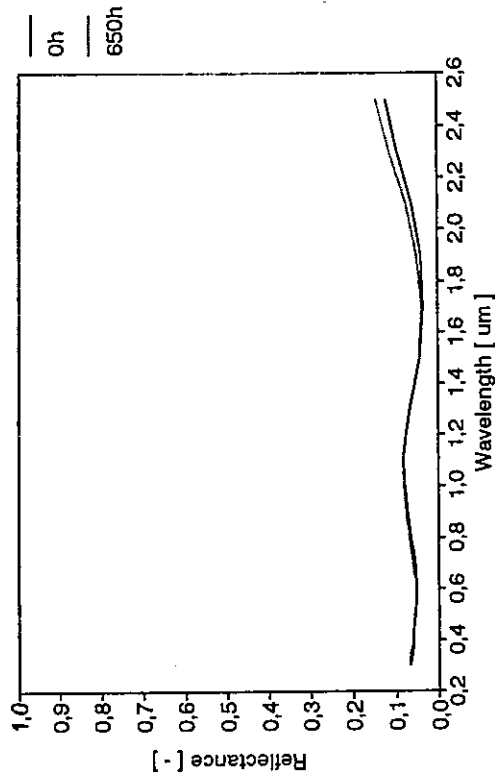
Table 5;15   Results from high-humidity tests and condensation tests for the MTI black chrome absorber coating

High Humidity Tests

Cabinet: 50 °C, 95 % RH
Sample: 50 °C

Time, h	α_s	ε_n(373 K)
0	0.956	0.206
150	0.952	0.215
300	0.955	0.229
800	0.955	0.234

Cabinet: 70 °C, 95 % RH
Sample: 70 °C

Time, h	α_s	ε_n(373 K)
0	0.966	0.134
150	0.964	0.134
300	0.964	0.136
800	0.963	0.136

Reflectance [-]   Wavelength [um]   0h   800h

5:57

Table 5;15 cont.

Reflectance charts — Cabinet: 90 °C, 95 % RH, Sample: 90 °C (0h / 800h) and Cabinet: 50 °C, 99 % RH, Sample: 50 °C (0h / 900h), plotted against Wavelength [µm].
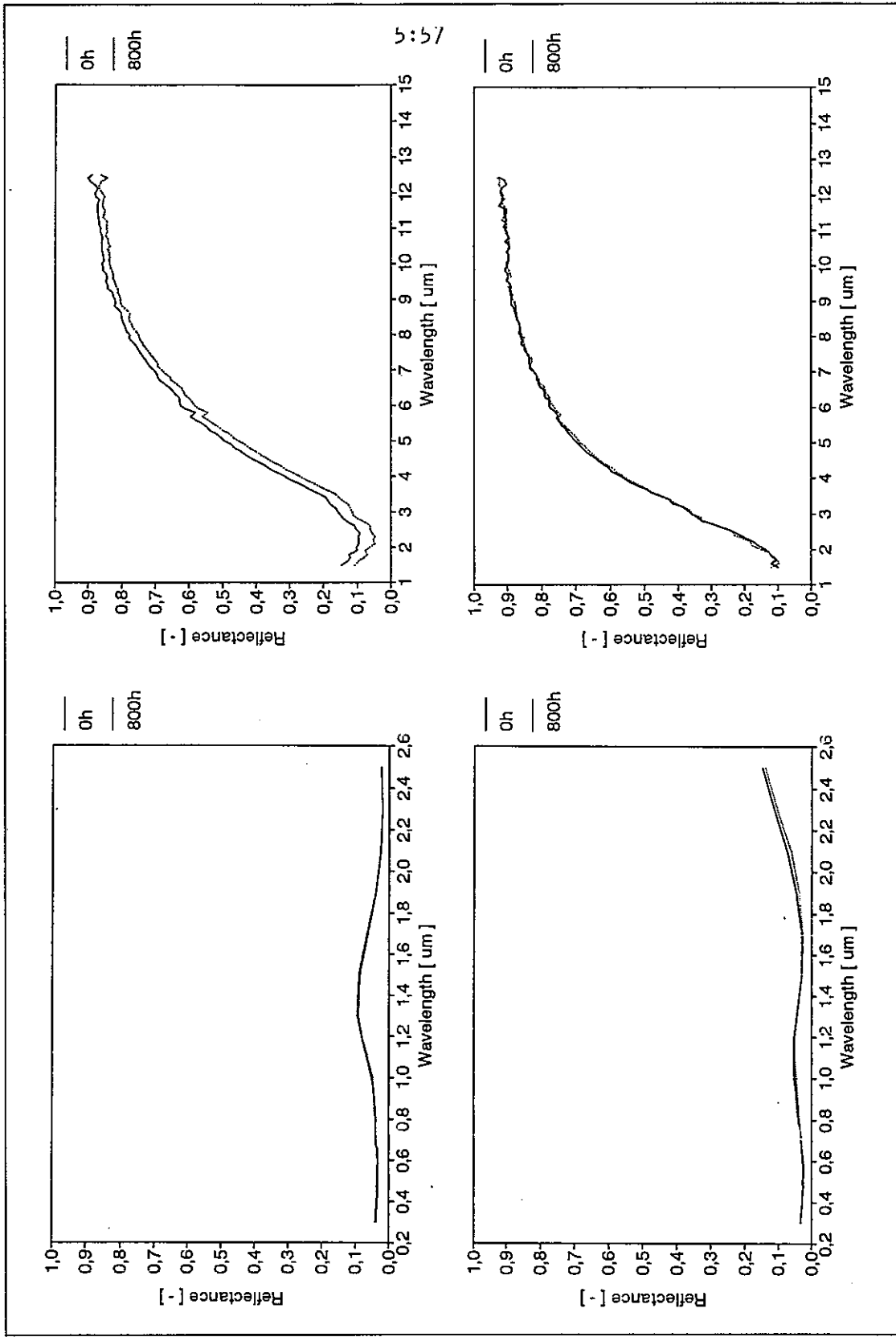
Cabinet: 90 °C, 95 % RH
Sample: 90 °C

Time, h	α_s	$\varepsilon_n(373\ K)$
0	0.966	0.142
150	0.970	0.137
300	-	-
800	0.968	0.137
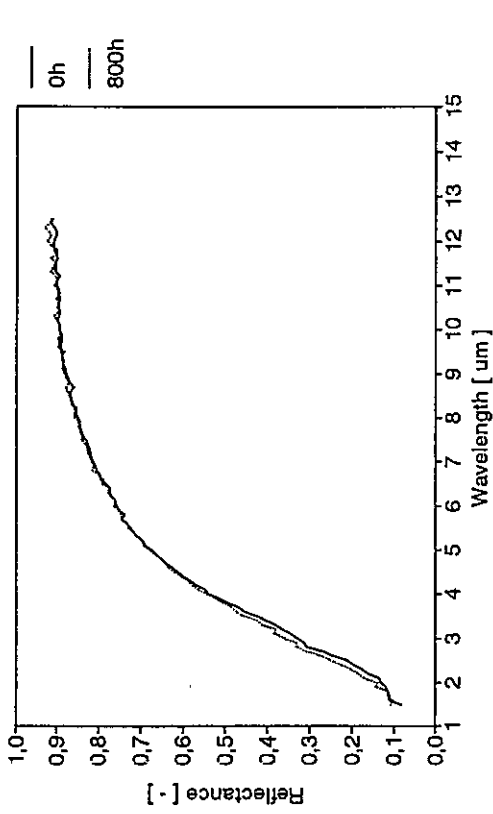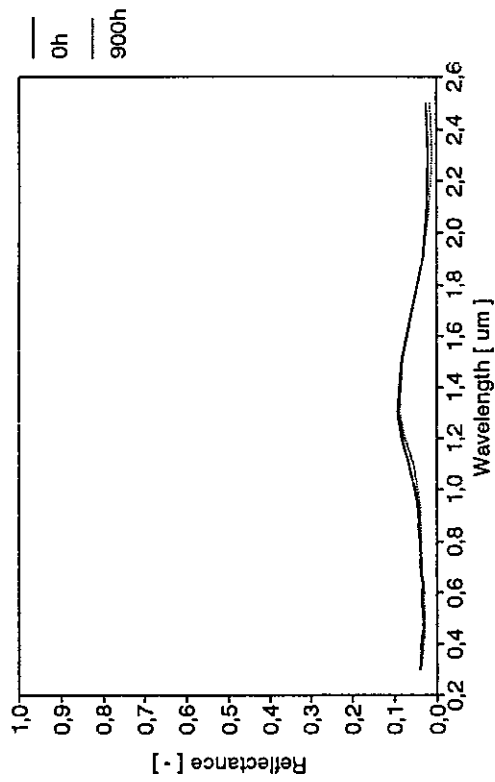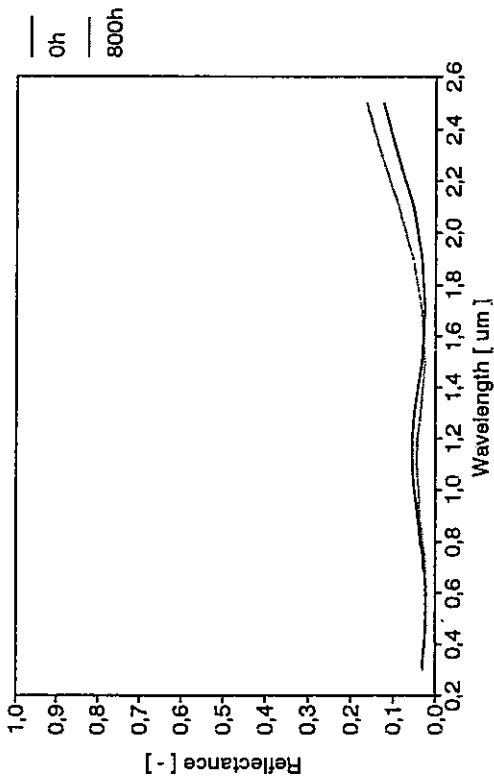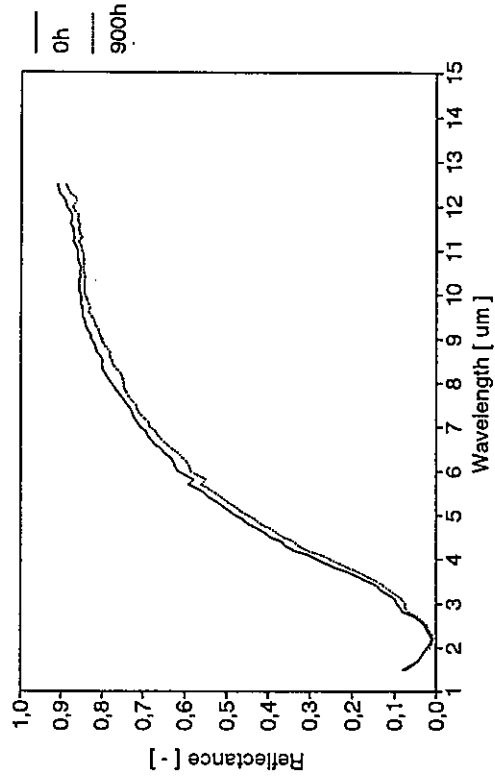
Cabinet: 50 °C, 99 % RH
Sample: 50 °C

Time, h	α_s	$\varepsilon_n(373\ K)$
0	0.956	0.213
150	0.962	0.231
300	0.961	0.239
900	0.960	0.231

Table 5;15 cont.

Cabinet: 90 °C, 99 % RH
Sample: 90 °C

Time, h	α_S	ε_n(373 K)
0	0.956	0.211
150	0.956	0.220
300	0.956	0.210
1000	0.964	0.208
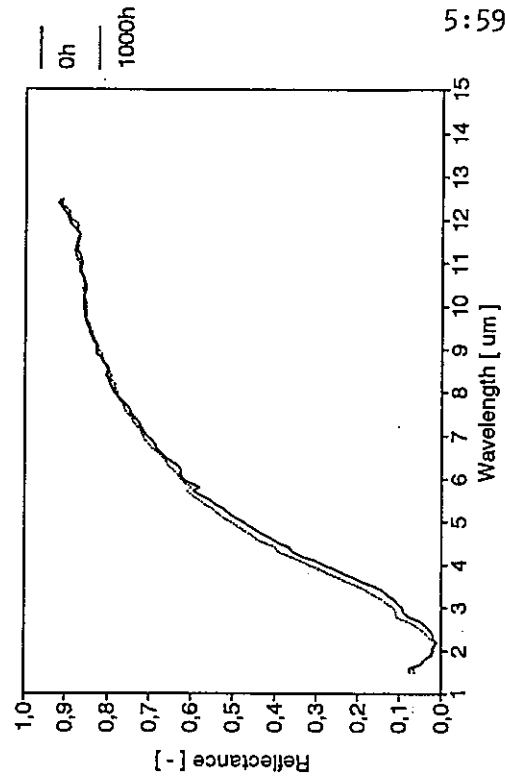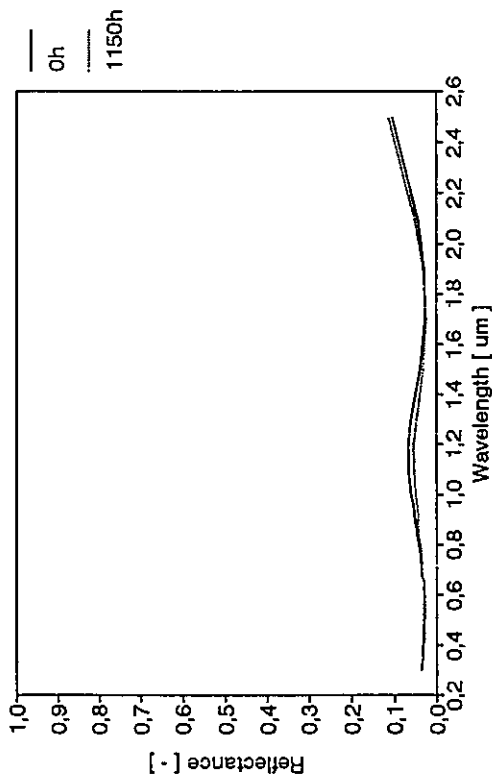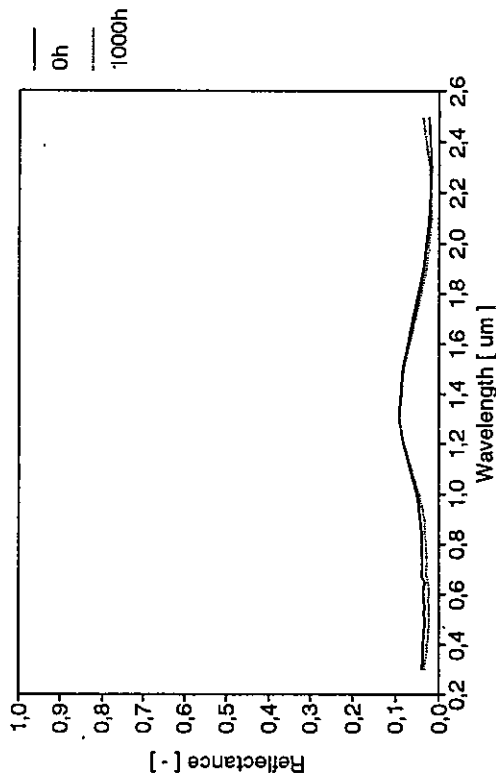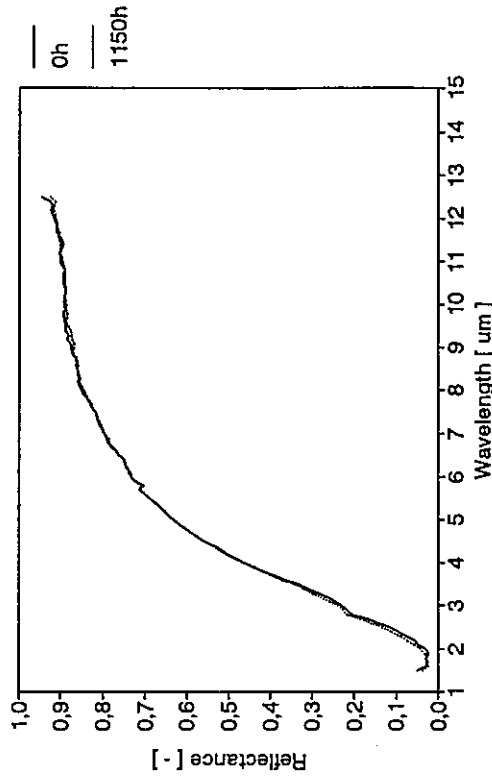
Condensation tests

Cabinet: 18 °C, 95 % RH
Sample: 12 °C

Time, h	α_S	ε_n(373 K)
0	0.959	0.154
3	0.964	0.159
10	0.964	0.156
110	0.965	0.161
300	0.967	0.159
650	0.967	-
1150	0.963	0.157

Table 5;15 cont.

5:60

Cabinet: 50 °C, 95 % RH
Sample: 45 °C

Time, h	α_S	ε_n(373 K)
0	0.956	0.204
3	0.958	0.209
10	0.965	0.200
50	0.967	0.199
150	0.967	0.201
300	0.968	0.205
650	0.967	0.203
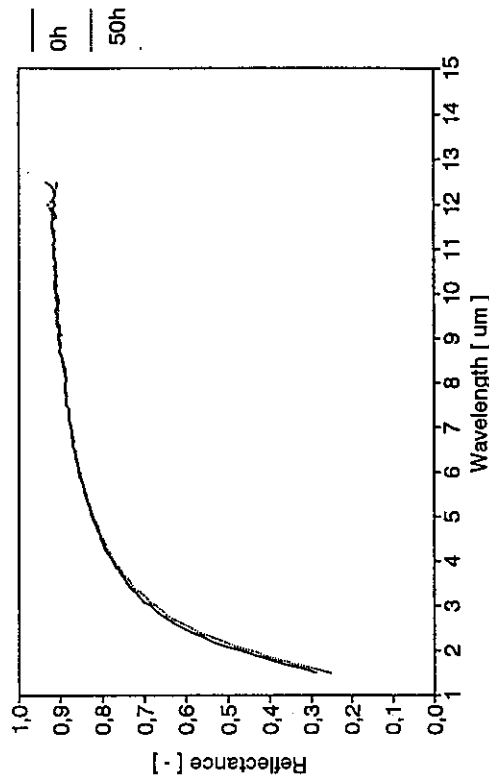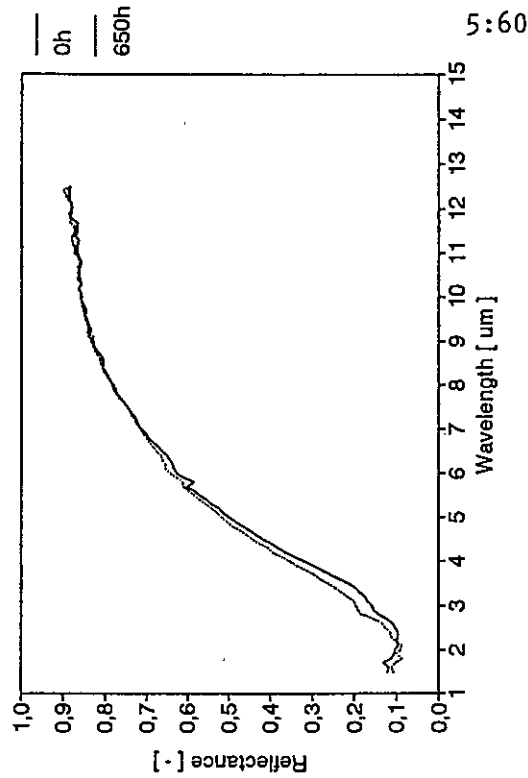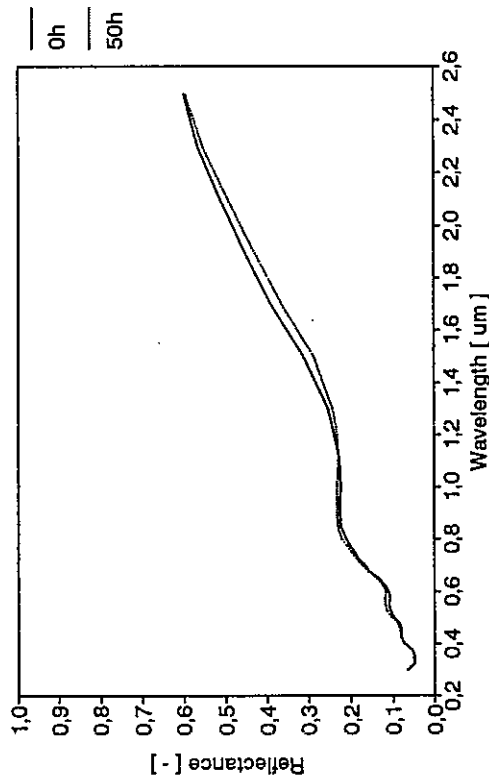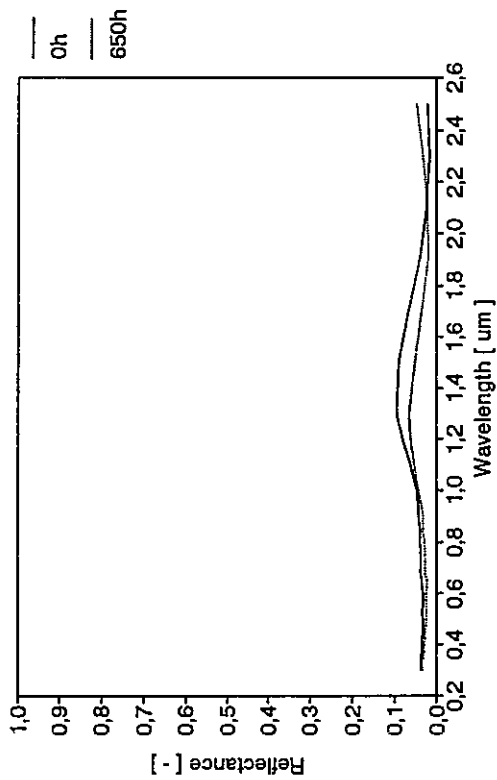
Cabinet: 50 °C, 95 % RH
Sample: 45 °C[1]

Time, h	α_S	ε_n(373 K)
0	0.806	0.105
3	0.802	-
10	0.806	0.105
50	0.804	0.106

1) Condensation test followed after a high temperature test at 400 °C.

Table 5;15 cont.

Cabinet: 70 °C, 95 % RH
Sample: 65 °C

Time, h	α_s	ε_n(373 K)
0	0.965	0.138
3	0.963	0.141
10	0.965	0.138
50	0.966	0.133
150	0.964	0.136
300	0.961	0.134
650	0.963	0.134
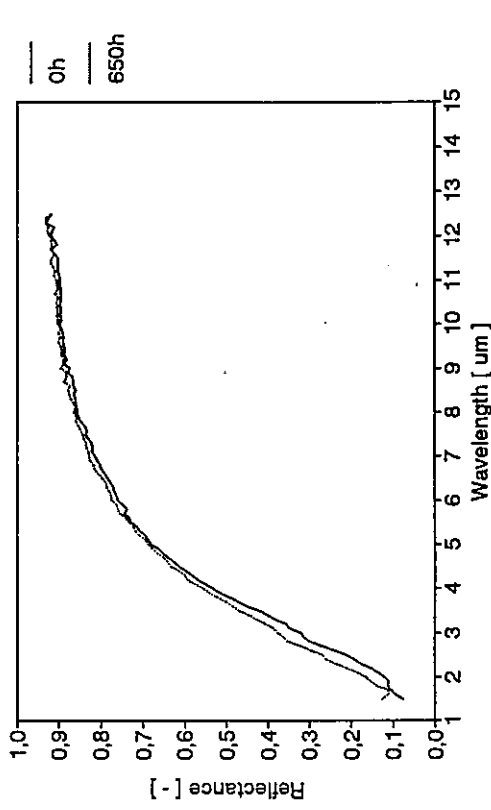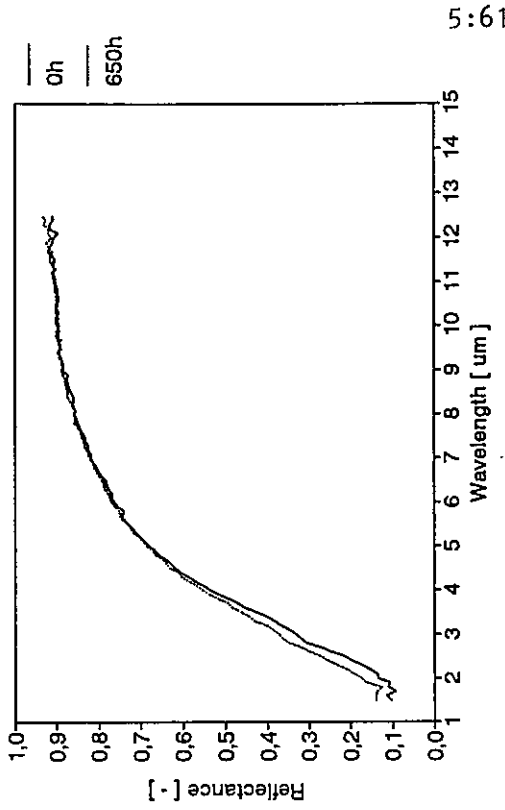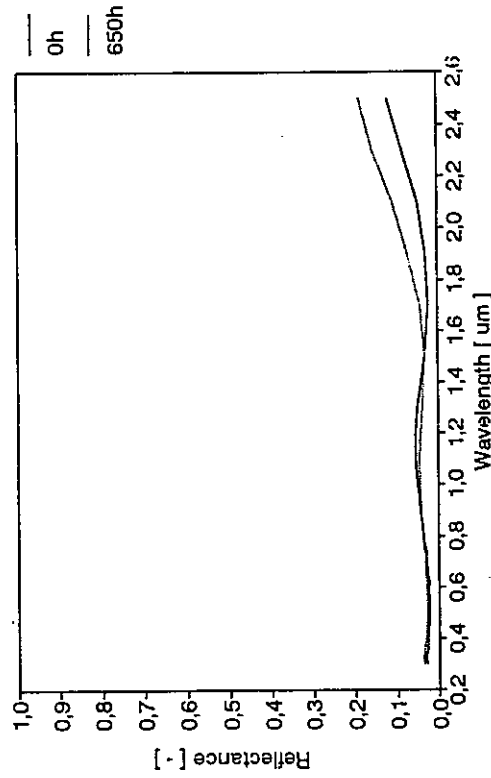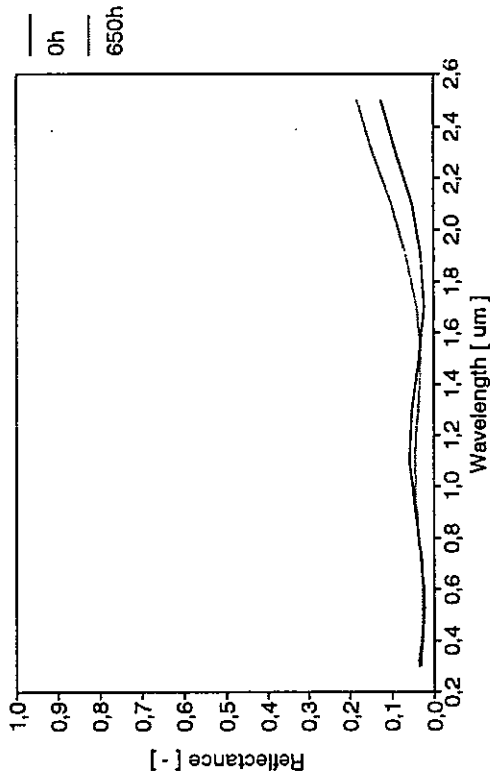
Cabinet: 90 °C, 95 % RH
Sample: 85 °C

| Time, h	α_s	ε_n(373 K)
0	0.965	0.142
3	0.968	0.139
10	0.970	0.139
50	0.971	0.135
150	0.966	0.135
300	0.966	0.133
650	0.961	0.131

5.4 Sulphur Dioxide Exposure Tests

A series of long-term laboratory exposure tests was conducted in order to study the combined effect of sulphur dioxide, high air humidity and temperature on coating degradation in the case study,

5.4.1 Equipment and ageing procedure

The test procedure employed was similar to that described in ISO 10062 "Corrosion tests in artificial atmosphere at very low concentrations of polluting gases". In each test performed, test samples were placed in a climatic cabinet and there exposed to circulating air of specified temperature, humidity and containing a fixed concentration of sulphur dioxide.

The climatic cabinet used for testing is described in *Figure 5;4* and a specification of relevant parts of the equipment is given in *Table 5;16*.

1. Climate chamber
2. External control
3. Inner chamber
4. Lead-trough, inner chamber
5. Lead-trough, climate chamber
6. Inlet for circulation
7. Outlet for circulation
8. Analysis point (movable)
9. Temperature sensor
10. Intake of conditioned air
11. Outlet from system
12. Mixing tube
13. Circulation pump
14. Evacuation pump
15. Gas analyzer
16. Connection to logger
17. Flowmeters
18. Regulation valves
19. Shut off valve
20. Magnetic valve
21. Gas bottle
22. Intake of clean air to climate chamber
23. Particle filter
24. Active coal filter
25. Air inlet

Figure 5;4 Climatic cabinet used for long-term exposure tests in high-humidity air containing sulphur dioxide.

Climatic Cabinet	
Type	WEISS 1000 SB
Volume	1.045 m^3
Internal dimensions	1100 x 1000 x 950 mm
Temperature range with humidity control	+10 - +95 °C
Humidity range	15 - 95 % RH
Materials	Stainless steel, glass and silicone gaskets and seals
Working space (Inner chamber)	
Type	WEISS
Volume	0.520 m^3
Internal dimensions	840 x 790 x 740 mm
Material	Teflon-coated stainless steel
Instruments for measurement and control of test conditions	
Temperature	Pt 100 sensors
Humidity	Psychrometer with Pt 100 sensors
Gas analyser for SO$_2$	Electrochemical cell INTERSCAN 1248 0 - 2, 0 - 10, 0 - 25 ppm
Gas flow system	
Flow rate of circulating air through inner chamber	4 m^3/h (1.7.10^{-3} m/s)
Flow rate of recirculated test atmosphere	2 m^3/h
Rate meter for air flow	Rotameter (0 - 9.2 m^3/h)
Sulphur dioxide gas	1000 ppm SO$_2$ in N$_2$ (ALFAX Pro Analysi)
Rate meter for sulphur dioxide gas flow	Rotameter (0 - 0.005 m^3/h)
Materials	Glass and Teflon

*Table 5;16   Specification of climatic cabinet, see **Figure 5;4**, used for long-term exposure of absorber coatings.*

In the design of a test cabinet for sulphur dioxide exposure testing, important parameters are: (a) materials of the relevant parts of the test equipment, (b) design of air flow and sulphur dioxide injection system, and (c) regulation and control systems for the test conditions in the inner chamber or working space, where the test samples are placed during the exposure test.

Test equipment must be made of inert materials, eg. Teflon or glass, to avoid or minimize adsorption of sulphur dioxide on surfaces other than of that of the test samples.

The air flow and sulphur dioxide injection system must be designed to ensure uniform test conditions in the working space. The test atmosphere in the working space is obtained by continuously introducing the necessary quantity of sulphur dioxide into a damp air flow to obtain the required concentration. Sulphur dioxide and conditioned air are mixed outside the cabinet. The conditioned air is taken from the outer chamber of the climatic cabinet. The air flow after injection of sulphur dioxide is then mixed with a flow of recirculated test atmosphere and the resulting gas flow admitted into the inner chamber or working space of the cabinet. Half of the flow of the test atmosphere through the inner chamber is recirculated.

To ensure uniform test conditions in the working space, the test atmosphere is supplied to the working space from the bottom and the outlet is placed at the top. Perforated plates are placed in front of the openings to assure uniform air flow through the working space. Uniformity of temperature in the working space should be better than ± 1 °C and uniformity of relative humidity better than ± 3 %.

The damp air flow should be within the tolerance for the specified temperature and relative humidity and be free of water droplets or aerosols. The air used is introduced to the outer chamber of the cabinet after filtration and purification by activated charcoal and a particulate filter. The sulphur dioxide gas is taken from a pressurized cylinder filled with 1000 ppm high-purity sulphur dioxide gas in high-purity nitrogen gas.

The working space should not be filled with test specimens in such a way that they shield one another, disturb the uniformity of air flow across the chamber or cause a change of sulphur dioxide concentration in the circulating air of more than 10 % during passage through the working space.

During the sulphur dioxide exposure tests the absorber coating samples were vertically placed in a special Teflon stand/holder at a distance of 3 cm apart from each other.

Pt 100 sensors are used for regulation and monitoring of temperature and humidity conditions during test. Humidity is measured psychrometrically from the difference between wet and dry bulb temperatures. The sensors and the uniformity of temperature and humidity within the working space are checked regularly between tests by use of a combined temperature and capacitance humidity sensor (Rotronic YA 100).

The concentration of sulphur dioxide in the air flow is adjusted to the correct level at the beginning and during testing, based on measurements of it at sampling points placed close to the inlet and outlet of the air flow through the working space, see *Figure 5;4*. An electrochemical cell device (INTESCAN 1248) is used for these measurements. The instrument is calibrated regularly by use of standard gas mixtures of sulphur dioxide in nitrogen gas.

The uniformity of the test conditions in the working space is also checked regularly by exposing a number of copper coupons, placed at different positions in the working space during sulphur dioxide exposure. The differences in weight change of the metal coupons indicate if the uniformity of test conditions is within specified range.

When performing a sulphur dioxide exposure test, the specified levels of temperature, air humidity and air flow rate are first adjusted. After stable conditions have been reached, the sulphur dioxide gas flow is adjusted to the specified level. When stabilized conditions have been reached after this step, the test specimens are placed in the working space. The test conditions are regularly checked during the test and, if necessary, adjusted to the specified levels.

When measuring the extent of degradation after a certain test time, the test specimens are removed from the working space and placed in a desiccator over silica gel. If, however, the test conditions are such that condensation would occur on the specimen surfaces upon removal from the working space, the humidity of the cabinet is first reduced before the test specimens are removed.

After making measurements, the test specimens are reintroduced to the working space after stabilized test conditions at the specified levels have been confirmed.
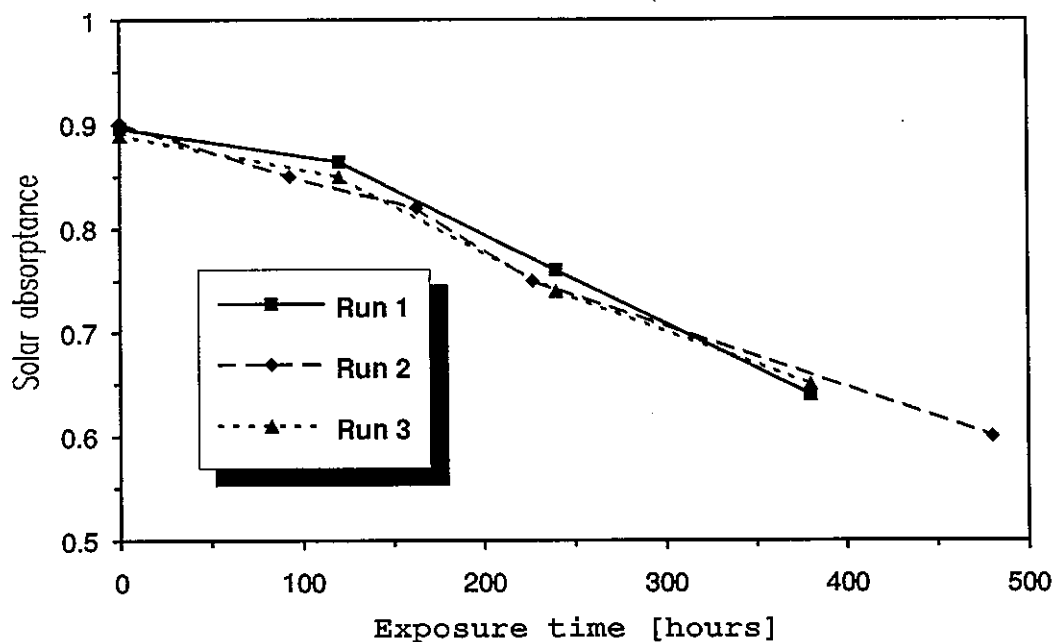
Figure 5;5   Results from reproducibility check of sulphur dioxide exposure test performed at 20 °C with the Sunstrip coating material.

To check the reproducibility of results obtained from the sulphur dioxide exposure tests, a series of tests were performed using the same test condition. The results are shown in *Figure 5;5*. As can be seen from this figure, the variations in results between the different tests performed are fairly small.

5.4.2 Ageing test results

The results from the sulphur dioxide exposure tests performed in the case study are presented in *Tables 5;17 - 5;20*.

In all tests, the sulphur dioxide concentration was 1 ppm except in one test where no sulphur dioxide addition was made. The concentration dependence was investigated separately by adsorption studies, presented in **Chapter 6** of this report.

The relative humidity level was 95 % in all tests performed except one. The dependence of the degradation on the relative humidity level was also investigated separately by adsorption studies, cf. above.

In the tables presenting the results of tests, only spectral data for the solar wavelength range are given. For the infrared wavelength region, spectral changes resulting from exposure testings were investigated by use of a special FTIR diffuse reflectance measurement technique. The results of these measurements are presented in **Chapter 6** of this report.

Data on weight changes of exposed metal coupons under the different test conditions used are presented in *Table 5;21*.

Table 5;17 *Results from sulphur dioxide exposure testings for the Showa nickel-pigmented anodized aluminium absorber coating.*

20 °C, 95 % RH, 1 ppm SO$_2$

Time, h	α_s	ε_n(373 K)
0	0.930	0.102
120	0.932	0.102
240	0.849	0.140
480	0.720	0.163
1000	0.605	0.181
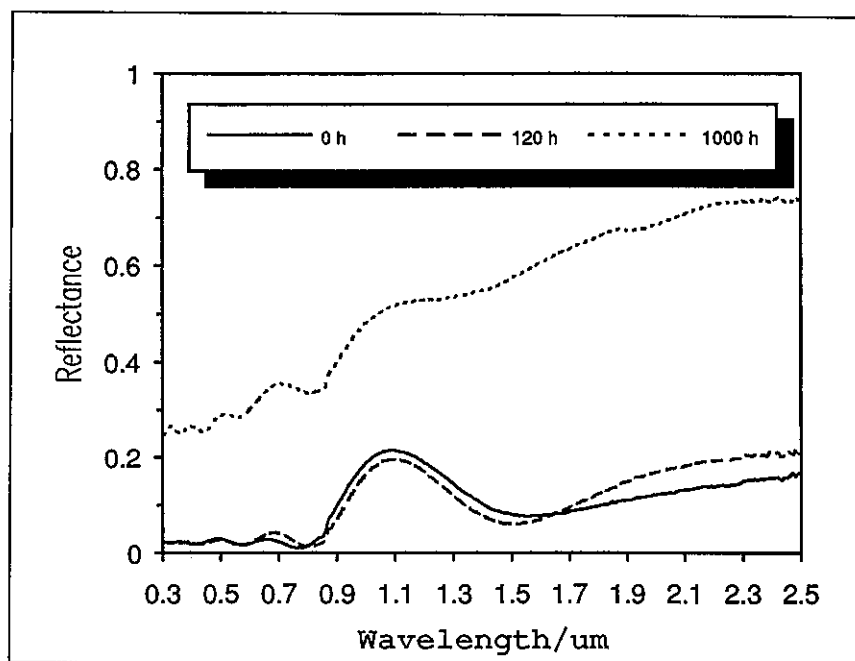
20 °C, 95 %, no addition of SO$_2$

Time, h	α_s	ε_n(373 K)
0	0.932	0.102
240	0.932	0.110
480	0.932	0.109
1000	0.933	0.108
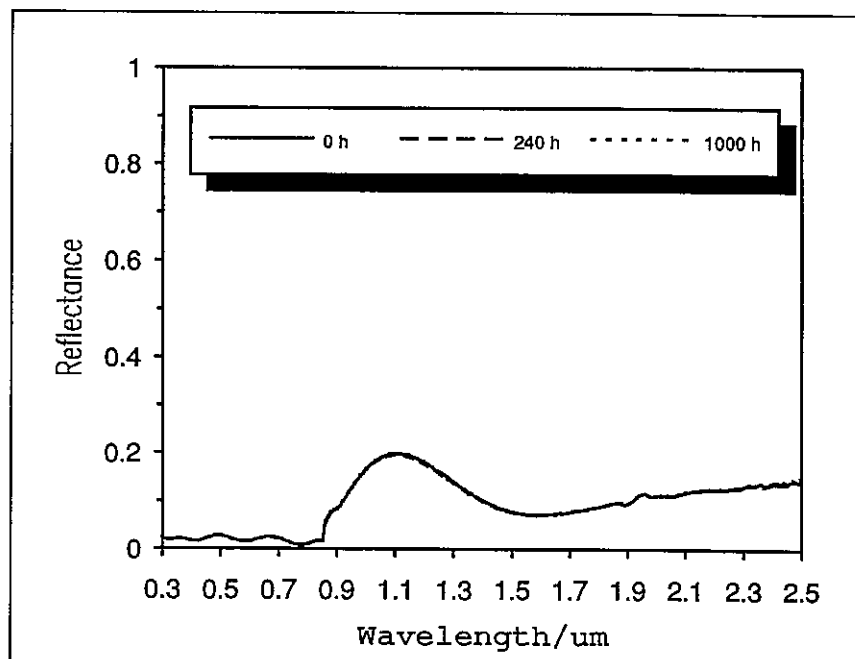
Table 5;17 cont.

20 °C, 75 % RH, 1 ppm SO$_2$

Time, h	α_s	ε_n(373 K)
0	0.932	0.101
240	0.931	0.103
480	0.933	0.103
1000	0.932	0.105
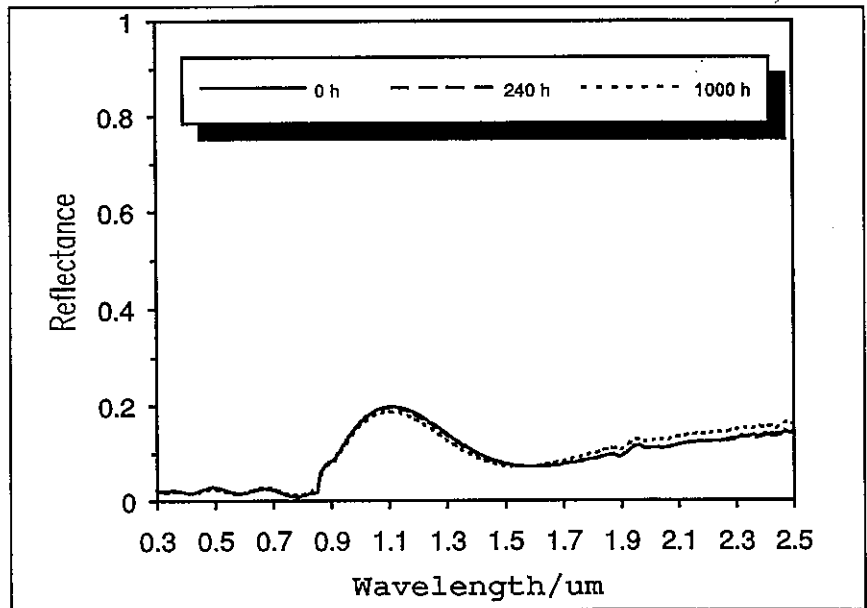
50 °C, 95 % RH, 1 ppm SO$_2$

Time, h	α_s	ε_n(373 K)
0	0.928	0.105
120	0.917	0.104
240	0.903	0.110
480	0.891	0.122
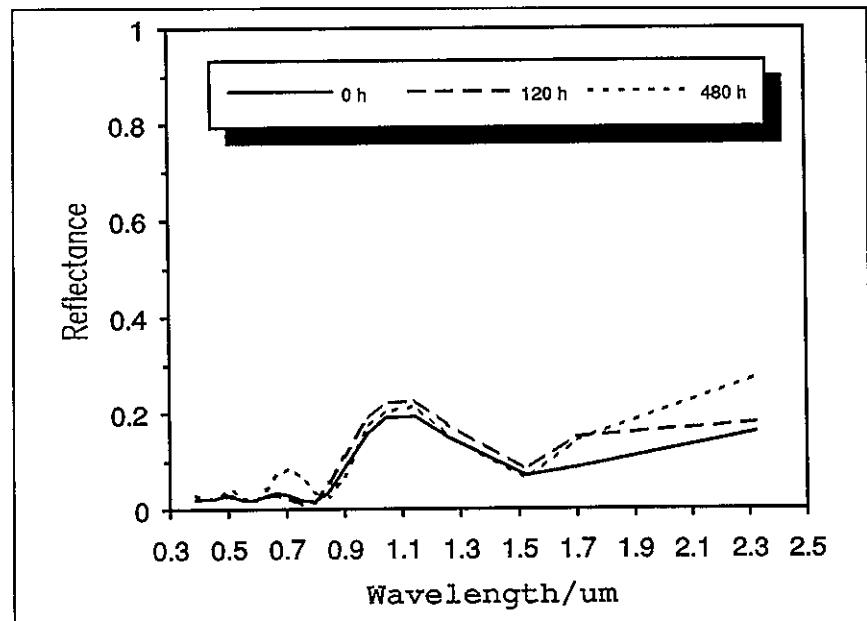
Table 5;17 cont.

70 °C, 95 % RH, 1 ppm SO$_2$

| Time, h	α_s	ε_n(373 K)
0	0.920	0.107
120	0.916	0.108
240	0.904	0.111
480	0.888	0.106
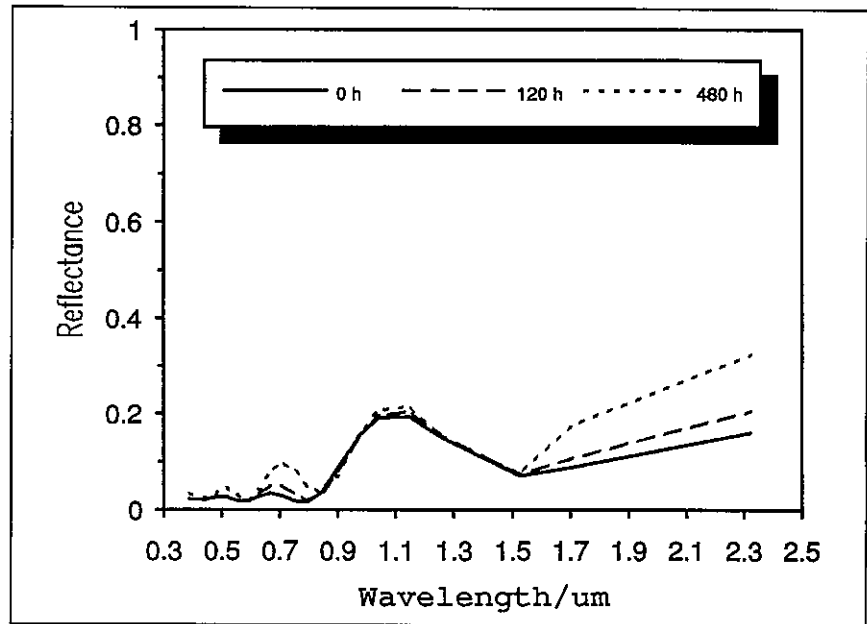
Table 5;18 *Results from sulphur dioxide exposure tests for the Sunstrip nickel-pigmented anodized aluminium absorber coating*

20 °C, 95 % RH, 1 ppm SO$_2$

Time, h	α_S	ϵ_n(373 K)
0	0.896	0.108
120	0.864	0.112
240	0.76	0.133
480	0.695	0.160
1000	0.632	0.171
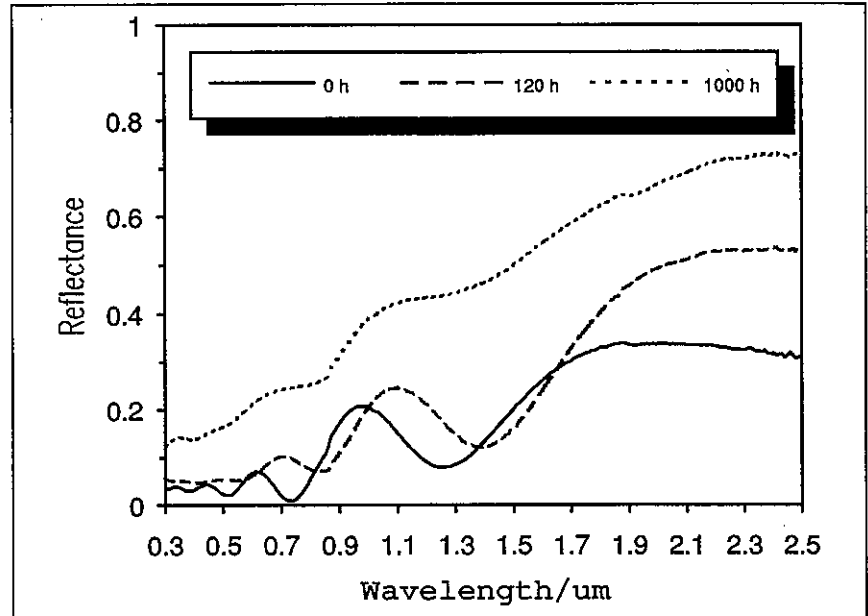
20 °C, 95 % RH, no addition of SO$_2$

Time, h	α_S	ϵ_n(373 K)
0	0.888	0.110
240	0.886	0.112
480	0.885	0.111
1000	0.887	0.115
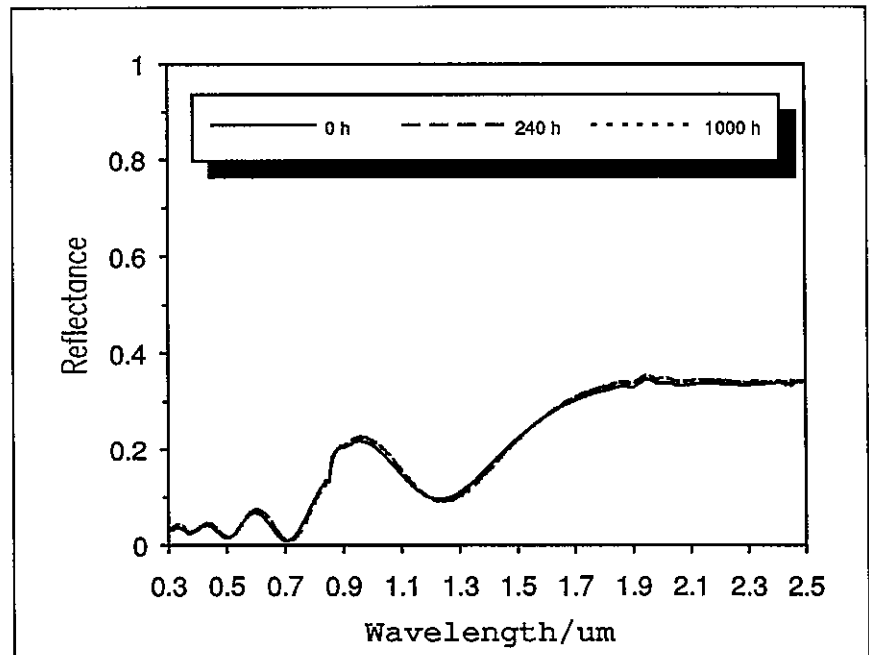
Tabel 5;18 cont.

20 °C, 75 % RH, 1 ppm SO$_2$

Time, h	α_S	ε_n(373 K)
0	0.891	0.109
240	0.887	0.113
480	0.888	0.111
1000	0.887	0.117
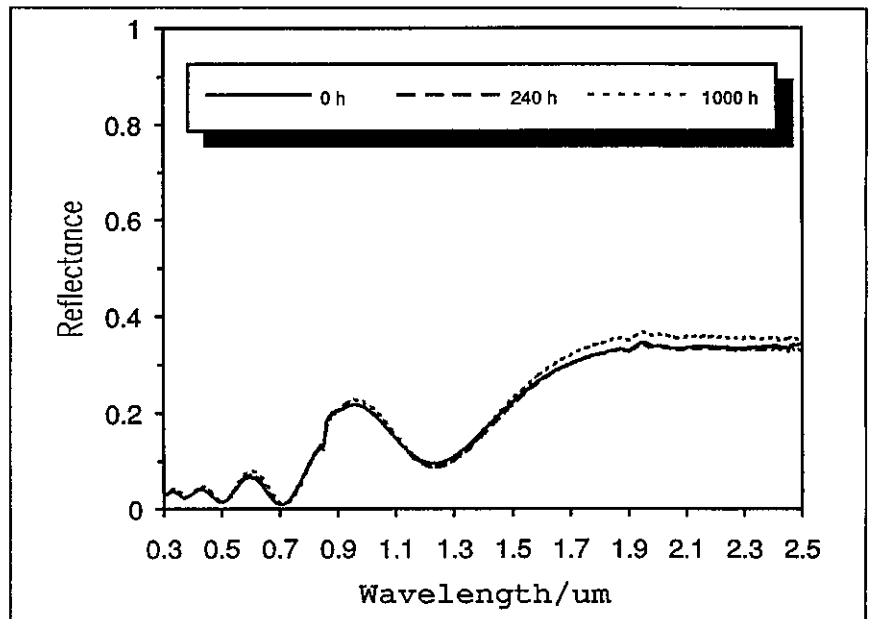

50 °C, 95 % RH, 1 ppm SO$_2$

Time, h	α_S	ε_n(373 K)
0	0.887	0.101
120	0.855	0.103
240	0.832	0.106
480	0.793	0.130
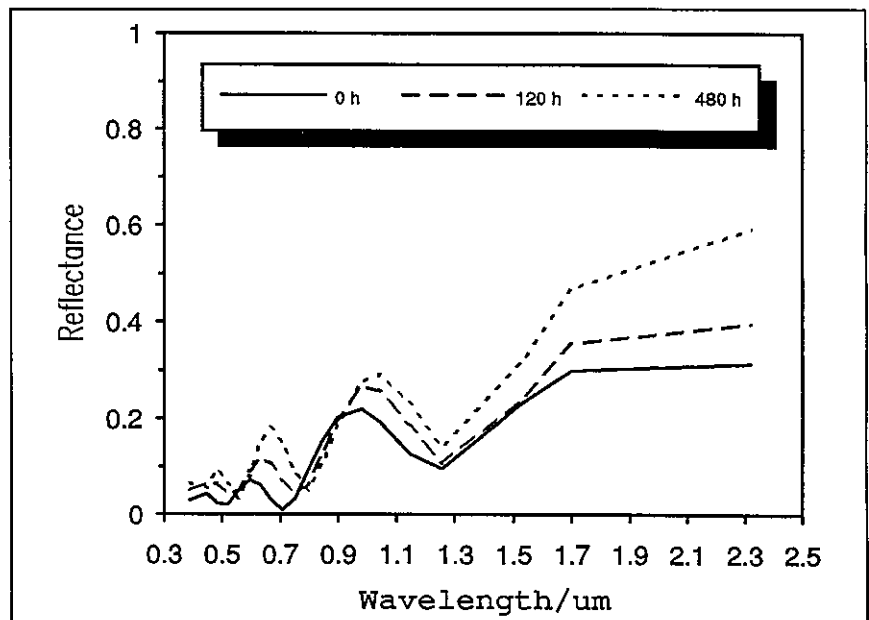
Table 5;18 cont.

70 °C, 95 % RH, 1 ppm SO$_2$

Time, h	α_s	ε_n(373 K)
0	0.878	0.087
120	0.815	0.099
240	0.637	0.222
480	0.613	0.220
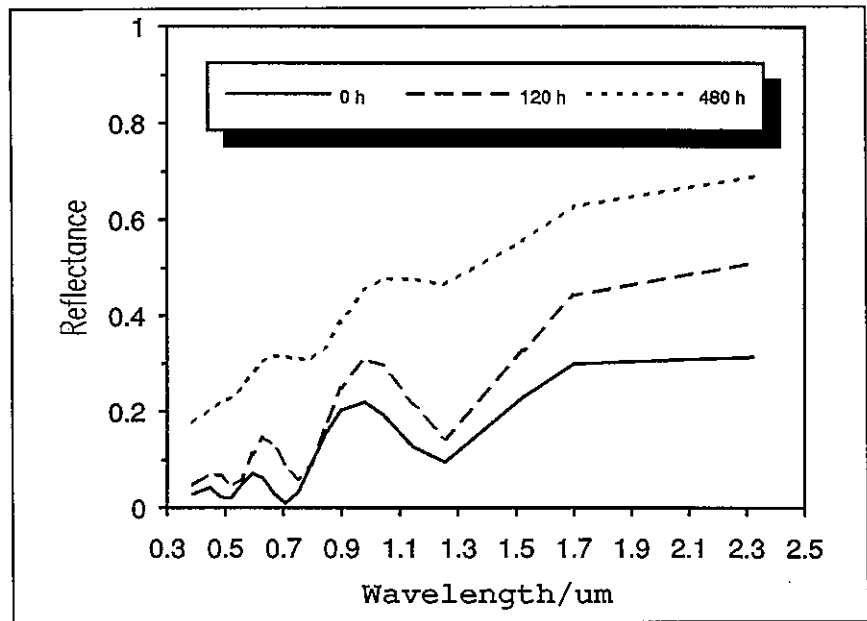
Table 5;19 *Results from sulphur dioxide exposure tests for the Energie Solaire black chrome absorber coating*

20 °C, 95 % RH, 1 ppm SO$_2$

Time, h	α_S	ε_n(373 K)
0	0.931	0.159
120	0.936	0.158
240	0.935	0.160
480	0.929	0.160
1000	0.928	0.162
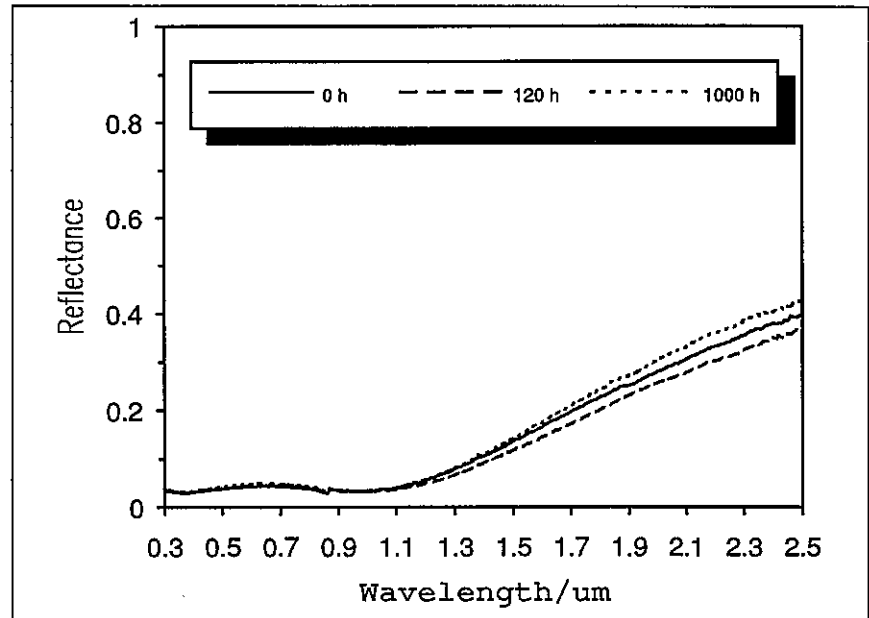
50 °C, 95 % RH, 1 ppm SO$_2$

Time, h	α_S	ε_n(373 K)
0	0.941	0.217
120	0.938	0.215
240	0.934	0.223
480	0.930	0.220
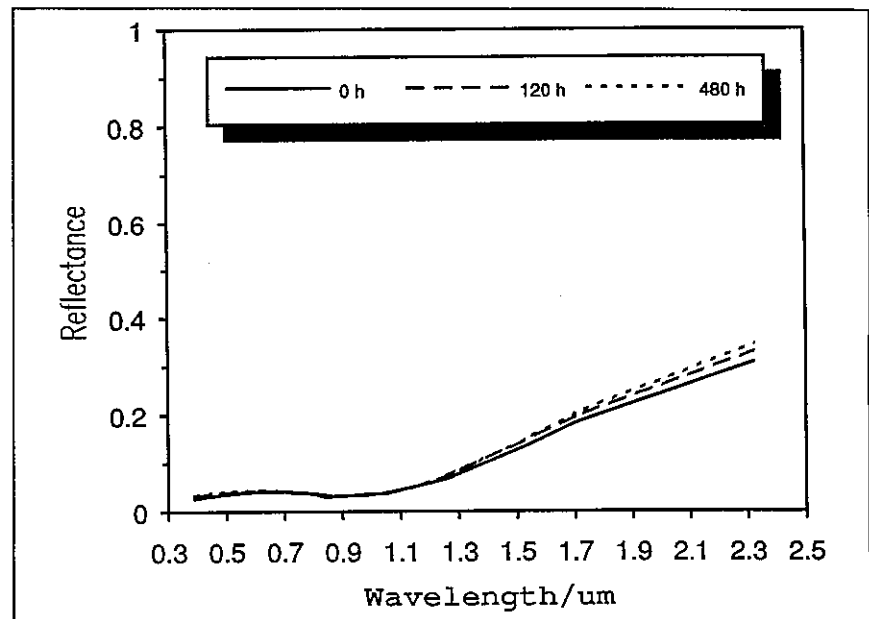
Table 5;19 cont.

70 °C, 95 % RH, 1 ppm SO$_2$

Time, h	α_s	ε_n(373 K)
0	0.930	0.156
120	0.929	0.162
240	0.922	0.171
480	0.920	0.173
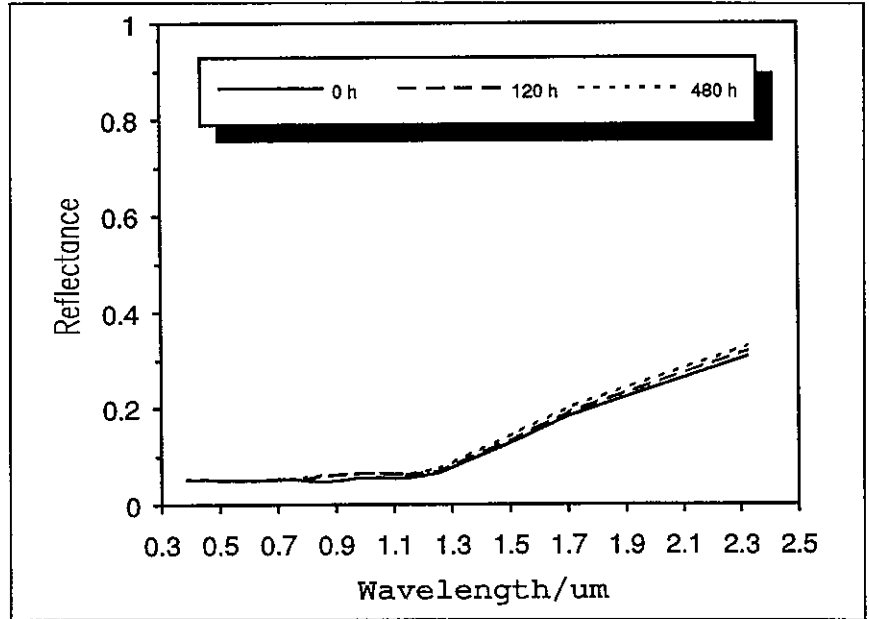
Table 5;20   *Results from sulphur dioxide exposure tests for the MTI black chrome absorber coating*

20 °C, 95 % RH, 1 ppm SO$_2$

Time, h	α_S	ε_n(373 K)
0	0.965	0.139
120	0.967	0.129
240	0.966	0.135
480	0.966	0.137
1000	0.965	0.145
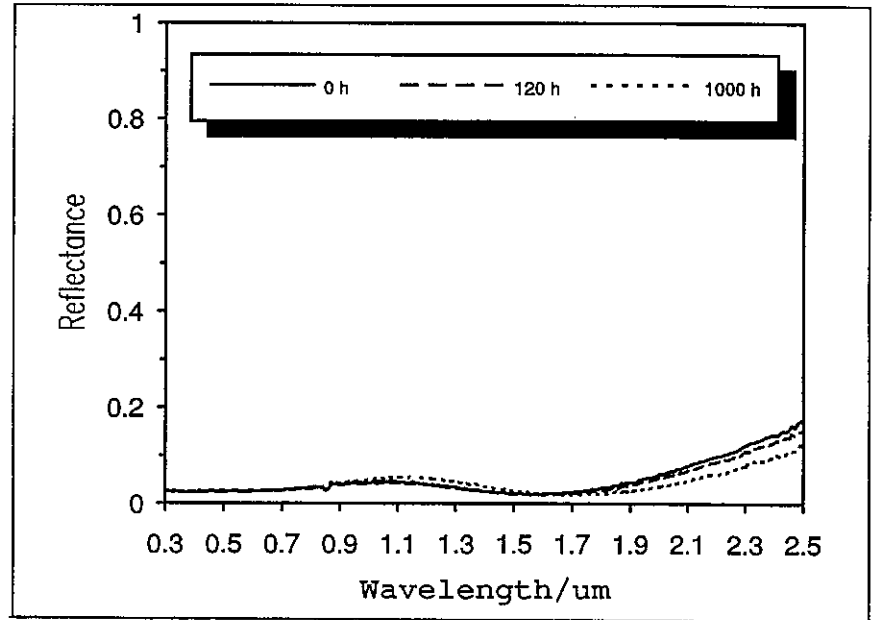
50 °C, 95 % RH, 1 ppm SO$_2$

| Time, h	α_S	ε_n(373 K)
0	0.966	0.130
120	0.961	0.133
240	0.954	0.136
480	0.951	0.132
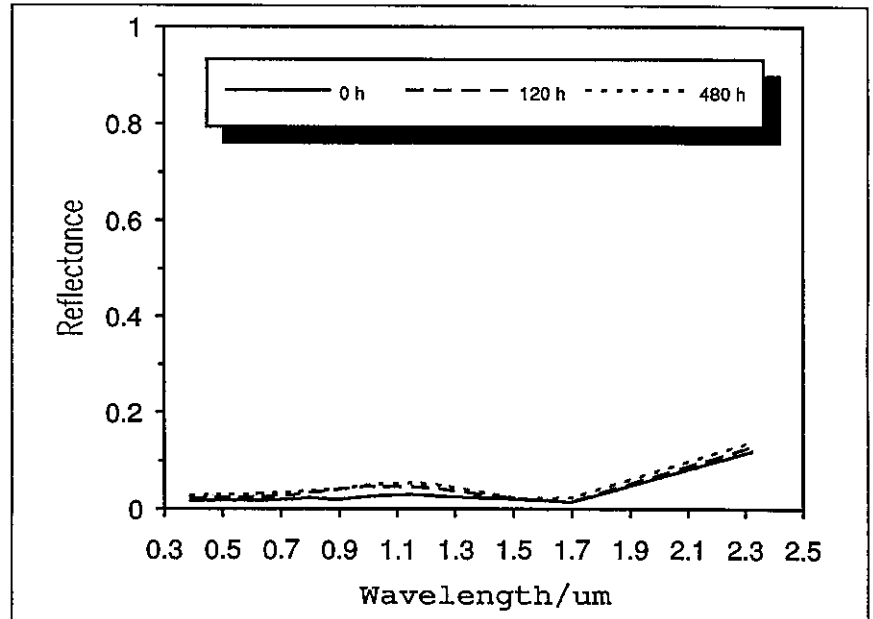
*Table 5;20* cont.

70 °C, 95 % RH, 1 ppm SO$_2$

Time, h	α_s	ε_n(373 K)
0	0.967	0.140
120	0.959	0.151
240	0.957	0.165
480	0.953	0.178
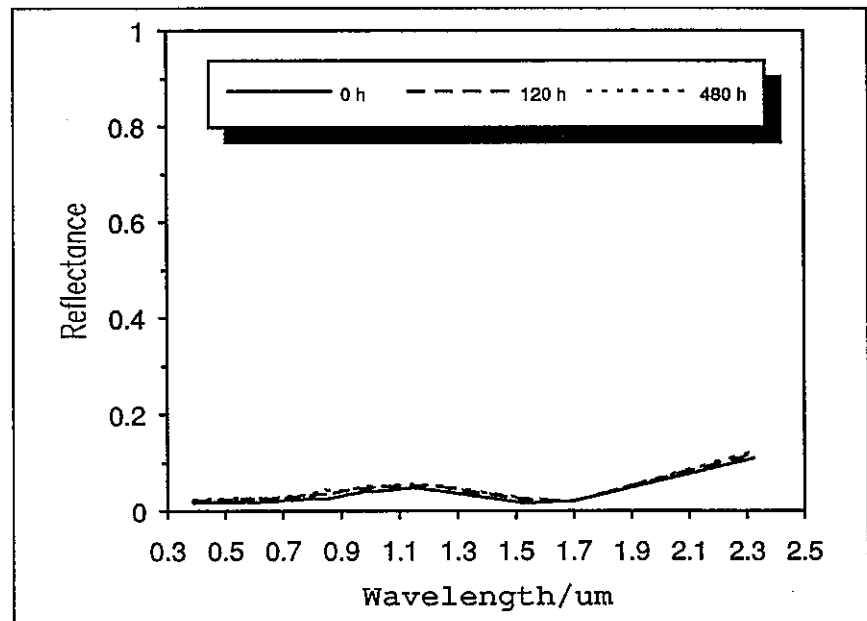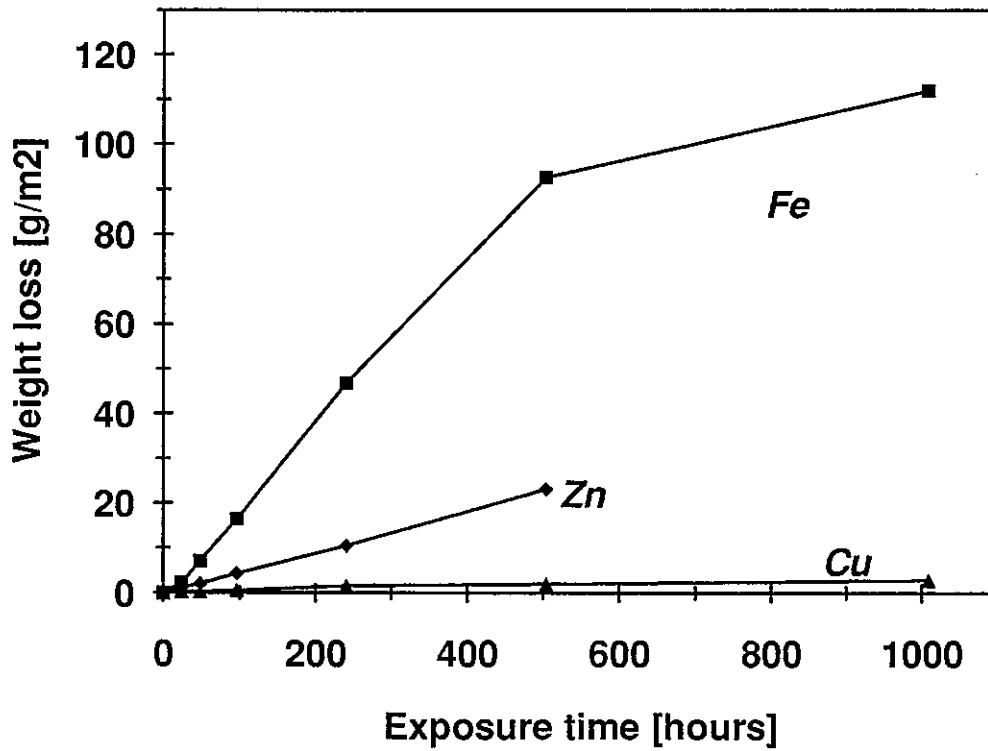
Exposure time (hours)	Metal weight loss of coupons (g/m^2)		
	Steel	Zinc	Copper
24	2.2	1.1	0.24
48	7.0	2.0	0.25
96	16.3	4.3	0.54
240	46.9	10.4	1.61
504	92.6	23.2	1.93
1008	111.9		2.82

Table 5;21 *Metal weight losses of standard metal specimens exposed to 1 ppm SO_2, 95 % RH, and 20 °C for testing times indicated in the table.*
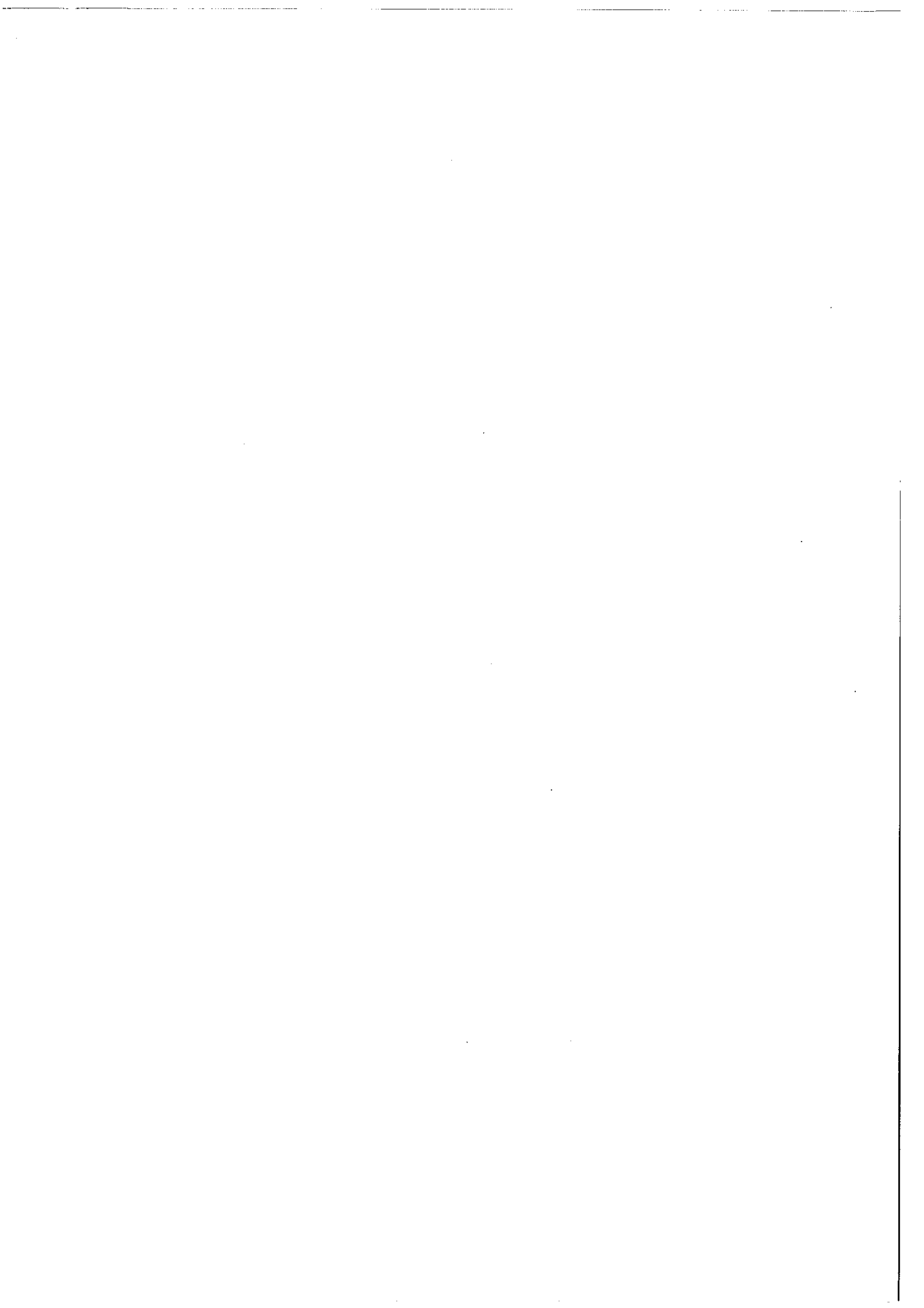
CHAPTER 6

INTERPRETATION OF AGEING TEST RESULTS

6.1 Purpose and Scope of Work

In interpreting the observed loss in coating performance caused by accelerated ageing, use was made of both qualitative and quantitative techniques for analysis.

The first step of analysis was merely qualitative in nature. Work was directed to the identification of the degradation mechanisms or the changes in composition, structure and morphology of coatings accompanying the loss in optical performance observed in the accelerated ageing tests.

Loss in optical performance is directly connected to changes in the reflectance spectrum of coatings in the visible, near infrared and infrared wavelength regions. Consequently, the main efforts were made to interpret those spectral changes in terms of chemical and physical degradation processes.

As a complement to these studies, aged coatings were also analysed by use of such techniques as Scanning Electron Microscopy (SEM), Energy-dispersive X-ray Spectroscopy (EDX), Auger Electron Spectroscopy (AES) depth profiling, and X-Ray Diffractiometry (XRD). In the interpretation work, use was made also of the effective medium theory model to calculate optical characteristics of the nickel-pigmented coatings used in the case study, the model previously described in *Chapter 3* of this report.

The intent of using such a variety of techniques for analysis was twofold. The first was the generation of information about degradation of coatings which, independently of other results, could provide evidence as to whether a hypothesized degradation mechanism had been operative or not during an ageing test. The second was demonstration what kind of conclusions that could be drawn from results obtained with the different techniques adopted for analysis in the case study.

The next step in the interpretation work was analysis of the kinetics of degradation observed during the accelerated ageing tests. This analysis involved modelling the changes in solar absorptance and thermal emittance observed during the ageing tests, as functions of the various test parameters used. Efforts here were directed to finding simple models to describe kinetic data based on the results of the qualitative analysis mentioned above. Some complementary studies were also performed in the form of high-temperature ageing under vacuum conditions, combined high-temperature ageing and condensation testing and studies of the absorption of sulphur dioxide on the nickel-pigmented coatings under various experimental conditions, as already mentioned in *Chapter 5* of this report.

The purpose of this work was also twofold. The first to develop kinetic models to describe degradation data for life data analysis, and second to identify critical properties of coatings, or weak points in coating design as regards resistance to different environmental agents. It should be pointed out, however, that in order to rank the im-

portance of different environmental factors, the in-use conditions of environmental influence have to be taken into account, as dealt with later in *Chapter 7*.

6.2   High - temperature Degradation of Coatings.

6.2.1   Dominant mechanisms of degradation causing loss in optical performance of coatings.

Black chrome absorber coatings

From the reflectance spectra given in *Chapter 5 Tables 5;5* and *5;6* at different temperatures and testing times of high-temperature ageing, the following qualitative information can be obtained.

For the Energie Solaire black chrome coating, an initial degradation process seems to occur, strongly increasing the reflectance in the near infrared, while the reflectance in the visible wavelength range is only slightly decreased. In the infrared wavelength region, the wide absorption bands with maxima around 3.0 and 6.4 µm visible in the spectrum of the unaged sample, suggest the existence of absorbed water, disappear. Thus, desorption of water from the coating is likely to occur. Similar spectral changes, in the visible, near infrared and infrared wavelength region, can also be observed for degradation caused by high-temperature exposure of the sample under vacuum conditions. However, at longer testing times under high temperature testing in air, the solar absorptance decreases steadily and the increase in reflectance is observed mainly in the visible wavelength region, while the reflectance in the near infrared approaches a limiting value. The development of an interference pattern suggests the formation of a compact layer structure. The extrema of the interference pattern stay at the same wavelengths as the degradation proceeds. Therefore it must be assumed the layer thickness remains the same while the absorptivity or attenuation coefficient of coating, mainly determined by the concentration of metallic chromium, decreases.

The spectral behaviour during the ageing of the MTI black chrome absorber coating resembles that observed for the Energy Solaire black chrome absorber coating. The interference pattern observed in the reflectance spectrum of the latter is, however, less pronounced.

Accordingly, the spectral changes observed after high-temperature ageing of the two black chrome absorber coating materials is consistent with the following two mechanisms being operative:

- Desorption of water from the coating during the initial phase of degradation.

- Oxidation of metallic chromium to chromium oxide as the high temperature degradation progresses.

That these two mechanisms are dominant in the high-temperature degradation of black chrome coatings is quite well known [6.1].

Of interest for the Task X group was therefore to see if the assumed mechanisms of degradation could also be confirmed by using other kinds of techniques for analysis.

SEM, AES depth profiling and XRD studies were therefore undertaken by Tanemura et al [6.2 - 6.4] on some of the aged samples of case study.

AES depth profiles for some aged samples of the two black chrome coatings are presented in *Figures 6;1 and 6;2*. As can be seen, the O/Cr ratio increases with the extent of degradation. This is consistent with oxidation of metallic chromium to chromium oxide occuring during high - temperature ageing of samples.

a) Unaged sample

b) Sample degraded at 350 °C for 100 hrs ($-\Delta\alpha_s$= 0.061)

c) Sample degraded at 450 °C for 50 hrs ($-\Delta\alpha_s$ = 0.101)

d) Sample degraded at 500 °C for 4 hrs under vacuum conditions
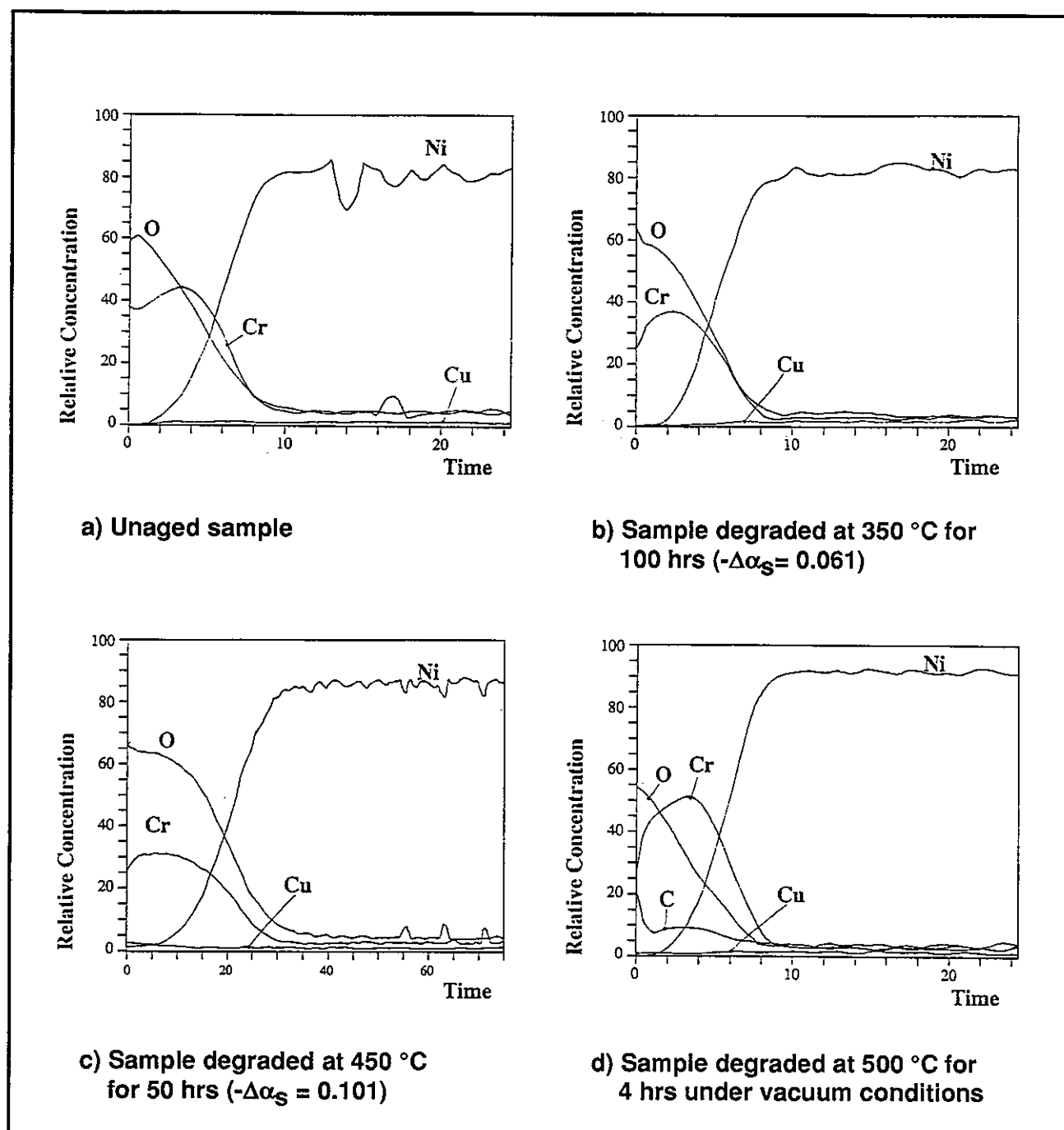
Figure 6;1 AES depth profiles for the MTI black chrome absorber samples recorded after high-temperature ageing.
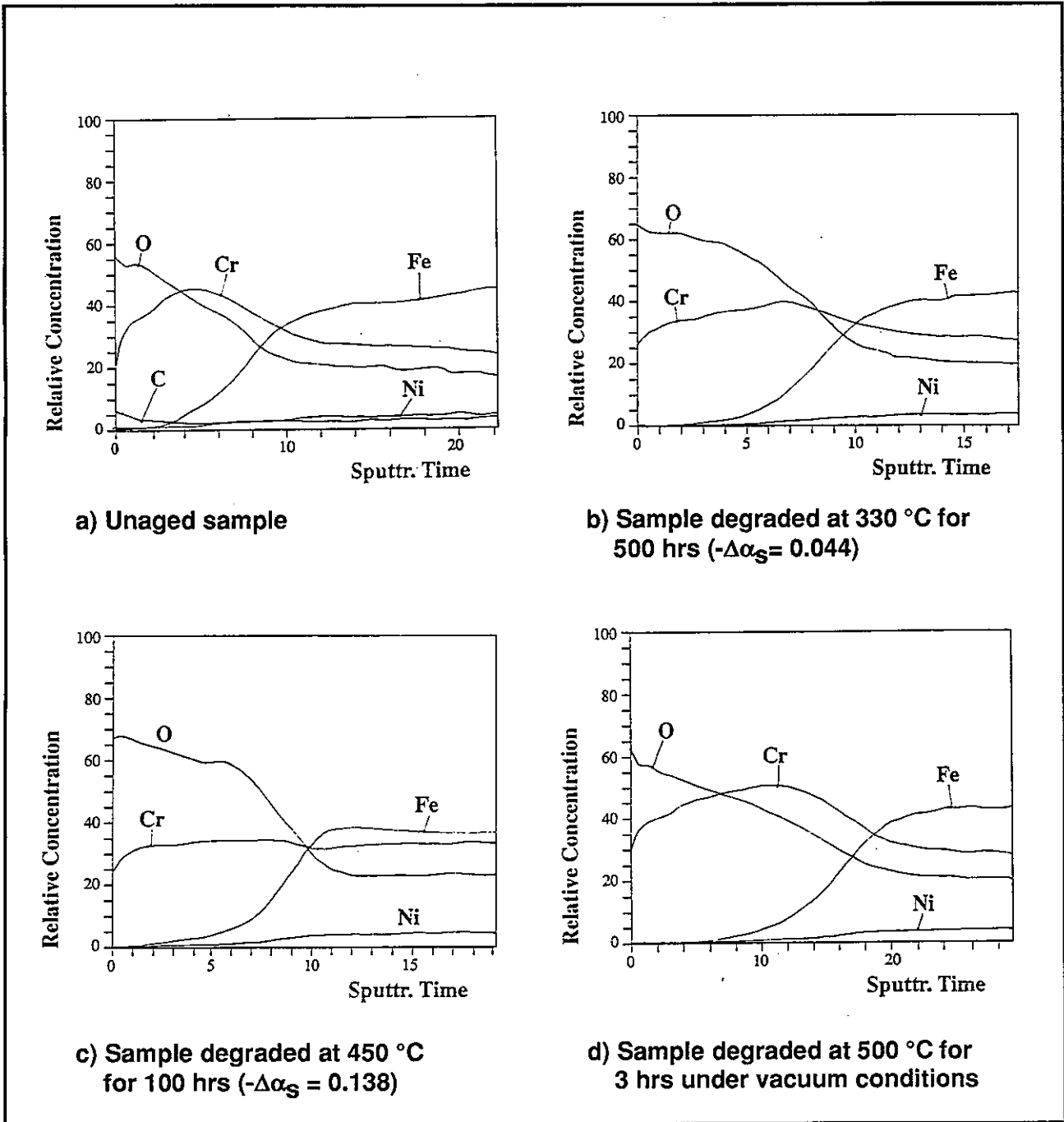
Figure 6;2 AES depth profiles for the Energie Solaire black chrome absorber coating samples recorded after high-temperature ageing.

For the samples degraded under vacuum conditions, the O/Cr ratios are lower compared with the corresponding ratios for the undegraded samples. This effect is particularly pronounced for the MTI absorber coating. Consequently, the desorption of water from the coatings aged under vacuum conditions and during the initial phase of high-temperature degradation in air seems likely to occur.

From SEM studies, it could be concluded that the surface morphology of the two coatings is hardly affected by the high-temperature ageing. At testing performed under vacuum conditions of the Energy Solaire coating, however, small craters, which may have been formed due to the escape of water from the coating, can be observed, see *Figure 6;3*.

a) Unaged sample (x 1500)

b) Sample degraded at 450 °C for 100 hrs ($-\Delta\alpha_s$= 0.138) (x 2000)
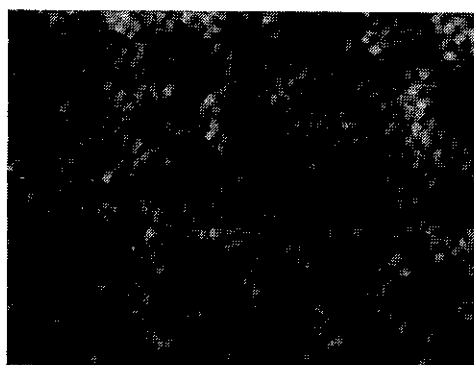
c) Sample degraded at 500 °C for 3 hours under vacuum conditions (x 1500)

Figure 6;3 SEM micrographs of samples of the Energie Solaire black chrome absorber coating degraded by high-temperature testing.

Studies of some high-temperature aged samples of the MTI black chrome absorber using XRD were also undertaken by Tanemura et al. Experimental details and complete results of these studies are given in [6.3]. From a comparison between the diffraction patterns of aged coatings and that of an undegraded coating, it is, however, hard to draw any far-reaching conclusions about the reaction mechanisms, which may have contributed to the observed loss in optical performance at high-temperature ageing of the coating.

Nickel-pigmented anodized aluminium absorber coatings

From a qualitative point of view, the spectral changes observed as a result of high - temperature ageing of the two nickel-pigmented anodized aluminium absorber coatings are essentially the same, as can be seen from the reflectance spectra given in *Chapter 5, Tables 5;7* and *5;8*.

In the initial phase of high-temperature exposure in air, a rapid change in reflectance occurs at the same time, the pronounced maxima in the interference pattern of reflectance is shifted to shorter wavelengths. Below testing temperatures of 400 °C, the initial change in reflectance seems to be of the same magnitude irrespective of temperature. As degradation proceeds, the main effect in the spectrum of coating upon ageing is a gradual increase in reflectance, especially at wavelengths longer than 1 µm.

It should be noted that high - temperature ageing under vacuum conditions results in minor changes. The change in reflectance spectrum is qualitatively the same, but only slight compared with the corresponding change occuring for the test performed in air at the same temperature. This finding strongly suggests, as expected, that oxidation of metallic nickel to nickel oxide is the main degradation process for high-temperature ageing in air.

Based on this assumption Niklasson extended his effective medium theory calculations, see *Chapter 3*, in order to simulate spectral changes which should result from oxidation of metallic nickel taking place as a result of ageing of the coatings.

The rate of oxidation of metallic nickel may be limited by diffusion processes taking place at or below the surface of a metallic particle, or by processes related to the transport of oxygen from the coating surface to the surface of the individual metallic particles within the coating. In the former case, the oxidation of nickel will take place uniformly in the coating. In the latter case an oxidation front will develop moving deeper and deeper into the coating as the oxidation progresses.

To simulate the spectral changes which should occur if the oxidation of nickel took place uniformly in the coating, Niklasson [6,5] made a series of calculations. He simply varied the concentration of metallic nickel in his model, i.e. the filling factor, f, of metallic nickel in the composite layer, see *Figure 6.4.(a)*. As can be seen, the qualitative features of the spectral changes with decreasing values of the filling factor are essentially the same as observed experimentally with increasing testing time or extent of degradation in optical performance. The calculated series of spectra does not, however, simulate the small initial shift of the interference pattern to shorter wavelengths as observed experimentally. For wavelengths longer than 1.5 µm, the calculated reflectance values increase somewhat with wavelength, while the experimental reflectance values do not. However, these discrepancies are only minor and

Niklasson's calculations, therefore, give strong support to the hypothesis that the degradation in optical performance is due to a fairly uniform oxidation of the metallic nickel particles throughout the composite layer.

To simulate the case of an oxidation front moving deeper and deeper into the coating, Niklasson also made a series of calculations. He then gradually decreased the thickness of the composite layer while keeping its filling factor constant and increased the thickness of the second layer from the top so that the sum of the two remained the same. As can be seen from *Figure 6;4 (b)*, this yielded, from a qualitative point of view, quite different changes in the reflectance spectrum than were observed experimentally. Moreover, the results indicate that the solar absorptance increases slightly when the normalized amount of metallic nickel, Q, decreases, which is in contradiction to experimental results.
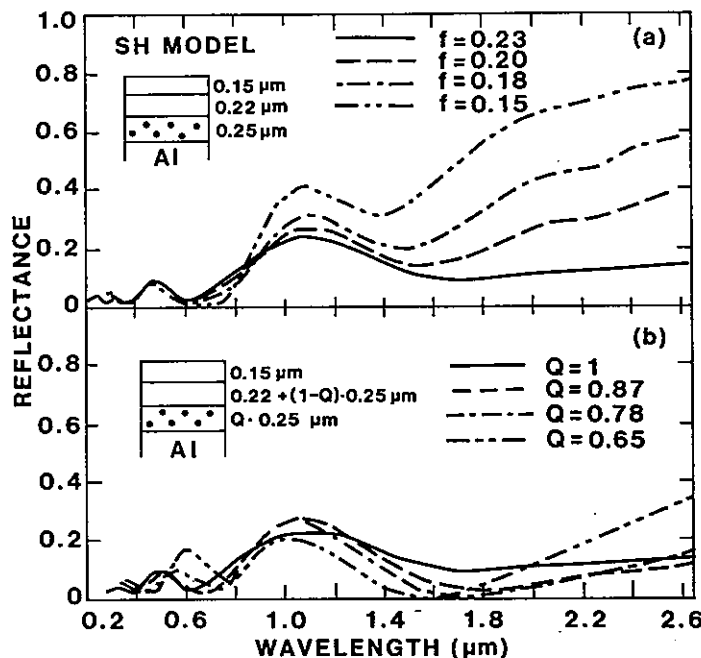
Figure 6;4 Calculated reflectance spectra for nickel-pigmented anodized aluminium coatings performed by Niklasson [6.5]. The calculations were carried out using parameters pertinent to the Showa coating, see Figure 3;13. In a), calculations for four filling factors, f, are shown. In b), results for four different thicknesses of the composite layer with a filling factor of 0.23 are depicted. The parameter Q denotes the normalized nickel content in the film. The structural models and parameters used in the calculations, as well as the differently indicated curves, are shown in the inserts.

It is not possible to draw any conclusions from the AES depth profiles recorded by Tanemura et.al. [6.2] whether oxidation of metallic nickel takes place as a result of high-temperature ageing in air or not. The O/Ni ratio is essentially the same for all samples studied: see examples of AES depth profiles for the Sunstrip coating in *Figure 6;5*.
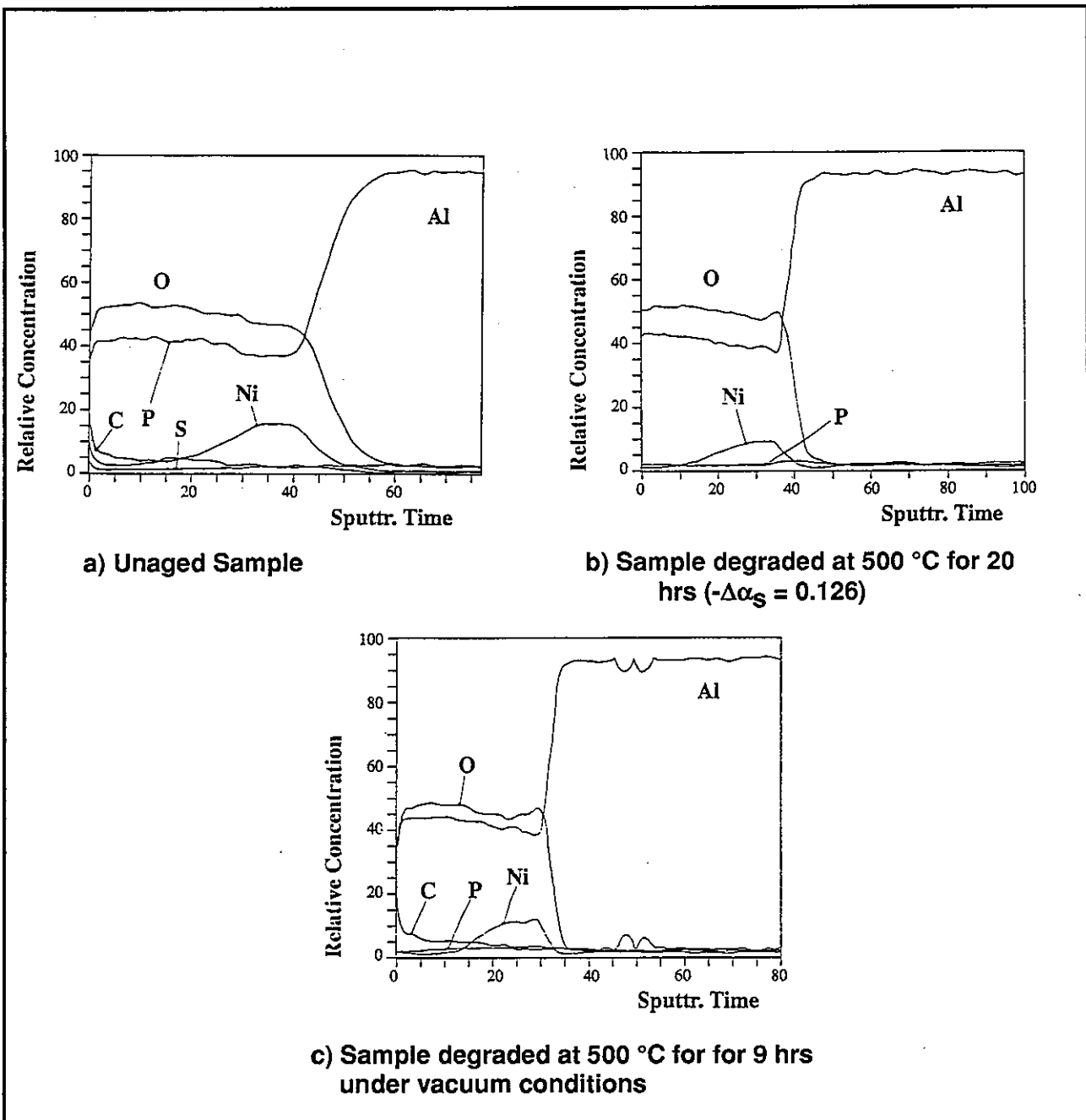
Figure 6;5 AES depth profiles for the Sunstrip nickel-pigmented anodized aluminium absorber coating samples recorded after high-temperature ageing.

Changes observed, for example between depth profiles b) and c) in *Figure 6;5*, are small and the increase in O/Ni ratio when going from c) to b) cannot be considered significant when compared with other depth profiles studied.

With XRD technique, however, Tanemura et.al. could observe diffraction peaks originating from NiO on high - temperature aged samples. These peaks could not be seen in the diffraction pattern of the undegraded sample [6;4].

No significant changes in surface morphology caused by high-temperature ageing could be observed from SEM investigations of aged samples in the case of the Showa coating. The surface morphology of the Sunstrip coating was, however, somewhat affected, as can be seen in *Figure 6;6.*

a) Unaged Sample
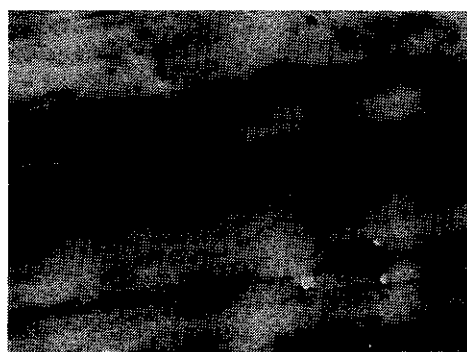
b) Sample degraded at 500 °C for 20 hrs ($-\Delta\alpha_S$ = 0.126) (x 2000)
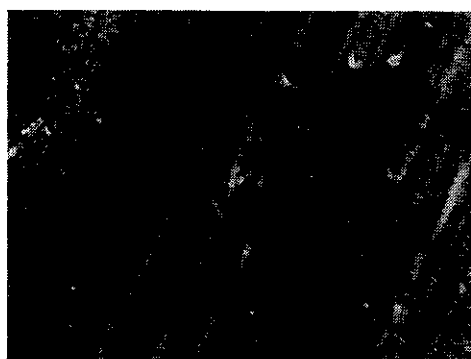
c) Sample degraded at 500 °C for for 9 hrs under vacuum conditions (x 1500)

Figure 6;6 SEM micrographs of samples of the Sunstrip nickel-pigmented anodized aluminium absorber aoating degraded by high-temperature testing.

For the high-temperature aged sample in air, deterioration of the surface morphology can be seen. Bright small particles also appear on the surface. On the surface of the sample exposed under vacuum conditions, craters appear, which probably originate from heavy boiling of water inclusions in the coating during exposure.

6.2.2 Kinetics of degradation, temperature dependence and time transformation functions for accelerated life testing

For modelling of the kinetic data from the high-temperature tests, the following analysis may be taken as a point of departure.

As only the temperature differs between the tests performed, the time transformation function according to equation (2,6) may be written as

$$\frac{y_R}{y} = g\,(\bar{S}\,)/\,g\,(\bar{S}_R) = h\,(T)/h(T_R) \tag{6,1}$$

To model the temperature dependence, the Arrhenius equation may then be used and thus

$$h(T)/h(T_R) = \exp\,(-E/R(T^{-1} - T_R^{-1})) \tag{6,2}$$

and

$$y = y_R \cdot \exp\,(E/R(T^{-1} - T_R^{-1})) \tag{6,3}$$

where E = action energy according Arrhenius and R = ideal gas constant.

The failure time y denotes the time needed to reach a certain extent of degradation at the temperature T and y_R is the corresponding time needed to reach the same extent of degradation at the temperature T_R.

By use of equation (6,3), thus, the activation energy E could, in principle, simply be evaluated from y - versus - T relationships at different extents of degradation, i.e. for different-$\Delta\alpha_s$ values. However, such a procedure is complicated by the facts that y-values for low extents of degradation are difficult to determine at high temperatures because of too high rate of degradation and y-values for high extents of degradation are difficult to determine at low temperatures because of too low rate of degradation.

One way to proceed is therefore to make use also of equation (2,5), which may be rewritten as

$$y_R = g^{-1}(\bar{S}_R) \cdot B(\alpha_{s,0}, \alpha_s, y_R) \approx C\,(-\Delta\alpha_s) \tag{6,4}$$

as $g(\bar{S}_R)$ can be considered a constant and the variation in $\alpha_{s,0}$ between different high - temperature tests in relatively small.

Combining eqs (6,3) and (6,4) then yields

$$y = \exp\,(E/R \cdot (T^{-1} - T_R^{-1})) \cdot C(-\Delta\alpha_s) \tag{6,5}$$

or

$$\ln y = E/R \cdot (T^{-1} - T_R^{-1}) + \ln\,(\,C(-\Delta\alpha_s)) \tag{6,6}$$

According to eq. (6,6) In y should be plotted versus $-\Delta\alpha_s$ for the different high - temperature tests. If the distance in In y between the different curves obtained is constant for all $-\Delta\alpha_s$ values, this means that the mechanism of degradation is dominated by one process being the same for all the high - temperature tests performed. If this is not the situation this means that more than one process contribute to the degradation observed.

If at a fixed value of degradation, In y plotted versus T^{-1} is not linear. This may indicate that the activation energy E varies with temperature. However, such a behaviour may also give an indication that the mechanism of degradation changes when shifting from one temperature region to another temperature region. One reason for such change in kinetic behaviour may be that a phase transition in the material takes place at a certain temperature inbetween the two temperature regions considered.

One complication, which may arise when analyzing the data from the tests performed, is that the degradation indicators used, i.e. $\Delta\alpha_s$ and $\Delta\varepsilon$, may be composed of contributions from more than one process of degradation.
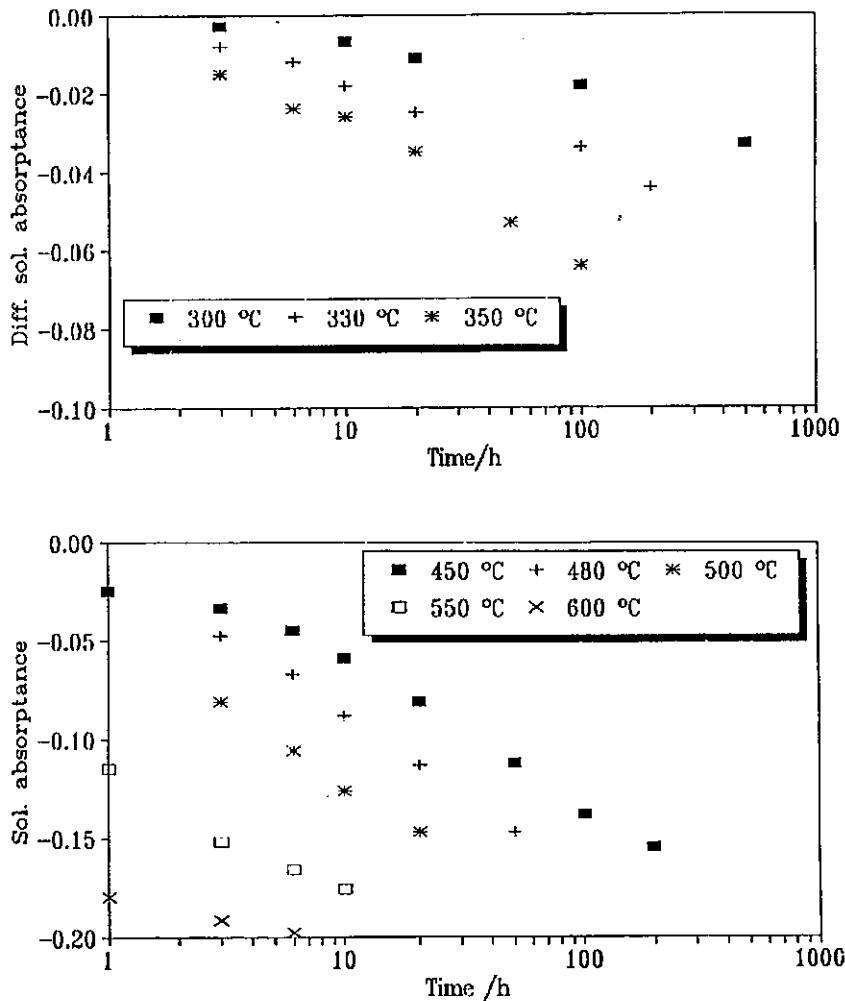
Figure 6;7 Changes in the solar absorptance with testing time for the different high-temperature tests performed on the Energie Solaire black chrome absorber coating.

As $\Delta\alpha_S = \Sigma\Delta\alpha_{S,\lambda}$, changes in one part of the solar range spectrum may be smoothed out or in some cases even be completely compensated by other spectral changes of reverse direction taking place in another part of the spectrum.

Black chrome coatings

In *Figures 6;7 and 6;8*, $-\Delta\alpha_S$ has been plotted versus ln y, i.e. the testing time in logarithmic form, for the different tests performed on the two black chrome coatings of the case study.
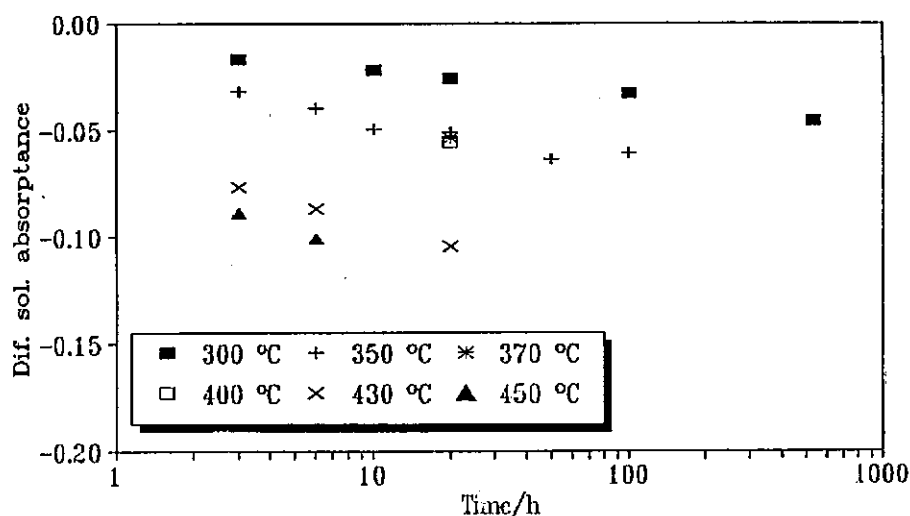
Figure 6;8 Changes in the solar absorptance with testing time for the different high-
temperature tests performed on the MTI black chrome absorber coating

For the Energie Solaire coating, the $-\Delta\alpha_S$ versus ln y plots exhibit a pattern which suggests that only one process with a fairly constant activation energy is dominating the kinetic behaviour at high temperature, above 350 °C. All curves except the one for 430 °C may be shifted into one single curve by a simple ln y transformation according to equation (6,6).

However, the curves for temperatures at or below 350 °C do not fit into this pattern. This may be more clearly seen if ln y is plotted versus temperature at certain $-\Delta\alpha_S$ values, see *Figure 6.9*. In this plot you can observe two branches; one for temperatures above 350 °C and one for temperatures at or below 350 °C. The change in kinetic behaviour when increasing the temperature of test above 350 °C strongly suggests that a conversion of the coating into another structural form takes place just above 350 °C. Its consequence for accelerated life testing may be realized if an estimated life time at 300 °C from the high temperature branch is compared with the experimental results obtained for this temperature. In the former case the estimated life time is in the order of ten years; experimental results indicate a value at around 1000 hours.

Energie Solaire black chrome coating
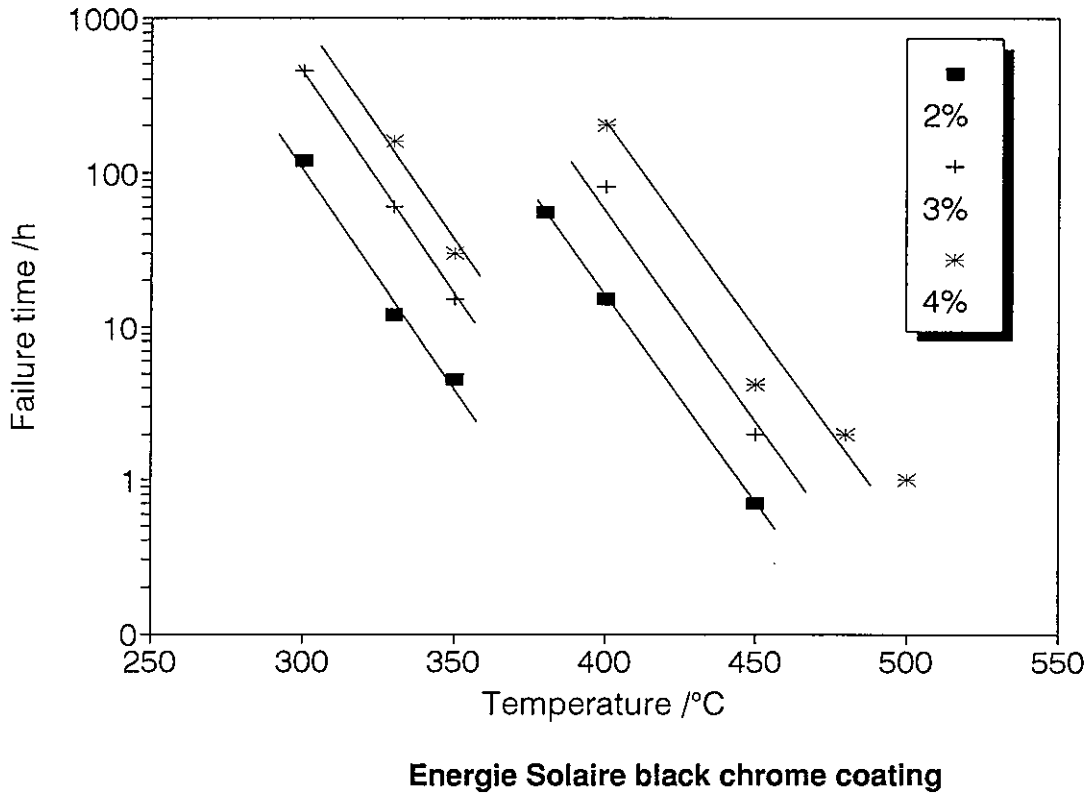
Figure 6;9 Required testing time of high-temperature ageing to reach specified extents of degradation in solar absorptance.

Equation (6,6) may form the basis for elaborating numerical expressions useful for service life prediction. The function $C(-\Delta\alpha_s)$ may be expressed as e.g. a power serie, i.e.

$$C(-\Delta\alpha_s) = \sum_{n=0}^{n} c_n (-\Delta\alpha_s)^n \qquad (6,7)$$

and its parameters c_n be determined by regression analysis using experimental data.

In *Figure 6;10* the results of such calculations are shown. The variable $-\Delta\alpha_s$ has been plotted versus ln y to forecast expected results for a test performed at 200 °C. Although maybe misleading two curves are given; one representing extrapolation of data obtained for tests at and below 350 °C and the other data obtained for tests above 350 °C. It should be noticed that the activation energy evaluated from the test data in the two different temperature regions is nearly the same.
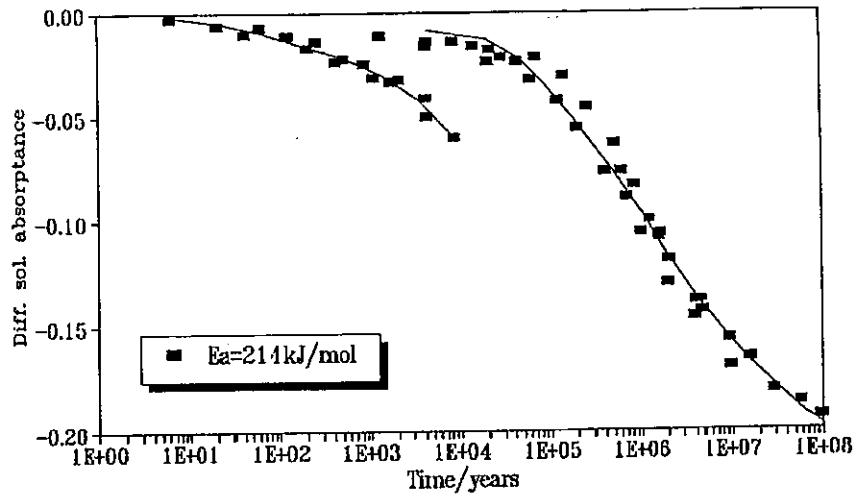
Energie Solaire black chrome coating
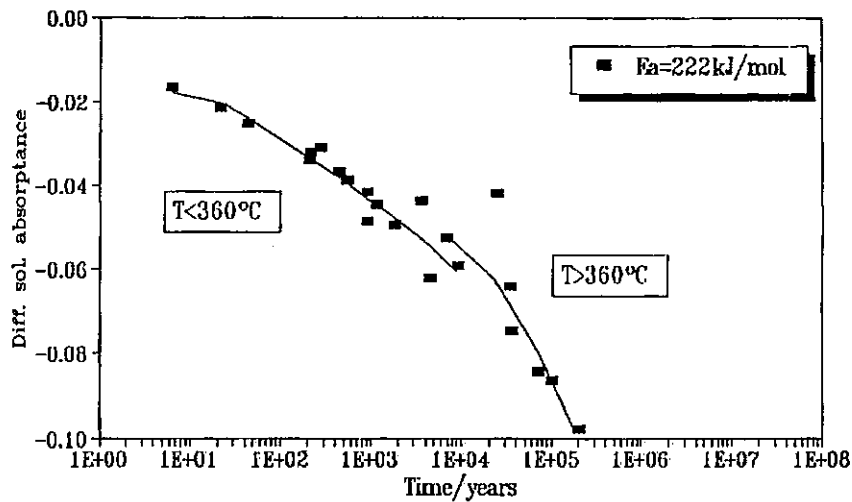
MTI black chrome coating

Figure 6;10 *Predicted change in the solar absorptance with time for a test to be performed at 200 °C on the black chrome coatings of the case study. Points in the diagrams refer to experimental data which has been transformed to 200 °C according to eq. (6;6) and by making use of the determined values for the activation energies indicated in the diagrams.*

The test data obtained for the MTI black chrome coating exhibits the same kind of change in kinetic behaviour at around 350 °C, but much less pronounced compared with the situation for the Energie Solaire coating, see *Figures 6;9 and 6;10*.

In the initial phase of high - temperature testing of the black chrome coatings there is a fast change in the reflectance for the near infrared and infrared wavelength regions. This affects the thermal emittance to some degree, but causes a nearly neglectible change in the solar absorptance. As mentioned in *Section 6.2.1* the spectral change observed is most probably caused by desorption of water from the coating. For the Energie Solaire coating the decrease in the thermal emittance is in the order of 0.06 and for the MTI coating in the order of 0.02. These changes will decrease the PC function, see equation (2,1) by about 0.015 and 0.005, respectively. Consequently, such changes are of less importance for the service lives of coatings as will be dealt with later in *Chapter 7* of this report.

For service life prediction, thus, primarily the numerical expressions used to calculate the curves illustrated in *Figure 6;10* and based on the test results for temperatures below or at 350 °C should be of interest.

Oxidation of metallic chromium in air at high temperature is, as has been discussed in *Section 6.2.1*, most probably the main cause for the decrease in the solar absorptance observed in the high temperature tests of the two black chrome coatings. Concerning the oxidation of bulk metals the literature contains a lot of information; for a review, see eg. [6,6]. It, however, falls outside the scope of the case study and the present report to make a deeper analysis how this information might be utilized in the interpretation of the high - temperature degradation data for the two black chrome coatings.

Nickel-pigmented anodized aluminium coatings

In *Figures 6;11 and 6;12*, $-\Delta\alpha_S$ is plotted versus the logaritmic testing time for the different high-temperature tests performed on the nickel-pigmented anodized aluminium coatings of the case study.
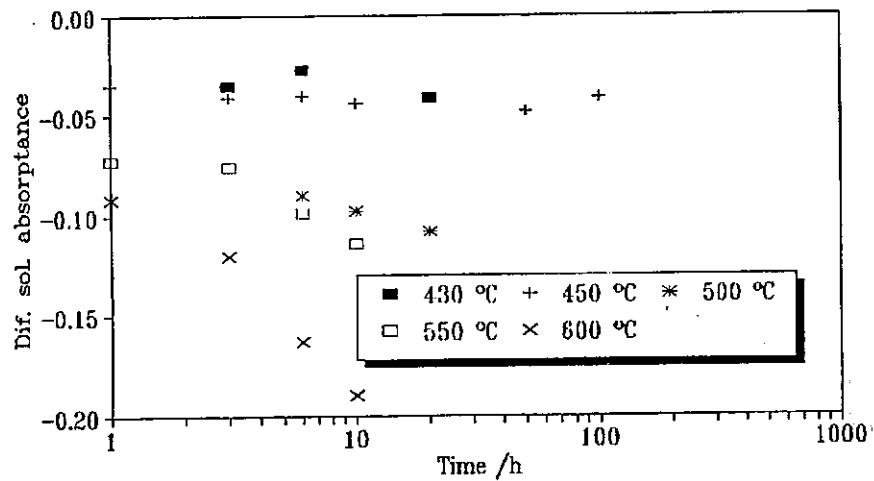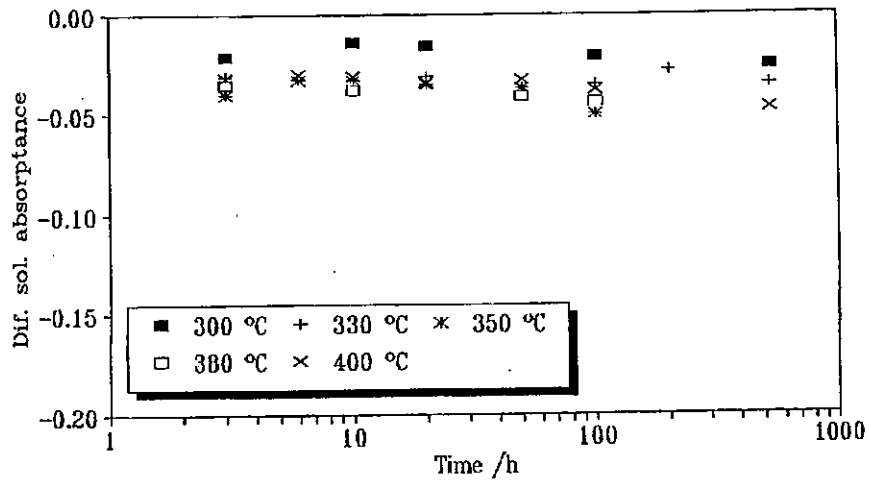
Figures 6;11 Changes in the solar absorptance with testing time for the different high temperature tests performed on the Showa nickel-pigmented anodized aluminium absorber coating.
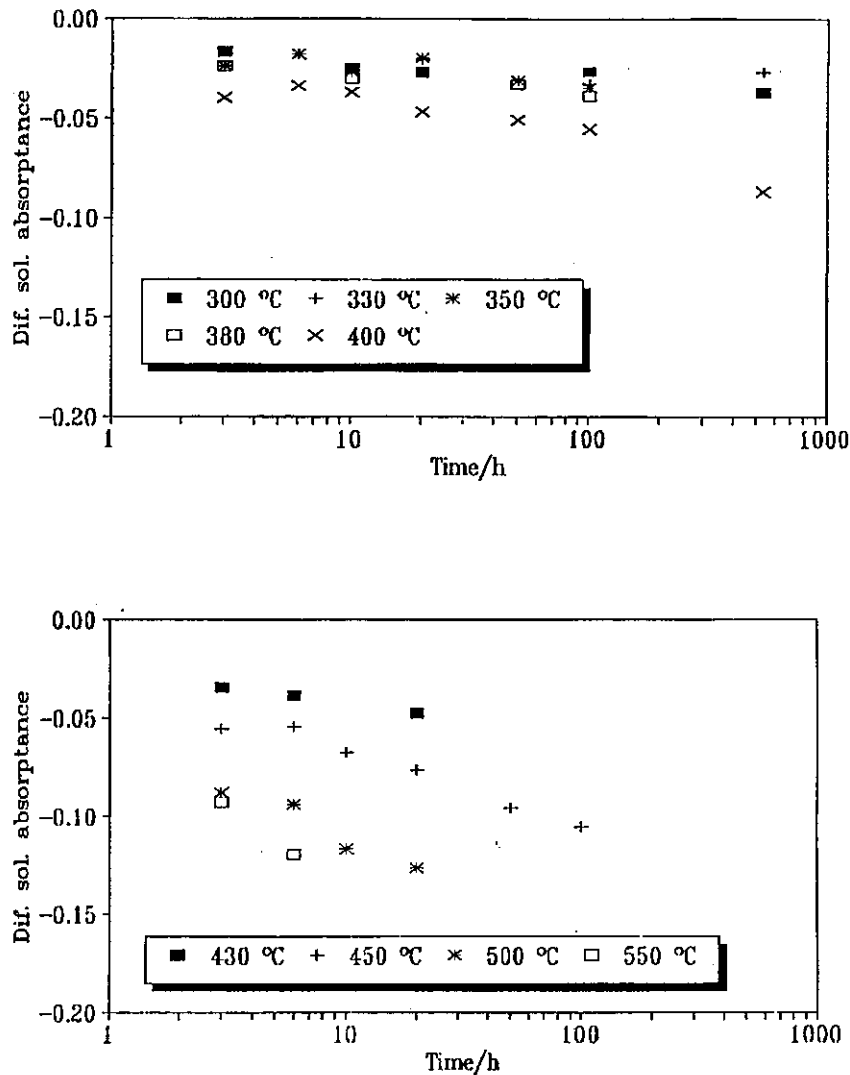
Figure 6;12 Changes in the solar absorptance with testing time for the different high temperature tests performed on the Sunstrip nickel pigmented anodized aluminium absorber coating.

As can be seen from the data in the two figures; after an initial fast decrease in the solar absorptance its change with testing time is only small for test temperatures below 400 °C. At the shortest testing time of 3 hours, the decrease in the solar absorptance for the Showa coating is nearly constant at a value of around 0.035, for temperatures below 450 °C, see *Figure 6;13*. For the Sunstrip coating the situation is similar as can also be seen in the same figure. A constant $-\Delta\alpha_S$ value appears at around 0.02 for temperatures below 400 °C.

As can be observed in *Figures 6;11* and *6,12* the initial decrease in the solar absorptance as is illustrated in *Figure 6;13* may for some tests even be reduced at longer testing times.
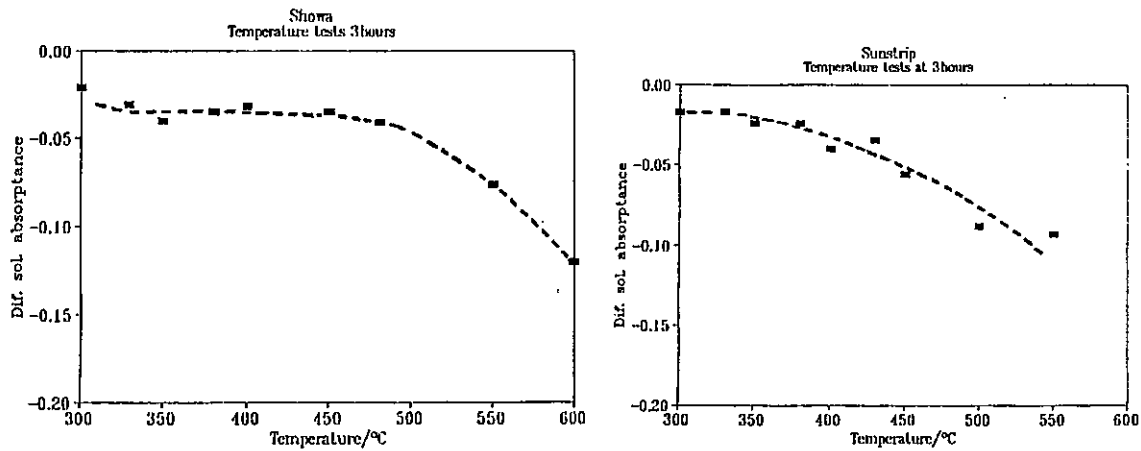
Figure 6;13 *Change in the solar absorptance after a testing time of 3 hrs for the different high temperature tests performed on the nickel-pigmented anodized aluminium coatings of the case study.*

In **Figure 6;14** the expected change in the solar absorptance versus testing time for a temperature of 200 °C is illustrated for the two coatings based on calculations making use of all the experimental data and eqs. (6,6) and (6,7). The calculations were made in the same way as described previously, meaning first the activation energy E and the parameters c_n were determined by way of regression analysis and then all the experimental data transformed to 200 °C by making use of the activation energy E determined.

As can be seen from the figure the change in the solar absorptance with testing time is very small for $-\Delta\alpha_s$ values less than about 0.02 - 0.04. This makes it difficult to determine testing times needed to reach $-\Delta\alpha_s$ values less than 0.02 for the Sunstrip coating and 0.04 for the Showa coating.
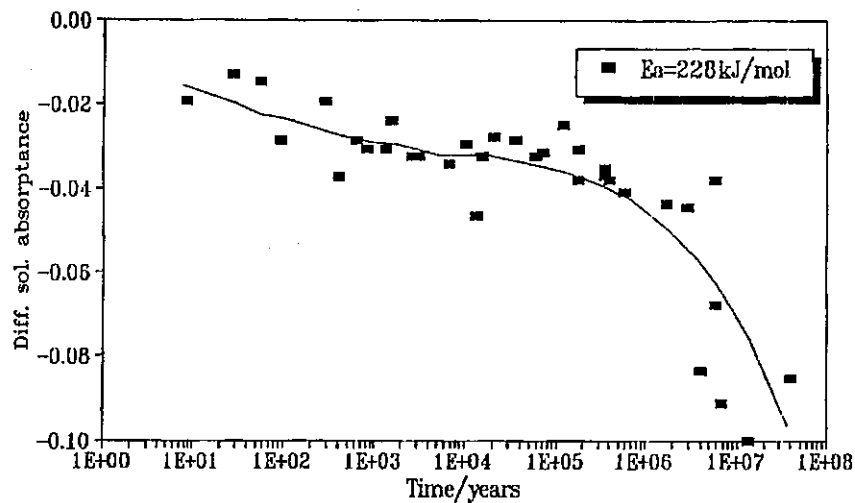
Showa nickel-pigmented anodized aluminium coating
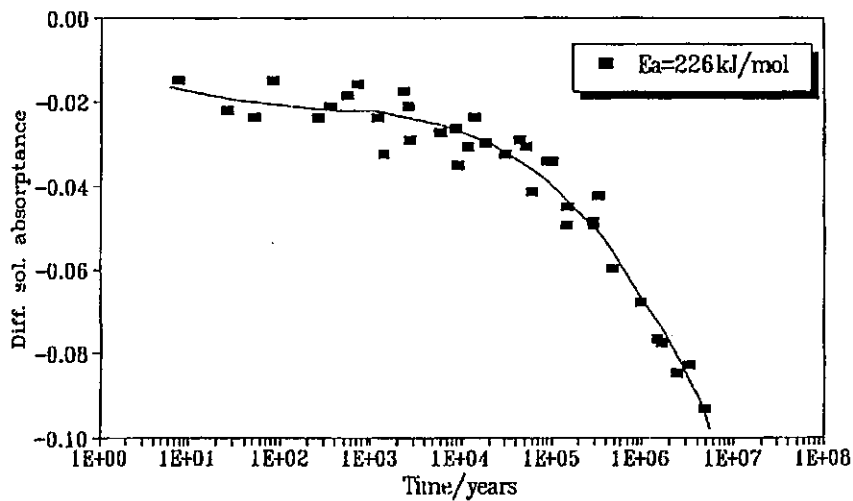
Sunstrip nickel-pigmented anodized aluminium coating

Figure 6;14 *Predicted change in the solar absorptance with time for a test to be performed at 200 °C on the two nickel-pigmented anodized aluminium coatings of the case study. Points given in the diagram refer to experimental data which has been transformed to 200 °C according to eq. (6,6) using the determined values for the activation energy given in the diagrams.*

To better understand the kinetics of the nickel-pigmented anodized aluminium coatings, Niklasson [6,5] made a theoretical analysis based on his relationship between decrease in the solar absorptance and decrease in the metallic nickel content, see equation (3,13).

To model the kinetic data he used a power law relationship which in terms of equation (6,6) may be understood as

$$\ln (C (-\Delta\alpha_s)) = \ln (-\Delta\alpha_s/\Delta\alpha_{s,0})/\gamma \qquad (6,8)$$

By combining equation (6,8) with equation (3,13) the resulting equation he used may be expressed as

$$\ln y = \frac{E}{R} (T^{-1} - T_R^{-1}) + \frac{\beta}{\gamma} \ln (1 - Q) \qquad (6,9)$$

For the two different nickel-pigmented anodized aluminium coatings he found $\gamma = 0.17$ and $\frac{\gamma}{\beta} = 0.07$ for the Sunstrip coating and $\gamma = 0.08$ and $\frac{\gamma}{\beta} = 0.03$ for the Showa coating. The activation energy was found the same for the two coatings and equal to 2.4 eV (231 kJ/mol), cf. *Figure 6;14*.

From the Cabrera and Mott theory, concerning oxidation of bulk metal, the following rate equation for the oxide thickness X may be derived for a situation when the diffusion of ions is the rate limiting step:

$$\frac{dX}{dt} = A \ \sinh \ (X_0/X) \hspace{5cm} (6,10)$$

where A is a constant and X_0 is a thermally activated quantity. For thick films $(X >> X_0)$ the Cabrera and Mott rate law crosses over to a diffusion limited behaviour characterized by a parabolic rate law.

By making use of the experimental data for oxidation of bulk metal from an investigation made by Sales et. al. (6,7), Niklasson was able to first show that the Cabrera and Mott rate law, eq. (6,9), could be used to describe the oxidation rate of bulk metallic nickel. Secondly, to show that the experimental oxidation rate data could fairly well be described by a power law relationship, i.e. equation (6,8). From the experimental data on the degradation of the two nickel-pigmented anodized aluminium coatings he could estimate that a change in the normalized solar absorptance of 0.1, i.e. $-\Delta\alpha_s/\alpha_{s,0}$, should correspond to oxide thicknesses in the order of 25 - 30 Å. For bulk metallic nickel, however, an oxide thickness of 50 Å is obtained after approximately one minute at 300 °C, which is orders of magnitude shorter than for the oxidation of the metallic nickel particles in the absorber coatings.

From the investigation by Sales et. al. [6,7] it was found that the activation energy changes remarkably at the Curie temperature of nickel at 358 °C. Below this temperature the activation energy was found to be 2.65 eV (265 kJ/mol) but above this temperature the activation energy was 1.60 eV (154 kJ/mol).

Niklasson's theoretical analysis involving comparison of experimental data from oxidation of bulk metallic nickel and from the high - temperature degradation of the nickel-pigmented absorber coatings of the case study points to the facts that there are many similarities but also differences in behaviour, which are needed to be more fully investigated.

However, for service life estimations in the case study the numerical expressions as illustrated in *Figure 6;14* may be taken as the point of departure.

The change in the thermal emittance of the two nickel pigmented coatings at high temperature ageing is small, in the order of maximally 0.02, which in terms of the PC function, see eq. (2,1), means a contribution of only 0.005. Consequently, such changes are of minor interest in connection with service life estimations.

6.3 Degradation of Coatings Caused by High-humidity and Condensation of Water

6.3.1 Dominant mechanisms of degradation causing loss in optical performance of coatings.

From the test results given in *Tables 5;12 - 5;15* it can be concluded that the sensitivity to degradation in high humidity air and by the action of condensed water varies considerably for the different coatings of the case study. Only slight degradation can be observed for the black chrome coatings. This is also true for tests performed at air humidities equal to or below 95 % RH for the nickel-pigmented coatings. However, when the air humidity is approaching the condensation limit, heavy degradation in the thermal emittance of coating occurs, see *Table 6;1*.

Test Condition: 95 % RH, 90 °C; 800 hrs	$\Delta\alpha_s$	$\Delta\varepsilon_n$(373 K)
- Energie Solaire black chrome coating	0.000	-0.004
- MTI black chrome coating	+0.002	-0.005
- Showa nickel-pigmented anodized aluminium coating	-0.002	+0.001
- Sunstrip nickel-pigmented anodized aluminium coating	-0.007	+0.003
Test Condition: Condensation, 45 °C sample; 650 hrs	$\Delta\alpha_s$	$\Delta\varepsilon_n$(373 K)
- Energie Solaire black chrome coating	+0.004	+0.003
- MTI black chrome coating	+0.011	-0.001
- Showa nickel-pigmented anodized aluminium coating	-0.028	+0.631
- Sunstrip nickel-pigmented anodized aluminium coating	-0.005	+0.645

Table 6;1 Comparison between changes in the solar absorptance and the thermal emittance of the different coatings of the case study after one humidity test and after one condensation test, cf. Tables 5;12 - 5;15.

Black chrome absorber coatings

The slight degradation in the optical properties of the black chrome coatings, observed after the humidity and condensation tests, is difficult to interpret in terms of physical and chemical processes of degradation. From the results of the humidity tests carried out at 95 % RH, it can be seen that at 50 °C the reflectance decreases in the near infrared and infrared wavelengths regions. For the test at 90 °C, the situation is the reverse. The spectral changes resembles those observed during the initial phase of the high-temperature tests in air. One possible explanation of the phenomenon observed may then be that at 90 °C, desorption of water from the coating takes place whereas at 50 °C it is the effect of water adsorption on the coating

that is observed. However, essentially the same variations with temperature can be seen looking at the results from the condensation tests. As a matter of fact, the temperature at which the reflectance starts to increase instead of decreasing is even lower compared with the situation at 95 % RH. Consequently, the changes observed cannot simply be explained as being due to adsorption/desorption of water on the coating only. Changes in structure, transparency or refractive index of the coating may be initiated due to the influence of water, and such changes might alter the reflectance in many different ways, difficult to foresee.

However, as the observed changes in the solar absorptance and the thermal emittance of the black chrome coatings are small, such changes are of little importance as regards loss in the optical performance of the two coatings. From a practical point of view, the two black chrome coatings can, accordingly, be considered insensitive to the action of water vapour and condensed water.

Nickel-pigmented anodized aluminium coatings

The increase in the thermal emittance of the nickel-pigmented anodized aluminium coatings, as observed mainly after the condensation tests, is far more important. The changes in the infrared spectrum of coatings are drastic and can be seen as being due to the evolution of absorption bands around 3 µm, 4.5 µm between 6 and 7 µm, and around 9.5 µm. These characteristic changes appear in the spectrum of the coatings in all condensation tests performed, see *Figure 6;15*.

In the humidity tests at 95 % RH, the increase in the thermal emittance of coatings is only slight, but despite that an increased absorption around 3 µm can be distinguished in the spectrum of coatings after the longest testing times. In the humidity tests at 99 % RH, a slight increase in absorption at around 6.5 µm and at around 9.5 µm can also be seen.
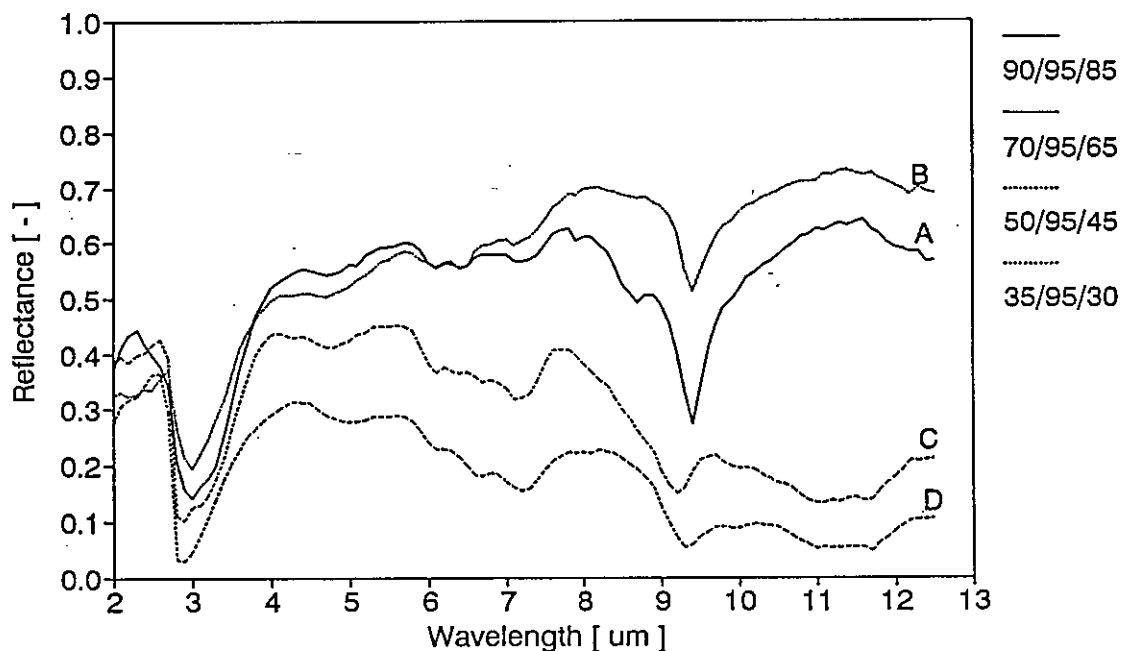
Figure 6;15   Infrared spectra after different condensation tests performed with the Showa nickel-pigmented anodized aluminium coating.
(A, B, and C represent a testing time of 650 hrs and D 200 hrs.)

As the absorption band at around 3 µm is characteristic of the stretching vibration of water, i.e. O-H, the spectral change observed is consistent with water being absorbed on the coatings during the tests. To explain the origin of the other absorption bands, one has to assume that the absorbed water reacts with the aluminium oxide, converting the latter into a hydrated form. *Figure 6;16* shows infrared spectra of some aluminium oxide hydroxides, originating from data published by Takahasi et.al. [6,8]. In order of increasing water content, the solid phases are: Boehmite, γ-AlO·OH, Pseudoboehmite, AlO·OH·X H_2O ; X = 0.4 - 1, Bayerite, β-Al_2O_3 · 3 H_2O, and Gibbsite, $Al(OH)_3$. Besides those solid phases, amorphous phases of hydrated aluminium oxide may exist also.
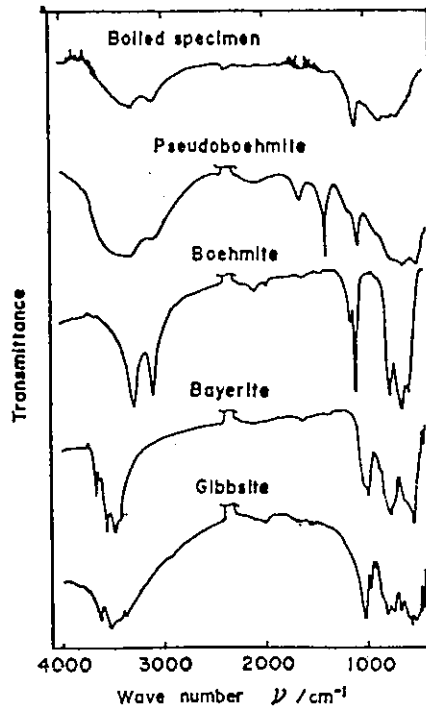
Figure 6;16 Infrared absorption spectra for different hydrated forms of aluminium oxide according to Takahasi et.al. [6,8]

As can be seen, all these solid phases exhibit absorption bands in the regions of around 3 µm and 9.5 µm. Only the Pseudoboehmite has absorption bands in the wavelength region between 6 to 7 µm. Tanemura et.al. [6,4] therefore concluded that it is most probably Pseudoboehmite that is formed in the nickel-pigmented anodized aluminium coatings of the case study. The absorption bands between 6 to 7 µm are probably due to bending vibrations of water in the hydrated aluminium oxide, the absorption band at around 9.5 µm due to wagging vibration of AlO-H and the absorption bands in the wavelength region 12.5 µm to 16.5 µm due to vibrations in the octahedron of AlO_6.

Consequently, the analysis of the spectral changes that occur in the infrared wavelength region as a result of high - humidity and condensation testing provide strong evidence for the assumption that aluminium oxide is converted into hydrated form under the influence of water vapour and condensed water.

The change in the reflectance spectrum in the visible and near infrared wavelength regions of the Sunstrip coating varies in a systematic way with the extent of degradation of the thermal emittance, although the change in the spectrum and the solar absorptance is less pronounced, With increasing thermal emittance, the interference pattern of the reflectance spectrum in the visible and near infrared shifts to longer wavelengths and is gradually smoothed out. For the most heavily degraded samples, no interference pattern at all can be observed. These changes may, therefore, be interpreted as being due to a change in the surface morphology and the growth of the optical thickness of the coating. For the most heavily degraded samples an increased absorption or scattering of light in the upper part of the layer prevents an interference pattern from being developed.

The change in the visible and near infrared spectrum observed can, therefore, be explained as being due to the build-up of a hydrated aluminium oxide layer on the coating surface during the high - humidity and condensation tests.

The same pattern of change can be observed for the Showa coating. However, samples with varying optical properties had to be used for the high - humidity and condensation tests of the Showa coating, as illustrated in *Figure 6;17.*
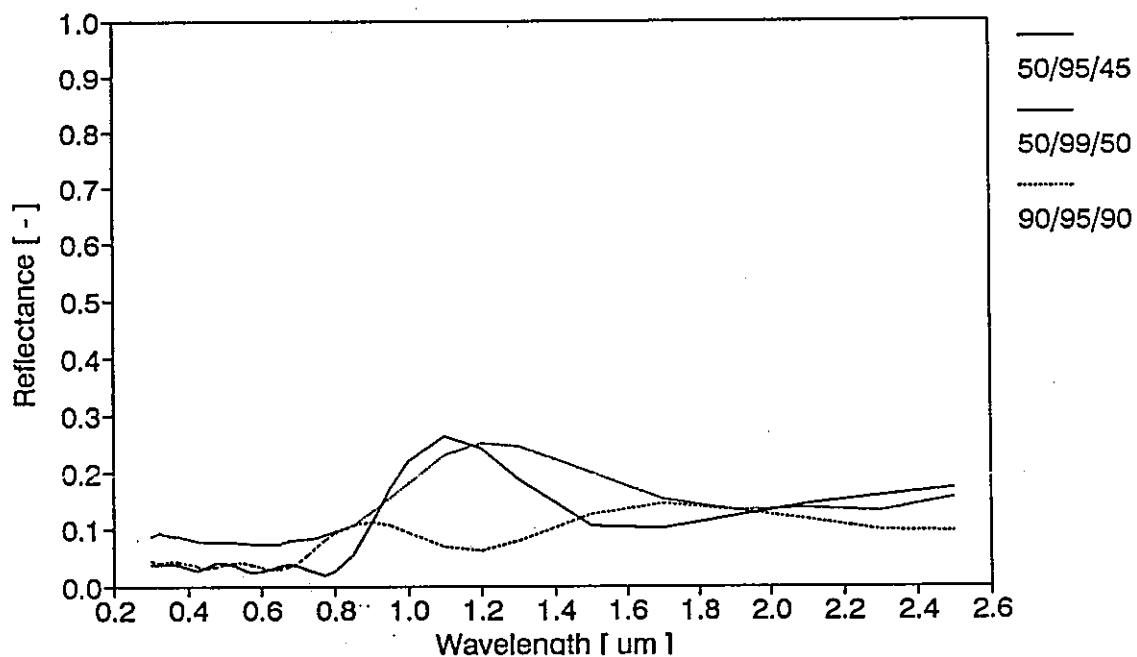
Figure 6;17 Spectra of different "unaged" samples of the Showa coating used in the different high-humidity and condensation tests.

The samples that exhibited a more diffusely reflecting spectrum, however, change during the first phase of reaction. After this period, their spectra exhibited the same characteristic interference pattern as was normally observed for an unaged sample tested, see *Figure 6;18*.
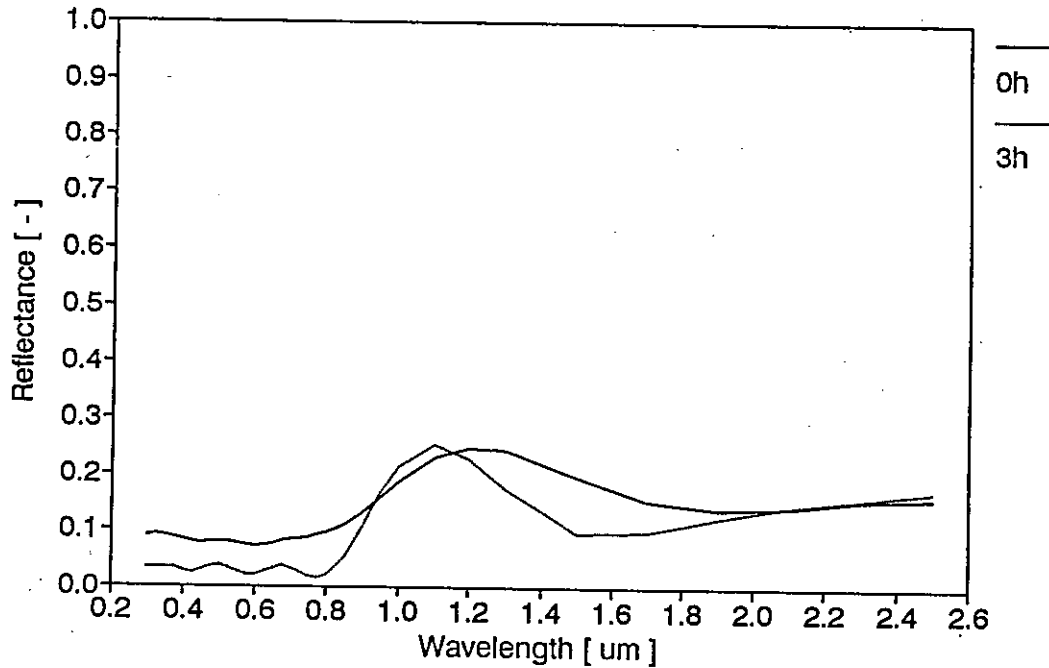
Figure 6;18 Change in the reflectance spectrum of a Showa coating sample after the initial phase of testing at 50 °C and 99 % RH.

One possible explanation of the phenomenon observed is that an initial absorption of water in the coating transforms the outer layer of the coating into a more transparent and less light-scattering state. However, the fact that some of the samples tested exhibited a diffusely reflecting spectrum with a lower solar absorptance seems not to have affected the overall kinetic behaviour related to the increase in the thermal emittance of the coatings during condensation testing. However, the change in the solar absorptance during condensation testing seems not possible to describe by a single and reasonable kinetic model.

Considerable changes in the surface morphology of samples after condensation testing could be observed in the SEM studies made by Tanemura et.al. [6,2], see *Figure 6;19*.
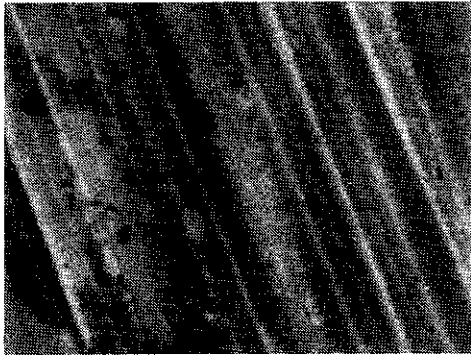
a) Unaged sample
   (x 1500)
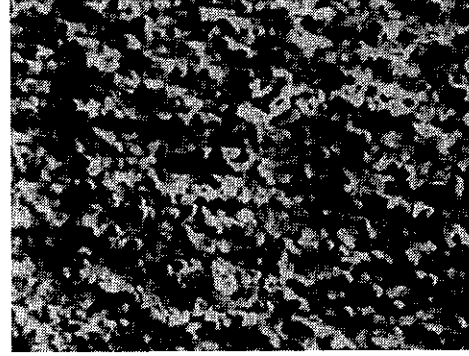
b) Sample degraded as a result of
   condensation testing at 45 °C (sample)
   for 650 hrs ($\Delta\varepsilon$ = 0.631) (x 1500)
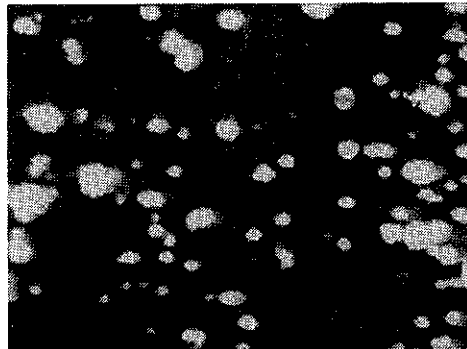
c) Sample degraded as a result of
   condensation testing at 65 °C (sample)
   for 650 hrs ($\Delta\varepsilon$ = 0.200) (x 700)

Figure 6;19 SEM micrographs of samples of the Showa nickel-pigmented anodized absorber coating degraded by condensation testing.

For the sample from the condensation test at 45 °C, a dense layer with a polycrystalline structure can be seen on the surface, which might be a layer of hydrated aluminium oxide. For the sample from the condensation test at 65 °C, particles and cracks can be observed on the surface.

With the sample from the condensation test at 45 °C, it was not possible to record any AES depth profile for either the Showa or the Sunstrip coating because of surface charging problems. This fact was probably due to the hydrated aluminium oxide layer formed, see *Figure 6;19*, which may have acted as an electric insulator.

With the sample from the condensation test at 65 °C, however, an AES depth profile could be recorded for the Showa coating, see *Figure 6;20*. The AES depth profile indicates that the structure of coating has been very much affected. The change in the O/Al ratio with sputtering time are, however, more difficult to explain.
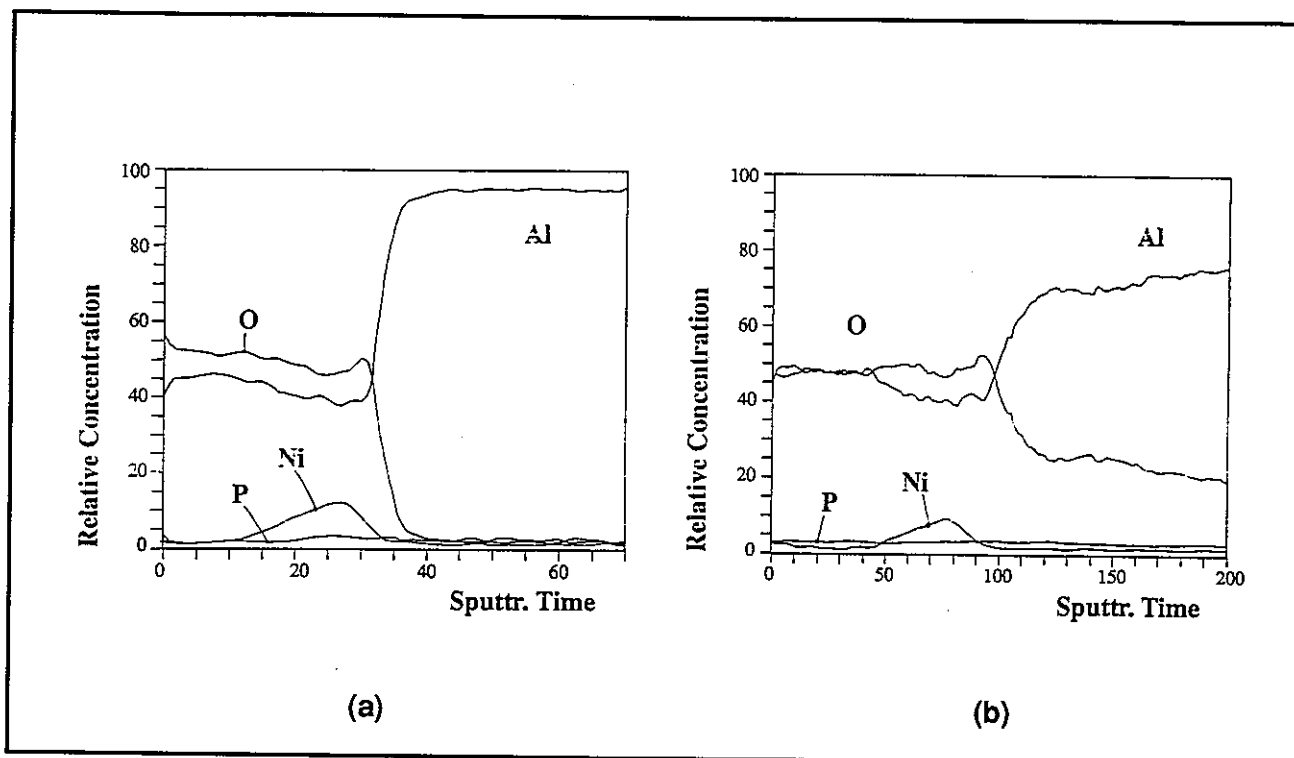
Figure 6;20   AES depth profiles for: (a) a sample of the Sunstrip coating after 1000 hrs testing at 90 °C, 99 % RH ($\Delta\varepsilon = 0.024$) and (b) a sample of the Showa coating after 650 hrs condensation testing at 85 °C (sample) ($\Delta\varepsilon = 0.200$).

As can also be seen from the figure, the high humidity test does not cause any significant changes in the AES depth profile except for a slight increase of the oxygen concentration just at the surface of coating. With SEM analysis, slight changes in the surface morphology could be observed in the form of the appearance of some particulates and cracks.

However, the AES and SEM studies provide evidence for the assumption that the deterioration in thermal emittance resulting from high - humidity and condensation testing is caused by conversion of the aluminium oxide into hydrated form. From these studies it can also be concluded that the hydrated aluminium oxide formed at temperatures below or at 45 °C seems different from the form appearing at temperatures above 65 °C. This affects to a certain degree also the shape of the absorption bands

in the infrared wavelength region, see *Figure 6;15*. However, as will be dealt with later, the kinetics of degradation in the condensation test changes drastically for temperatures above 45 °C.

It should be pointed out that there exists a critical temperature in the oxidation of aluminium in distilled water between 60 - 70 °C. Below this temperature an amorphous film of hydrated aluminium oxide is formed at first, which then converts into Boehmite and finally into Bayerite. Above the critical temperature, only a film of Boemite is formed on the top of the initial amorphous film, see eg. [6;9].

Anodized aluminium coatings are widely used in many different applications. One example is decorative coatings for architectural purposes, in which nickel pigmentation may also be applied for colouration. However, decorative coatings manufactured for outdoor use have coating thicknesses in the order of 25 µm. The pores of these coatings are also sealed by treating them in boiling water after pigmentation. As a result of this treatment Boehmite is formed, closing the pores.

The nickel-pigmented anodized aluminium absorber coatings, on the other hand, have thicknesses less than 1 µm and cannot be sealed by treating the coatings in boiling water. The Boehmite formed in such a treatment should increase the thermal emittance of the coatings. However, as has been observed, formation of hydrated forms of aluminium oxide may occur on the absorber coatings if the humidity conditions are close to condensation.

It is known that Boehmite converted into aluminium oxide by heat treatment at temperatures above 300 °C is. From the reflectance spectra in *Tables 5;12 and 5;13* for the combined test: condensation testing at 45 °C followed by high-temperature ageing at 400 °C, such a process may also be seen to occur . However, during the high-temperature treatment, a high rate of oxidation of the metallic nickel can be noted from the test results.

6.3.2 Kinetics of degradation, humidity/temperature dependence and time transformation functions for accelerated life testing

Nickel-pigmented anodized aluminium coatings

In the high humidity and condensation test both humidity and temperature levels need to be considered in kinetic modelling of the test results. The time transformation function according to equation (2,6) may be assumed to have the following form:

$$\frac{y_R (T_R, RH_R)}{y(T, RH)} = g\ (S)/g(S_R) = h(T,RH)/h(T_R, RH_R) \cdot (k(RH)/k(RH_R)) \qquad (6,11)$$

where h is a function describing mainly the temperature dependence and k is a function describing the humidity dependence.

It is most convenient to use a condensation test as a reference test. To model the temperature dependence, the Arrhenius equation may be used, as previously, and thus

$$\frac{h(T, RH_R)}{h(T_R, RH_R)} = \exp\left(\frac{-E(RH_R)}{R} \cdot (T^{-1} - T_R^{-1})\right) \qquad (6,12)$$

where E is the activation energy which may be a function of the relative humidity RH. The time $y(T, RH_R)$ needed to reach a certain degree of degradation can, thus, be expressed as:

$$y(T, RH_R) = y_R(T_R, RH_R) \cdot \exp\left(\frac{E(RH_R)}{R} \cdot (T^{-1} - T_R^{-1})\right) \qquad (6,12)$$

In analogy with equation (6,6), the following expression may be derived for describing the increase in the thermal emittance $\Delta\varepsilon$ with testing time $y(T, RH_R)$

$$\ln(y(T, RH_R)) = \frac{E(RH_R)}{R}[T^{-1} - T_R^{-1}] + \ln(D_R(\Delta\varepsilon)) \qquad (6,14)$$

In *Figure 6;21* and *Figure 6;22* the change in the thermal emittance versus testing time is plotted for the different condensation tests performed on the Showa and the Sunstrip coating, respectively. As can be seen from the two figures the two coatings behave nearly the same. At temperatures of samples at or less than 45 °C the degradation pattern is such that all curves may be shifted into one single curve by a simple ln y transformation according to equation (6,14).

By expressing D_R ($\Delta\varepsilon$) in equation (6,14) as a power serie and applying the same procedure as used in the evaluation of the high - temperature test data, all experimental data for the condensation tests at temperatures at and lower than 45 °C may be tranformed to one temperature, see *Figure 6;23*.
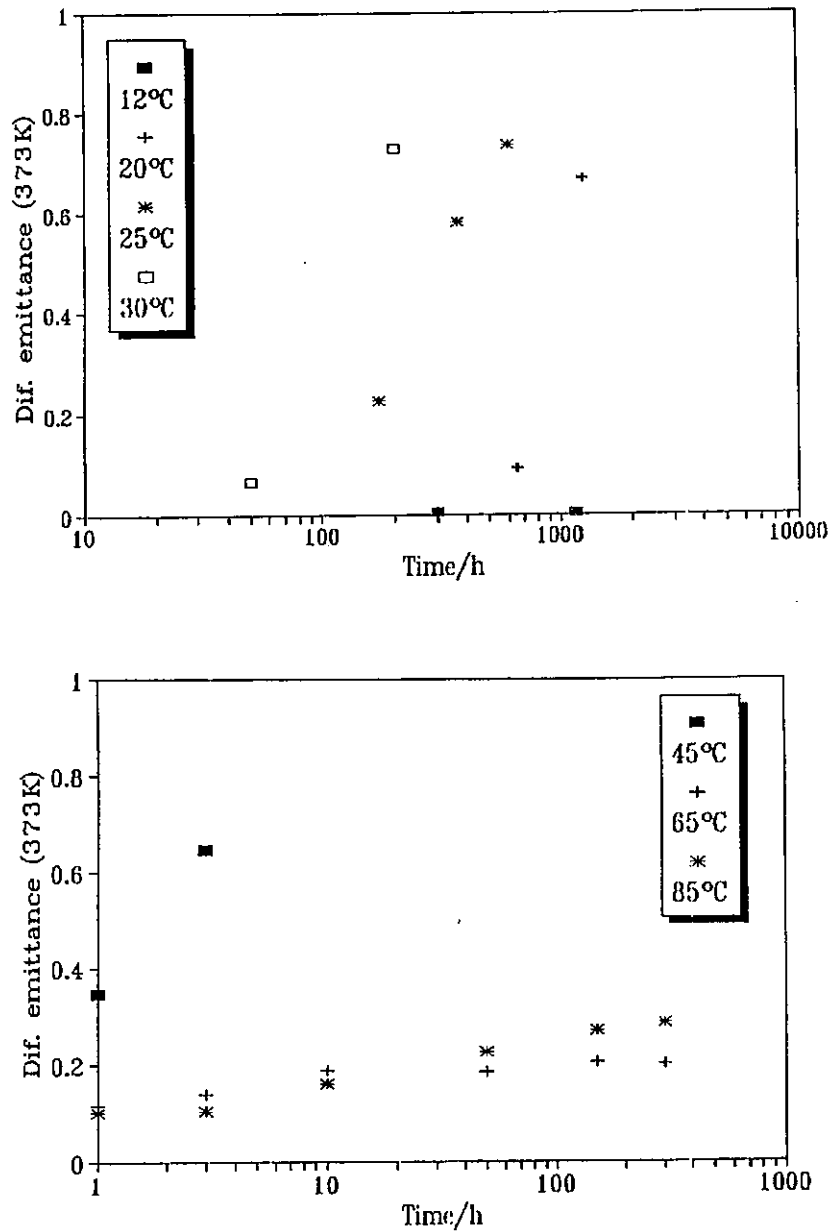
Figure 6;21 Change in the thermal emittance with testing time for the different condensation tests performed on the Showa nickel-pigmented anodized aluminium coating.

As can be seen the activation energies determined for the two coatings are close to each other. The testing times needed to reach certain Δε-values are also of the same order of magnitude for the two coatings.
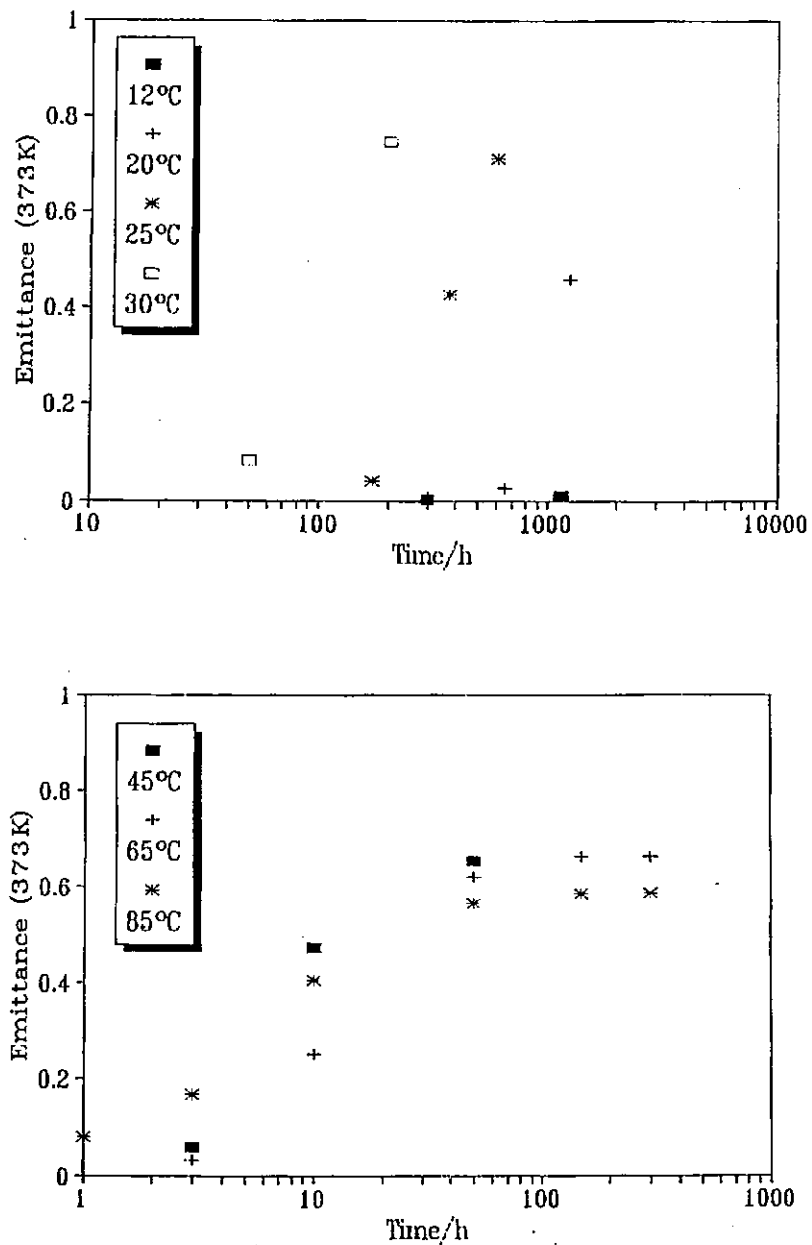
Figure 6;22   *Changes in the thermal emittance with testing time for the different con-densation tests performed on the Sunstrip nickel-pigmented anodized aluminium coating.*
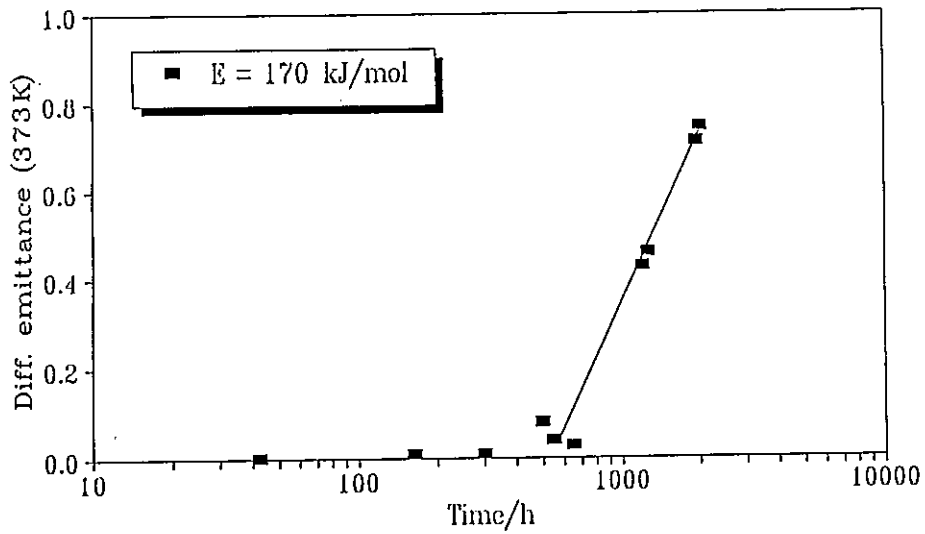
The Sunstrip nickel-pigmented anodized aluminium coating
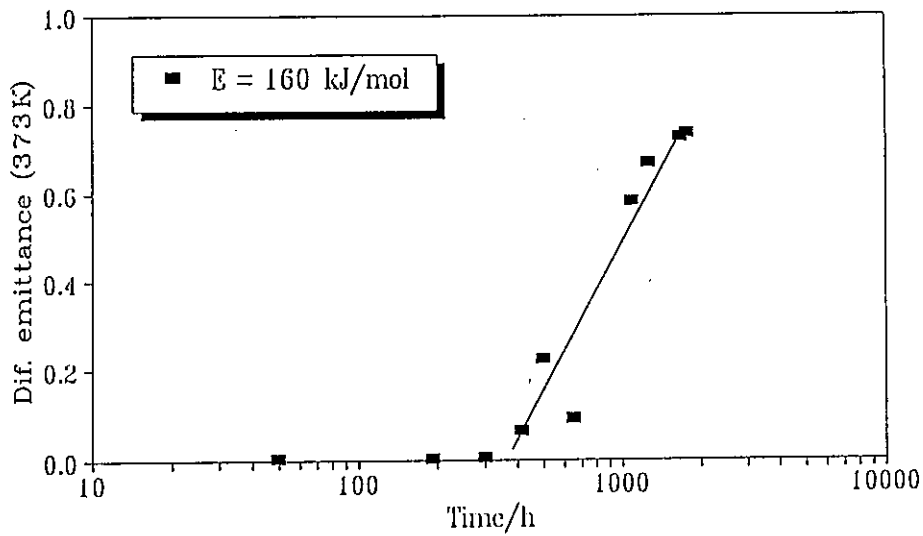
The Showa nickel-pigmented anodized aluminium coating

Figure 6;23   *Predicted change in the thermal emittance with time for a condensation test to be performed at 20 °C on the two nickel-pigmented coatings of the case study. Points given in the diagrams refer to experimental data which has been transformed to 20 °C according to equation (6,14) using the determined values for the activation energy given in the diagrams.*

For temperatures 65 °C and 85 °C the rate of degradation in the condensation tests is considerably lower. As mentioned in *Section 6.3.1* this may be due to the fact that at and below 45 °C hydratization of aluminium oxide may proceed from Boehmite, Pseudoboehmite to Bayerite whereas above 45 °C hydratization of aluminium oxide may proceed only to Boehmite. However, from the data of the microclimate for absorbers presented in *Chapter 4*, it can be concluded that situations when the relative humidity may approach values close to condensation will never occur at temperatures above 45 °C.

Equation (6;11) can be written in the following form when comparing results from tests carried out at different humidities but at the same temperature T_A

$$\frac{y(T_A, RH_R)}{y(T_A, RH)} = \exp\left(-(E(RH) - E(RH_R))/T_A \cdot \frac{k(RH)}{k(RH_R)}\right) \qquad (6,15)$$

However, as RH_R is representing a condensation test this means that $y(T_A, RH_R)/y(T_A, RH)$ is extremely small even for values of RH = 99 %. From the data in *Tables 5;12* and *5,13*, this ratio can be estimated to be in the order of 10^{-3}.

From measurements of microclimate in collectors, as described in *Chapter 4* of this report the following conclusions can be made:

- The humidity level on the absorber surface may during certain time periods approach 100 % RH, but a real condensation seems not to occur in the middle part of the collector as indicated by the time-of-wetness measurements.

- It is not possible to measure humidity with a higher precision than 1 %.

From the high humidity test it is not possible and not meaningful to apply equation (6,15) for a more detailed analysis of test data. However, in the humidity interval between 99 % and 100 % RH it may be reasonable to express this equation as

$$\frac{y(T_A, RH_R)}{y(T_A, RH)} \approx \frac{k(RH)}{k(RH_R)} = X \qquad (6,16)$$

where X is a factor representing the mean rate of degradation in the interval $99 \le RH \le 100$ %.

To summarize the approximations made:

- For RH < 99 % the time transformation function

$$g(\bar{S})/g(\bar{S}_R) = 0 \qquad (6,17)$$

meaning that the rate of degradation is negligible and therefore the critical humidity level according to equation (2,8) can be set equal to 99 %.

- For $99 \% \le RH < 100 \%$ the time transformation

$$g(\bar{S})/g(\bar{S}_R) = \exp\left(\frac{-E(RH_R)}{R}(T^{-1} - T_R^{-1})\right) \cdot X \qquad (6,18)$$

To be able to estimate the factor X, results from the in-service tests of collectors have to be utilized in combination with the numerical expressions used to calculate the curves illustrated in *Figure 6,23*. This will be dealt with in *Chapter 7 and 8* of this report.

The decrease or in some cases even increase in the solar absorptance accompanying the increase in the thermal emittance during the condensation tests influences the value of the PC function according to equation (2,1), only to a small extent. For service life estimations based on the condensation tests, thus, the changes in the solar absorptance may be neglected.

However, one so called synergistic effect, that should have been investigated in more detail in the case study, is the combination of a period of condensation at low temperature followed by a period of exposure at high temperature. The results from the serial tests in *Table 5;12* and *Table 5,13* indicate that the decrease, in the solar absorptance in the high temperature test at 400 °C after 3 hrs, is about ten times as high as that found for the corresponding single load high temperature test after the same testing time.

6.4 Degradation of Coatings Caused by Sulphur Dioxide as an Airborne Pollutant

6.4.1 Dominant mechanisms of degradation causing loss in optical performance of coatings

The results from the sulphur dioxide exposure tests presented in *Tables 5;17 - 5;20* show that the black chrome coatings in the case study are only slightly affected after performing the different tests. The nickel - pigmented anodized aluminium coatings, however, became heavily degraded in some tests.

For the test performed at 20 °C after 100 hrs, the changes in the solar absorptance and thermal emittance of the different coatings differ markedly from each other, as shown in *Table 6;2*.

	$-\Delta\alpha_s$	$\Delta\varepsilon_n$ (373K)
- Energie Solaire black chrome coating	0.003	0.003
- MTI black chrome coating	0.000	0.006
- Showa nickel-pigmented anodized aluminium coating	0.298	0.079
- Sunstrip nickel-pigmented anodized aluminium coating	0.264	0.063

Table 6;2 *Comparison between changes in the solar absorptance and the thermal emittance for the different coatings in the case study after a sulphur dioxide exposure test (1 ppm SO_2, 95 % RH, 20 °C) for1000 hrs.*

As the degradation of the black chrome coatings is only slight in comparison with the degradation of the nickel-pigmented anodized aluminium coatings, the main efforts in the case study were directed to the analysis of the degradation of the latters only.

Nickel-pigmented anodized aluminium absorber coatings

The spectral changes in the visible and near infrared wavelength regions observed as a result of the sulphur dioxide-induced degradation of the Showa and the Sunstrip coatings resemble those observed after high-temperature ageing of the two coatings.

One difference, however, is that during the initial phase of degradation the interference pattern shifts to longer wavelengths in the former case, but is shifted to shorter wavelengths in the latter case. However, the dominating features of spectral changes are the same in the two cases, strongly suggesting oxidation of metallic nickel to be the main process of degradation in the sulphur dioxide-induced degradation process as well.

To investigate this further, use was made of some previous results obtained by Anderson, Hundari and Granquist [6;10]. They found a strong correlation between the amount of nickel, γ, present in the coating and the wavelength λ_c at which the absorber coatings switch from the absorbing state to the reflecting state.

The wavelength λ_C being defined as the wavelength at which the reflectance is equal to 50 %. If the amount of metallic nickel γ increases, λ_C shifts towards longer wavelengths. The relation they found is simply:

$$\lambda_C = 6.3 \ \gamma \tag{6,19}$$

where λ_C is expressed in µm and γ in g/m².

The wavelengths λ_C for the reflectance spectra recorded at the different testing times of test (1 ppm SO_2, 95 % RH, 20 °C) were evaluated as described in *Figure 6;24*.
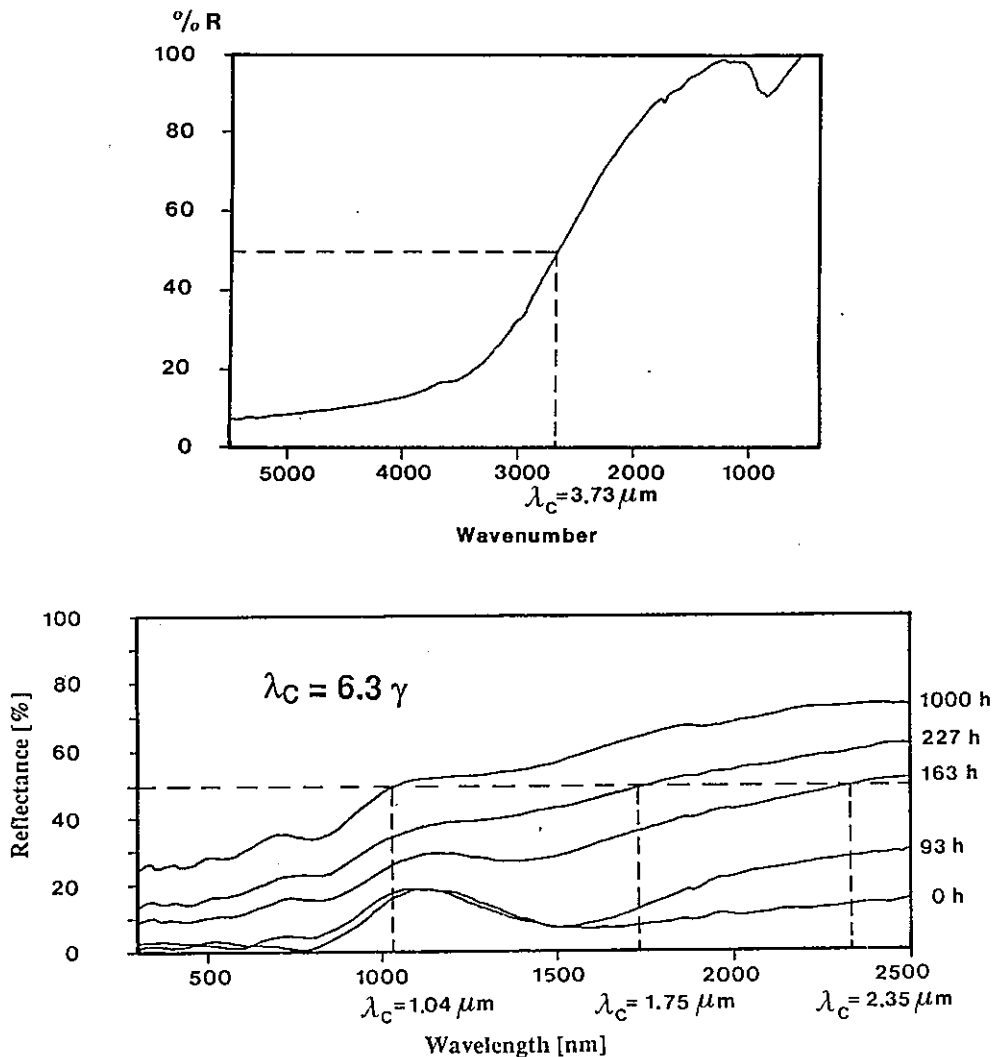
Figure 6;24 *Evaluation of λ_C from reflectance spectra of the unaged and aged Showa absorber coating. Ageing conditions: 1 ppm SO_2, 95 % RH, 20 °C. The positions of λ_C for different testing times are indicated in the figures. The upper figure presents result for unaged coating. In this case λ_C was determined by use of the specular reflectance ,which could be done as the non-specular component is more or less negligible for an undegraded coating [6,16]. The lower figure presents results for aged coatings.*

The next step in the analysis was to make use of the relationship between normalized change in absorptance and normalized change in metallic nickel content suggested by Niklasson [6,5], see *Figure 3;14* of this report. In numerical form the relationship can be expressed as

$$1 - (\alpha_s/\alpha_{s,0}) = 0.84 \, (1 - Q)^{2.5} \qquad\qquad (6;20)$$

where Q is defined as $Q = \gamma/\gamma_0$. The parameter γ_0 denotes the initial amount of metallic nickel in the coating.

By combining eqs. (6,19) and (6,20) "theoretical" values for α_s using the experimental λ_c values could be calculated. The results are presented in *Figure 6;25*.
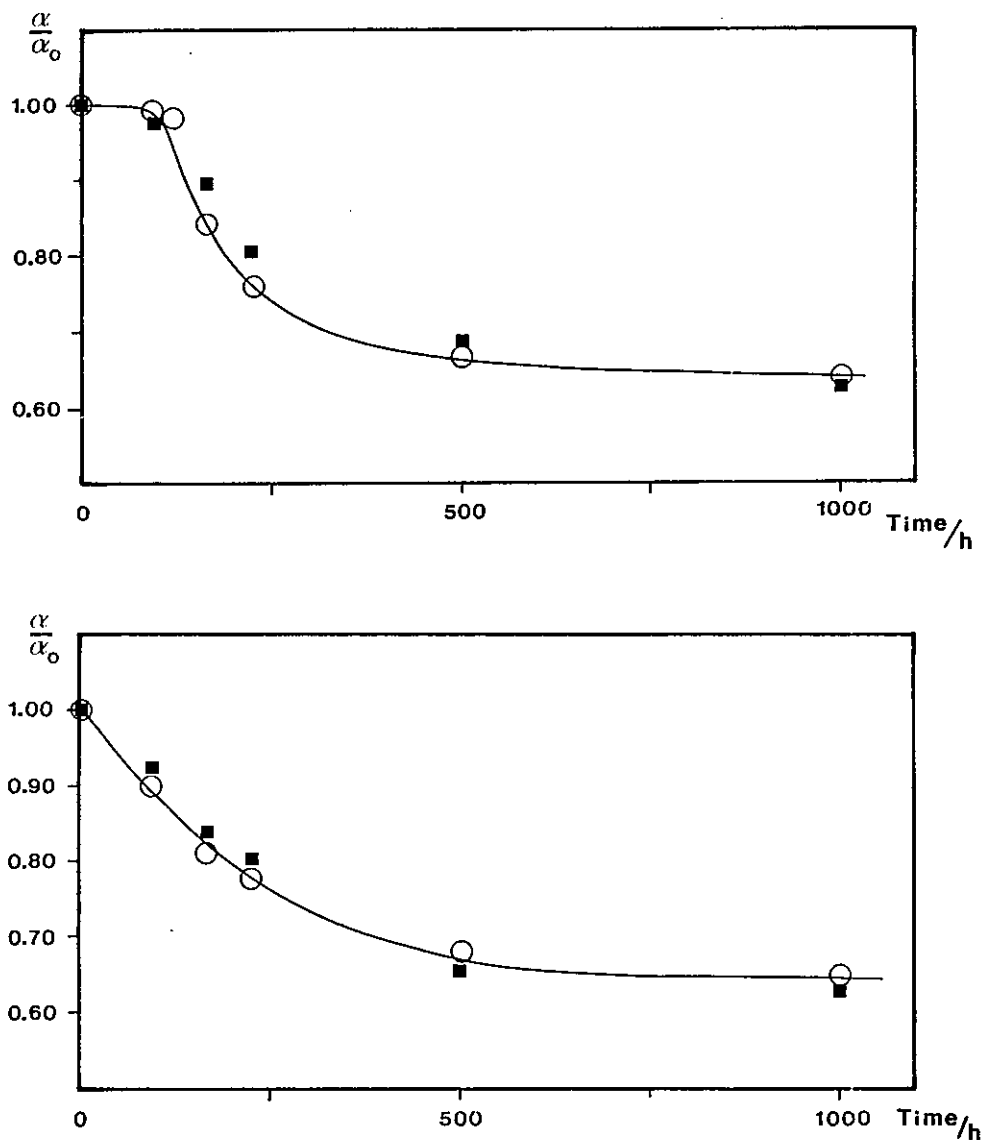
Figure 6;25 *Experimental and calculated solar absorptance values (normalized) plotted versus testing time for the ageing of the Showa coating (upper figure) and the Sunstrip coating (lower figure). Filled squares represent calculated values. Ageing conditions: 1 ppm SO_2, 95 % RH, 20 °C.*

As can be seen, there is good agreement between the experimental and the calculated values. The results, therefore, imply that the decrease in absorptance is most probably due to oxidation decreasing the amount of metallic nickel in the coating.

As can also be seen from the figure, the solar absorptance decreases with time to what seems to be a constant value in the range of 0.6 - 0.7. This value is considerably higher than the solar absorptance value of around 0.27, which can be determined for an unpigmented but anodized aluminium surface. This indicates that although metallic nickel is still present, its rate of degradation or oxidation terminates before reaching full completion. An explanation could be that the pores of the aluminium oxide in the coating are blocked by reaction products formed during degradation, and thereby preventing complete oxidation of the metallic nickel particles.

Another striking observation is the very low or negligible degradation rate for the Showa coating observed in the initial stage of degradation. However, after an initiation period, the degradation proceeds at a rate which is equal to or even higher than that observed for the Sunstrip coating.

From the results presented in *Chapter 5, Tables 5;19* and *5;20*, it can be seen that a less pronounced increase in the thermal emittance accompanies the decrease in the solar absorptance is. This pattern of degradation in optical properties is quite the opposite to what is observed at the high - humidity and condensation tests performed as described previously in the report.

In this latter case formation of hydrated phases of aluminium oxide gave rise to drastic changes in the infrared spectrum, leading to a considerable increase in the thermal emittance. For the sulphur dioxide induced degradation, the changes appearing in the infrared reflectance spectrum are less drastic. Accompanying the decrease in solar absorptance is the appearance of quite well-defined absorption bands in the infrared wavelength region of around 9.2 µm, 6.0 µm and 3 µm. These bands, which are characteristic for salt hydrates of nickel sulphate, increase in intensity with the extent of degradation in the solar absorptance, see *Figure 6;26*.
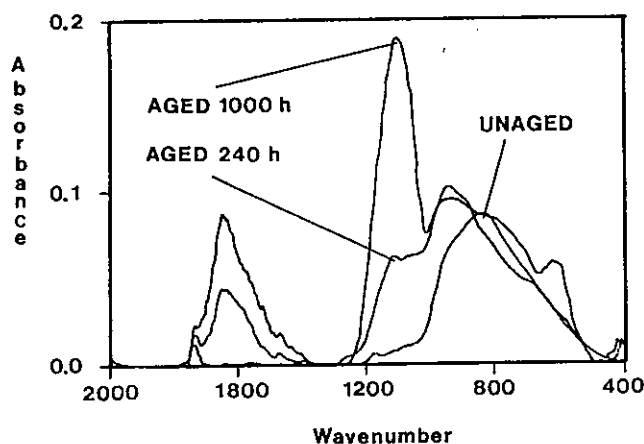
Figure 6;26 FTIR spectra obtained by using an attachment for diffuse reflectance measurements on unaged and aged Sunstrip coatings. Ageing conditions:1 ppm SO_2, 95 % RH, 70 °C.

It seems therefore reasonable to assume that the oxidation of metallic nickel is of a electrochemical nature, leading by the action of sulphur dioxide to the formation of nickel sulphate.

In order to verify that the decrease in metallic nickel content is due to a reaction with sulphur dioxide, an EDX investigation was performed. Some of the results obtained are illustrated in *Figure 6;27*.
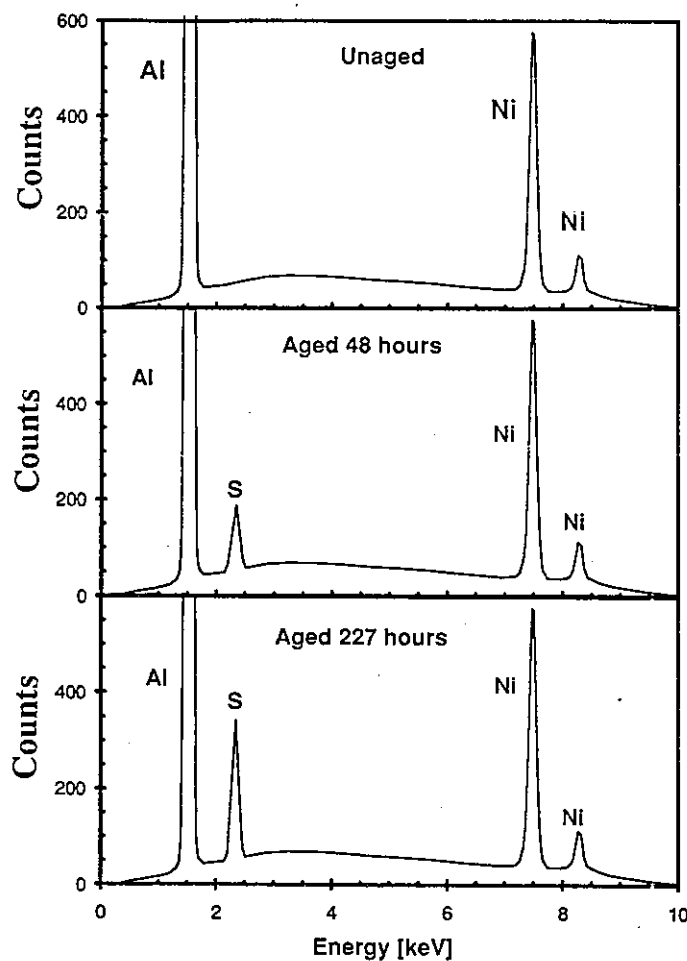
Figure 6;27 EDX spectra from unaged and aged Sunstrip coatings. Ageing con-ditions: 1 ppm SO_2, 95 % RH, 20 °C.

In *Figure 6;28* the sulphur content, as determined from the EDX spectra exemplified in *Figure 6;27*, is plotted versus testing time. In the same figure also the α_S values are plotted in the same figure. As can be seen, there is very good correlation between the decrease in solar absorptance and the increase in the amount of sulphur, i.e. sulphur dioxide, absorbed in the coating during degradation.
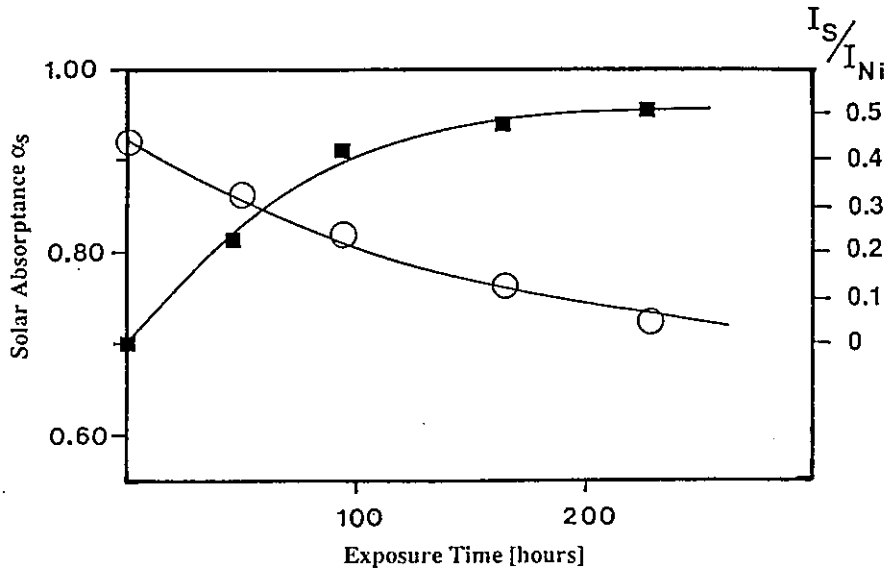
Figure 6;28 *Normalized solar absorptance and sulphur content, as determined from EDX spectra, plotted versus testing time for the Sunstrip coating. Ageing conditions. 1 ppm SO_2, 95 % RH, 20 °C.*

By the use of AES depth profiling on a severely degraded Sunstrip coating sample, Tanemura et.al [6,2] was also able to provide evidence for the formation of nickel sulphate in the sulphur dioxide induced degradation of the coating, as is illustrated in *Figure 6;29.*
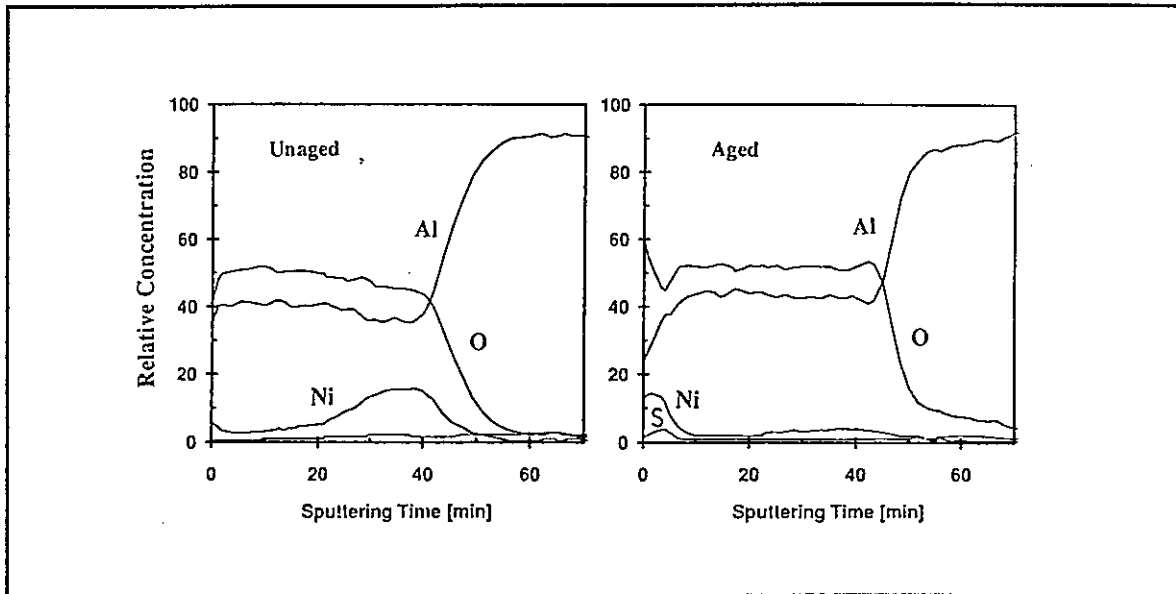
Figure 6;29 *AES depth profile for a Sunstrip absorber coating samplebefore ageing and after 1000 hrs ageing in 1 ppm SO_2, 95 % RH, 70 °C ($\Delta\alpha$ = 0.265)*

As can be seen from the figures there is an accumulation of sulphur and nickel at the entrance of the pores of aluminium oxide. This strongly suggests that nickel ions formed by oxidation of metallic nickel migrate to the entrance of the pores due to an electrochemical redox/corrosion process.

That the surface morphology is strongly affected by the sulphur dioxide-induced degradation of the nickel pigmented anodized aluminium coatings is illustrated in *Figure 6;30*.

| Unaged sample (x 11000) | Sample degraded for 227 hrs (x 11000)($\Delta\alpha_S = 0.756$) |
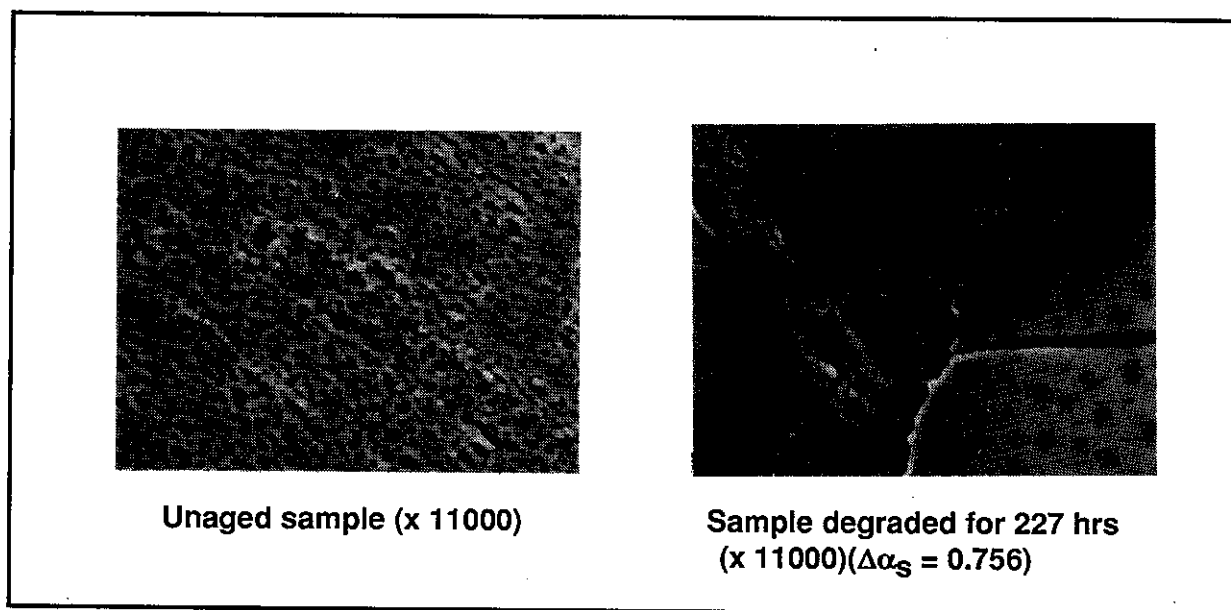
Figure 6;30   *SEM micrographs of unaged and aged samples of the Showa coating. Ageing conditions: 1 ppm SO_2, 95 % RH, 20 °C.*

It should be pointed out that the corresponding changes in the surface morphology of the Sunstrip coating are even more pronounced. As can be seen from *Figure 6;30*, there exist a lot of pores filled with reaction products on the surface of the aged samples. By EDX analysis, it could be confirmed that the reaction products in such a filled pore consisted mainly of nickel sulphate, i.e. nickel, sulphur and oxygen.

Based on the results of the different analysis performed, the following principle scheme of reactions leading to the observed degradation may be hypothesized:

Initiation

(1) $SO_2(g) \Leftrightarrow SO_2(aq)$ (Absorption)

(2) $SO_2(aq) + H_2O + \frac{1}{2} O_2(aq) \rightarrow 2H^+ + SO_4^{2-}$ (Oxidation and lowering of pH)

(3) $2H^+ + NiO(s) \rightarrow Ni^{2+} + H_2O$ (Depassivation of the surface of metallic nickel particles)

Electrochemical corrosion
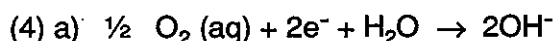
(4) a) $\frac{1}{2}$ O_2 (aq) + 2e$^-$ + H_2O $\rightarrow$ 2OH$^-$ (Cathodic reaction taking place on the surface of pores near the outer surface of coating)

or

(4) b) SO_2(aq) + O_2(aq) + 2e$^-$ $\xrightarrow{H_2O}$ SO_4^{2-}
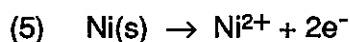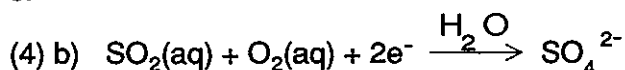
(5) Ni(s) $\rightarrow$ Ni^{2+} + 2e$^-$ (Anodic reaction taking place at the surface of metallic nickel particles)

Termination

(6) Ni^{2+} + SO_4^{2-} + XH_2O $\rightarrow$ $NiSO_4 \cdot XH_2O$ (s)   (Precipitation of nickel sulphate near the pore entrance)
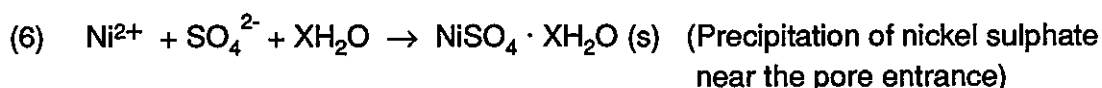
The first two steps, involving the adsorption or absorption of sulphur dioxide on the surface of the porous aluminium oxide, require the existence of adsorbed water on the coating surface, and therefore air humidities above at least 80 % RH, to be efficient, as well known from corrosion science. That no degradation was observed either at under the ageing conditions of 1 ppm SO_2, 75 % RH, 20 °C or for the test performed at   95 % RH without the addition of SO_2, cf *Table 5;19* and *5;20*, is consistent with reactions (1) and (2) being essential for initiation of the degradation in the pertinent case.

Absorbed sulphur dioxide in water, or in a liquid film of water, undergoes an oxidation leading to sulphate ions and to a decrease in pH, which may depassivate surfaces covered by oxides. From Pourbaix diagrammes, see eg [6, 11], one can conclude that for pH value less than 6, nickel oxide will dissolve according to reaction (3). If the pH values is less than 3, the aluminium oxide will also dissolve and aluminium ions be formed. As a result, the surface of the metallic particles will be opened for corrosion attacks.

As the change in pH needed to depassivate the metallic nickel surface is small, one can expect the initiation period to be relatively short. But if, on the other hand, the metal particles are entirely or partly embedded in a matrix of aluminium oxide, considerable change in pH is required for depassivating the surface of the metal. As a consequence, the initiation period will be much longer. Consequently, the difference in kinetic behaviour between the Sunstrip and the Showa coating, which can be seen from *Figure 6;25*, may be attributed to the fact that the metal particles in the Showa coating are embedded in the aluminium oxide, but not in the Sunstrip coating examined in the case study.

The next phase of reactions, which may take place after a depassivation of the metal surface has occurred, is an electrochemical corrosion process. This may lead to anodic oxidation of metallic nickel and a cathodic reduction of dissolved oxygen, in which process sulphur dioxide may also play a part, as has been suggested in reaction (4)b). It is reasonable to assume that the anodic surfaces are well separated from the cathodic surfaces of this electrochemical corrosion process. The former being located at the surface of the metallic particles, while the latter are located near the pore entrance, where there is good availability of oxygen needed for the cathodic reaction. As a consequence of such an electrochemical corrosion process, nickel ions will be transported in a direction towards the entrance of the pore. An explanation for the termination of the degradation process may then be precipitation of solid nickel sulphate salt hydrates formed during the corrosion process. This will close the pore and thus prevent further oxidation of metallic nickel..

As can be seen from the data in *Table 5;19* and *5;20*, the rate of degradation decreases with temperature. Such a behaviour seems strange at first sight, but may be explained by the reaction scheme postulated, as being due to a decreasing absorbitivity with increasing temperature of oxygen and sulphur dioxide on the coating surface. Moreover, the reaction scheme points to the fact that the most important step in the degradation process, as regards influence of environmental factors, is the initial absorption of sulphur dioxide on the surface of the coating.

6.4.2 Kinetics of degradation, sensitivity to different environmental factors and time-transformation functions for accelerated life testing

In order to investigate how the absorption kinetics of sulphur dioxide depend on humidity of the air and the concentration of sulphur dioxide in the air, some complementary studies were undertaken. Measurements of a more introductory character were carried out in equipment specially designed for such studies at the Department of Inorganic Chemistry at the Chalmers Technical University in Sweden, see *Figure 6;31*.

In the study, reported in more detail in [6, 12], the deposition rate of sulphur dioxide on samples of the Sunstrip coating was measured from the difference in sulphur dioxide concentration between inlet and outlet flow of conditioned air through a reaction cell where the absorber sample was placed. The composition of the conditioned air was varied from one experiment to another so that both the humidity and the sulphur dioxide concentration dependence could be investigated.

A typical deposition rate/time relationship obtained for an experimental run is given in *Figure 6; 32*.
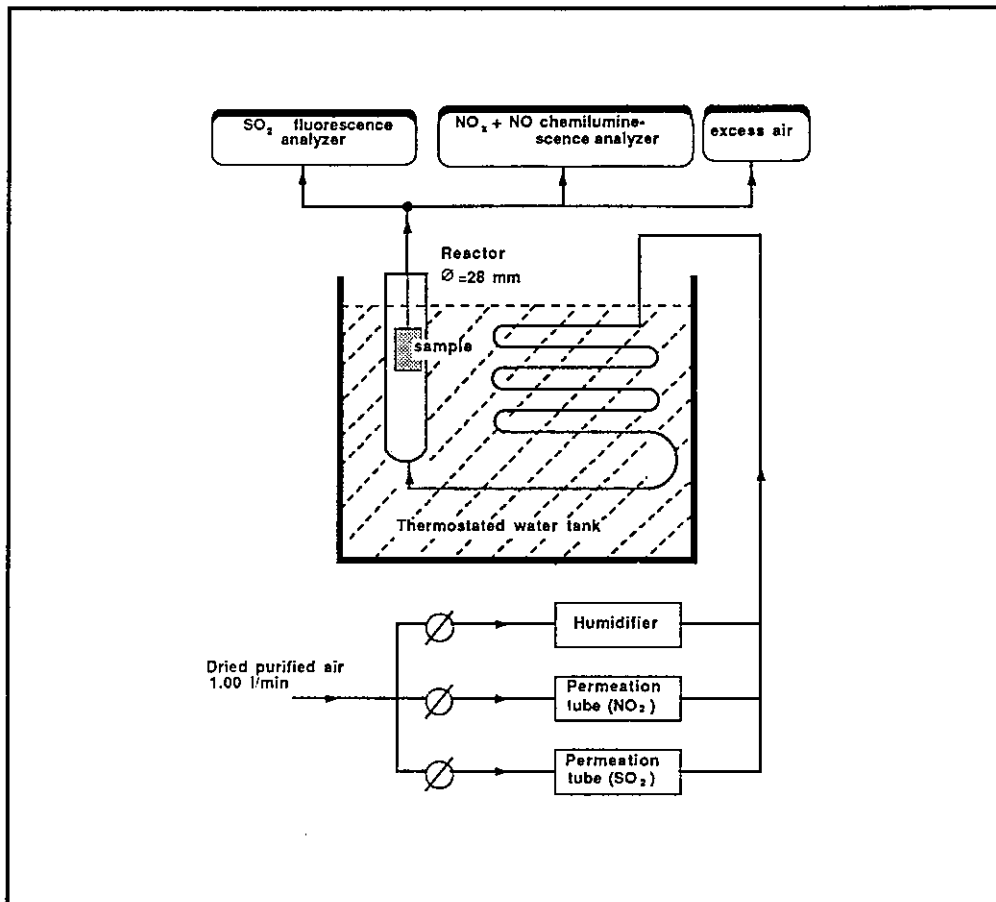
Figure 6;31   *Experimental set up used for deposition rate measurements.*
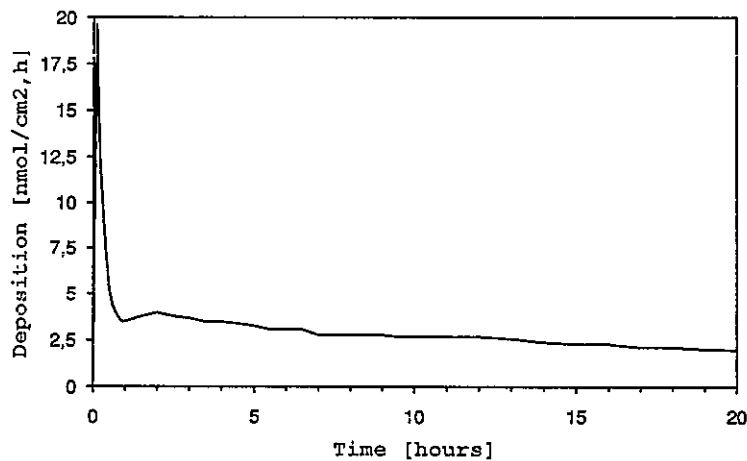
Figure 6;32   *Sulphur dioxide deposition rate versus time on a sample of the Sunstrip nickel-pigmented absorber coating. Experimental conditions: Composition of conditioned air 986 ppb SO$_2$, 99 % RH, 22 °C. Linear flow rate of conditioned air 27 mm/s.*

As can be seen, the initial deposition rate decreases with time until a constant rate is reached. The first phase of deposition behaviour with time may be interpreted in terms of the equilibrium reaction (1) being operative, see above. The steady-state condition then reached, characterized by the deposition rate being constant, gives evidence for the assumption that absorbed sulphur dioxide is consumed by oxidation reactions, see also above.

Figure 6;33 illustrates how the steady-state deposition rate, as determined from the different experiments performed, varies with the concentration of sulphur dioxide and with the humidity of air.

As can be seen in the lower figure, the steady-state deposition rate of sulphur dioxide does not seem to be proportional to its concentration in air. Although the experimental points vary in a somewhat inconsistent way due to experimental difficulties, the dashed curve, given in the figure to illustrate a power law relationship with an exponent of 0.5, seems better to describe the experimental data.

As can be seen in the upper figure, the humidity dependence is very drastic. However, it nicely reflects the expected characteristic features for the adsorption of water on the porous coating surface, as is indicated in the figure.

From a kinetic modelling point of view, therefore, three different regions may be distinguished:

I   At air humidities below 70 - 80 % RH, the overall reaction leading to oxidation of metallic nickel cannot take place. No liquid film of water exists on the porous coating surface, which is necessary for the absorption/oxidation of sulphur dioxide to occur.

II   At air humidities above 70 - 80 % RH, the conditions for absorption and oxidation of sulphur dioxide prevail, which may lead to oxidation of metallic nickel. The rate is dependent on the concentration of sulphur dioxide in the air and the mass transfer of sulphur dioxide to the surface of coating. It should be pointed out that the deposition rate of sulphur dioxide on the coating was found not to be dependent on the presence of metal particles as almost the same result was obtained for an unpigmented coating, as for an pigmented coating.

III At air humidities above 95-97% RH, capillary or pore condensation of water takes place, drastically increasing the steady-state deposition rate of sulphur dioxide on the coating. This should also lead to a drastic increase in the oxidation rate of metal. However, the rate-limiting step may change and the availability of sulphur dioxide in the air near the coating surface may become the rate-limiting factor.

Due to the complex nature of the degradation caused by sulphur dioxide, it is consequently difficult to formulate a theoretical model to describe the kinetics of it. Even if the kinetics of the chemical reaction could be quantitatively described in terms of temperature dependence, humidity dependence and sulphur dioxide concentration dependence nothing would have really been gained. The most difficult modelling problem concerns the transport of sulphur dioxide into the solar collector and the sorption of sulphur dioxide on the surface of all the materials inside the collector.
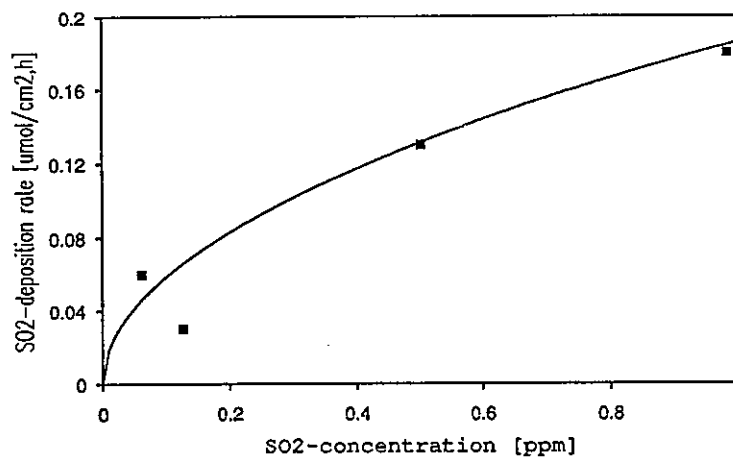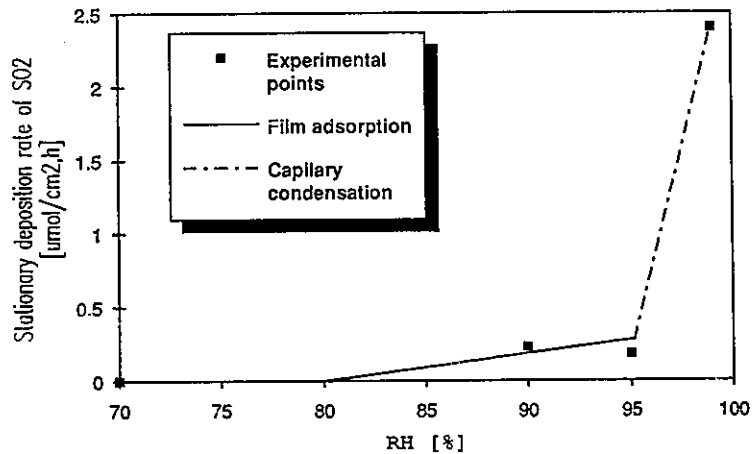
Figure 6;33 *Steady state deposition rates of sulphur dioxide on samples of the Sunstrip nickel-pigmented absorber coating.*
Upper figure: Deposition rates after 20 hrs of exposure for conditioned air with 0.99 ppm SO₂ in different experiments of varying air humidities.
Lower figure:Deposition rates after 20 hrs of exposure for conditioned air of 95 % RH in different experiments of varying concentrations of sulphur dioxide. The curve represents a power law relationship with an exponent of 0.5

*For other experimental details, see **Figure 6;32.***

An alternative evaluation procedure was therefore adopted based on comparative testing. Metal coupons were used to determine the atmospheric corrosivity in the accelerated sulphur dioxide tests and the atmospheric corrosivity inside the collectors tested. The degradation rate in the solar absorptance of the coatings, thus, considered to be a simple function of the corrosion rates of the different metal coupons used.

As an additional comparative test method measurements of the deposited amounts of sulphur dioxide on the surface of the absorber coatings in the accelerated laboratory tests and in the solar collector tests could be utilized, see *Chapter 7* and *8*.
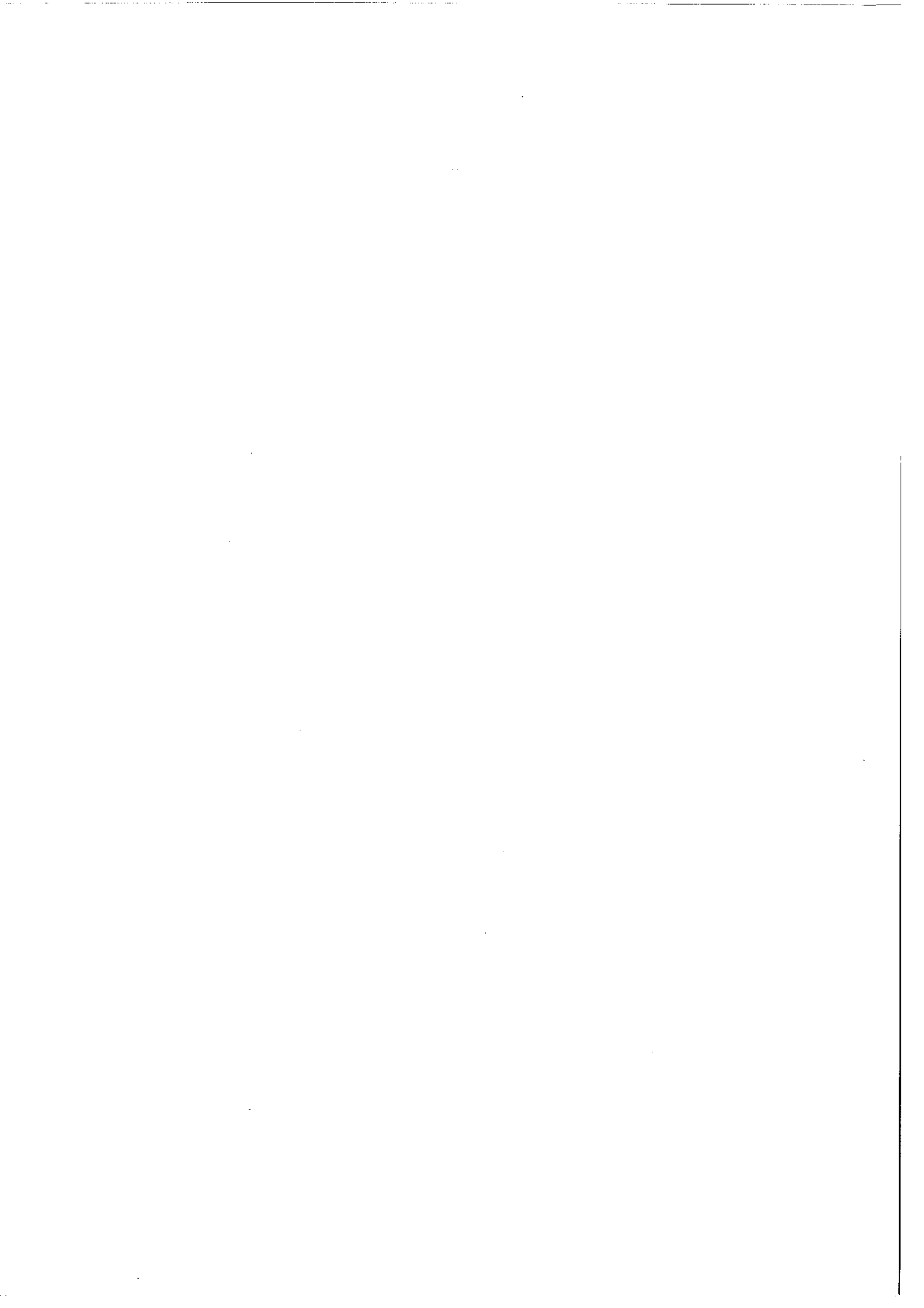
CHAPTER 7

PERFORMANCE CRITERIA FOR ACCELERATED AGEING TESTS AND ESTIMATION OF SERVICE LIVES OF STUDIED COATINGS

7.1   Purpose and Scope of Work

By use of time-transformation functions expected service lives of materials can be estimated from results of accelerated ageing tests.

The most essential question in design work is, however, not the actual value of the service life. Rather, the question is if the material tested can be expected to have a service life longer than a certain value; the latter dictated by life cost considerations taking into account all the materials, material combinations, design and needs of maintenance of the total system or component.

Methods for service life assessment may in its most simplest form be based on theoretical analysis making use of results from previous durability studies of similar materials. They may involve testing and the life data analysis be based on results from so called qualification or acceptance durability tests. The life data analysis may be based on results from more extensive work as accelerated life testing as performed in the present case study. For all methods adopted it is, however, important to carry out also long-term in-service exposure tests to finally verify the accuracy of predicted or estimated service lives.

The objectives of the case study work were to make use of the experimental results for the black chrome and the nickel-pigmented anodized aluminium coatings:

- for formulating failure criteria for accelerated ageing tests to be used primarily in the assessment of the service life of new absorber coating materials by qualification testing,

- to estimate the service life of the four different coatings of the case study,

- to predict expected decrease in the optical performance of the coatings of the case study after the three years of testing of the eight solar collectors at Rapperswil.

By comparison of predicted and actually measured decrease in optical performance, the validity of the derived models for service life prediction in the case study may then be evaluated, see *Chapter 8* of the present report.

As the first step in the analysis of life data, effective mean levels of the degradation factors under service conditions were evaluated. Micro-climatic data measured or calculated as described in *Chapter 4* of the present report were utilized as a point of departure for this evaluation.

As the second step performance or failure time requirements for the constant load accelerated aging tests were evaluated. The third step was the estimation of the expected service lives of the coatings in the case study.

7.2 The Effect of High-temperature Degradation on Service Life of Absorbers

7.2.1 Effective mean temperatures for high temperature degradation of absorbers in collectors

To elaborate a useful expression for calculating the effective mean temperature of absorber from micro-climatic data, the equations given in *Chapter 2* of the present report were used as a starting point.

For high temperature degradation in optical performance of the coatings, equation (2.8) can be written as follows.

$$\frac{1}{n_A} = \int_0^{y_A} (g_A\,(T)/g_A\,(T_{R,\,A})) \cdot \frac{1}{y_{R,\,A}} \cdot dt \qquad (7,1)$$

By introducing the temperature distribution or frequency function $f(T)$ for one year, equation (7,1) may be rewritten

$$\frac{1}{n_A} = \int_{T_{min}}^{T_{max}} (g_A(T)/g_A(T_{R,A})) \cdot \frac{1}{y_{R,\,A}} \cdot f(T) \cdot dT \qquad (7,2)$$

By inserting the expression for the time-transformation function, as elaborated in *Section 6.2.2*, and expressing all time values in years, the expected service life $n_A = y_{A,S}$ can be written

$$y_{A,S} = y_{R,A} \cdot \left(\int_{T_{min}}^{T_{max}} \exp\left(\frac{-E_A}{R}(T^{-1} - T^{-1}_{R,A})\right) \cdot f(T) \cdot dT \right)^{-1} \qquad (7,3)$$

If now the effective mean temperature $T_{eff,A}$ is introduced defined by

$$\exp\left(-\frac{E_A}{R}(T^{-1}_{eff,A} - T^{-1}_{R,A})\right) = \int_{T_{min}}^{T_{max}} \exp\left(\frac{-E_A}{R}(T^{-1} - T^{-1}_{R,A})\right) \cdot f(T) \cdot dT \qquad (7,4)$$

it is evident that equation (7,3) can be expressed in a much simpler form, namely

$$y_{A,S} = y_{R,A} \cdot \exp\left(\frac{E_A}{R}\left(T^{-1}_{eff,A} - T^{-1}_{R,A}\right)\right) \qquad (7,5)$$

It should be noted that the effective mean temperature $T_{eff,A}$ depends on both the temperature distribution or frequency function $f(T)$ and the activation energy E_A.

Test collectors see *Figure 4;9*		Arithmetic mean temperature (°C)	Effective mean temperatures according to the Arrhenius equation at activation energies of		
			50 kJ/mol (°C)	100 kJ/mol (°C)	200 kJ/mol (°C)
Teknoterm	- stagnation	36	96	124	145
	- operation	20	43	82	114
Showa	- stagnation	33	84	110	128
	- operation	21	38	68	96
Sessatherm	- stagnation	37	98	127	148
	- operation	22	42	76	105
Azur III	- stagnation	35	93	121	141
	- operation	22	41	74	105
Simulated collector in the calculations made by Hollands et.al. [4,5], see *Figure 4;12* (operation)		20	41	61	83
Simulated collector in the calculations made by van der Linden et.al. [4,2], see *Figures 4;15* and *4;16*					
- operation		17	24	29	36
- stagnation		31	78	102	120

Table 7;1   *Characteristic mean temperature data based on measured and calculated absorber temperatures*

In *Table 7;1* characteristic mean temperature data based on both measured and calculated absorber temperatures are presented. As can be seen from the table, the effective mean temperature varies very strongly with the activation energy of the degradation reaction. At the high activation energies determined for high temperature degradation of the coatings of the case study, only the highest absorber temperatures contribute significantly to the effective mean temperature.

The variation in effective mean temperatures between the four collectors tested is as to be expected small. The very large deviation of the values obtained from the calculations made by van der Linden et.al. for the collector working under operating conditions is attributed to the fact that no period of stagnation is included, which is the case for the calculation carried out by Hollands et.al. Hollands et.al. included a stagnation period of fourteen days per year. Because of the pump failure during the collector tests previously mentioned, the effective mean temperatures based on measured absorber temperatures are accidentally influenced by a period of fourteen days during the three years of test period when the collectors were under stagnation conditions. Despite that, the effective mean temperatures based on calculated mean absorber temperatures differ markedly from those that are based on measured mean temperatures.

To be able to set up a more general service life requirement or failure time requirement for a constant load high temperature test, a reference temperature frequency function was designed based on the measured absorber temperatures. This function shown in *Figure 7;1* was formed by calculating the mean frequency of the absorber temperatures measured in all test collectors assuming that a collector works under operation conditions for eleven months per year and under stagnation conditions for one month per year. The measured values of absorber temperatures refer to three years of the collector test executed in the case study.
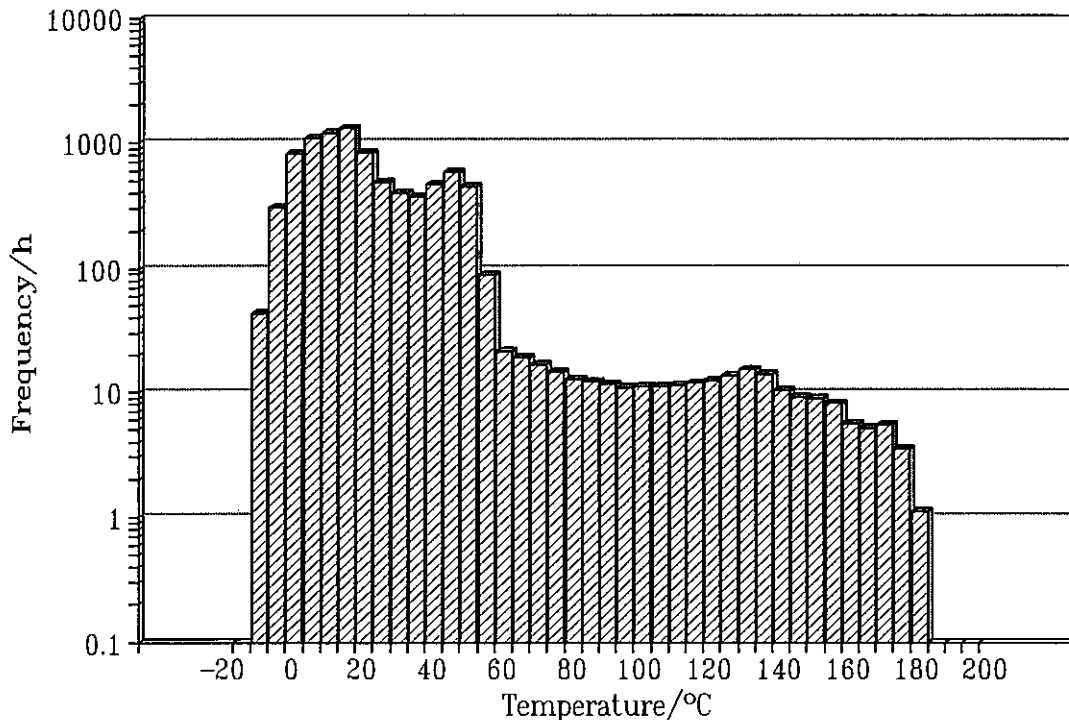
Figure 7;1 Reference absorber temperature frequency function for one year based on measured absorber temperatures in the collectors tested.

In *Figure 7;2* the effective mean temperature versus activation energy is plotted for the reference temperature load profile in *Figure 7;1*.
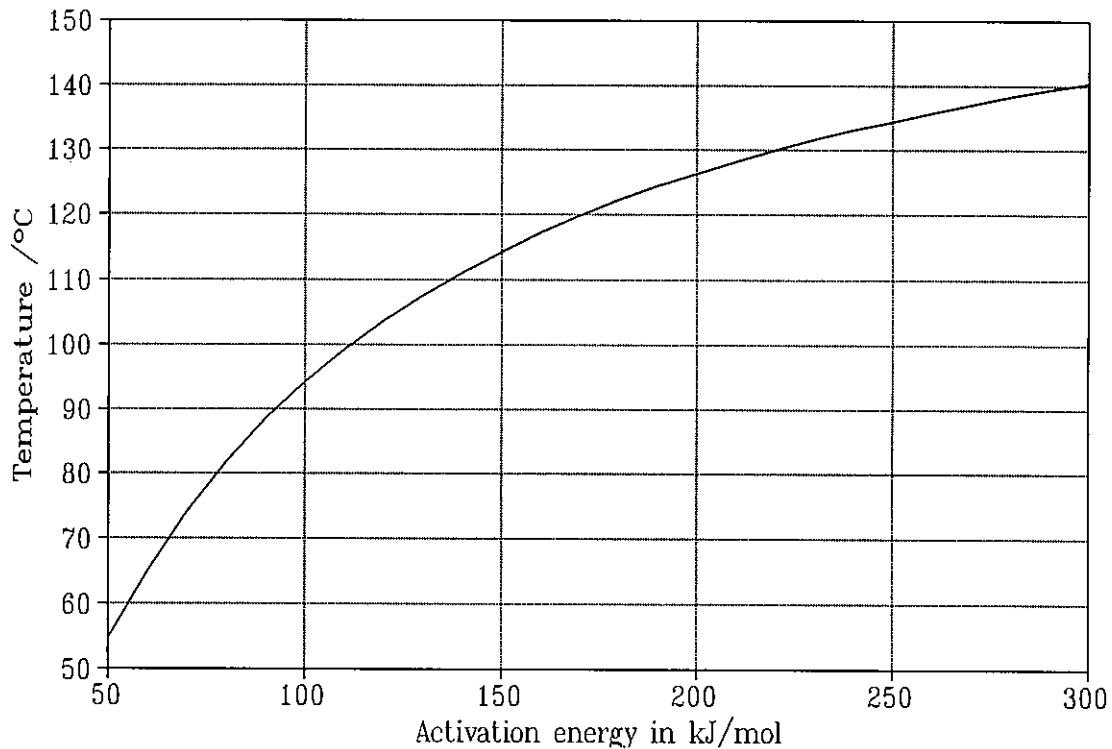
Figure 7;2 Effective mean temperature versus activation energy for the reference temperature frequency function given in *Figure 7;1*.

7.2.2. Performance and service life requirements for absorbers related to high temperature testing

In order to formulate failure time requirements for absorbers in constant load high-temperature tests, the following qualification rules were set up.

- An absorber coating should fulfil the performance requirement, ie

$$PC = - \Delta\alpha_s + 0.25 \, \Delta\varepsilon \leq 0.05 \qquad\qquad (7,1)$$

cf equations (2,1) and (2,2), during a service time of at least 25 years, ie the expected service life with PC <0.05 should be at least 25 years.

- During its service life, the absorber coating should be exposed to a thermal stress defined by the temperature frequency function given in *Figure 7;2*.

Equation (7,5) and the relation between effective mean temperature for the reference thermal load and activation energy, as illustrated in *Figure 7;2* could thereafter be applied. As a result, the qualification rules set up for service conditions could be transformed into useful failure time requirements for absorber coatings in accelerated high temperature tests, as are illustrated in *Figure 7;3*. In *Table 7;2* the numerical data, on which *Figure 7;3* is based, are presented.
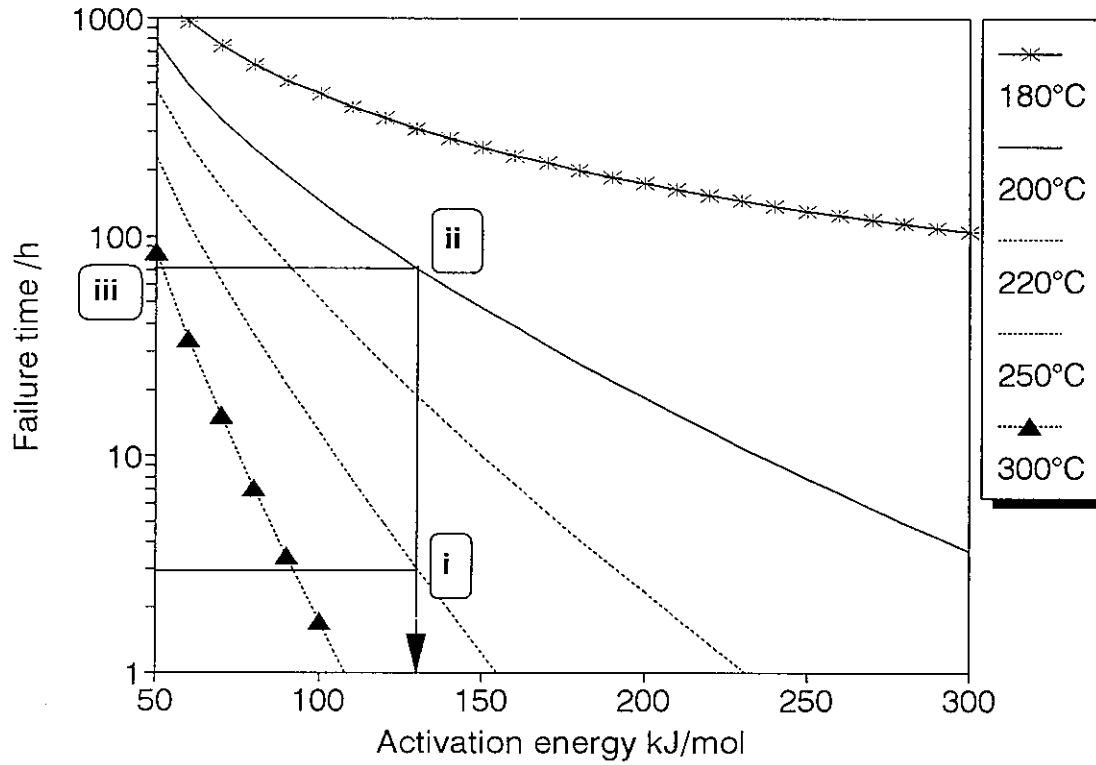
Figure 7;3 *Shortest acceptable failure time for absorber coatings in different high
temperature tests given as a function of the activation energy for the
degradation reaction. The failure time given corresponds to a service life
with PC <0.05 of 25 years.*
*Solid lines in the figure define the circumstances for an absorber coating
with a service life with PC <0.05 of 25 years and with an activation energy
of 130 kJ/mol for its degradation reaction.*

*Table 7;2 Numerical data upon which **Figure** 7,3 are based.*

Activation energy (kJ/mol)	Failure times corresponding to a service life *with PC <0.05* of 25 years for high temperature tests at					
	150 °C (hrs)	180 °C (hrs)	200 °C (hrs)	220 °C (hrs)	250 °C (hrs)	300 °C (hrs)
50	3470	1354	773	462	229	84
60	2947	953	486	262	113	34
70	2768	741	338	164	62	15.2
80	2742	608	248	109	36	7.1
90	2799	515	188	74	21	3.5
100	2917	444	145	52	13	1.7
110	3085	389	113	37	7.8	0.9
120	3303	345	90	26	4.9	0.4
130	3572	309	72	19	3.1	0.2
140	3896	280	58	14	1.9	0.1
150	4282	254	47	10.1	1.2	0.1
160	4738	233	39	7.4	0.8	0
170	5274	215	32	5.5	0.5	
180	5900	199	27	4.1	0.3	
190	6633	186	22	3.1	0.2	
200	7489	174	18	2.3	0.1	
210	8487	163	16	1.8	0.1	
220	9653	154	13	1.3	0.1	
230	11013	145	11	1.0	0	
240	12602	138	9.3	0.8		
250	14459	131	7.9	0.6		
260	16631	125	6.7	0.5		
270	19174	119	5.8	0.4		
280	22154	114	4.9	0.3		
290	25649	109	4.2	0.2		
300	29753	105	3.6	0.2		

The plots in *Figure 7;3* can be used as follows as is illustrated by the example given in the figure.

Consider an absorber coating which fails after a testing time of about 1.5 hour in a test performed at 250 °C (solid line i). This means that the absorber coating will meet the service life requirement, ie PC <0.05 for 25 years, only if the activation energy of its degradation reaction is higher than 130 kJ/mol (solid line ii). If so, the failure time for the absorber coating in a test performed at 200 °C should be longer than about 70 hrs (solid line iii).

A qualification test procedure for an absorber coating with respect to thermal stability can accordingly be designed as follows:

(a) Perform a constant load high-temperature test at 250 °C and determine, or estimate the failure time, ie the testing time at which PC = -$\Delta\alpha_s$ + 0.25 $\Delta\varepsilon$ = 0.05[1].

   If the failure time exceeds 200 hrs measure the extent of degradation and proceed to point (g)

(b) Determine the lowest acceptable activation energy by use of *Figure 7;3*, ie use the curve for the 250 °C test and determine the activation energy which corresponds to the pertinent failure time of the coating at that temperature.

(c) Use this value for the activation energy and determine, the corresponding or shortest acceptable failure time in a test to be performed at 200 °C.

(d) Perform a high temperature test at 200 °C and determine or estimate by extrapolation the actual failure time for the coating at that temperature.

(e) Compare the actual failure time at 200 °C for the coating with the shortest acceptable failure time at that temperature according to (c).

(f) The absorber coating is qualified as regards its thermal stability if the actual failure time at 200 °C exceeds the shortest acceptable failure time at that temperature by at least 50 %.

(g) If the failure time exceeds 200 hrs according to point (a), execute a new test at 300 °C for 80 hrs and measure the extent of degradation after that testing time. If the extent of degradation is then higher than that found after the test at 250 °C for 200 hrs, the coating is qualified. If no significant change can be measured in the optical properties of coating, ie the change in PC <0.01, it is most probable that the thermal stability of the coating is good enough for its intended use in a DHW-system.

It should be pointed that this qualification test procedure is only relevant for the application area of this case study. The absorber coatings are considered for use in single glazed solar collectors installed in typical DHW systems.

---

[1] The performance criterion can of course be set at a higher level, eg 0.10. In this case the service life corresponds to the time when the DHW system performance will be at a level of at least 90 % of its original value.

7.2.3 Thermal stability of the coatings of the case study

For the coatings of the case study, effective mean temperatures were calculated based on temperature data from the collector in which the absorber coating was installed. The corresponding shortest acceptable failure times for a constant load temperature test at 200 °C were also calculated for each test collector, see *Table 7,3*.

As can be seen from this table, the shortest acceptable failure times at 200 °C are several orders of magnitude shorter than the estimated actual failure time at that temperature. It can be concluded that the coatings are more than qualified for their intended use in the application area of the case study, as far as thermal stability is concerned.

Test collector		Effective mean temperature (°C)	Shortest acceptable failure time for high temperature test at 200 °C corresponding to a service life with PC <0.05 of 25 years (hrs)	Extrapolated failure time at 200 °C from accelerated test results in the programme of case study, see *Section 6.2.2* (years)
Teknoterm (Sunstrip)	- stagnation	148	~ 200	>10^5
	- operation	118	~ 1	
Showa (Showa)	- stagnation	131	~10	>10^6
	- operation	100	~ 0.01	
Sessatherm (MTI)	- stagnation	150	~ 300	>10^3
	- operation	109	~ 0.5	
Azur III (Energie Solaire)	- stagnation	143	~ 100	>10^3
	- operation	107	~ 0.3	

Table 7;3 *Effective mean temperatures for the absorber coatings in the different test collectors of the case study together with the corresponding shortest acceptable failure times at 200 °C and estimated failure times for the coatings based on the accelerated test results from the case study.*

A maybe more informative measure on the thermal stability of the absorber coatings of the case study is to give the effective mean temperature of an absorber coating that corresponds to an expected service life with PC <0.05 of 25 years. This is done in *Table 7;4*.

Absorber coating	Effective mean temperature corresponding to a service life with PC <0.05 of 25 years (°C)
Sunstrip	~ 290
Showa	~ 310
MTI	~ 240
Energie Solaire	~ 250

Table 7;4   Effective mean temperatures corresponding to a service life with PC <0.05 of 25 years for the absorber coatings in the case study.

According to the data in the table the nickel-pigmented anodized aluminium coatings, can be used in solar systems characterized by absorber effective mean temperatures up to around 300 °C. The black chrome coatings are somewhat less stable and can be used in solar systems characterized by absorber effective mean temperatures up to around 250 °C.

It should be pointed out that the service life data calculated are based on the presumption that an absorber coating fails when its PC value exceeds 0.05. Degradation in optical performance of the absorber coatings which is less than this PC value may eventually occur only after a short time period under service conditions. Other processes faster than the main degradation process which is the dominating one at the high temperatures of the accelerated tests performed may take place, see *Section 6.2*.

Difficulties, therefore, arose when trying to estimate the expected extent of degradation in optical performance of the coatings after the three-years of collector test executed in the case study. However, rough estimates could be made to predict the maximum change to be expected based on the accelerated test data presented in *Figures 6;10* and *6;14*.

The testing time of three years under the conditions of the collector tests was first transformed into corresponding testing times at 200 °C. For the black chrome coatings this time period was in the order of 10^{-3} years for the stagnation case and 10^{-5} years for the operation case. It is clear from *Figure 6;10* that the reduction in solar absorptance to be expected as a result of thermal degradation after three years of collector test should be less than 0.001 for the Energie Solaire coating and less than 0.01 for the MTI coating.

Using the same extrapolation procedure for the Showa coating and the Sunstrip coating may be not fully correct because of the fast initial change in the absorptance of these coatings observed in the high temperature tests, see *Figure 6;13*. However, by taking this effect into account, the expected reduction in the solar absorptance caused by thermal degradation after three years of collector test should be less than 0.02 for the Showa coating and less than 0.01 for Sunstrip coating.

7.3 Degradation of Absorbers Caused by High-humidity and Condensed Water

Degradation caused by the action of high-humidity air and condensed water on an absorber coating may reduce its service life in a way which can be estimated by use of the equations presented in *Section 6.3.2*.

The kinetic model, on which these equations are based, requires primarily test results from condensation tests. As a consequence, the life date analysis could be carried out analogous to what was described in *Section 7.2*.

7.3.1 Effective mean temperatures for degradation

Effective mean temperatures for absorbers in collectors were calculated for different humidity intervals near the condensation limit. For the calculations measured micro-climatic data from the Teknoterm collector tested under simulated operation conditions were used, see *Chapter 4*.

Temperature frequency diagrammes, based on those measured data are shown in *Figure 7;4* together with two comparable sets of data of results from the calculations made by van den Linden et.al. , see *Section 4.3.2*.
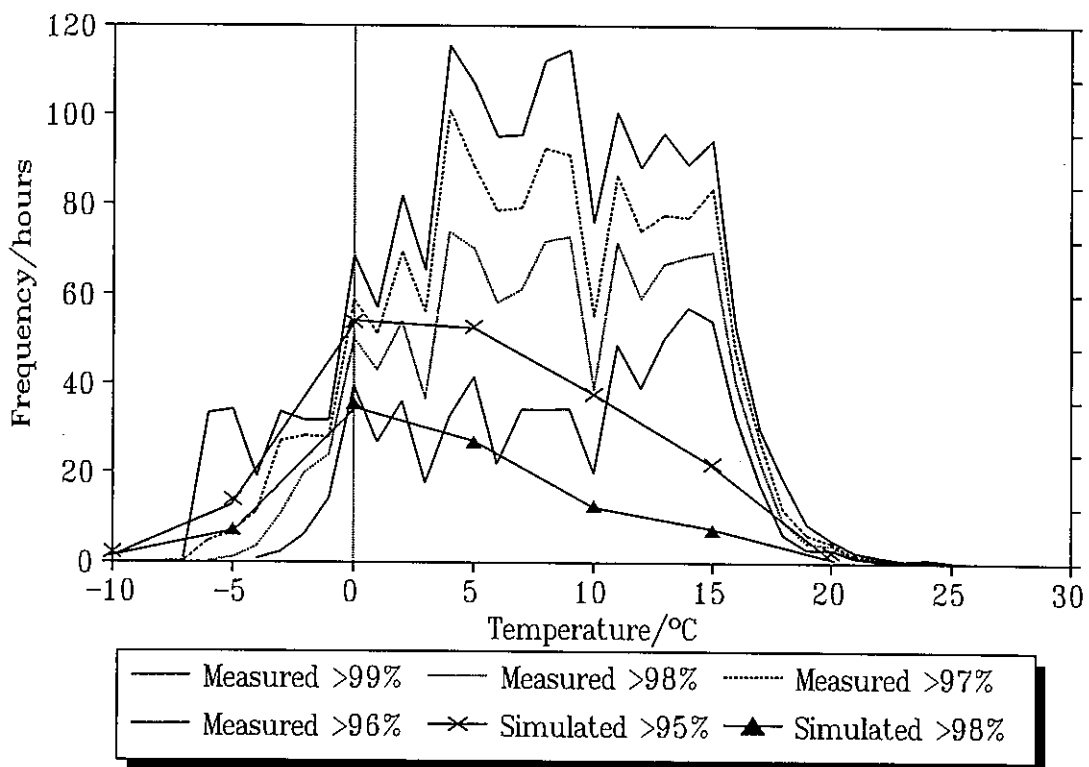
Figure 7;4 Temperature frequency diagrammes in different humidity intervals based on measured and calculated micro-climatic data for absorbers in collectors.

It should be pointed out that the relative humidities which are referred to in *Figure 7;4* are defined in a somewhat different way as concerns the diagrammes based on measured data compared to the diagrammes based on calculated data. The calculated air humidities refer to absolute humidities which have been transformed into relative humidities valid for the corresponding mean absorber plate temperatures. The temperature frequency diagrammes based on measured humidities refer, however, to relative humidities recorded in the air gap between absorber and cover plate in the upper part of the collector. The relative humidities are, thus, only strictly valid for the air gap temperature at the measuring point used.

The difference between the calculated and measured temperature frequency diagrammes is in the order of a factor of two. Possible explanations to this difference might be many.

When optimizing the calculation model, van der Linden et.al. [4,2] found relatively large deviations between calculated and measured relative humidities in the air gap during night conditions, see *Figure 4;19*. The measured air humidities were about 5-10% higher than the calculated humidities. If a 4% deviation is assumed, this should mean that the "simulated >95%" diagram in *Figure 7;4* should correspond to the "measured >99%" diagram in the same figure. Thus, if this deviation was corrected for, the agreement should be considerably better. Moreover, the different measures for humidity used, cf above, lead to an effect, which when corrected for, should reduce the temperature frequencies measured in the humidity intervals considered and, thus, also lead to a better agreement.

In view of the high complexity involved both in the measurement and modelling of the humidity conditions, the agreement between measured and calculated humidities is fairly good.

Because of the difficulties faced in getting information on the actual humidity conditions on the surface of the absorber plate, it is ,thus, important to verify calculated degradation data for service conditions with actual degradation data determined from collector tests under in-use conditions, as already has been pointed out in *Section 6.3.2*.

To generated service life data based on results from the laboratory condensation tests, the temperature frequency diagram based on measured micro-climatic data and valid for the relative humidity interval 99%-100% was mainly considered, see *Section 6.3.2*.

The equations used for the life data analysis were derived from equations (2,8), (6,18) and (7,4). The service life $y_{B,S}$ was expressed related to the fraction of a year η when the relative humidity exceeds a certain value RH_c as

$$y_{B,S} = y_{B,\eta}/\eta \qquad\qquad (7,6)$$

where

$$y_{B,n} = y_{R,B} \cdot \exp\left(\frac{E_B}{R}\left(\frac{1}{T_{eff,B}} - \frac{1}{T_{R,B}}\right)\right) \cdot \frac{1}{X} \qquad\qquad (7,7)$$

The parameters $T_{eff,B}$ and η were defined as follows

$$\exp\left(\frac{-E_B}{R}\left(\frac{1}{T_{eff,B}} - \frac{1}{T_{R,B}}\right)\right) = \int_{T_{min}}^{T_{max}} \exp\left(\frac{-E_B}{R}\left(\frac{1}{T} - \frac{1}{T_{R,B}}\right)\right) \cdot f((T, RH > RH_c) \cdot dT \quad (7,8)$$

and

$$\eta = \int_{T_{min}}^{T_{max}} f(T, RH > RH_c) \cdot dT \quad (7,9)$$

The parameter X was set equal to 1 and RH_c varied from 96% to 99%. The value of T_{min} was set equal to 0 °C which is reasonable as for temperatures below this value ice instead of condensed water should exist on the surface of absorber.

Calculated effective mean temperatures versus activation energy for RH_c values ranging from 96% to 99% are given in *Figure 7;5*.
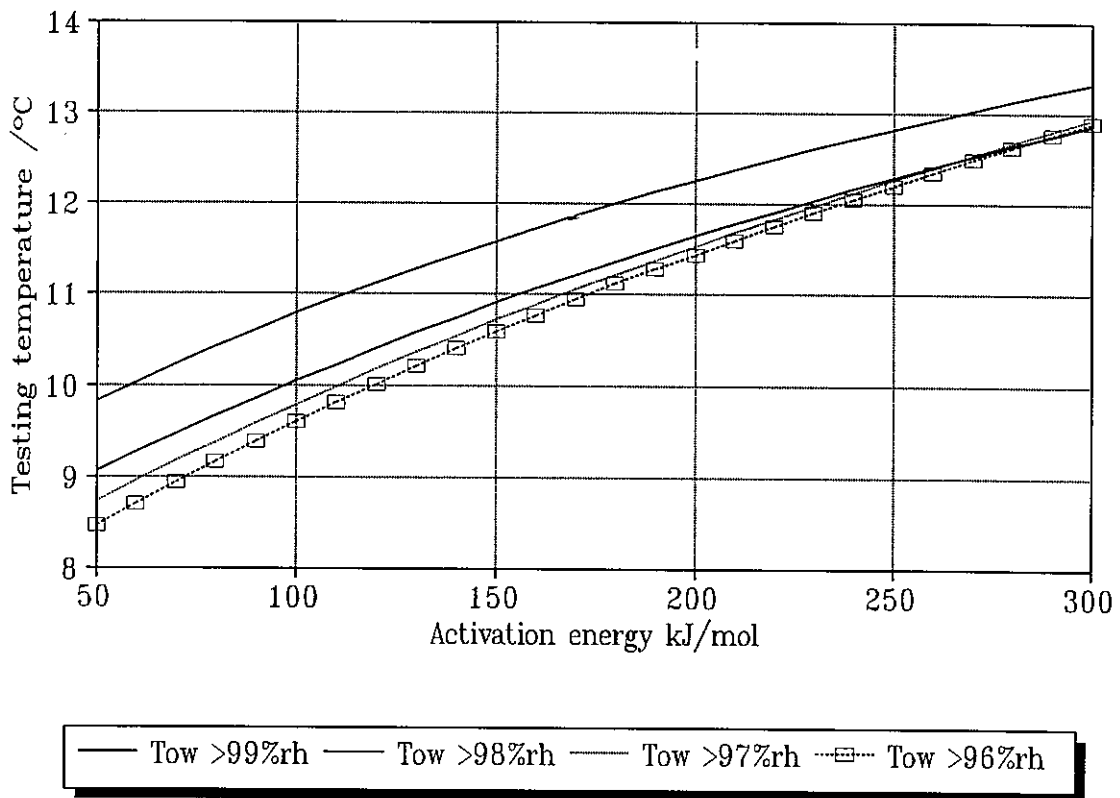
Figure 7;5 *Calculated effective mean temperatures versus activation energy for RH_c values ranging from 96% to 99%, see equation (7,8). Temperature frequency functions based on measured micro-climatic data illustrated in Figure 7;4 were used for the calculations. The time of a year when T>0°C and RH>RH_c are: 1507 hrs when RH_c = 96%, 1260 hrs when RH_c = 97 %, 995 hrs when RH_c = 98 %, and 610 hrs when RH_c = 99%.*

When formulating a more general service life requirement or failure time requirement for absorbers in a condensation test, the humidity - temperature frequency function valid for $RH_c = 99\%$ was used as the reference load. Its temperature frequency function is shown in *Figure 7;7*.
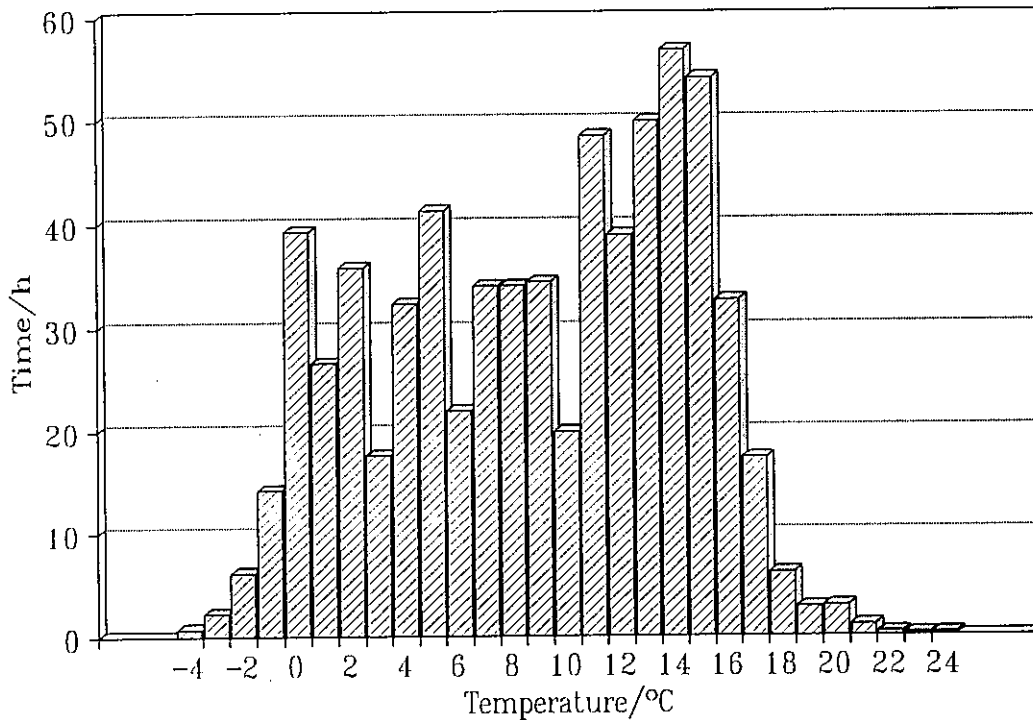
Figure 7;7 Reference humidity/condensation load used for life data analysis. The temperature frequency function is based on measured micro-climatic data for the Teknoterm collector tested under simulated operation conditions and is valid for $RH_c = 99\%$, see equations (7,6) to (7,9).

7.3.2 Performance and service life requirements related to condensation testing

Failure time requirements for absorbers in condensation tests were thereafter formulated based on the requirements that on absorber coating should have a service life of at least 25 years and during that time be capable to meet the requirement PC <0.05 for a moisture or humidity load defined by the temperature/humidity frequency function given in *Figure 7;7*.

By use of the relation between effective mean temperature and activation energy, as is illustrated in *Figure 7;5*, and the equation (7,6) to (7,9), failure time requirements for condensation tests could be calculated, see *Figure 7;8*.
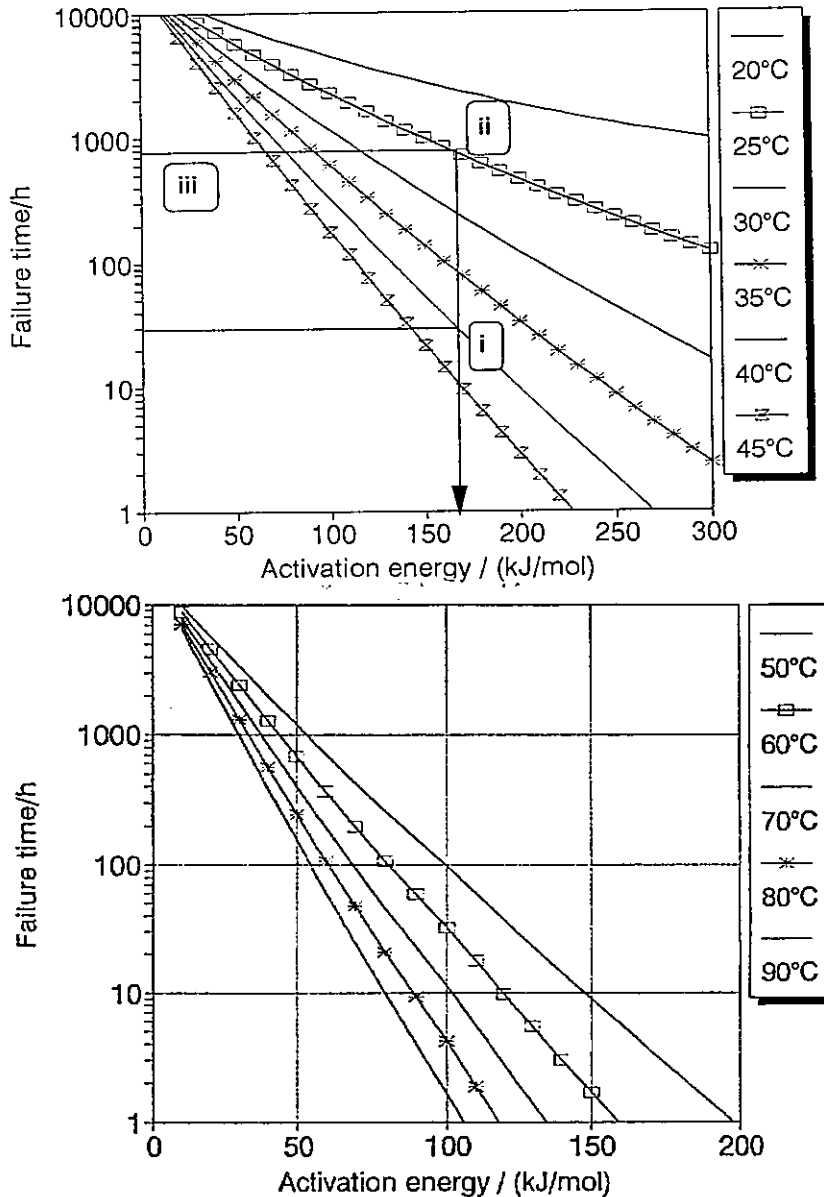
Figure 7;8 *Shortest acceptable failure time for absorber coatings in different condensation tests given as a function of the activation energy for the degradation reaction. The failure time given should correspond to a service life with PC <0.05 of 25 years.*
Solid lines in the upper figure define the circumstances for an absorber coating with a service life with PC <0.05 of 25 years and with an activation energy of 170 kJ/mol.

The example given in the figure may be interpreted in the following way. If in a condensation test at 40 °C an absorber coating fails after a testing time of about 30 hrs (solid line i). This means that the coating will be qualified only if the activation energy of its degradation reaction is higher than 170 kJ/mol (solid line ii). The failure time for the coating in a condensation test performed at 25 °C should then be longer than about 800 hrs (solid line iii).

A qualification test procedure, related to resistance to humidity involving condensation of water on the absorber coating, can accordingly be designed in a similar way as presented in *Section 7.2.2.*

(a) Perform a condensation test at 40 °C and determine or estimate the testing time at which
$$PC = - \Delta\alpha_S + 0.25 \ \Delta\varepsilon = 0.05^1$$

If the failure time exceeds 800 hrs measure the extent of degradation and proceed to point (g)

(b) If the failure time is less than 800 hrs determine the lowest acceptable activation energy by use of *Figure 7;8*, ie use the curve for the 40 °C test and determine the activation energy which corresponds to the pertinent failure time of the coating at that temperature.

(c) Use this value for the activation energy and determine the corresponding or shortest acceptable failure time in a test to be performed at 30 °C.

(d) Perform a condensation test at 30 °C and determine, or estimate by extrapolation, the actual failure time for the coating at that temperature.

(e) Compare the actual failure time at 30 °C for the coating with the shortest acceptable failure time at that temperature according to (c).

(f) The absorber coating is qualified as regards its humidity resistance if the actual failure time at 30 °C exceeds the shortest acceptable failure time at that temperature.

(g) If the failure time exceeds 800 hrs according to point (a), execute a new test at 60 °C[2] for 250 hrs and measure the extent of degradation after that testing time. If the extent of degradation is then higher than that found after the test at 40 °C for 800 hrs, the coating is qualified.
If no significant change can be measured in the optical properties of coating, ie the change in PC <0.01, it is most probable that the moisture resistance of coating is good enough.

The assumptions made mean that the qualification procedure proposed is based on micro-climatic data measured for the middle part of an absorber in a rather highly ventilated solar collector operating under the conditions of a DHW system.

---

[1] The performance criterion can of course be set at a higher level, eg. 0.10. In this case the service life corresponds to the time period when the DHW system performance will be at a level above 90 % of its original value.

[2] If the coating is based on anodized aluminium this high temperature can not be used. In this case a set of lower test temperatures must be used requiring longer test periods to be comparable with the test scheme presented above.

However, it should be pointed out that the macro-climate of the collector test site is rather dry compared to the situation for a DHW system located for example in the Netherlands, cf *Figure 4;16 and 4,17*. Thus, further investigations are needed to clarify how appropriate the reference humidity load proposed is for other climates and for other collector designs.

7.3.3 Service life with regard to resistance to humidity loads for the coatings of the case study

Of the absorber coatings of the case study only the nickel-pigmented anodized aluminium coatings were seen to degrade markedly under the influence of high-humidity and condensed water in the laboratory tests. Their expected service lives with PC <0.05 were estimated under the assumption that they were both exposed to the reference moisture load defined in the case study.

Test collector	Absorber coating	Expected service life with PC <0.05 (years)
Teknoterm (operation)	Sunstrip	9
Teknoterm (operation)	Showa	6

Table 7;5. Estimated service lives of nickel-pigmented anodized aluminium coatings of the case study when being installed in the Teknoterm collector placed at the test site in Rapperswil. The service life has been defined as the time when Δε = 0.20. The service lives predicted for the absorbers are based on a moisture load corresponding to RH$_c$ = 99 %. Accelerated ageing data for the two coatings which were used for the calculations are presented in Figure 6;23.

As can be seen from *Table 7;5*, the nickel-pigmented anodized aluminium coatings are not qualified as regards their durability for the moisture load set up as a reference load in the case study. How reliable the predicted service lives, however are will be further discussed in *Chapter 8* of this report.

For validation purpose and using the same calculation procedure, the expected increase in the thermal emittance after three years of collector test was estimated for the Sunstrip absorber in Teknoterm collector working under simulated operation conditions. The expected increase was 0.03±0.02.

7.4 Degradation of Absorbers Caused by Sulphur Dioxide and High Humidity

The life data analysis with respect to degradation caused by the action of sulphur dioxide and high humidity air observed for the nickel pigmented aluminium of the case study was based on comparative testing. For that purpose, determined corrosion rates of the metal coupons exposed inside the test collectors, see *Table 4;2*, and determined corrosion rates

of the metal coupons exposed in the laboratory sulphur dioxide tests ,see *Table 5;17* and *5;18* were utilised.

7.4.1 Effective levels of atmospheric corrosivity

To be able to make use of the corrosion rates determined for the metal coupons for the purpose of service life prediction the following assumptions had to be made:

- Of the coupons exposed inside the test collectors it is those mounted at the bottom part of a collector which best reflect the level of corrosivety at the absorber surface.

  For the Showa collector this statement is not needed because no significant differences exist between corrosion rates determined at the bottom part and at the top part of a collector, except maybe for copper. This is true both for the DHW collector and the stagnation collector. For the Teknoterm collectors, however, this holds true only for zinc in the DHW collector, but not for steel and copper. For the stagnation collector there exists a marked difference between all corrosion rates determined for the top and bottom parts of the collector which might be an effect caused by the untightness of this collector, see *Section 4.3.2*.

  That the zinc coupons at the top part of the DHW collectors of Sessatherm and Azur III are more affected than the zinc coupons at the bottom might be an effect caused by sulphur dioxide which during night conditions enters the collectors from the top. The high rate of corrosion of zinc in those collectors compared to the two other DHW collectors can be explained as an effect of sorption of sulphur dioxide by the nickel-pigmented anodized aluminium absorber coatings.

- Of the different metals used it is mainly zinc and steel which give corrosion rates that most probably can be interpreted in terms of the total period of time-of-wetness at the absorber surface and the effective level of sulphur dioxide during such time periods.

  The reason for that is that the corrosion rate of copper is most probably too much influenced by temperature at lower humidity levels. The corrosion rates of copper are much higher in the stagnation collectors, in particular at the top part of those collectors. The corrosion rates of zinc and steel are, however, generally somewhat lower in the stagnation collectors compared to the DHW collectors. The exceptions are the top part of the stagnation Teknoterm collector previously discussed and the Azur III stagnation collector during the third year of test after the pipe failure had happened, see *Section 4.3.2*. It should be recalled that the temperature dependence of the sulphur dioxide-induced degradation of the nickel-pigmented anodised aluminium coatings was small and even such that the rate of degradation decreased somewhat with increasing temperature, see *Tables 5;17* and *5;18.*.

After making these two assumptions equivalent accelerated exposure periods, t_{eq} for the accelerated laboratory sulphur dioxide test at 1 ppm SO_2, 95% RH, and 20 ^{o}C were determined from the corrosion rates of the metal coupons mounted at the bottom parts of the Teknoterm and the Showa collectors by use of the laboratory test data given in *Figure 7;9*, which is a more detailed version of *Figure 5;21*.

The results are shown in *Table 7;6*.

Collector	Equivalent accelerated exposure periods (hours)		
	Steel	Zinc	Copper
Simulated operation conditions			
Teknoterm	16±5	21±2	(145±5)
Showa	11±5	7±2	(35±5)
Stagnation conditions			
Teknoterm	120±5	14±2	(240±5)
Showa	11±5	10±2	(70±5)

Table 7;6 *Equivalent exposure periods, t_{eq}, for the Teknoterm and Showa collectors tested in DHW and stagnation modes. The equivalent exposure period, t_{eq}, represents three years of coupon exposure in the tested collectors.*
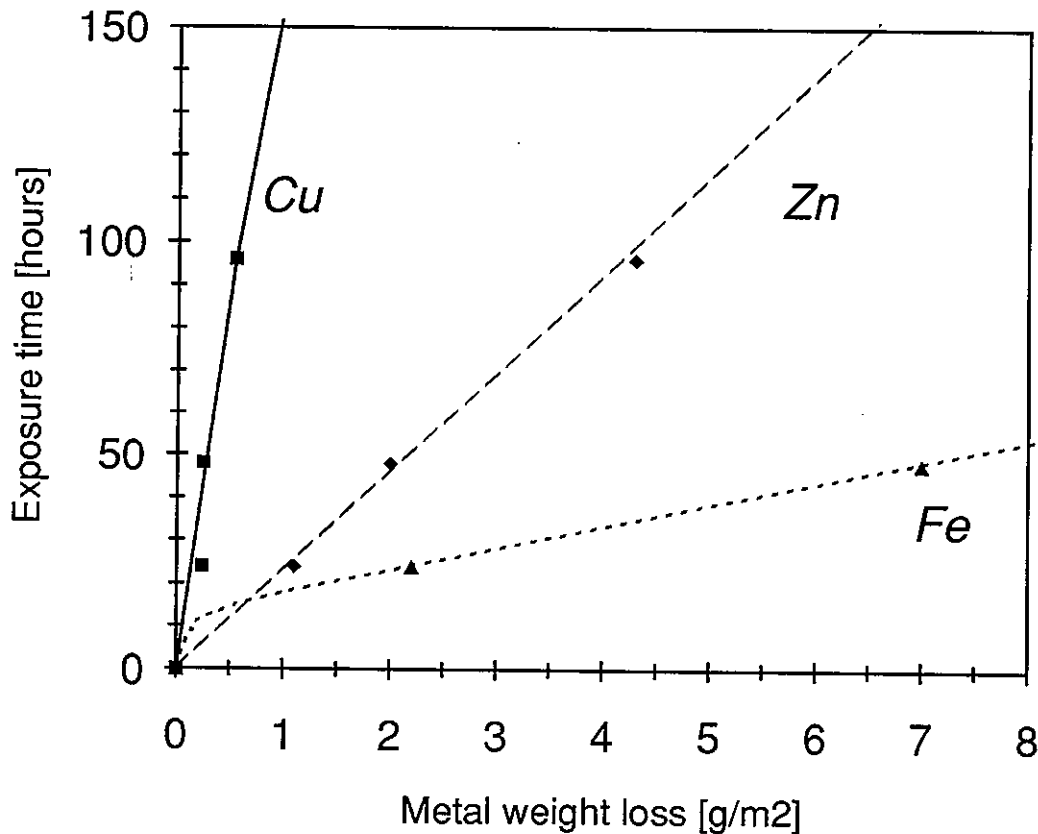
Figure 7;9 *Exposure time for metal coupons exposed in accelerated SO_2-test vs. metal weight loss. Ageing conditions: 25 °C, 95% RH, and 1 ppm SO_2. Not all experimental points are shown in the figure, since they are out of scale, i. e., the curves are based on more points than are shown in the figure.*

For steel, the curve in *Figure 7;9* contains an induction period of about 5-10 hours, which makes the determination of equivalent exposure periods uncertain. However, for the DHW collectors the equivalent exposure periods based on corrosion rate data for zinc and steel are in fair good agreement with each other. The corresponding equivalent exposure periods based on corrosion rate data for copper are about one order of magnitude longer.

For the Teknoterm stagnation collector, the equivalent exposure period is about one order of magnitude longer than what should be expected. This period is of about the same order of magnitude as the one based on corrosion rate data for copper. However, the equivalent exposure period based on corrosion rate data for zinc is of a reasonable order or what should be expected. However, the very high corrosion rate observed only for steel at the bottom part of the Teknoterm stagnation collector cannot be explained. The untightness of this collector, which has previously been discussed in *Section 4.3.2* may eventually be of importance.

Of the three metals used for measurements of the atmospheric corrosivity inside the collectors, it is thus only zinc that behaves in a consistent way.

As will be further discussed in *Section 8.1.3*, the corrosion rates of the zinc metal coupons at the bottom part of the collectors consequently correlate quite well with the deposited amount of sulphur, i.e. sulphur dioxide that were determined on the surface of absorber coatings in the Teknoterm and the Showa collectors after three years of collector tests.

7.4.2 Performance and service life requirements related to sulphur dioxide testing

As pointed out above zinc is regarded as the most representative metal of the three tested to characterize the corrosivety of the micro climate inside the collectors.

The measured corrosion rates of zinc were accordingly taken as a point of departure for formulating failure time requirements related to accelerated testing of absorber coatings in a test atmosphere containing 1 ppm SO_2, 95 % RH, and 20 °C.

As the failure time requirement for the accelerated test will be dependent on the design of the solar collector, two classes of collectors needed to be considered.

Type A: Tight solar collector with controlled low rate of ventilation characterized by an atmospheric corrosivity level at the bottom part of the collector corresponding to a corrosion rate of zinc of 0.1 g/m^2 per year (Showa collector).

Type B: Untight solar collector with more or less uncontrolled high rate of ventilation characterized by an atmospheric corresponding to a corrosion rate of zinc of 0.3 g/m^2 per year (Teknoterm collector).

The service life requirements on an absorber coating should accordingly be to meet the performance requirement PC < 0.05 for a service time of at least 25 years at a corrosivity level set by either the Type A or Type B collector. The shortest acceptable failure times for the two cases in the accelerated test can be calculated from the data for zinc in *Table 7;6*.

A tentative qualification test procedure related to the resistance to atmospheric corrosivity of an absorber coating may be formulated as follow:

(a)   Perform a sulphur dioxide test under the ageing conditions of 1 ppm SO_2, 95 % RH, and 20 °C for at least 175 hours.

(b)   Measure the solar absorptance and thermal emittance before the start of the test, after a testing time of 60 hours and 175 hours.

(c)   Determine the values of the PC-function

$$PC = -\Delta\alpha_s + 0.25 \Delta\epsilon$$

at the two testing times given in (b).

(d)   - If the value of the PC - function after a testing time of 60 hours is less than 0.05, the service life of the coating with PC < 0.05 is longer than 25 years when being installed in a type A solar collector.

-If the value of the PC - function after a testing time of 175 hours is less than 0.05, the service life of the coating with PC < 0.05 is longer than 25 years when being installed in a type B solar collector.

It should be pointed out that the qualification procedure is very tentative.

One important question needed to be answered is how the outdoor climate influence the atmospheric corrosivety inside the collector.

If only the results from the third year of test is considered (when the collectors were placed on the roof of the ITR - building) there is an even larger difference between the conditions in the Teknoterm and the Showa collector than given in the qualification test procedure presented above.

For the DHW Teknoterm collector the shortest acceptable failure time in the accelerated test increases from 175 hours to 300 hours. For the Showa collector the shortest acceptable failure time is the same.

More work is consequently needed to clarify the dependence of atmospheric corrosivety inside collectors on collector design and on outdoor climate.
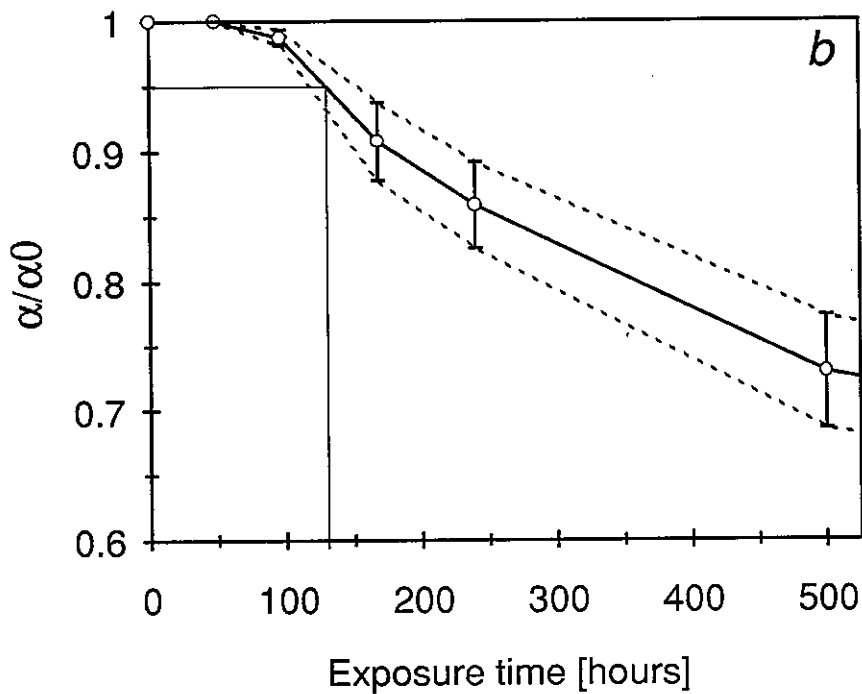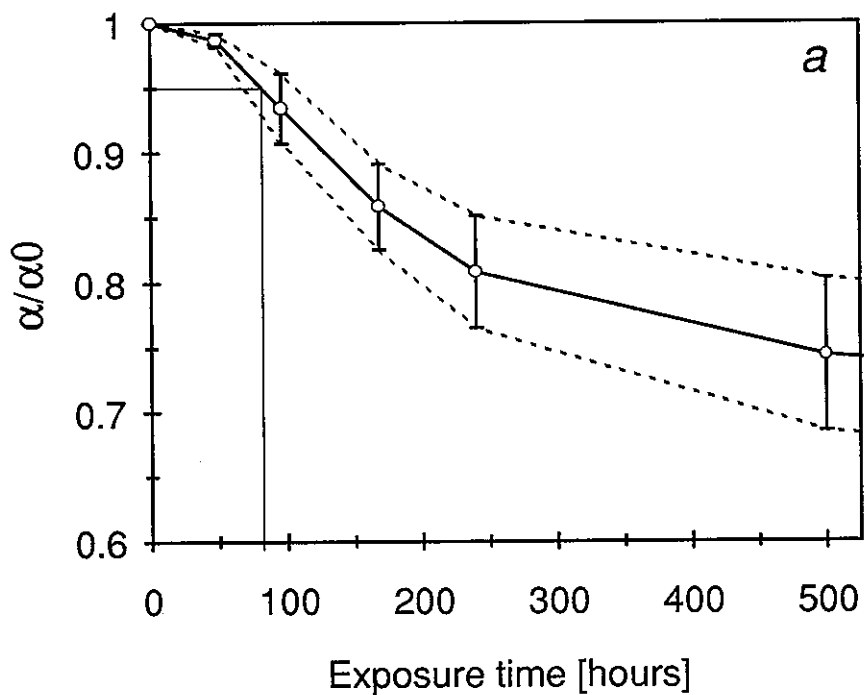
Figure 7;10 α/α_0 plotted vs. exposure time in the accelerated SO_2-test at 1 ppm SO^2, RH = 95 %, 20 °C. Figure **a** refers to the Sunstrip coating, while figure **b** refers to the Showa coating. The solid curves represent average values. The vertical bars and the broken lines represent the standard deviation. In the figures are also indicated the exposure times for a decrease in α_s of 5 %.

7.4.3 Service life with regard to resistance to sulphur dioxide as an airborne pollutant

In *Figures 7;10* the normalized solar absorptance α_s/α_{s0} is plotted as a function of exposure time in the accelerated SO_2-test for the Sunstrip and Showa coatings, respectively. The solid lines in the diagrams represent the average decrease in α_s for a number of different samples exposed in different test runs. The exposure times corresponding to a decrease in α_s of 5 % are also indicated in the figures. Since the change in ε is quite small in the accelerated SO_2-test a decrease in α_s of 5 % fairly well corresponds to a value of the PC-function equal to 0.05.

As is seen in the figures a decrease in α_s of 5 % is reached after an exposure time of 82 hours for the Sunstrip coatings and after 130 hours for the Showa coatings. The inaccuracy in the determination is roughly -15 and + 25 hours.

The inaccuracy in the determination is mainly caused by different behaviour of different samples, but also by the high sensitivity in degradation rate to changes in relative humidity.

By use of the data in *Table 7;6* and the equivalent exposure periods corresponding to $-\Delta\alpha_s$ = 0.05 for the Sunstrip and the Showa coatings, see *Figure 7;10*, expected service lives with PC < 0.05 were calculated. The results are shown in *Table 7;7* for the two defined types of collectors A and B both working under typical DHW conditions.

Absorber coating	Predicted service lives with PC<0.05 (years)	
	Type A collector	Type B collector
Sunstrip	34	12
Showa	54	19

Table 7;7 Predicted service lives with PC < 0.05 for the two types of collectors A and B working under typical DHW conditions.

As can be seen the predicted service lives depends strongly on the type of collector. How reliable the predicted service lives are will be further discussed in *Chapter 8*.

Using the same calculation procedure the expected decrease in the solar absorptance after the three years of collector tests was calculated. For the Sunstrip coating in the DHW Teknoterm collector, the expected decrease was 0.006 and in the stagnation Teknoterm collector only 0.002. For the Showa coating in the Showa collectors, however, no decrease in the solar absorptance after three years of collector tests is to be expected.

CHAPTER 8

VALIDATION OF METHODS USED FOR ACCELERATED LIFE TESTING BASED ON RESULTS FROM IN-SITU TESTS

The collector tests described in **Chapter 4** had two main purposes. The first to generate a set of measured microclimatic data prevailing for absorbers in collectors. These data were used as a base for interpretations of the accelerated ageing data in terms of service lives of absorbers, as outlined in **Chapter 7** of this report. The second purpose of the collector tests was to expose the absorber coatings of the case study to service conditions during a longer time period in order to measure the actual extent of degradation in optical performance of the coatings. With these results a validation of the methods used for accelerated life testing should be able to perform. This was, however, complicated by the fact that the time available for the collector tests was limited to only three years by the IEA Task X work programme.

8.1 Results from Long-Term Tests of Collectors at Rapperswil

To determine the change in the optical properties of the absorber coatings in the collectors tested, samples for measurements were cut out from the absorbers at the bottom, middle and top of the collectors before the start of the test, after two years and three years of test. However, due to the design of the Energie Solaire absorber in the Azure III collector, being a preformed, welded double plate absorber, it was only possible in this case to cut out samples from the absorber after the completion of the three years of test. For the fin and tube collectors samples were always cut out from the same fin. The latter located in the middle of the shortest side of the collector.

8.1.1 Changes in the optical properties of the nickel pigmented anodized aluminium coatings during the collector tests.

The results from the optical measurements on the Sunstrip nickel-pigmented anodized aluminium coating during the collector tests are given in *Table 8;1*. The spectral changes which are accompanying the change in optical performance during the tests are illustrated in *Figures 8;1* and *8;2*.

Under DHW conditions the thermal emittance of coating increases with time. Affected is above all the top and bottom parts of the absorber. Accompanying the increase in the emittance is the evolution of absorption bands in the infrared wavelength region at 3 µm, 4.5 µm between 6 and 7 µm and at around 9.5 µm, see *Figure 8;5*. These absorption bands may, thus, indicate the formation of hydrated forms of aluminium oxide, probably Pseudoboehmite, as discussed in *Section 6.3.1*.

The solar absorptance of coating decreases with time and the interference pattern in the visible and near infrared reflectance spectrum is shifted somewhat towards longer wavelengths, see *Figure 8;1*. The shift in the interference pattern, thus, suggests that the optical thickness of coating increases, see *Section 6.3.1*.

Sunstrip Coating in the Teknoterm Collector	α_s (start of test)	α_s (2 years)	α_s (3 years)	ϵ (start of test)	ϵ (2 years)	ϵ (3 years)	PC (2 years)	PC (3 years)
DHW conditions								
- top of the collector	0.891	0.900	0.885	0.086	0.111	0.126	-0.012	0.016
- middle of the collector	0.906	0.907	0.896	0.086	0.114	0.109	0.006	0.016
- bottom of the collector	0.906	0.894	0.877	0.094	0.105	0.138	0.015	0.043
Stagnation conditions								
- top of the collector	0.899	0.903	0.893	0.094	0.101	0.102	-0.002	0.008
- middle of the collector	0.895	0.888	0.906	0.086	0.099	0.112	0.010	-0.004
- bottom of the collector	0.894	0.881	0.881	0.089	0.102	0.107	0.016	0.018

Table 8;1 Results from optical measurements on the Sunstrip coating during the collector tests. The parameter PC = - $\Delta\alpha_s$ + 0.25 $\Delta\epsilon$.

Showa Coating in the Showa Collector	α_s (start of test)	α_s (2 years)	α_s (3 years)	ϵ (start of test)	ϵ (2 years)	ϵ (3 years)	PC (2 years)	PC (3 years)
DHW conditions								
- top of the collector	0.941	0.925	0.937	0.119	0.122	0.129	0.017	0.007
- middle of the collector	0.941	0.925	0.928	0.117	0.123	0.131	0.018	0.017
- bottom of the collector	0.938	0.911	0.905	0.120	0.116	0.110	0.026	0.031
Stagnation conditions								
- top of the collector	0.939	0.922	0.897	0.111	0.130	0.110	0.022	0.042
- middle of the collector	0.940	0.943	0.911	0.118	0.125	0.121	-0.001	0.029
- bottom of the collector	0.943	0.923	0.919	0.113	0.118	0.114	0.021	0.024

Table 8;2 Results from optical measurements on the Showa coating during the collector tests. The parameter PC = - $\Delta\alpha_s$ + 0.25 $\Delta\epsilon$.

8:3

top of the collector   middle of the collector   bottom of the collector
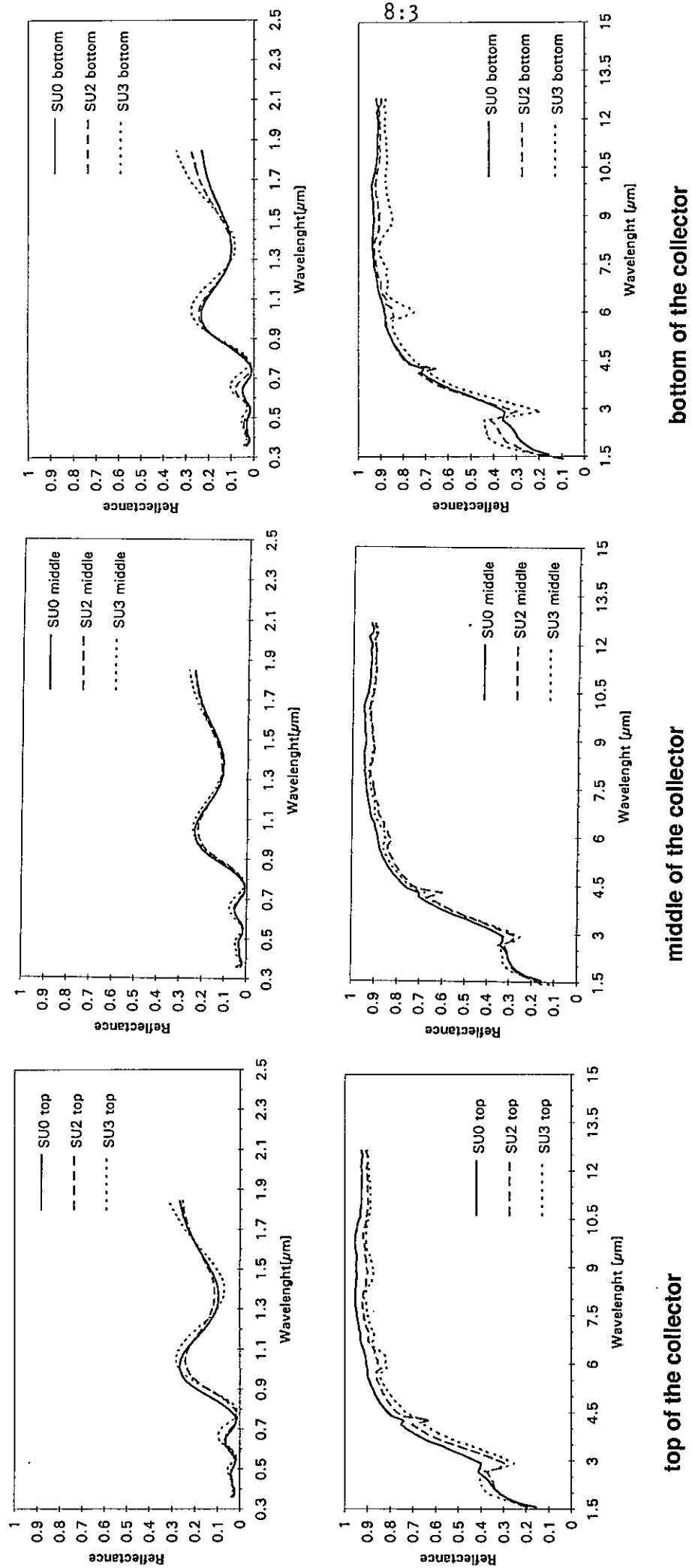
Figure 8;1 Spectral changes observed for the Sunstrip coating during the collector test under DHW conditions (The notation SU X, where X = 0, 2 or 3, means the Sunstrip coating after X years of test).

8:4

top of the collector

middle of the collector

bottom of the collector

Figure 8:2 Spectral changes observed for the Sunstrip coating during the collector test under stagnation conditions. (The notation SU X, where X = 0, 2 or 3, means the Sunstrip coating after X years of test).

As consequence of the increase in the thermal emittance and the accompanying decrease in the solar absorptance, the mean PC value of the coating reaches a level 50 % of the acceptable 0.05 after the three years of test under DHW conditions.

For the absorber tested in the collector working under stagnation conditions the overall pattern of degradation is very much the same although less pronounced, see *Table 8;1* and *Figure 8;2*.

The corresponding results for the Showa coating are given in *Table 8;2* and *Figures 8;3* and *8;4*.

Here the dominating change is a decrease in the solar absorptance with time. The spectral changes in the visible and near infrared wavelength regions may indicate that the coating becomes more transparent or less light scattering as an interference pattern evolves in the reflectance spectrum, see *Figures 8;3* and *8;4*.
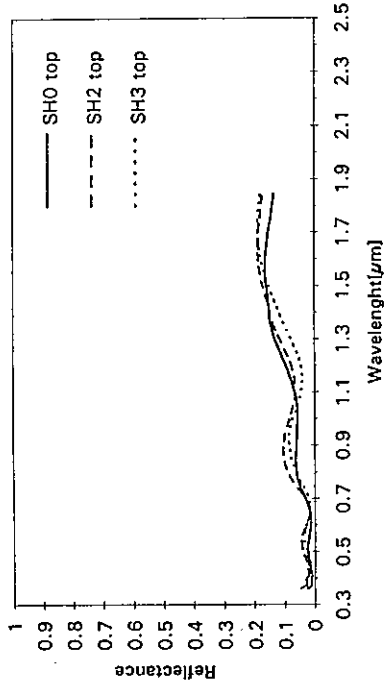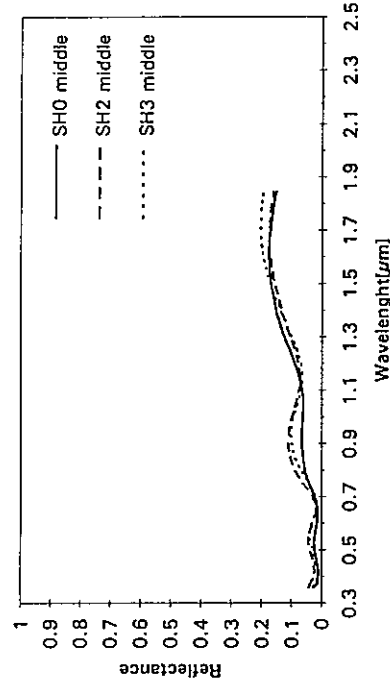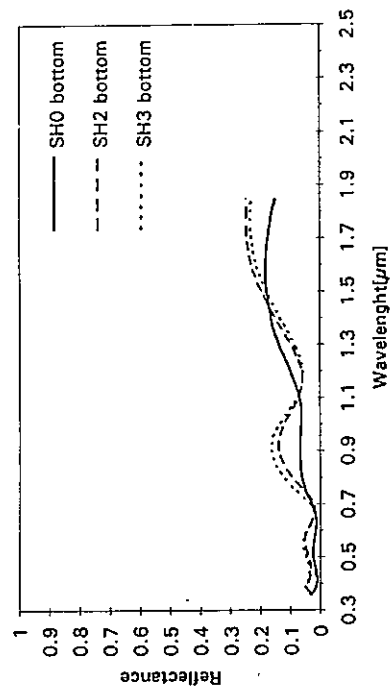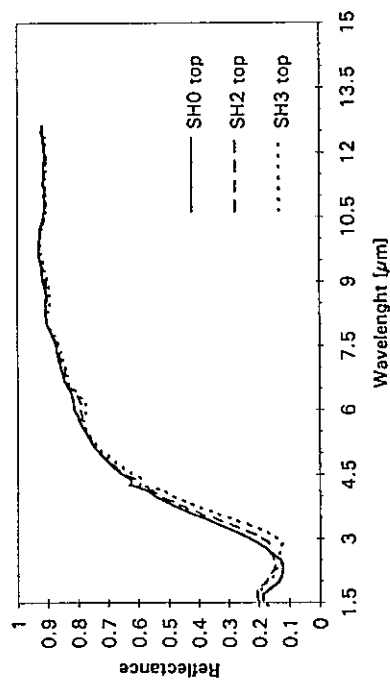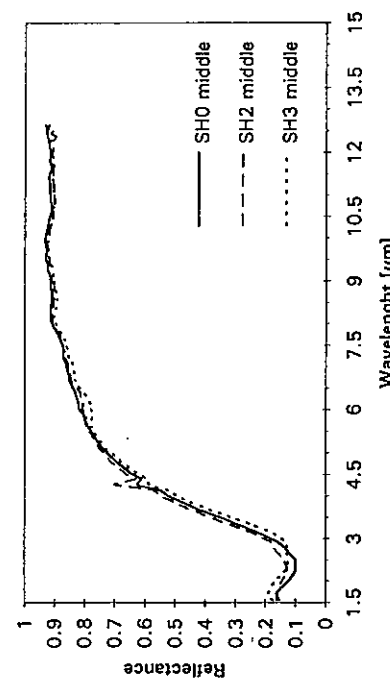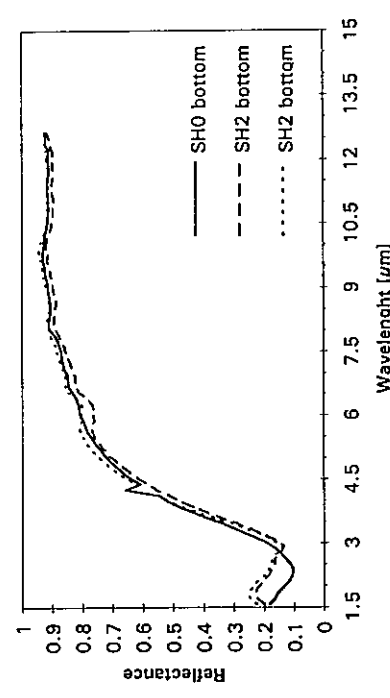
top of the collector　　　**middle of the collector**　　　**bottom of the collector**

Figure 8;3 Spectral changes observed for the Showa coating during the collector test under DHW conditions (The notation SHX, where X = 0, 2 or 3, means the Showa coating after X years of test).

top of the collector

middle of the collector

bottom of the collector
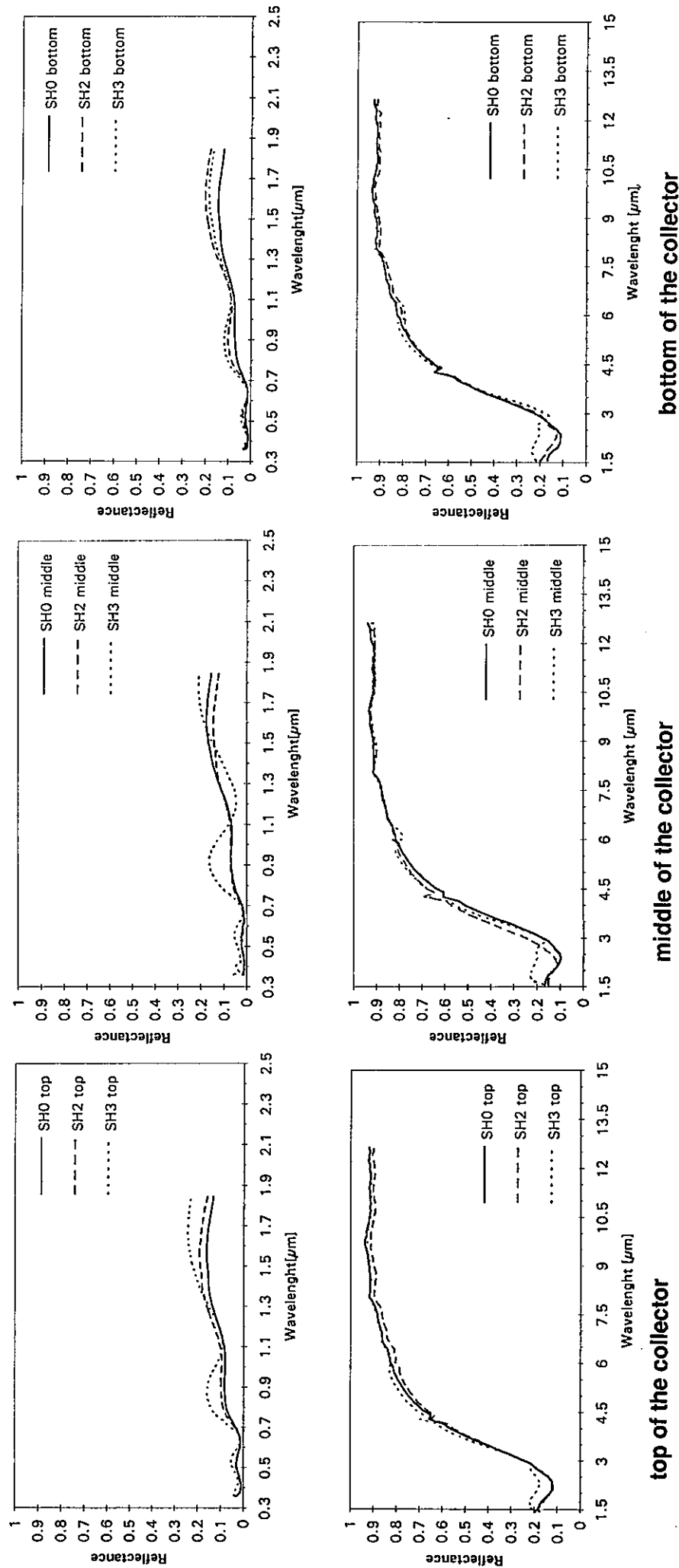
Figure 8;4 Spectral changes observed for the Showa coating during collector test under stagnation conditions (The notation SHX where X = 0.2 or 3 means the Showa coating after X years of test).

The increase in the thermal emittance with time is significant but slight at the middle and top of the collector. At the bottom part of the collector the thermal emittance even decreases. In the infrared wavelength region you can observe weak absorption bands at 3 µm and 6 µm.

Under stagnation conditions the thermal emittance values after three years of test are nearly the same as those measured at the start of the test.

As a result mainly of the decrease in the solar absorptance the PC value increases. For the collector tested under stagnation conditions its mean value has after three years of test reached a level about 60 % of the acceptable value of 0.05.

8.1.2 Changes in the optical properties of the black chrome absorber coatings during the collector tests.

The results from the optical measurements on the MTI black chrome absorber coating in the collector tests are given in *Table 8;3* and *Figures 8;5* and *8;6*.

MTI coating in the MTI Collector	α_s (start of test)	α_s (2 years)	α_s (3 years)	ε (start of test)	ε (2 years)	ε (3 years)	PC (2 years)	PC (3 years)
DHW conditions								
- top of the collector	0.950	0.947	0.949	0.108	0.116	0.102	0.005	-0.001
- middle of the collector	0.957	0.951	0.947	0.110	0.116	0.082	0.008	0.003
- bottom of the collector	0.948	0.946	0.953	0.119	0.105	0.083	-0.002	-0.012
Stagnation conditions								
- top of the collector	0.954	0.940	0.941	0.082	0.101	0.101	0.019	0.018
- middle of the collector	0.953	0.940	0.941	0.104	0.094	0.087	0.011	0.008
- bottom of the collector	0.947	0.943	0.943	0.106	0.1052	0.082	0.004	-0.002

Table 8;3 Results from optical measurements on the MTI coating during the collector tests. The parameter $PC = -\Delta\alpha_s + 0.25\ \Delta\varepsilon$.

top of the collector

middle of the collector

bottom of the collector
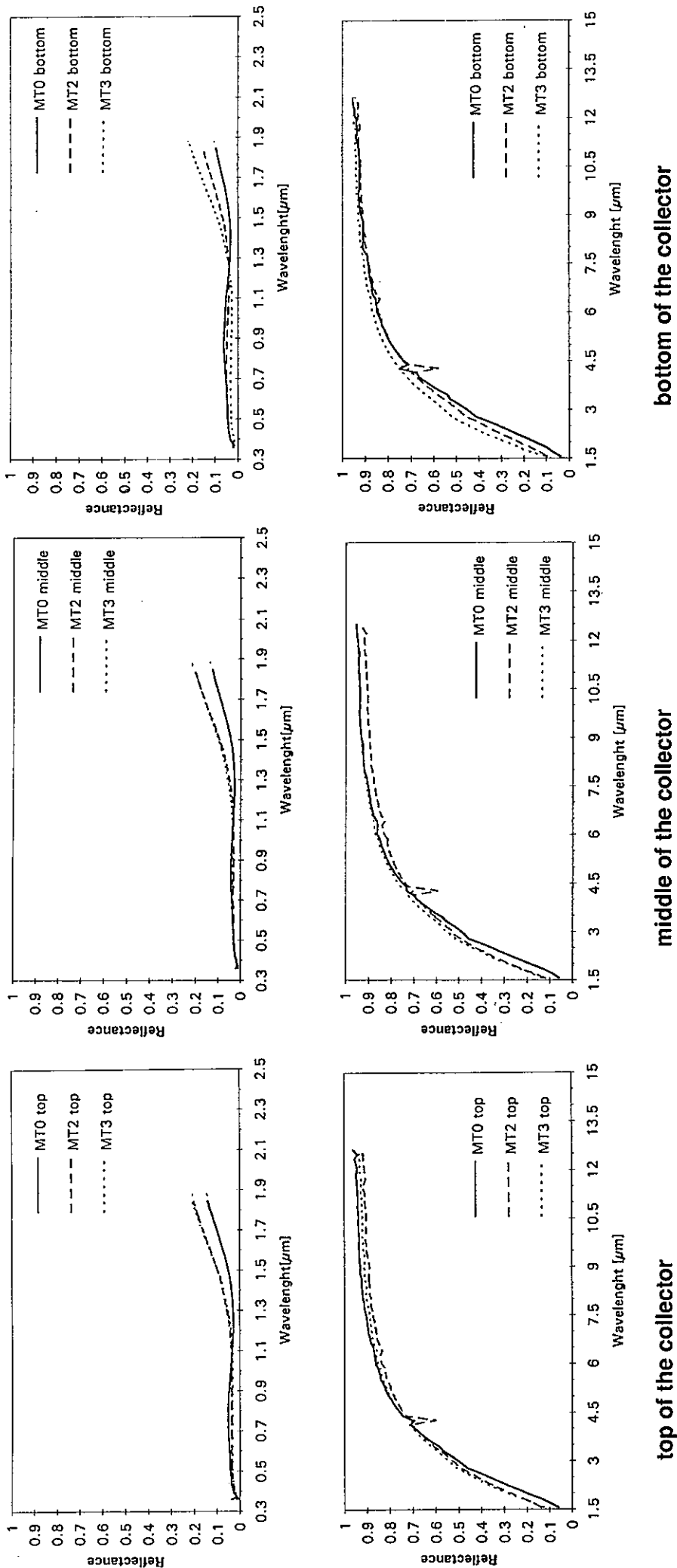
Figure 8;5 Spectral changes observed for the MTI black chrome coating during the collector test under DHW conditions.
(The notation MTX where X = 0, 2, 3, means the MTI coating after X years test).

top of the collector

middle of the collector

bottom of the collector
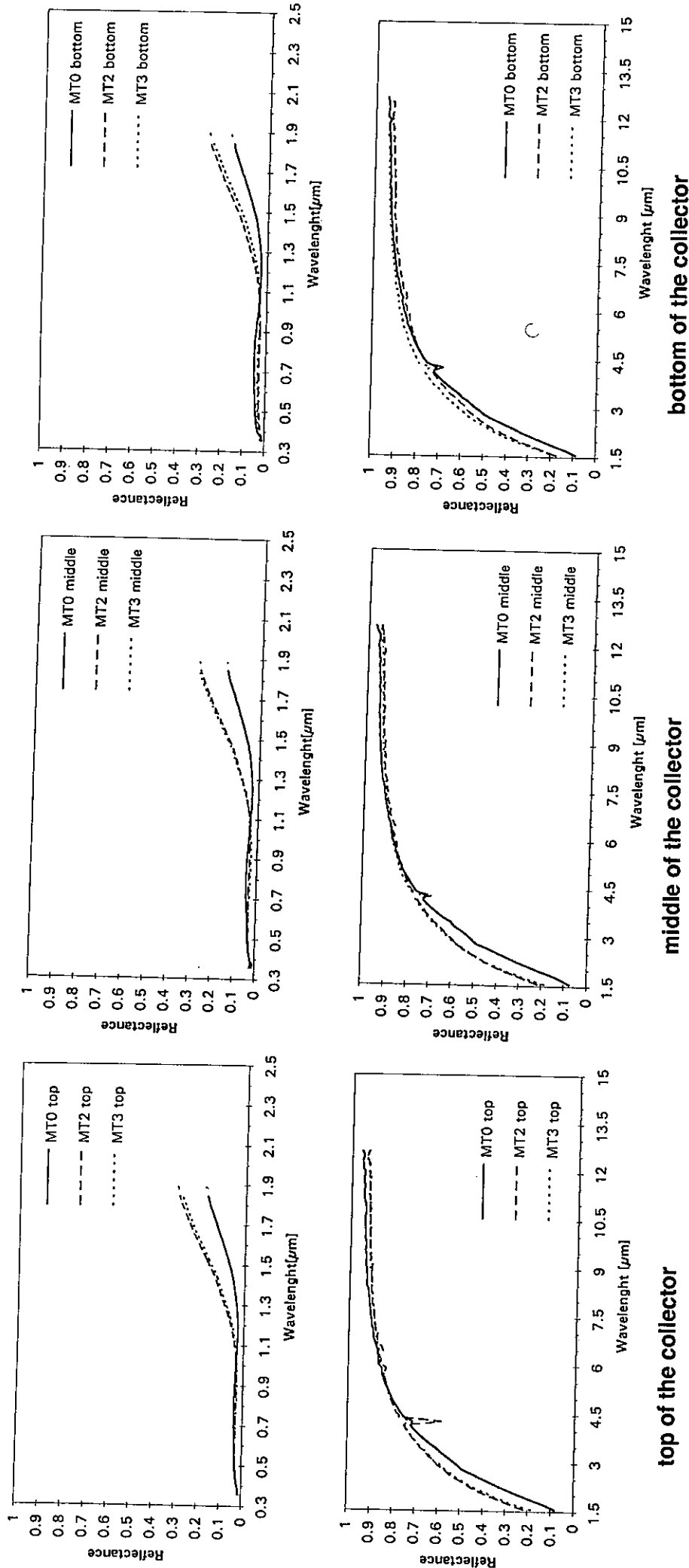
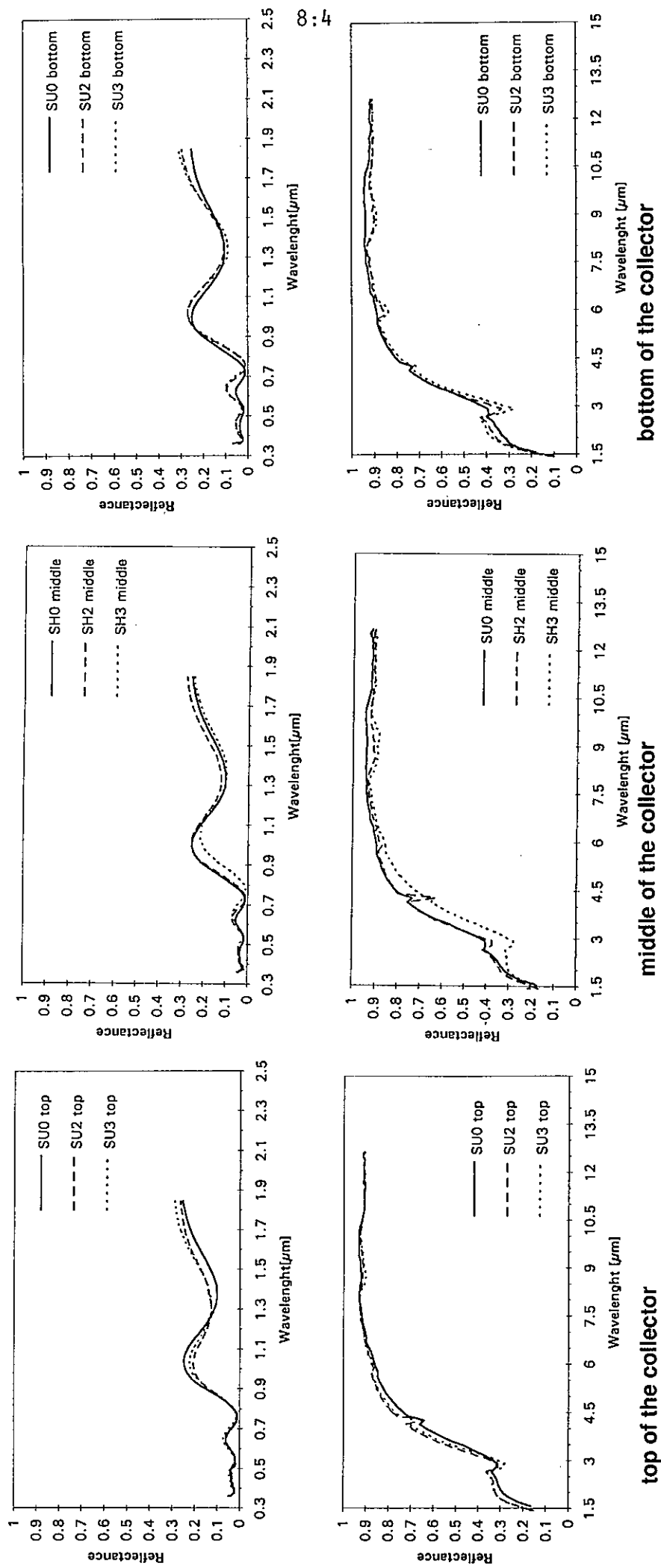*Figure 8;6 Spectral changes observed for the MTI black chrome absorber coating during the collector test under stagnation conditions. (The notation MTX, where X = 0, 2 or 3, means the MTI coating after X years of test).*

For the samples taken from the DHW collector, the mean value of decrease in solar absorptance after three years of test is 0.002. For the samples taken from the collector tested under stagnation conditions the corresponding mean value of decrease in the solar absorptance is 0.010. The spectral changes in the reflectance after testing are particularly pronounced in the near infrared wavelength region, see *Figure 8;5* and *8;6*. The reflectance at 1.9 μm is increased by as much as 0.08 - 0.12 for all samples. This increase, however, causes only a minor decrease in the solar absorptance and accompanying this decrease is also a decrease in the emittance. As a consequence, the combined effect of these two decreases leads to a nearly unchanged value for the PC function. The optical performance as reflected by the value of the PC function is even slightly improved in some cases especially for absorber samples taken from the DHW collector. For the absorber in the collector tested under stagnation conditions the mean increase in the PC value after two as well as after three years of test is about the same and in the order of one sixth of the maximum allowed value of 0.05.

The change in optical properties of the Energie Solaire absorber coating during the collector test could not be measured because the design of the absorber made it not possible to cut out samples for measurements without destroying it. The values of its optical properties after three years of test are, however, given in *Table 8;4*. The corresponding reflectance spectra for the solar and infrared wavelength regions are shown in *Figure 8;7*.

The Energie Solaire coating samples used in the accelerated aging tests had optical properties corresponding typically to α_s = 0.940 and ε = 0.20. From the values presented in *Table 8;4* it can be concluded that the absorber coating materials in the two collectors tested had a higher optical quality compared to the first mentioned.

Solaire coating in the Azure III collector	α_s (3 years)	ε (3 years)
DHW conditions		
- top of the collector	0.952	0.148
- middle of the collector	0.955	0.162
- bottom of the collector	0.948	0.161
Stagnation conditions		
- top of the collector	0.963	0.184
- middle of the collector	0.960	0.191
- bottom of the collector	0.957	0.194

Table 8;4   *Results from optical measurements on the Energie Solaire coating after the collector tests.*
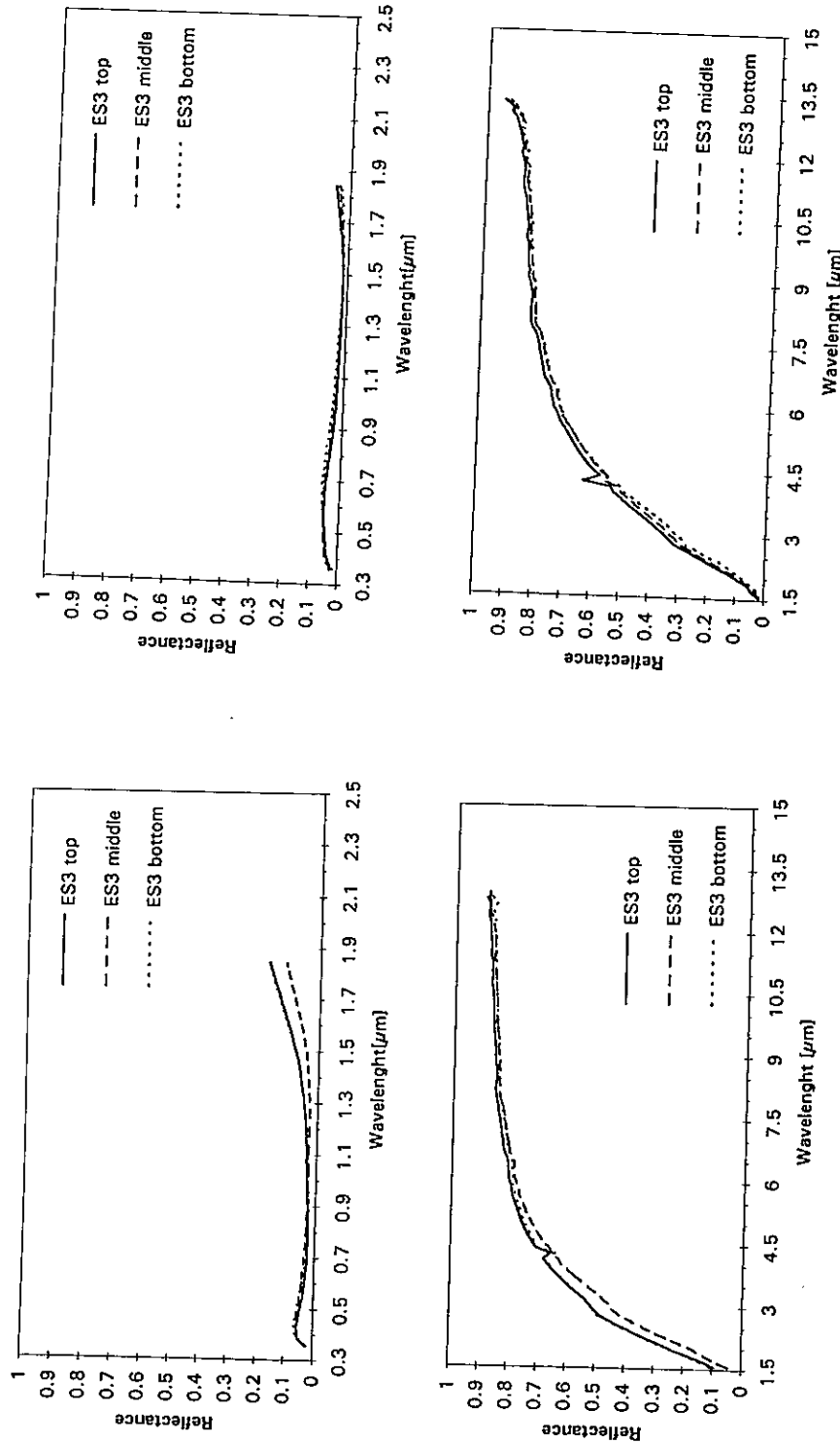
DHW conditions

Stagnation conditions

Figure 8;7 Reflectance spectra for the Energie Solaire black chrome coating after three years of collector tests
(The notation ES3 means the Energie Solaire coating after three years of test.

As changes in the optical properties with time could not be determined from measurements, the effect of aging is difficult to verify. However, high temperature aging seems to be one operative aging process as the reflectance of the absorber coating in the near infrared wavelength region is generally higher at the top of the collector.

8.1.3 Deposition of sulphur dioxide on the absorber coatings during the collector tests

For validation of the results from accelerated sulphur dioxide tests, an EDX-investigation was performed on absorber coatings after three years of collectors test.

In this investigation no significant amounts of sulphur were found on the black chrome absorber coatings (Energie Solaire and MTI). However, significant amounts of sulphur were found on the surfaces of the nickel pigmented aluminium oxide absorber coatings (Sunstrip and Showa). This result is in agreement with the investigation of the sulphur dioxide content in the atmosphere inside the collectors presented in *Table 4;4, Section 4.2.3.*

It was found that the SO_2-level was zero in both of the nickel pigmented aluminium collectors (Teknoterm and Showa) when the weather was cloudy, i. e., when the absorbers were relatively cold and the humidity level was high. The SO_2-level in the black chrome collectors (Sessatherm and Azur III) was almost the same as the outdoor level. When the weather was sunny on the other hand, i. e., when the absorbers were warm and the humidity low, the SO_2-levels were almost the same in all collectors. The SO_2-levels inside the collectors were also the same as the outdoor level. This observation indicated that the nickel pigmented aluminium absorbers can absorb SO_2 when they are relatively cold and the humidity high. The EDX-investi-gation verify this observation, see *Table 8;5.*

Location of sample	Relative EDX-signal I_S/I_{Ni}	
	Sunstrip in Teknotem Collectors	Showa in Showa Collectors
Collectors tested under simulated operation Conditions		
top	0.23	0.07
middle	0.07	0.07
bottom	0.10	0.08
Collectors tested under stagnation conditions		
top	0.10	0.05
middle	0.04	0.04
bottom	0.09	0.09
Unexposed samples		
	0	0

Table 8;5   *Relation between the EDX-signal from sulphur, I_S, and nickel, I_{Ni}, from nickel pigmented aluminium oxide coatings (Sunstrip and Showa) after three years of collector test.*

As is seen in *Table 8;5* the relation in intensities between the signals from sulphur and nickel varies between 4 and 23 %. The highest values are found at the top and at the bottom of the collectors.

There are no large differences between the collectors working under simulated in use conditions and those in stagnation. This indicates that the coatings are affected by sulphur dioxide mainly during relatively cold and high humidity weather conditions.

By combining data relating the decrease in solar absorptance, α_s, as a function of exposure time in an accelerated SO_2-test and the increase in EDX-signal, I_S/I_{Ni}, as a function of exposure time, the relation between α_s and the sulphur content can be determined. Such a diagramme is presented in *Figure 8;8*.
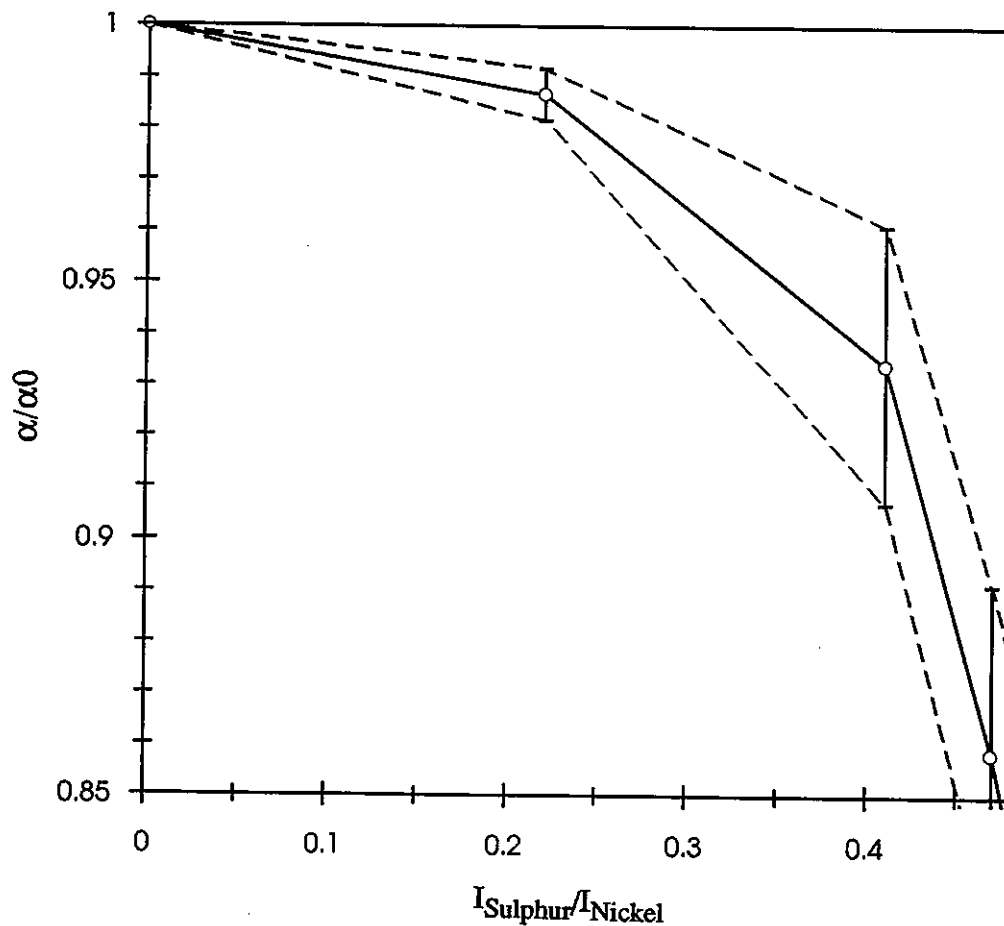
Figure 8;8 α/α_0 plotted vs. relative EDX-signal (I_S/I_{Ni}) in the accelerated SO_2-test (1 ppm SO2, 95 % RH, and 20 °C) for the Sunstrip absorber coating. The solid curve represents average values. The vertical bars and the broken lines represent the standard deviation.

8.2 Validity of the Results from the Accelerated Life Test Programme of the Case Study

In validating the reasonableness of the results from the accelerated life test programme of the case study, the following scheme of questions were set up:

a) Can the observed changes in α_s and ε after the three years of collector tests be qualitatively explained in terms of the three different degradation mechanisms investigated and evaluated in the accelerated life test programme?

b) Are the spectral changes in qualitative and quantitative agreement with those observed in the three different kinds of accelerated laboratory tests performed?

c) Are the predicted or estimated changes in α_s and ε from the results of the accelerated tests in quantitative agreement with what was found after the three years of collector tests?

d) How reliable are the predicted service lives of the coatings of the case study?

It should be pointed out, that the validation procedure was found very complicated. The main reasons for that were the following:

- There existed for most coatings marked differences in the optical properties between absorber samples used in the laboratory tests and the absorbers used in the collector tests. This complicated above all the analysis of the results for the Energie Solaire and the Showa coatings.

- The extents of degradation in the optical properties of the coatings after the three years of collector tests were in some cases too small to be used properly for the intended purpose of validation.

- The experimental results from the laboratory tests were in some respects incomplete. The laboratory tests were carried out and had to be terminated before any reliable results from the collectors tests were available.
In the design and modification of the accelerated test programme, consequently, no feed back of experience from an in-service test carried out in parallel with the laboratory tests could be utilized.

8.2.1 Comparison between predicted and measured in-service degradation of the black chrome coatings of the case study

For the black chrome coatings of the case study the reasonableness of the results from the accelerated life test programme could only be judged in the case of the MTI coating.

As described in *Chapter 7* of this report only the high temperature tests generated results for this coating which could be used for the purpose of service life prediction. The effect of high humidity and condensed water on the optical properties of the coating was found to be slight and also hard to interpret. The degradation pattern appearing resembled, however, in the 70 °C and 90 °C high humidity tests and in the condensation tests performed very much with what was observed during the initial phase of the high temperature tests. The effect of exposing samples of the coating in a corrosive atmosphere containing high humidity and sulphur dioxide was found even slighter and should therefore not be an important factor for the service life of the coating.

As a consequence, the expected change in the optical properties of the black chrome coating should be able to interpret solely in terms of the results from the high temperature tests. The changes in the optical properties of the coating observed after the collector tests also evolve in a direction which supports this hypothese.

- The decrease in the solar absorptance and the accompanying decrease in the thermal emittance are in general more significant for samples taken from the collector tested under stagnation conditions than for samples taken from the DHW collector, see *Table 8;3*.

- The spectral changes which were caused by the high temperature exposure in the laboratory tests, see *Table 5;6*, are qualitatively the same as those observed after the collector tests, see *Figure 8;5* and *Figure 8;6*.

After the collector tests the most dominating aging effect observed in the reflectance spectrum is an increase of the reflectance in the near infrared wavelength region. At 1.9 µm, the mean increase in the reflectance after three years of collector test is 0.08 for samples from the DHW collector and 0.13 for samples from the collector working under stagnation conditions. It should, however, be observed that this increase in the reflectance at 1.9 µm is reached already after two years of collector tests, see *Figure 8;5* and *8;6*. For the constant load high temperature test at 300 °C the increase in the reflectance at 1.9 µm is 0.17 after 3 hrs, 0.20 after 10 hrs, and 0.22 after 20 hrs.

As discussed in **Section 6.2.1** of this report, the degradation of the black chrome coating may be explained by assuming two mechanisms being operative:

- Desorption of water from the coating during the initial phase of degradation

- Oxidation of metallic chromium to chromium oxide as the high temperature degradation progresses.

The first process characterizing the initial phase of degradation gives rise to spectral changes mainly in the near infrared wavelength region and influences therefore the solar absorptance to a small extent. In the collector tests performed, the observed degradation should thus be understood as a result of the first mechanism being operative mainly.

However, to understand fully the results from the collector tests, two questions need to be answered:

- Why does the reflectance in the near infrared wavelength range reach a nearly constant value only after two years of testing both in the case of the DHW collector and of the stagnation collector?

- Why is the difference between the reflectance changes in the near infrared not larger for the absorber in the DHW collector and for the absorber in the stagnation collector?

To answer the first question you may have to make the assumption that a sorption/desorption equilibrium reaction with water involved is operative rather than only a desorption of water process. The equilibrium or maybe better stationary state determined by the collector test conditions, is established rather fast. The equilibrium state varies with the temperature and the higher the temperature the smaller amount of water is contained in the coating. The answer to the second question will consequently be, that the temperature dependence of the equilibrium reaction, being the dominating mechanism at low temperatures and during the initial phase of reaction in the high temperature tests, is quite different and weaker than that of the second mechanism involving oxidation of metallic chromium. However, the first mechanism seems to generate only a minor decrease in the solar absorptance value, see the degradation curve in *Figure 6;10*.

In the analysis of the accelerated life data presented in *Chapter 7* of this report, an attempt was made to predict or estimate the expected decrease in the solar absorptance after the three years of collector tests. As the appearance or shape of the degradation curve in *Figure 6;10* for extents of degradation between 0 and 1.5 % was difficult to foresee it could only be claimed that the expected decrease should be less than 0.01. In the collector tests the mean decrease in the solar absorptance was 0.010 (arithmetic mean 0.012) for the absorber in the stagnation collector and 0.002 (aritmethic mean 0.001) for the absorber in the DHW collector.

To reach an extent of degradation of 0.05 in the solar absorptance should then most probably require an extremely long time period, more than 10^3 years, if the degradation curve shown in *Figure 6;10* reflects the degradation behaviour during the collector tests as seems reasonable. The oxidation of metallic chromium to chromium oxide should be the dominating degradation process at this extent of degradation and then the temperature dependence of the degradation reaction be as strong as indicated in *Figure 6;10*.

It can be concluded that the results from the collector tests seem to be in fairly good agreement with the results of the life data analysis presented in *Chapter 7*. The coating seems more than qualified for its intended use in a DHW system collector.

As a consequence, the value of the maximal effective mean temperature corresponding to a service life of 25 years presented in *Table 7;4* also should be in the right order of magnitude.

As the Energie Solaire Black chrome absorber coating behaved very much the same in the laboratory tests as the MTI coating, it is reasonable to assume that the conclusions presented in *Chapter 7* about the stability and service life of the Energie Solaire coating also should be essentially correct.

8.2.2 Comparison between predicted and measured in-service degradation of the nickel pigmented anodized aluminium coatings of the case study

In the accelerated life test programme of the case study, the nickel pigmented anodized aluminium coatings were seen to degrade

a) under the influence of a high temperature, reducing the solar absorptance and causing in the case of the Showa coating a slightly lower decrease in the thermal emittance of the coating,

b) under the influence of condensed water increasing the thermal emittance of the coatings and initially also their solar absorptance but to a much smaller extent

c) under the influence of high humidity decreasing the solar absorptance and slightly increasing the thermal emittance, and

d) under the influence of a corrosive atmosphere of high humidity and sulphur dioxide reducing the solar absorptance of the coatings but causing only a slight increase in their thermal emittance.

The degradation results from the collector tests can be summarized as in *Table 8;6* below.

Conditions during collector test	Showa coating in the Showa collector		Sunstrip coating in the Teknoterm collector	
	$-\Delta\alpha_s$	$\Delta\varepsilon$	$-\Delta\alpha_s$	$\Delta\varepsilon$
DHW	0.020 (2 years) 0.017 (3 years)	0.002 (2 years) 0.005 (3 years)	0.001 (2 years) 0.015 (3 years)	0.021 (2 years) 0.036 (3 years)
Stagnation	0.011 (2 years) 0.032 (3 years)	0.010 (2 years) 0.001 (3 years)	0.005 (2 years) 0.003 (3 years)	0.011 (2 years) 0.017 (3 years)

Table 8;6 Mean values of the changes in the optical properties of the nickel pigmented anodized aluminium coatings after two and three years of collector test.

Degradation of the Sunstrip coating

Under DHW conditions, the dominating degradation effects of the Sunstrip coating are an increase in time of the thermal emittance of coating. Also observed is a decrease in the solar absorptance which is particularly pronounced between the second and the third year of collector test.

The increase in the thermal emittance is, thus, consistent with a moisture or high humidity induced degradation process to be operative. Associated with the increase in the thermal emittance is the evolution of absorption bands in the infrared reflectance spectrum at wavelengths around 3 μm, 4.5 μm between 6 and 7 μm and at about 9 μm, see the difference reflectance spectra in *Figure 8;9*.
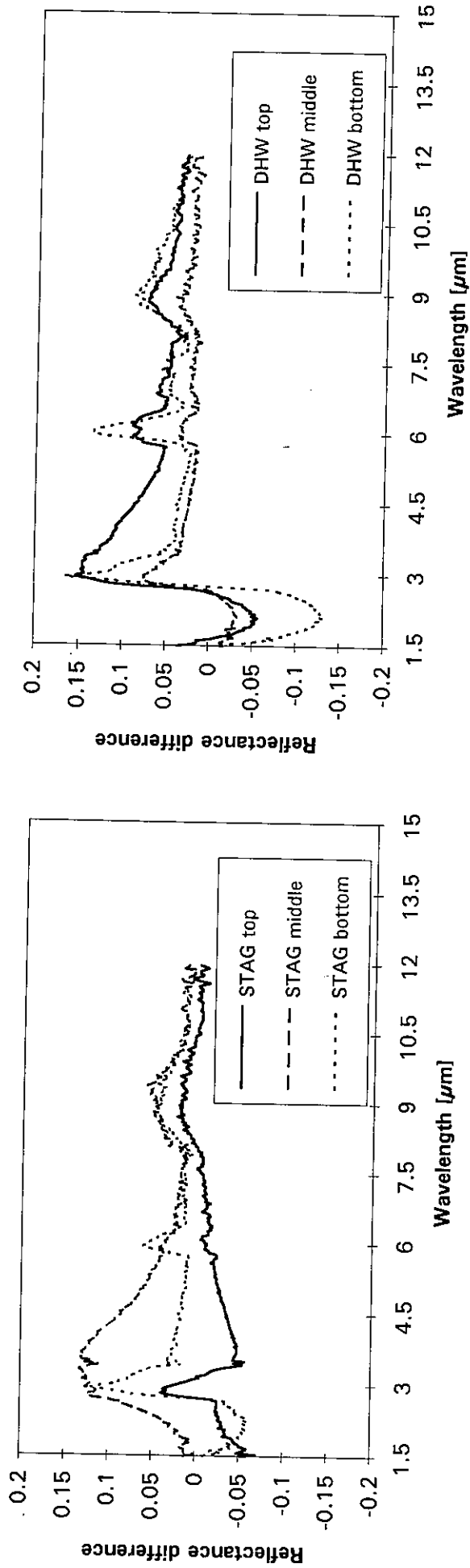
Stagnation conditions

DHW Conditions

Figure 8:9   Difference reflectance infrared spectra for the Sunstrip coatings based on the results obtained after three years of collector tests.

In *Figure 8;10* some reflectance spectra are, for the reason of comparison, also shown for some laboratory condensation and high humidity tests.

The reflectance difference spectra at wavelengths longer than about 4 µm are for the top and bottom parts of the absorber in the DHW collector, both from a qualitative and a quantitative point of view, agree fairly good with the reflectance spectrum from the 20 °C condensation test after 650 hrs. The absorption peak at 6 µm, particularily strong in the spectrum for the bottom part of the collector is, however, not so pronounced in the reflectance spectra from the condensation tests. For wavelengths shorter than about 4 µm the agreement is not that good which is reflected also in the value of the solar absorptance. This increases initially in the condensation test but was found to decrease in the DHW collector test.

For wavelength shorter than 4 µm the agreement with the reflectance spectra from the high humidity test is much better. Here you also have a slight decrease in the solar absorptance. However, the absorption bands between 6 - 7 µm are missing in the reflectance spectra from the high humidity test. This suggests that Boehmite rather than Pseudoboehmite is formed in this high humidity test as already discussed in *Section 6.3.1*.

The reflectance difference spectrum from the middle part of the DHW collector fits fairly well with the reflectance difference spectrum from the condensation test at 20 °C after 300 hrs. The influence of moisture is thus considerably less severe at the middle part of the absorber than at the top and bottom parts of it. This is also evident from the changes in the thermal emittance observed after the collector test. The mean value of increase in the thermal emittance after the three years of DHW collector test is 0.036 and thus in agreement to 0.03 ±0.02 which value was predicted from the accelerated test data, see *Section 7.3.3*.

The predicted value of the service life with PC <0.05 of 9 years should then be in the right order if the degradation curve presented in *Figure 6;23* truly reflects the degradation behaviour of the absorber in the DHW collector also at higher extents of degradation. It should be pointed out that a service time corresponding to twice the defined service life should give rise to an increase in the thermal emittance of about 0.6 - 0.7 which should corresponds to PC values of 0.15 - 0.17 ie the thermal performance of the DHW system should be reduced by about 15 % - 17 % at that time. However, one weak point in the validation procedure is that the steep increase in the rate of degradation in the thermal emittance should start first after a time period of 6 years according to the degradation curve in *Figure 6,23* but the test had to be terminated after three years.

What can be seen from the collector test carried out for three years under DHW conditions, however, is that the mean thermal emittance increases nearly linear with time. If an linear extrapolation procedure is employed in this case the expected service life with PC <0.05 should be in the order of 18 years. The true service life with PC <0.05 then is most probably less than this value.

In order to finaly verify the estimated service life from the accelerated life test programme of the case study experience of absorber durability from real solar installation should be utilized. However, it should be pointed out that the service life estimated depends strongly on the design of the collector which will be further discussed later on.
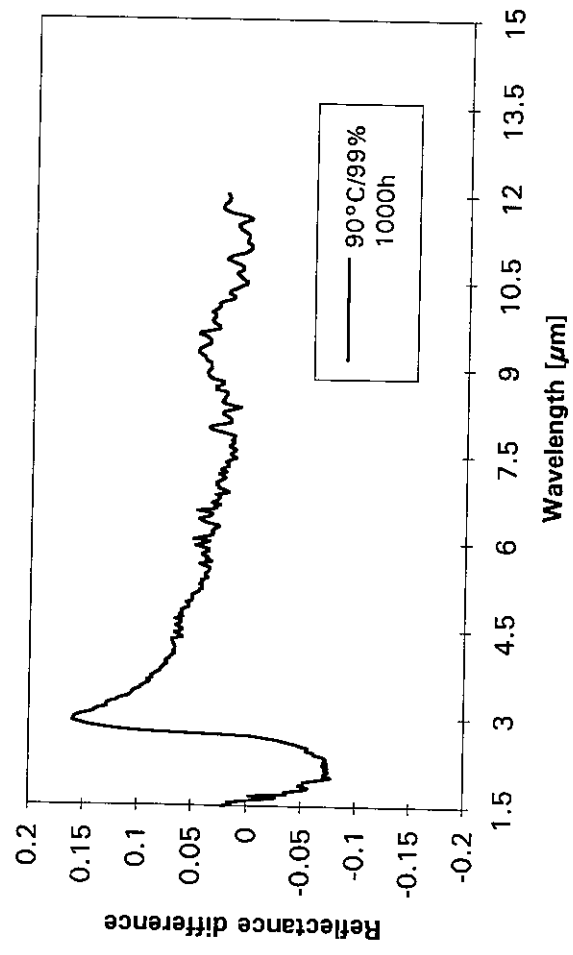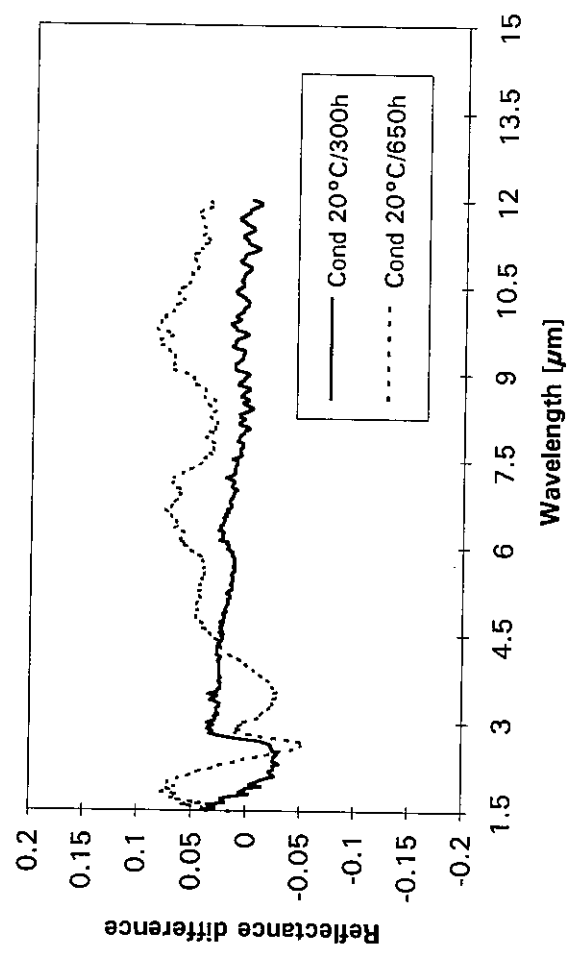
High humidity test at 90 °C and RH = 99 %   Condensation test with a sample temperature of 20 °C

Figure 8;10 Reflectance difference infrared spectra for the Sunstrip coating based on the results from some laboratory high humidity and condensation tests in the accelerated life test programme to the case study.

In the case of the stagnation collector the degradation pattern in the thermal emit-
tance and changes in the reflectance in the infrared wavelength region are essentially
the same but less pronounced, see *Figure 8;9*. The mean rate of degradation in the
thermal emittance is about half of that found for the absorber coating in the DHW col-
lector.

It seems reasonable to assume that the high temperatures which are often reached in
the stagnant collector should change the composition of the hydrated aluminium oxide
formed when the temperature is low and the humidity is at the condensation limit.
Pseudoboehmite might at least partly be transformed into Boehmite which should
lower the level of degradation in the thermal emittance.

Concerning the change in the solar absorptance of the Sunstrip coating several
mechanisms may be involved. However, the decrease in the solar absorptance is
significantly higher in the DHW collector compared to the stagnation collector.

If the degradation in the solar absorptance should have been caused by the same
kind of process as observed in the initial phase of the high temperature tests, the
extent of degradation should have been higher in the stagnation collector.

Thus, the decrease observed in the solar absorptance after the collector tests is most
likely caused by the influence of high humidity and most probably also by the action
of sulphur dioxide on the coating during the collector tests. That sulphur was depo-
sited on the absorber coating during the collector tests was confirmed by the EDX
analysis presented in *Section 8.1.3*.

If the deposited amounts of sulphur found on the absorber coatings after the collector
tests are converted into equivalent exposure periods for the accelerated sulphur
dioxide test, which was selected as a reference test for the life data analysis
presented in *Section 7.4*, essentially the same result is obtained as shown in *Table
7;6*, see *Table 8;7*.

Equivalent exposure period for the sulphur dioxide test at 1 ppm SO_2, RH = 95 %, 20 °C	Sunstrip in the Teknoterm collector tested for three years under	
	DHW conditions	Stagnation conditions
- based on mean values of I_S/I_{Ni} ratios after three years of collector tests, see *Table 8;5* and *Figure 6;28*	~ 23 hrs	~ 12 hrs
- based on corrosion rate of zinc at the bottom of collec-tors according to *Table 7,6*	21 ±2 hrs	14 ±2 hrs

Table 8;7   *Equivalent exposure periods for accelerated sulphur dioxide test (1 ppm
SO_2, RH = 95 %, 20 °C) calculated from I_S/I_{Ni} ratios determined by EDX
and from metal weight loss measurements for zinc at the bottom part of
collectors*

The observed mean decrease in the solar absorber of the coating after the three years of collector tests of 0.014 for the DHW collector and of 0.003 for the stagnation collector are in reasonable agreement to what can be predicted from the results of the accelerated sulphur dioxide test. Estimated decreases in the solar absorptance based on the measured corrosion rates of zinc are 0.006 for the DHW collector and 0.002 for the stagnation collector. The corresponding decreases are 0.007 for the DHW collector and 0.004 for the stagnation collector, if instead the mean deposited amounts of sulphur found on the coatings in the collectors are used as a base for the predictions.

As the extent of degradation in the solar absorptance measured on the coatings in the collectors is small, it is difficult to judge how reasonable the predicted service lives with PC<0.05 are. One weak point in the validation procedure in this case is that a steeper decrease with time is to be expected after a time period of around six years for the coating in DHW collector. The test, however, had to be terminated after three years.

It can, however, be concluded that the predicted extents of degradation in the solar absorptance of the coatings in the collectors are reasonable. The close agreement between the predicted decreases in the solar absorptance based on data for deposited amounts of sulphur on the coating and the measured decreases in the solar absorptance of coating is of great interest. This method can be used in estimating the loss in the solar absorptance of coatings taken from real solar installations.

For the Sunstrip coating in the Teknoterm collector, thus, two degradation mechanisms, contributing to its service life have been identified. The first mechanism, related to degradation caused by moisture or condensed water on the absorber, should limit the service life with PC<0.05 to 9 years for the coating in the DHW collector. The second mechanism related to degradation caused by sulphur dioxide and high humidity, should limit the service life with PC<0.05 to 12 years for the coating in the DHW collector.

If these two mechanisms are acting independently of each other, the requirement PC<0.05 should not be met after a time period of 5 years according to equation (2,9). After three years of testing the mean increase in the value of the PC function was found to be 0.023 for the coating in the DHW Teknoterm collector. The increase in the PC value after three years of testing, consequently, is in fair agreement with this assumption.

Degradation of the Showa coating

Concerning the Showa coating, it should be pointed out that the reflectance spectra of the samples of the unaged coating in the collector tests were quite different from those recorded for the unaged samples used in the major part of the laboratory tests. The observed spectral changes after the collector tests therefore are difficult to interpret in terms of the results from the laboratory tests.

The dominating degradation effect observed after the collector tests is a significant decrease in the solar absorptance of the coating. The change in the thermal emittance is much less significant.

For the coating tested under DHW conditions the thermal emittance is steadily increasing at the top and middle part of the collector. At the bottom, however, the thermal emittance decreases steadily. The decrease in the solar absorptance is also much more significant at the bottom part of the collector than in the top and middle parts of it. In the infrared wavelength region of the reflectance spectrum absorption bands at around 3 μm and 6 μm can clearly be distinguished, see *Figure 8;11*.

For the coating tested under stagnation conditions the thermal emittance is essentially the same after the three years of collector test. But it can clearly be seen from the reflectance difference spectra in *Figure 8;11* that absorption bands around 3 μm and 6 μm have evolved. As this is an effect that should increase the thermal emittance, there is consequently, a process in operation that is working in the opposite direction to the first mentioned. It should be observed that the thermal emittance first increases and then decreases which is specially pronounced at the top part of this collector.

In *Figure 8;12* some reflectance difference spectra for the infrared wavelength region are shown to illustrate the spectral changes found in a condensation test and in a high humidity (RH = 99%) test executed in the accelerated life test programme.

As a result of the high humidity test at 90 °C and RH = 99 %, absorption bands evolve at wavelengths around 3 μm, 4.5 μm, 6 μm and 9.5 μm.

As a result of the condensation test with a sample temperature of 20 °C, absorption bands evolve at wavelengths around 3 μm, 4.5 μm, 6 μm, 7 μm, and 9.5 μm.
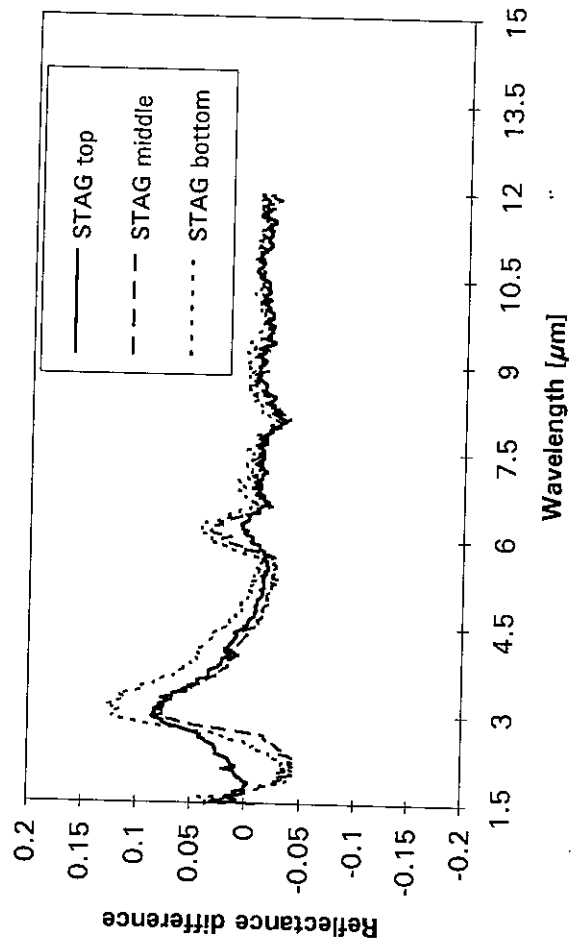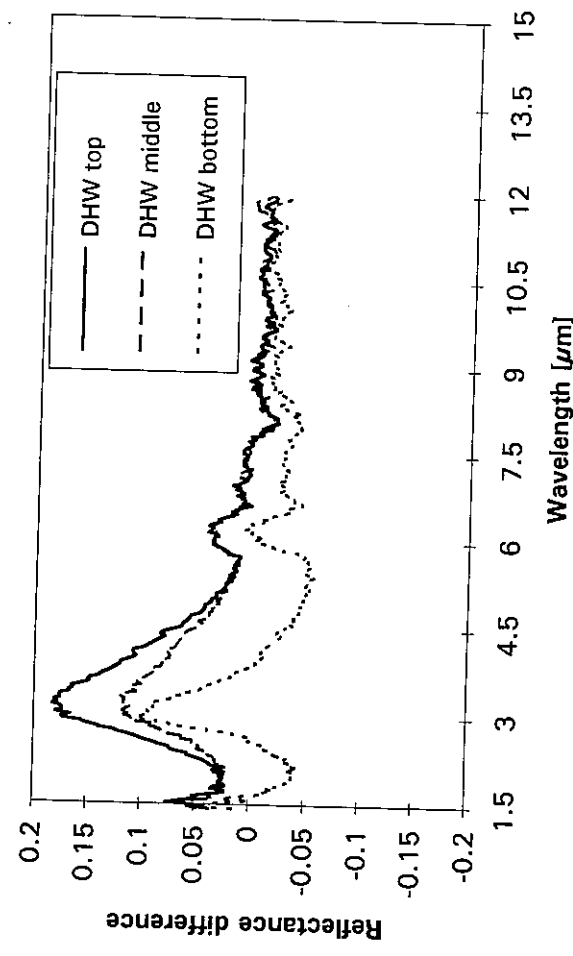
Figure 8:11 *Difference reflectance infrared spectra for the Showa coatings based on the results obtained after three years of collector tests.*
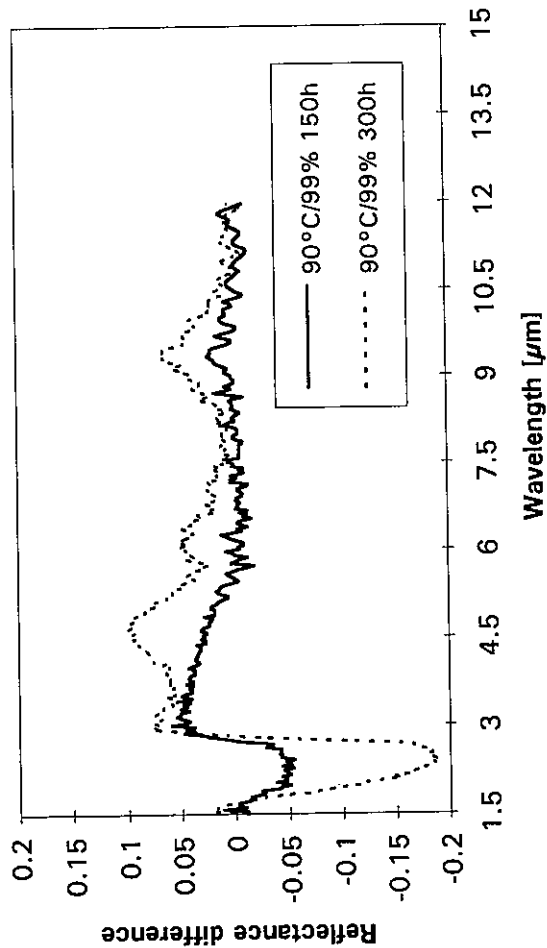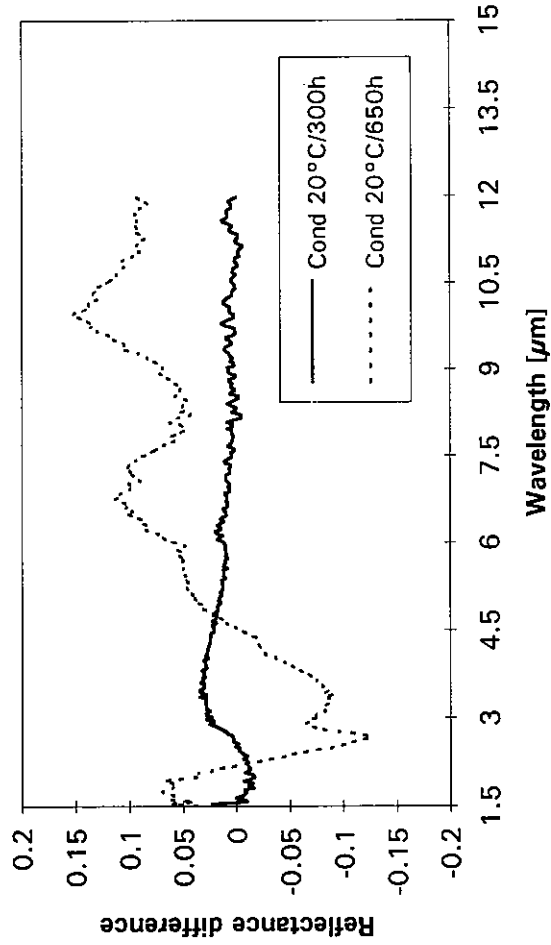
High humidity test at 90 °C and RH = 99 %

Condensation test of a sample temperature of 20 °C

Figure 8;12   *Reflectance difference infrared spectra for the Showa coating based on the results from some laboratory high humidity and condensation tests in the accelerated life test programme of the case study.*

Consequently, the absorption bands at 4.5 and 9.5 μm, being characteristic for Pseudoboehmite and Boehmite, are more or less missing in the reflectance spectra of the absorber samples taken from the two test collectors.

The results from the corrosivity measurements performed with the use of metal coupons placed in the collectors during the test, see *Table 4.2* clearly indicate that the Showa collector must be considerably dryer than the Teknoterm collector. The change in the thermal emittance with time in the DHW collector is about one fifth to one fourth of the corresponding increase in the thermal emittance of the Sunstrip coating in the DHW Teknoterm collector. It should be pointed out that in the laboratory condensation tests the Showa coating was found to be even more sensitive to moisture than the Sunstrip coating.

From the results of the collector tests it is not possible to judge whether degradation by moisture of the Showa coating, increasing its thermal emittance, is an important factor for its service life. The difference in results between the two nickel pigmented anodized aluminium coatings in the DHW collector tests, however, points to the importance of a proper collector design as regards ventilation.

The most important result after the collector tests of the Showa coating is, however, the rather strong decrease in its solar absorptance.

In the reflectance spectra for the visible and near infrared wavelength region you can observe the evolution of a more pronounced inference pattern with increasing testing time. You can also observe that the inteference pattern is shifted somewhat to longer wavelengths at increasing extents of degradation. These phenomena may be a result of absorption of water in the pores of the coating. The relatively strong absorption bands in the infrared wavelength region at 3 and 6 μm indicate that water is contained in the coating even if it seems not to be in the two hydrated forms of aluminium oxide previously discussed, ie Pseudoboehmite and /or Boehmite.

In the high temperature tests of the case study, the solar range reflectance spectrum of the unaged samples used all exhibited a characteristic interference pattern. At exposure of these samples for the thermal loads, the interference pattern of the reflectance spectrum remained essentially the same, although the overall level of reflectance increased steadily as the degradation process progressed, see *Table 5;12*. As a result of those tests, the solar absorptance decreased and the thermal emittance decreased.

In the sulphur dioxide tests of the case study also the solar range reflectance spectrum of the unaged samples used all exhibited the same characteristic inteference pattern. At exposure of these samples, the inteference pattern of the reflectance spectrum also remained essentially the same, although the overall level of reflectance increased steadily as the degradation process progressed. As a result of those tests, the solar absorptance decreased and the thermal emittance increased slightly. The expected change in the solar absorptance after the three years of collector test caused by the action of sulphur dioxide and high humidity should, however, be considerably less than 1 %. This conclusion is reached both when taking into consideration the metal weight losses for the coupons placed inside the collectors and the amount of sulphur dioxide being absorbed in the coating during the collector tests, see *Table 7;6* and *Figure 8;8*.

From the discussion above it is, thus, hard to find an explanation for the decrease in the solar absorptance observed. The main reason is that the samples used in the major part of the laboratory tests were compared to the absorber used in the collector tests, quite different as regards their optical characteristics in the visible and near infrared wavelength region. However, structural changes in the coating probably initiated by the adsorption of water seems to take place during the collector tests performed. Such processes may, as seems to be the only explanation, decrease the solar absorptance of coating and also decrease its thermal emittance. It should be pointed out that peculiar changes in the solar absorptance were observed in the high humidity and condensation tests, as discussed in *Section 6.3*.

As regards the service life with PC <0.05 for the Showa coating in the Showa collector, the results from the accelerated tests point to the fact that it should be more than 25 years. If however, the decrease in the solar absorptance observed in the collector tests progresses, the PC limit of 0.05 should probably be reached already after about 6 years of testing.

The conclusion from the case study work on the Showa coating is that it is of utmost importance to work with coatings with exactly the same optical characteristics in all kinds of tests performed.

A predicted service life is a service life predicted.

How long the actual service life will be, you can only guess. The more clever you are, or the more luck you have, the more accurate your guess.

But why bothering, when you can prevent a failure to happen that you know will happen and you know will result in an unacceptable service life.

This is the key point and the most important outcome of accelerated life testing

REFERENCES

CHAPTER 1

[1,1]   "Survey of service life prediction methods for materials in solar heating and cooling" ; IEA Solar Heating and Cooling Programme Task X "Solar Materials Research and Development"; B. Carlsson (Editor); Document D16:1989 Swedish Council for Building Research, Stockholm, Sweden (Report available from Svensk Byggtjänst S-17188 Solna, Sweden).

CHAPTER 2

[2,1]   "Prediction of Service Life of Building Materials and Components" CIB W 80 /RILEM 71-PSL; Draft report July 1985; see also "Overview of Methodologies for Prediction of Service Life" C. Sjöström in "Problems in Service Life Prediction of Building and Construction Materials", L.W. Masters (Editor) NATO ASI Series E No. 95, Martin Nijhoff Publishers, 1985.

[2,2]   "The Application of Encapsulation Material Stability Data to Photovolatic Module Life Assessment"; C.D. Coulbert; Jet Propulsion Laboratory, California Institute of Technology; Report DOE/JPL - 1012 - 84, 1983.

CHAPTER 3

[3,1]   "Performance criteria for new solar materials"; IEA Solar Heating and Cooling Programme Task X "Solar Materials Research and Development"; B. Brouwer (Editor); Report number 01N1244-1; 1991; (Report available from van Heugten Consulting Engineers Solar Energy Department, P.O. Box 305, 6500 AH Nijmegen, The Netherlands).

[3,2]   "Effect of Selective Surface Degradation on the Performance of Solar Water Heating Systems" K.G.T. Hollands, A. Karagiozis, A.P. Brunger and B. Brouwer; IEA Task X Working Document 1990 (Report available from Solar Thermal Engineering Centre, University of Waterloo, Waterloo, Ontario, Canada N2L3G1).

[3,3]   WATSON User Manuel, Version 11.2, WATSON Simulation Lab. Department of Systems Design Engineering, University of Waterloo, Ontario, Canada N2L3G1 (1989).

[3,4]   "Optical properties measurements of solar absorber surfaces: results of an international round-robin programme"; M.G. Hutchins, P.R. Dolley, K. Gindele, M. Köhl, U. Frei, B. Carlsson, S. Tanemura, K.G.T. Hollands, P.A. van Nijnatten, J. Havinga, A. Gonzales, and E. Mezquida; Proceedings SPIE Conference Volume 1272; Hague; March 1990.

[3,5]   "Results of Comparative Measurements of the Optical Properties of Solar Absorbers"; K. Gindele; Interim report for IEA Solar Heating and Cooling Programme Task XB; March 1989.

[3,6]   C.M. Lampert and J. Washburn; Solar Energy Mater. 1 (1979) 81.

[3,7]   J.N. Sweet, R.B. Pettit and M.B. Chamberlain; Solar Energy Mater. 10 (1984) 251.

[3,8]   "Results of Auger Depth Profile of the Designated Samples in the Work of Subtask B", S. Tanemura; Interim report for IEA Solar Heating and Cooling Programme Task XB; Oct. 1989.

[3,9]   G.B. Smith, R.C. Mc Phedran and G.H. Derrick; Appl. Phys. A 36 (1985) 193.

[3,10]   "Theoretical Model for the Durability of Solar Selective Absorber Coatings at Elevated Temperatures" G.A. Niklasson; Proceedings World Renewable Energy Congress Reading, UK; May 1990.

[3,11]   Å. Andersson, O. Hunderi and C.G. Granquist; J. Appl. Phys. 51 (1980) 754.

[3,12]   H. Uchino, S. Aso, S. Hozumi, H. Tokumasu and Y. Yoshioka; Matsuhita Electr. Ind. Natl. Techn. Rep. 25 (1979) 994.

[3,13]   "Improved Solar Optical Properties of a Nickel-pigmented Anodized Aluminium Selective Surface" E. Wäckelgård, T. Chibuye and B. Karlsson Proceedings North Sun Conference -90; Reading, UK; May 1990.

[3,14]   "Degradation of solar collector coatings: Model calculations for nickel-pigmented aluminium oxide"; G. Niklasson; Proceedings of SPIE Conference Volume 1272; Hague; March 1990.

CHAPTER 4

[4,1]   "Failure and Degradation Modes in Selected Solar Materials - A review"; Carl Lampert /Editor); IEA Solar Heating and Cooling ProgrammeTask X "Solar Materials Research and Development"; Report May 1989. (Report available from Applied Science Division, Lawrence Berkley Laboratory, 1 Cyclotron Road, Berkley, CA 94720, USA).

[4,2]   "Microclimate in Solar Collectors" J. van den Linden, J. Havinga, W. Kowalczyk; Reports TPD No. 914.012, and TPD-HWM-RPT-90-052 (1990) TNO-TU Delft, Report for IEA SHC Task X (Report available from TNO Institute of Applied Physics, P.O. Box 155, 2628 CK, Delft, The Netherlands)

[4,3]   Data file available form Ulrich Frei, School of Engineering, Solar Energy Laboratory, ITR, CH 8640, Rapperswil, Switzerland.

[4,4]   see [3,1].

[4,5]   "Histograms of Temperature and Humidity of Solar Collector Plate: Phase II and III", K.G.T. Hollands, A. Karagiozis and D. Shipley; IEA SHC Task X Working Document 1990 (Report available from Solar Thermal Engineering Centre, University of Waterloo, Ontario, Canada N2L3G1).

[4,6]   S.A. Svendsen (private communication) Thermal Insulation Laboratory, Technical University of Denmark, DK 2800, Lyngby, Denmark.

CHAPTER 5

[5,1]   see [4,1].

[5,2]   see [1,1].

[5,3]   "Ultraviolet irradiation, condensation and humidity testing of black chrome and nickel-pigmented aluminium oxide selective solar absorbers" P.R. Doley and M.G. Hutchins: Solar Energy Materials Research Laboratory School of Engineering. Oxford Polytechnic, Oxford, UK. Report for IEA SHC Task XB (March 1989)

[5,4]   "Round Robin Test Results on the Temperature Stability of a Black Chrome Coating" M. Köhl, K. Möller, B. Carlsson, U. Frei, P.R. Dolley, M.G. Hutchins, P.A. Nijnatten, J. Havinga, A. Gonzales, S. Tanemura Proceedings SPIE Conference Volume 1272; Hague, March 1990.

[5,5]   "Accelerated Ageing Test Procedures for Selective Absorber Coatings Including Lifetime Estimation and Comparison with Outdoor Test Results", M. Köhl, K. Gindele, U. Frei, T. Häuselmann, Solar Energy Materials 16 (1989) pp 257 - 313.

[5,6]   "Accelerated ageing of absorbers - Temperature tests", M. Köhl, Interim Report IEA SHC Task XB (March 1989).

CHAPTER 6

[6,1]   see [4,1]

[6,2]   see [3,8]

[6,3]   "Accelerated Ageing Testing of Black Chrome Coating under Heat and/or Condensation Loads and Degradation Mechanisms"; S. Tanemura, K. Yoshimura, K. Taga, R. Odaira, M. Inshida, S. Tsuboi, M. Yoshikawa; ISES Congress Kobe, Japan; Sept. 1989 (Pergamon Press N.Y. 1990).

[6,4]   "Accelerated Aging Testing of Ni-pigmented Anodized Al under Heat and/or Condensation Loads and Degradation Mechanism", S. Tanemura, K.Yoshimura, K. Taga, R. Odaira, M. Ishida, S. Tsuboi, M. Yoshikawa, ISES Congress Kobe, Japan; Sept. 1989 (Pergamon Press N.Y. 1990)

[6,5]   see [3,14]

[6,6]   F.P. Fehler and N.F. Mott, Oxidation of Metals, Vol 2 pp 59-99, 1970.

[6,7]   B.C. Sales and M.B. Maple Phys. Rev. Lett. vol. 39, pp 1636-1639, 1977;
        B.C. Sales, M.B. Maple and F.L. Vernon, Phys, Rev. B, vol 18, pp 486 - 491,
        1978.

[6,8]   Takahasi?

[6,9]   "An Introduction to Corrosion and Protection of Metals", G. Wranglén;
        (Chapman and Hall, London 1985).

[6,10] see [3,11].

[6,11] "The Corrosion and Oxidation of Metals"; U.R. Evans; pp 105-106 (Edvard
        Arnold (Publishers) Ltd. 1961).

[6,12] "SO_2-deposition on solar collector material of nickel-pigmented anodized alu-
        minium" P. Eriksson, L.G. Johansson, J.E. Svensson; Department of Inor-
        ganic Chemistry, Chalmers Technical University Gothenburg; Report for IEA
        SHC Task XB (in Swedish) April 1991.